Field-scale water flow and solute transport

SWAP model concepts, parameter estimation and case studies

Promotor: dr. ir. R.A. Feddes
Hoogleraar in de bodemnatuurkunde, agrohydrologie en het grondwaterbeheer

Jos C. van Dam

Field-scale water flow and solute transport

SWAP model concepts, parameter estimation and case studies

"Concepts without percepts are empty. Percepts without concepts are blind." (I. Kant)

Water flow and solute transport in top soils are important elements in many environmental studies. The agro- and ecohydrological model SWAP (Soil-Water-Plant-Atmosphere) has been developed to simulate simultaneously water flow, solute transport, heat flow and crop growth at field scale level. The main features and theoretical concepts of SWAP are described.

A serious limitation of many model applications is the availability of accurate input parameters. With the rapid increase of processor calculation speed and development of effective optimization algorithms, the optimization of input parameters by inverse modeling has become an attractive option. Typical and verifiable examples of the inverse modeling technique, are the laboratory One-step and Multi-step outflow experiments, which are used to determine the soil hydraulic functions. It is shown that in the One-step method the cumulative outflow data with time are insufficient to derive unique parameter estimates, and should be supplemented with retention data. In Multi-step experiments, where the air pressure is increased in several steps rather than one large step, the cumulative outflow data proved to be sufficient to derive unique and reliable soil hydraulic parameters.

The accuracy of field scale model predictions will increase if the inverse problem is also applied to measurements at field scale level. A prior method is presented to select the type of measurements and timing of observations that result in well-posed inverse problems. This method was applied to a theoretical field experiment at a drained loamy soil, cultivated with maize. SWAP in combination with the optimization shell PEST (Parameter ESTimation) were used to perform the prior inverse analysis. At least four selected parameters could be optimized uniquely, using ordinary, generated observations augmented with a random observation error. The prior analysis showed that inclusion of a crop, a tracer as well as measurements at periods with extreme and rapidly changing hydrological conditions improved the accuracy of the optimized parameters significantly.

An accurate and efficient numerical solution of Richards' water flow equation is presented. Special attention is given to proper selection of the top boundary condition during the iterative solution of Richards' equation. The stability of the scheme is shown for extreme events of infiltration, soil evaporation and rapidly fluctuating, shallow groundwater levels in two strongly non-linear soils. It is shown that in case of nodal distances of 1 cm and arithmetic spatial averages of the hydraulic conductivity, errors due to numerical discretization are small compared to errors due to hysteresis and horizontal spatial variability of the soil hydraulic functions.

Concepts for hysteresis and mobile-immobile regions due to water repellency have been incorporated in SWAP. Both concepts were applied to data sets from two locations with hysteretic and water repellent soils. In general hysteresis retards soil water movement, while preferential flow enhances soil water movement. Application of the hysteresis and mobile-immobile concept improved the correspondence between measured and simulated water and bromide contents.

Also an extended model concept for water and solute movement in cracked clay soils is discussed and applied to a field experiment. Inclusion of this concept in SWAP improved considerably the simulation of soil water contents and bromide leaching to the groundwater. The bromide amounts leached were especially sensitive to the saturated hydraulic conductivity of the top layer, the solute transfer from the soil matrix to crack water flow and the mean residence time of rapid drainage.

We may expect that in the coming years SWAP will be useful to explore new flow and transport concepts for agro- and ecohydrology, to analyse laboratory and field experiments, to select viable management options, to perform regional studies employing geographical information systems, and to illustrate transport processes for education and extension.

Additional index words: clay cracks, crop growth, heat flow, hysteresis, inverse modeling, outflow experiments, Richards' equation, salinization, transpiration, unsaturated zone, water repellency

Voorwoord

Dit proefschrift is samengesteld uit artikelen en onderzoeksrapporten waarvan ik eerste auteur was en die over een periode van 10 jaar zijn verschenen. Misschien had u meer verwacht dan een klein boekje na zo'n lange periode, maar bedenk dan dat u slechts de eindversie ziet, niet de vele conceptversies die het niet gehaald hebben. In de conceptversie van dit proefschrift gebruikte ik vaak 'wij' om aan te geven dat het resultaat voortvloeit uit het werk van veel mensen, en ik slechts gegevens en ideeën hoefde te combineren, abstraheren, implementeren, toetsen, aanvullen en opschrijven. Terwille van wetenschappelijk verantwoord taalgebruik zijn veel 'wij's' eruit gehaald. Dit voorwoord biedt wel de gelegenheid een aantal mensen bij name te noemen die een belangrijke bijdrage hebben geleverd.

Kort nadat ik in 1988 afgestudeerd was, nam Han Stricker me aan om onderzoek te doen voor een EG project naar variabiliteit van bodemfysische functies ten behoeve van atmosferische modellen. Hoewel de atmosferische modellen werken met gridafstanden van 100 – 200 km, begonnen wij als echte bodemfysici veel bescheidener: met bodemmonsters van 5 cm hoog en 5 cm diameter. Een paar jaar ervoor was een laboratorium-uitstromingsmethode ontwikkelt (One-step Outflow) voor het efficiënt meten van bodemfysische eigenschappen en die methode zouden wij toepassen op honderden bodemmonsters uit testgebieden in Nederland, Frankrijk en Spanje. Na het overwinnen van een aantal experimentele kinderziektes, bleek dat de methode niet tot éénduidige resultaten leidde. Een flinke tegenslag, die een groot aantal metingen waardeloos maakte en de relevantie van onze bijdrage in het EG project in de waagschaal bracht. Om toch in korte tijd een groot aantal bodemmonsters te kunnen meten, zochten we naar verbeteringen van de uitstromings-methode. Ik kreeg versterking van Peter Droogers, die in het bodemfysische laboratorium veel werk heeft verzet en enorm geholpen heeft bij de verwerking en analyse van de gegevens. Uiteindelijk konden we duidelijke suggesties voor een betrouwbare en efficiënte uitstromingsmethode doen, welk werk leidde tot de artikelen die aan de basis liggen van hoofdstuk 3.

In 1990 kon ik bij de sectie Waterhuishouding een functie gaan vervullen als wetenschappelijk medewerker in bodemfysische transportverschijnselen. Reinder Feddes was niet lang daarvoor aangesteld als hoogleraar. Een van zijn oogappels was het agrohydro-logische model SWATRE, en hij onderkende het strategische belang van verdere ontwikkeling van dit model. Vanaf 1990 hebben Jan Wesseling, Pavel Kabat, Barend van de Broek, Jaap Huygen van het voormalige Staring Centrum en Reinder Feddes en ik van de sectie Waterhuishouding urenlange besprekingen gehouden over mogelijke verbeteringen. Naast het nodige literatuuronderzoek en uitgebreide tests, kregen we ondersteuning met specifieke expertise vanuit het Staring Centrum voor regionale drainage (Piet Groenendijk), opgeloste stoffen (Jos Boesten), zwel en krimp in kleigronden (Hans Bronswijk) en oppervlaktewater (Paul van Walsum). In 1997 heeft Joop Kroes de coördinerende taak van

Barend van den Broek met verve overgenomen. Inmiddels vindt het model steeds meer toepassing (zie hoofdstuk 8) en konden we cursussen over SWAP gegeven in Wageningen en Warschau, die hoge waardering ontvingen.

Met de jaren groeide mijn idee om een proefschrift te schrijven waarin numerieke modellering van waterstroming en transport van opgeloste stoffen op veldschaal en het schatten van parameters belangrijke elementen zouden vormen. In het kader daarvan verbleef ik in 1994 drie maanden op de University of California in Davis en drie maanden op het Soil Salinity Laboratory in Riverside. De vakgebieden en onderzoeksvelden van UCDavis hebben veel gemeen met die van de Universiteit Wageningen, en we zouden in de toekomst meer samenwerking moeten hebben. Ik heb er op heel prettige wijze gewerkt met Jan Hopmans en Volker Clausnitzer van de afdeling Land, Air and Water Resources. Op het Soil Salinity Laboratorium heeft de onderzoeksgroep Soil Physics van Rien van Genuchten (in 1994 Feike Leij, Nobuo Toride, Kangle Huang, Antonella Sciortino, Binayak Mohanty, Jirka Šimunek en Peng-Hsiang Tseng) een grote indruk op me gemaakt: een kleine, maar zeer gemotiveerde, doelgerichte en productieve groep jonge onderzoekers. Het liet zien dat er geen grote instituten nodig zijn om grensverleggend onderzoek te doen.

In de jaren 1989-1994 voerde Klaas Groen in Flevoland drie grote veldexperimenten uit naar het vochttransport en de uitspoeling van bromide en gewasbeschermingsmiddelen. De gronden varieerde tussen zavel en sterk gerijpte klei met permanente scheuren onder de ploegzool, en het landgebruik tussen fruitboomgaarden en de verbouw van tulpenbollen en aardappelen. Het RIZA in Lelystad, waar Klaas Groen was gedetacheerd, maakte het financieel mogelijk uitgebreide metingen op de experimentele velden te doen en een ideale dataset voor modelverificatie op te bouwen. In de begeleidingsgroep van de experimenten en de analyse, bestaande naast Klaas Groen uit Bart Schultz, Jos Boesten, Reinder Feddes, Ruurd Koopmans en mijzelf, heb ik veel geleerd tijdens de besprekingen over meetstrategieën, foutenbronnen, modelalternatieven, validatie en calibratie. Ook bleek het een zeer nuttige oefening voor het model SWAP. In 1997 ronde Klaas Groen dit promotieonderzoek af met een fraai proefschrift boordevol experimentele gegevens.

Als ergens het belang van een goede analyse van waterstroming- en stoffentransport duidelijk wordt, is dat wel in de geïrrigeerde landbouw van Pakistan en India waar watertekorten en verzouting van de wortelzone de gewasopbrengsten ernstig belemmeren. We werkten samen met IWASRI (International Waterlogging and Salinity Research Institute) via NRAP (Netherlands Research Assistance Project) en IWMI (International Water Management Institute), beide in Lahore, Pakistan, via studenten en promotie-onderzoekers. Driemaal heb ik een aantal weken doorgebracht in Pakistan. De levendige discussies met Thijs Kelleners, Hussain Asher, Jelle Beekma, en Asad Sarwar zullen me altijd bijblijven, als ook de gastvrijheid, betrokkenheid en ijver van Marcel Kuper en Pierre Strosser. Hun huis was een sfeervolle oase voor diverse Europeanen en Aziaten in Lahore. Zij wisten de juiste randvoorwaarden te scheppen voor gezamenlijk en creatief onderzoek. In 1998 zijn Marcel

Kuper en Pierre Strosser op hun irrigatie-onderzoek gepromoveerd, deze maand zal Asad Sarwar zijn promotieonderzoek naar drainage afronden.

In de afgelopen 10 jaar is de capaciteit van de sectie Waterhuishouding helaas onder druk van bezuinigingen tot de helft teruggebracht. Ondanks de toegenomen werkdruk en geringe financiële ruimte, voelen de meeste medewerkers zich nog steeds sterk betrokken bij de taken in onderwijs en onderzoek. Hun interesse, ondersteuning en collegialiteit waren onmisbaar bij de totstandkoming van dit proefschrift.

Reeds jaren bestaat er een nauwe samenwerking tussen de sectie Waterhuishouding en de corresponderende teams op het vroegere Staring Centrum, nu Alterra. Zonder vrije uitwisseling van gegevens, ervaringen, en ideeën had het SWAP model niet bestaan. Nu het landbouwkundig onderzoek en onderwijs verder gaan in het WUR (Wageningen Universiteit- en Researchcenter) kunnen er nieuwe vormen aan die samenwerking worden toegevoegd. Hopelijk zal daarbij genoeg ruimte zijn voor fundamenteel, strategisch onderzoek, waartoe ook modelontwikkeling behoort.

Diverse gastmedewerkers (John Nieber, Matthew Bethune, Mehdi Homaee, Jose Louzada, Dinesh Sharma) en afstudeervak-studenten (Anne Verhoef, Desirée Huisman, Magali Garcia, Attila Nemes, Ronnie Daanen, Susanna Smets, Mariska Te Vaarwerk, Christiaan van der Tol en Marchien van Os) met wie ik heb kunnen samenwerken, hebben ieder op hun eigen wijze bijgedragen aan de inhoud van dit proefschrift.

Reviewers van professionele tijdschriften hebben mijn promotor Reinder Feddes voor het proefschrift veel werk uit handen genomen. Echter niet minder belangrijk, hij schiep de randvoorwaarden die dit onderzoek mogelijk maakte: tijd om aan modelontwikkeling te werken, contact met de juiste mensen, doelmatige besprekingen, organisatie van SWAP cursussen en stimuleren van publicatie. Zijn enthousiasme, pragmatisme, oog voor de rode lijn in het onderzoek, doortastendheid en ijver waren voor mij een grote stimulans.

Het schrijven van een proefschrift lijkt op het rijden van een Elfstedentocht of het lopen van een marathon: diegene die ermee bezig is wordt er volledig door in beslag genomen, terwijl de naaste omgeving niet veel meer kan doen dan enigszins meewarig toekijken. Daarom heb ik thuis en bij familie, vrienden en kennissen niet veel uitgeweid over de voortgang en problemen bij het schrijven. Echter, zonder hun hulp, vriendschap, relativering en vertrouwen had dit proefschrift hier nu niet gelegen. De afgelopen maanden leek het voor Ilse en mij een kwestie van wie eerder zou bevallen: zij van een echt kind of ik van dit boekwerk. Ik weet niet in hoeverre je hormonen kunt sturen, maar Ilse heeft gelukkig op me gewacht. Met de geboorte van onze tweede dochter breekt nu een nieuwe periode aan.

Jos van Dam

Contents

1. Introduction

Top soils, whether they belong to natural or agricultural fields, play a key role in our environmental conditions. They provide a supporting medium for plant roots and supply essential nutrients for all plant organs. Top soils form a habitat for numerous living organisms, from small mammals and reptiles to tiny insects and microscopic cells. Also top soils function as a flexible recycle system for human waste products and remains of plants and animals, and their basic products are made available for reuse by the next generation of life (e.g. *Brady and Weil*, 1996).

In the processes related to all these functions, the presence and behaviour of water in the top soil is of utmost importance. First of all, water itself is needed by plants to build up their tissues, as one of the main constituents of the photosynthesis process. This amount of water forms only 1% of the total plant water requirements, 99% of the water requirements is needed to compensate water loss through open stomata and to cool the plant environment. Plant nutrients adsorbed to soil particles and organic matter dissolve in water and come available to plant roots through the aquaous phase. Chemical soil reactions are governed by soil acidity, temperature and oxygen status, factors which are directly affected by the amount of water present. Also water determines physical properties which control the soil habitat function, like penetration resistance, soil structure and stability.
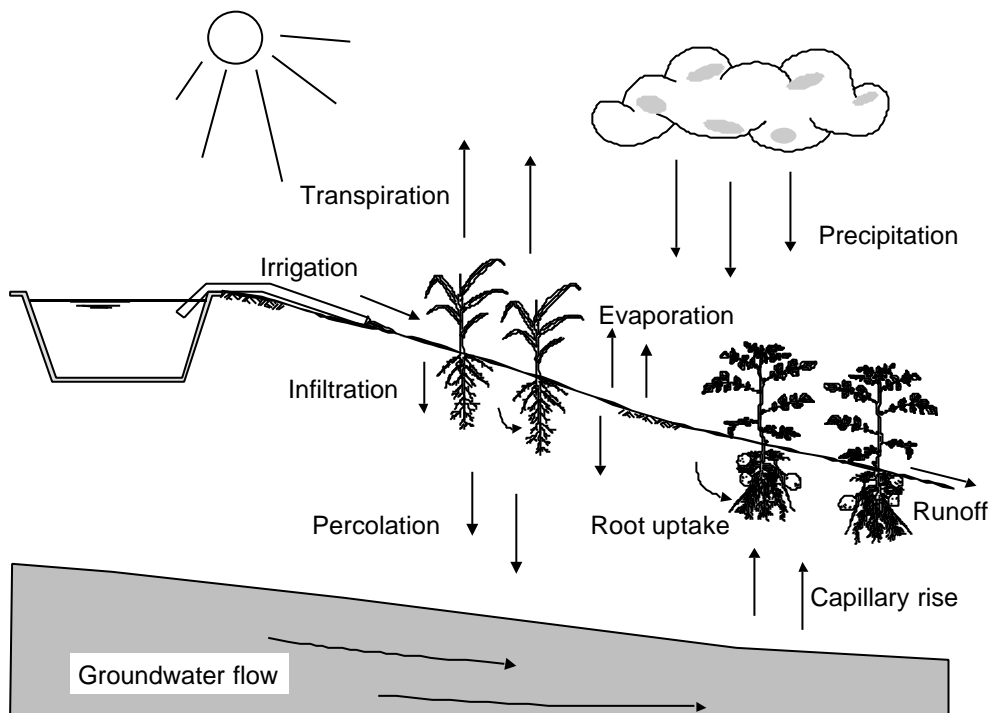
Figure 1.1 Hydrological flow processes at field scale level.

Top soils in combination with the vegetation play a major role in distributing precipitation among transpiration, evaporation and percolation, which form important components of the hydrological cycle (Fig. 1.1). Water which reaches the soil surface may infiltrate into the soil,

or, if the soil infiltration capacity is exceeded, may flow laterally as runoff to depressions. Once in the soil, water may be extracted by plant roots, evaporate from the soil surface or percolate to deeper soil layers. These flow processes depend to a large extent on the physical properties of the soil, in particular its water holding capacity and hydraulic conductivity. In this way important components of the hydrological cycle (transpiration, evaporation, runoff and groundwater recharge, see Fig. 1.1) are determined by the vegetation type and the top soil composition.

Therefore water flow and solute transport in top soils forms an essential part in many environmental studies. This is especially true for The Netherlands, where the population density is high, agriculture is intensive, chemical industry is well developed, soils are composed of permeable sediments, groundwater levels are shallow and average rainfall surpluss is generous. Only in The Netherlands, already a large number of doctoral theses have been written on water and solute movement in natural soils (among others *Feddes*, 1971; *Stroosnijder*, 1975; *De Laat*, 1980; *Boesten*, 1986; *Ten Berge*, 1986; *Van Bakel*, 1986; *Van Grinsven*, 1988; *Van Ommen*, 1988; *Van der Zee*, 1988; *Wösten*, 1990; *Bronswijk*, 1991; *Boekhold*, 1992; *Bouten*, 1992; *Finke*, 1992; *Schultz*, 1992; *Booltink*, 1993; *Kim*, 1995; *De Rooij*, 1996; *Schaap*, 1996; *Droogers*, 1997; *Groen*, 1997; *Heinen*, 1997; *Kuper*, 1997; *De Vos*, 1997; *Dekker*, 1998; *Ritsema*, 1998; *Van der Schaaf*, 1999; *Tiktak*, 1999; *Gehrels*, 1999; *Hack-ten Broeke*, 2000). Which information does this thesis add to all the information already available? Like many other research fields, agrohydrological research experiences rapid developments in knowledge and methodology. This thesis aims to contribute to three current trends in agrohydrological research: the trend from analytical to numerical modeling, from uniform to heterogeneous soils, and from measurements in the laboratory to measurements in the field.

In top soils occur numerous physical, chemical en biological processes, with all kind of complexity and interactions. Although analytical equations are elegant, provide insight and are rapidly transferable, they are in general insufficient for field conditions. The interaction between highly non-linear processes under irregularly changing boundary conditions, as occurring in the field, can not be solved by analytical equations. Numerical solutions of the governing relationships are much better equipped to solve these processes at the prevailing boundary conditions. Our increased knowledge of numerical stability, the exponential growth of computer speed and capacity, the accessibility of input data and availability of support through the Internet, and the increasing interface user's friendliness, have enhanced the development and application of numerical models. One of these agrohydrological models is the Soil-Water-Atmosphere-Plant (SWAP) model, which is described in Chapter 2. The rapid changing boundary conditions, especially at the soil surface, and the high non-linearity of the soil physical properties, require specific numerical methods, as discussed in Chapter 5.

The second trend is a shift from uniform to heterogeneous soils, which is closely related to the development of numerical techniques. Traditionally, the vertical variation of physical properties in the soil profile due to soil origin and development, was taken into account.

However, practical procedures to account for swelling and shrinking in clay soils or to account for water repellency in many agricultural and natural fields, were lacking. Measurements both in the field and in the laboratory show that these processes have a large impact on soil water and solute transport, and therefore should be included in environmental policy analysis. Both aspects, swelling and shrinking of clay soils and water repellency are considered in the Chapters 6 and 7.

The third trend is a shift from measurements in the laboratory to measurements in the field. The laboratory has certain advantages with respect to reproducable measurements due to the availability of usual facilities (e.g. electricity, gas, water and vacuum) and the control of boundary conditions (*Dirksen*, 1999). However, the volume and number of soil samples needed for a representative picture of layered and structured soil horizons, requires a huge investment of time and money. Unavoidable disturbances due to soil sampling and non-representative experimental conditions, further limit the value of laboratory measurements. Also, separate measurement in the laboratory of the large number of parameters describing the physical, chemical and biological processes, is rather inefficient. An alternative approach was developed when more efficient optimization algorithms in combination with reliable agrohydrological models, allowed optimization of model input parameters using physical data of natural fields. The development of non-destructive and stand-alone measurement techniques, such as remote sensing for soil surface wetness, surface temperature and evapotranspiration, scintillometers for evapotranspiration, time domain reflectrometry for water content, automatic sampling equipment for tracers, and diver instruments for groundwater levels, enhanced the focus on field experiments. The technique of using a transport model in combination with an optimization algorithm, so called inverse modeling, is explored with well-defined laboratory outflow experiments in Chapter 3 and applied in case of agrohydrological field experiments to improve measurement strategy in Chapter 4.

In the first part of this thesis, the basic features of the SWAP program are described. Next the inverse methodology, as a tool to derive model parameters and to select the most informative measurement scheme, is considered for laboratory and field experiments. Then recent improvements of the SWAP program, developed by the present author, are discussed, notably the numerical solution of the soil water flow equation, and concepts for water and solute movement in hysteretic, water repellent, and cracked soils. The last chapter provides an overview of recent SWAP applications. Two applications will be discussed in more detail, one with regard to irrigation management in the Punjab, Pakistan, and one with regard to surface water management in a former estuary De Grevelingen, in The Netherlands.

2. SWAP model description[1]

This Chapter contains the main features and theoretical concepts of the SWAP program, as far as they are not extensively discussed in the next chapters (e.g. numerical discretization of water flow, and water and solute movement in water repellent sand or cracked clay soils). The description below applies to SWAP version 2.07d, which is currently spread.

2.1 SWAP guidelines

During the past 10 years, the joint development of SWAP by Wageningen University, sub-department Water Resources, and Alterra Green World Research, department Water and Environment, was guided by the following main wishes:
- Allow direct interaction between water flow, solute transport, heat flow and plant growth
- Simulate physical, chemical and biological processes at field scale level
- Accomodate long term simulations, with multiple crops per year
- Employ experiences with SWATR and its derivatives
- Develop for researchers, engineers and students

In the soil numerous interactions occur between water flow, solute transport, heat flow and plant growth. For instance, water fluxes affect the rate of salinization, while salt concentrations affect actual root water uptake rate. Water and salinity stress may affect crop development and soil cover, which vice versa affects soil evaporation and crop transpiration. Pesticide decomposition is sensitive to soil temperatures, which on their turn are influenced by soil wetness. In order to analyse these kind of interactions, SWAP solves simultaneously the numerical equations for water flow, solute transport, heat flow and crop growth, and allows interaction at time step basis.

As spatial scale for the description of physical, chemical and biological processes near the soil surface, the farmer field scale is attractive. At this scale, the meteorological conditions, cultivation pattern, soil profile and drainage conditions are more or less the same and well defined. This is important, as the input data do not represent a weighted areal average, which generally requires calibration, but can be measured directly in the field, or derived from data banks with geographical information. Another important advantage of using physically defined characteristics at field scale level rather than some kind of effective properties, is that such models can be employed for scenario analysis covering a wide range of situations.

In most applications, we are not only interested in the systems behaviour in a particular or 'average' meteorological year, but also in its behaviour during extreme weather periods.

---

[1] *Adapted from Van Dam, J.C., J. Huygen, J.G. Wesseling, R.A. Feddes, P. Kabat, P.E.V. van Walsum, P. Groenendijk, and C.A. van Diepen, 1997. Theory of SWAP version 2.0. Simulation of water flow, solute transport and plant growth in the Soil-Water-Atmosphere-Plant environment. Report 71, Department Water Resources, Wageningen University, Technical Document 45, Alterra, Wageningen, The Netherlands, 167 pp.*

Furthermore some processes, like salinization and groundwater recharge, require analysis over a large number of years. Therefore long term simulations, without losing accuracy during rapidly changing conditions, formed one of the main demands.

Feddes et al. (1978) developed the agrohydrological model SWATR (Soil Water Actual Transpiration Rate) to describe transient water flow in cultivated soils with various soil layers and under the influence of groundwater. The model was further developed to accommodate more boundary conditions (*Belmans et al.*, 1983), crop growth (*Kabat et al.*, 1992), shrinkage and swelling of clay soils (*Oostindie and Bronswijk*, 1992), and salt transport (*Van den Broek et al.*, 1994). Gradually the need was felt for a completer program that included the options of the various SWATR derivatives, as well as updated numerical schemes, a clear program structure and a user's friendly interface.

The model should assist researchers in analysis of field experiments, in testing alternative theoretical concepts and in exploration of all kind of scenarios. Also the model should be useful to students to illustrate the interaction between agrohydrological processes and provide quantitative information on their relative importance. Furthermore, the model should be useful to engineers who face daily agrohydrological problems. However, in such a complex environment as existing in the top soil, basic knowledge of agrohydrological processes is essential for proper model use and result interpretation.

Figure 2.1 schematizes the hydrological processes incorporated in SWAP. The upper boundary is located just above the vegetation, the lower boundary in the top groundwater system. In the region between these boundaries, the main water flow processes are vertical, which allows a one-dimensional model structure. When a region is analyzed with horizontal variation of vegetation, soil or drainage conditions, the model should be applied either at each location separately, or a more or less representative situation should be defined. The SWAP soil column is divided in compartments, for which the transport and balance equations of water, solutes and heat are solved. Interaction between residence and movement of water, solute and heat occurs at each time step, which may range between seconds and hours, depending on how fast flow and transport conditions change in time. Interaction with plant growth processes, which show relatively slow changes in time, is calculated on a daily basis. SWAP makes a distinction between soil evaporation and plant transpiration, because both have clearly different extraction and reduction mechanisms. In the saturated zone, interaction with water management in canals/ditches at different levels may be calculated. At the bottom of the SWAP column, interaction with regional groundwater is defined. Soil heterogeneity is taken into account by providing options for soil layering, similar media scaling, water repellency and shrinkage cracks. In the next sections the various elements are described in more detail, starting with water, going from atmosphere to bottom boundary, then solutes, heat and soil heterogeneity, and ending with the user interface.
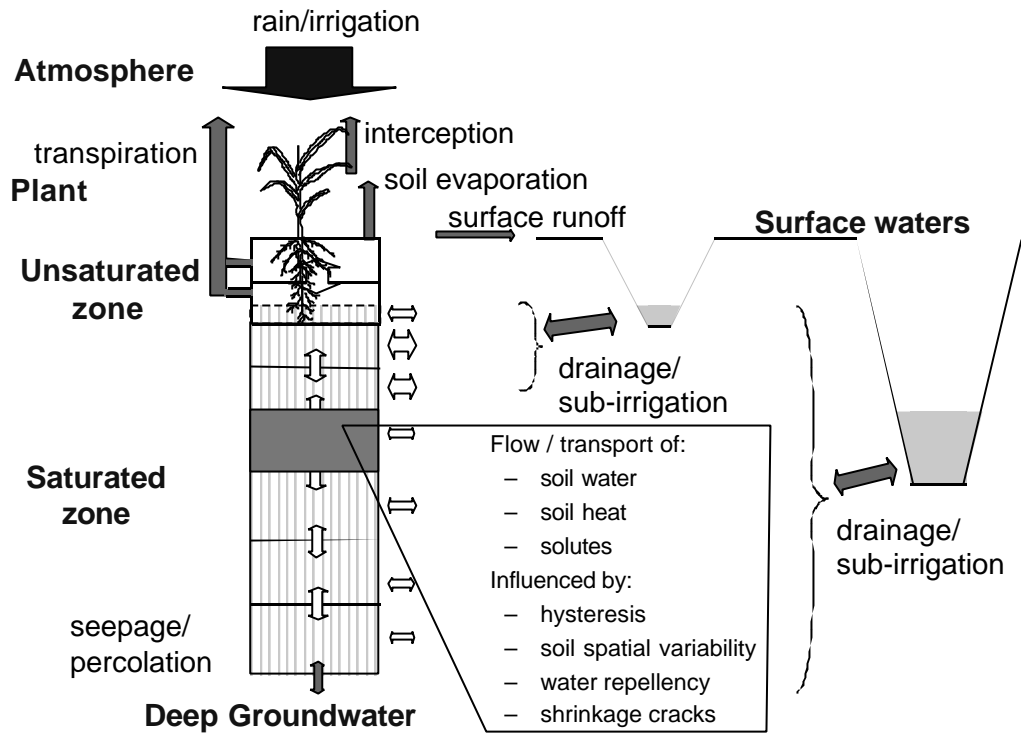
Figure 2.1 Schematization of hydrological processes incorporated in SWAP.

2.2 Potential evapotranspiration

The upper boundary conditions are determined by the rates of potential evapotranspiration, irrigation and precipitation. Daily meteorological data, consisting of air temperature, solar radiation, wind speed and air humidity, can be used to calculate daily potential evapotranspiration according to Penman-Monteith (*Monteith*, 1965, 1981; *Smith*, 1992; *Allen* et al., 1998):

$$ET_p = \frac{\dfrac{\Delta_v}{\lambda_w}\left(R_n - G\right) + \dfrac{p_1 \rho_{air} C_{air}}{\lambda_w}\dfrac{e_{sat} - e_a}{r_{air}}}{\Delta_v + \gamma_{air}\left(1 + \dfrac{r_{crop}}{r_{air}}\right)} \tag{2.1}$$

where ET_p is the potential transpiration rate of the canopy (mm d^{-1}), Δ_v is the slope of the vapour pressure curve (kPa K^{-1}), λ_w is the latent heat of vaporization (J kg^{-1}), R_n is the net radiation flux density above the canopy (J m^{-2} d^{-1}), G is the soil heat flux density (J m^{-2} d^{-1}), p_1 accounts for unit conversion (= 86400 s d^{-1}), ρ_{air} is the air density (kg m^{-3}), C_{air} is the heat capacity of moist air (J kg^{-1} K^{-1}), e_{sat} is the saturation vapour pressure (kPa), e_a is the actual vapour pressure (kPa), r_{air} is the aerodynamic resistance (s m^{-1}), γ_{air} is the psychrometric constant (kPa K^{-1}), and r_{crop} is the crop resistance (s m^{-1}).

If basic meteorological data are not available, potential evapotranspiration or reference evapotranspiration in combination with crop factors can be input (*Doorenbos and Pruitt*, 1977; *Feddes*, 1987; *Allen et al.*, 1998). Precipitation may be provided either at a daily basis or at actual intensities. In case of runoff and preferential flow simulation, actual rainfall intensities increase the reliability of the simulation results.

2.3   Irrigation

Irrigation may be prescribed at fixed times or scheduled according to a number of criteria, which allows the optimization of irrigation management. The timing criteria include allowable daily stress (as expressed by the reduction of potential crop transpiration), allowable depletion of readily available water in the root zone, allowable depletion of totally available water in the root zone and critical soil water pressure head or soil water content at a certain depth. The irrigation amounts can be prescribed, or can be calculated by SWAP as the difference between actual water storage in the root zone and water storage at field capacity. The calculated irrigation amounts can be increased to induce leaching, or decreased to account for expected rainfall.

2.4   Crop growth
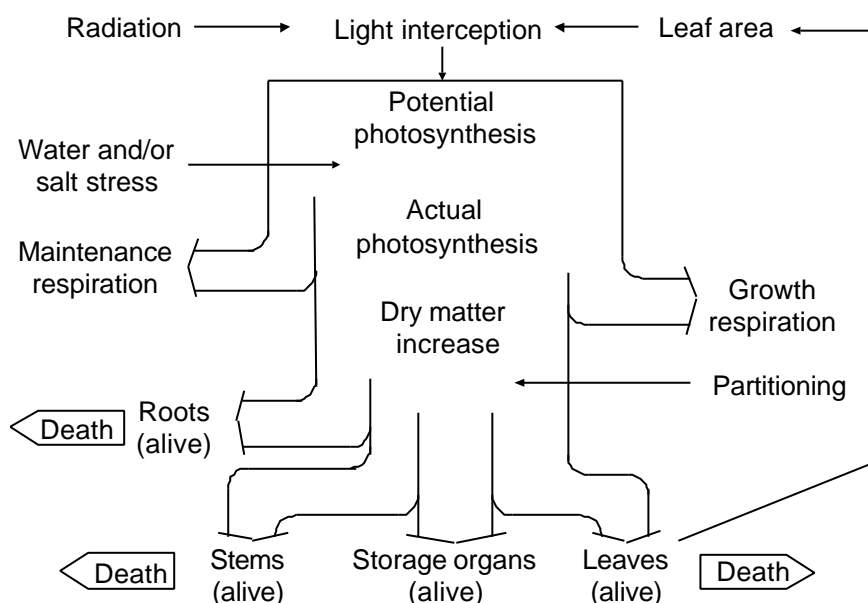
Figure 2.2 Schematization of the crop growth processes incorporated in WOFOST.

SWAP may simulate up to three rotating crops in a year and contains three crop growth routines: a detailed model (WOFOST 6.0; *Spitters et al.*, 1989; *Hijmans et al.*, 1994), the same model but attuned to simulate grass growth only, and a simple model. Figure 2.2 schematizes the processes incorporated in WOFOST. The program calculates the radiation energy absorbed by the canopy as function of incoming photosynthetic active radiation and crop leaf area. Using

the absorbed radiation and taking into account photosynthetic leaf characteristics, the potential photosynthesis rate is calculated. The latter is reduced due to water and/or salinity stress, as quantified by the relative transpiration rate, and yields the actual photosynthesis rate. Part of the carbohydrates (CH_2O) produced are used to provide energy for the maintenance of living biomass (maintenance respiration). The remaining carbohydrates are converted into structural matter. In this conversion, some of the weight is lost as growth respiration. The dry matter produced is partitioned among roots, leaves, stems and storage organs, using partitioning factors that are a function of the crop phenological development stage. The fraction partitioned to the leaves, determines leaf area development and hence the dynamics of light interception. The dry weights of the plant organs are obtained by integrating their growth rates over time. During crop development a part of the living biomass will die due to senescence.

The grass growth model is adapted from the general WOFOST crop growth model. The following assumptions apply to the grass growth model:
- the grass species grows and behaves similarly to perrennial ryegrass;
- the sward is regularly mowed and remains vegetative;
- grazing by cattle is excluded;
- the grassland is permanent.

In case crop growth doesn't need to be simulated or when crop growth data are insufficient, the simple crop development model can be used. For this model the user prescribes the leaf area index (or soil cover fraction), crop height and rooting depth as functions of crop development stage, which either is controlled by temperature or is linear in time. These data are sufficient to determine rainfall interception and potential transpiration and evaporation. In order to calculate yield reduction, yield response factors as function of growing stage can be used (*Doorenbos and Kassam*, 1979; *Smith*, 1992). Each growing stage k, the actual yield $Y_{a,k}$ (kg ha^{-1}) relative to the potential yield $Y_{p,k}$ (kg ha^{-1}) during this growing stage is calculated by:

$$1 - \frac{Y_{a,k}}{Y_{p,k}} = K_{y,k}\left(1 - \frac{T_{a,k}}{T_{p,k}}\right)$$
(2.2)

where $K_{y,k}$ is the yield response factor (-) of growing stage k, and $T_{p,k}$ (cm) and $T_{a,k}$ (cm) are the potential and actual cumulative transpiration, respectively, of growing stage k.

The relative yield of the entire growing season is calculated as product of the relative yields of each growing stage:

$$\frac{Y_a}{Y_p} = \prod_{k=1}^{n} \frac{Y_{a,k}}{Y_{p,k}}$$
(2.3)

where Y_a is the cumulative actual yield (kg ha^{-1}) of the whole growing season, Y_p is the cumulative potential yield (kg ha^{-1}) of the whole growing season, and n is the number of defined growing stages.

2.5 Rainfall interception

Von Hoyningen-Hüne (1983) and *Braden* (1985) measured interception of precipitation for various agricultural crops. They proposed the following general formula for canopy interception:

$$P_i = aLAI \left(1 - \frac{1}{1 + \dfrac{b\,P_{\mathrm{gross}}}{aLAI}} \right) \tag{2.4}$$

where P_i is intercepted precipitation (cm), *LAI* is the leaf area index (m^2 m^{-2}), P_{gross} is gross precipitation (cm), *a* is an empirical coefficient (cm) and *b* is the soil cover fraction ($\approx$ LAI/3.0) (-). For increasing precipitation amounts, the amount of intercepted precipitation asymptotically reaches the saturation amount *a LAI*. In principle *a* must be determined experimentally. In case of ordinary agricultural crops we may assume *a* = 0.25.

2.6 Potential soil evaporation and plant transpiration

The potential evaporation rate of a soil under a standing crop, E_p (cm d^{-1}), is derived from the Penman-Monteith equation by neglecting the aerodynamic term. The aerodynamic term will be small because the wind velocity near the soil surface is relatively small, which makes the aerodynamic resistance r_{air} very large (*Ritchie*, 1972). Thus, the only source for soil evaporation is net radiation that reaches the soil surface. Assuming that the net radiation inside the canopy decreases according to an exponential function, and that the soil heat flux can be neglected, we can derive (*Goudriaan*, 1977; *Belmans*, 1983):

$$E_p = ET_p\, e^{-k_{\mathrm{gr}}LAI} \tag{2.5}$$

where κ_{gr} is the extinction coefficient for global solar radiation (-). *Ritchie* (1972) and *Feddes* (1978) used $\kappa_{\mathrm{gr}} = 0.39$ for common crops. More recent approaches estimate κ_{gr} as the product of the extinction coefficient for diffuse visible light, κ_{df} (-), which varies with crop type from 0.4 to 1.1, and the extinction coefficient for direct visible light, κ_{dir} (-):

$$k_{\mathrm{gr}} = k_{\mathrm{df}}\, k_{\mathrm{dir}} \tag{2.6}$$

In case the leaf area index as function of crop development stage is unknown, the soil cover, *SC* (-), might be used to determine E_p:

$$E_p = (1 - SC)\, ET_p \tag{2.7}$$

Based on energy considerations, the potential transpiration rate, T_p (cm d^{-1}), equals the potential evapotranspiration rate ET_p, corrected for the time needed to evaporate interception water, and minus E_p:

$$T_p = \left(1 - \frac{P_i}{ET_{p0}} \right) ET_p - E_p \qquad \text{with} \qquad T_p \geq 0 \tag{2.8}$$

where ET_{p0} is the potential evapotranspiration rate of the wet crop, as calculated with Eq. 2.1, assuming $r_{\mathrm{crop}} = 0$.

2.7 Actual soil evaporation

In case of a wet soil, soil evaporation is determined by the atmospheric demand and equals potential soil evaporation rate E_p. When the soil becomes more dry, the soil hydraulic conductivity decreases, which may reduce E_p to a lower actual evaporation rate, E_a (cm d^{-1}). In SWAP the maximum evaporation rate which the top soil may deliver, E_{max} (cm d^{-1}), is calculated according to Darcy's law (see also Eq. 2.12):

$$E_{max} = K_{\frac{1}{2}} \left(\frac{h_{atm} - h_1 - z_1}{z_1} \right) \qquad (2.9)$$

where $K_{\frac{1}{2}}$ is the average hydraulic conductivity (cm d^{-1}) between the soil surface and the first node, h_{atm} is the soil water pressure head (cm) in equilibrium with the air relative humidity, h_1 is the soil water pressure head (cm) of the first node, and z_1 is the soil depth (cm) at the first node. Equation 2.9 excludes water flow due to thermal differences in the top soil and due to vapour flow, as on daily basis the concerned flow amounts are probably negligable compared to isothermal, liquid water flow (*Koorevaar et al.*, 1983; *Ten Berge*, 1986; *Jury et al.*, 1991). Note that the value of E_{max} in Eq. 2.9 depends on the thickness of the top soil compartments. Increase of compartment thickness, generally results in smaller values for E_{max} due to smaller hydraulic head gradients. For accurate simulations at extreme hydrological conditions, the thickness of the top compartments should not be more than 1 cm (see Chapter 5).

There is one serious limitation of the E_{max} procedure as described above. E_{max} is governed by the soil hydraulic functions $\theta(h)$ and $K(\theta)$. Still it is not clear to which extent the soil hydraulic functions, that usually represent a top layer of a few decimeter, are valid for the top few centimeter of a soil, which are subject to splashing rain, dry crust formation, root extension and various cultivation practices. Therefore also empirical evaporation functions may be used, which require calibration of their parameters for the local climate, soil, cultivation and drainage situation. SWAP has the option to choose the empirical evaporation functions of *Black* (1969) or *Boesten and Stroosnijder* (1986). SWAP will determine E_a by taking the minimum value of E_p, E_{max} and, if selected by the user, one of the empirical functions. This procedure implicitly assumes that E_{max} in general overestimates the maximum soil water flow near the soil surface.

2.8 Actual plant transpiration

The maximum root water extraction rate, integrated over the rooting depth, is equal to the potential transpiration rate, T_p (cm d^{-1}), which is governed by atmospheric conditions as discussed before. The potential root water extraction rate at a certain depth, $S_p(z)$ (d^{-1}), may be determined by the root length density, $\pi_{root}(z)$ (cm cm^{-3}), at this depth as fraction of the total root length density (e.g. *Bouten*, 1992):

$$S_p(z) = \frac{\boldsymbol{p}_{root}(z)}{\int_{-D_{root}}^{0} \boldsymbol{p}_{root}(z) \partial z} T_p \qquad (2.10)$$

where D_{root} is the root layer thickness (cm). A disadvantage of prescribing the potential root water extraction in this way, is that water stress in one part of the root zone can not be compensated by higher root water uptake in other parts of the root zone. Such situations occur when large water content differences exist in the root zone, e.g. in case of irrigation or a shallow groundwater table. Currently alternative expressions are evaluated which take into account these compensation effects.

Stresses due to dry or wet conditions and/or high salinity concentrations may reduce $S_p(z)$. The water stress in SWAP is described by the function proposed by *Feddes et al.* (1978), which is depicted in Fig. 2.3. For salinity stress the response function of *Maas and Hoffman* (1977) is used (Fig. 2.4), as this function has been calibrated for many crops (*Maas*, 1990). It is still not clear if under the conditions where both stresses apply, the stresses are additive or multiplicative (*Dirksen*, 1993; *Shalhevet*, 1994; *Šimunek et al.*, 1998b; *Homae*, 1999). In order to simplify parameter calibration and use of existing experimental data, we assume in SWAP the water and salinity stress to be multiplicative. This means that the actual root water flux density, $S_a(z)$ (d^{-1}), is calculated from:

$$S_a(z) = \alpha_{rw}\, \alpha_{rs}\, S_p(z) \tag{2.11}$$

where α_{rw} (-) and α_{rs} (-) are the reduction factors due to water and salinity stresses, respectively. Integration of $S_a(z)$ over the rooting depth yields the actual transpiration rate T_a.
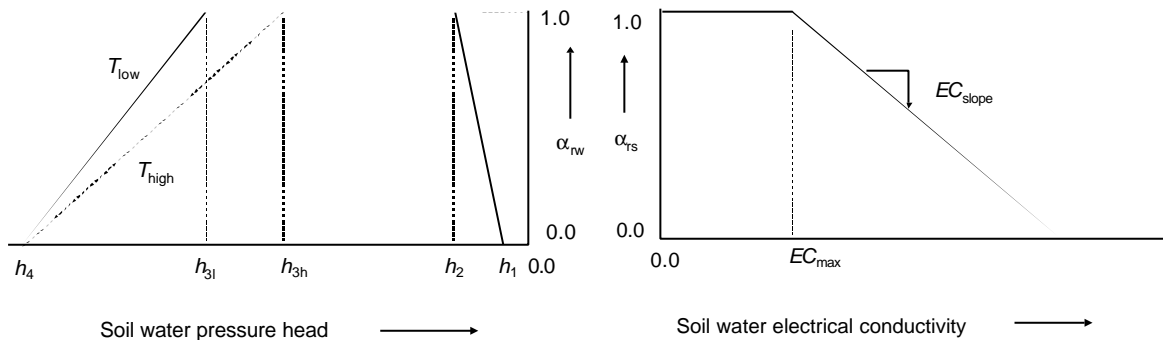
Figure 2.3 Reduction coefficient for root water uptake, α_{rw}, as function of soil water pressure head h and potential transpiration rate T_p (after *Feddes et al.*, 1978).

Figure 2.4 Reduction coefficient for root water uptake, α_{rs}, as function of soil water electrical conductivity EC (after *Maas and Hoffman*, 1977).

2.9   Soil water flow

Spatial differences of the soil water hydraulic head cause flow of soil water. Darcy's equation is used to quantify these soil water fluxes. For one-dimensional vertical flow, Darcy's equation can be written as:

$$q = -K(h)\frac{\partial (h + z)}{\partial z} \tag{2.12}$$

where q is soil water flux density (positive upward) (cm d^{-1}), K is hydraulic conductivity (cm d^{-1}), h is soil water pressure head (cm) and z is the vertical coordinate (cm) taken positively upward. Water balance considerations of an infinitely small soil volume result in the continuity equation for soil water:

$$\frac{\partial \boldsymbol{q}}{\partial t} = -\frac{\partial q}{\partial z} - S_a(z) \tag{2.13}$$

where θ is the volumetric water content (cm^3 cm^{-3}), t is the time (d) and S_a is the actual soil water extraction rate by plant roots (cm^3 cm^{-3} d^{-1}). Combination of Eq. 2.12 and 2.13 results in the well-known Richards' equation:

$$\frac{\partial \boldsymbol{q}}{\partial t} = C(h)\frac{\partial h}{\partial t} = \frac{\partial\left[K(h)\left(\dfrac{\partial h}{\partial z}+1\right)\right]}{\partial z} - S_a(z) \tag{2.14}$$

where C is the differential water capacity (dθ/dh) (cm^{-1}).

Richards' equation has a clear physical basis at a scale where the soil can be considered to be a continuum of soil, air and water. This physical basis allows the use of generally available soil physical data and the simulation of a wide range of management scenario's. SWAP solves Eq. 2.14 numerically, subject to specified initial and boundary conditions and soil hydraulic functions, which relate θ, h and K.

Although tabular forms of $\theta(h)$ and $K(\theta)$ have been used for many years, currently analytical expressions are generally applied for a number of reasons. Analytical expressions are more convenient as model input and a rapid comparison between horizons is possible by comparing parameter sets. In case of hysteresis, scanning curves can be derived by some modification of the analytical function. Also scaling, which is used to describe spatial variability of $\theta(h)$ and $K(\theta)$, requires an analytical expression of the reference curve. Another reason is that extrapolation of the functions beyond the measured data range is possible. Last but not least, analytical functions allow for calibration and estimation of the soil hydraulic functions by inverse modeling (Chapter 4).

Brooks and Corey (1964) proposed an analytical function of $\theta(h)$ which has been used for a number of years. Mualem (1976) derived a predictive model of the $K(\theta)$ relation based on their retention function. *Van Genuchten* (1980) proposed a more flexible $\theta(h)$ function than the Brooks and Corey relation and combined it with Mualem's predictive model to derive $K(\theta)$. This model has been used in numerous studies, forms the basis of several national and international data-banks (e.g. *Carsel and Parrish*, 1988; *Yates et al.*, 1992; *Wösten et al.*, 1994; *Leij et al*, 1996; *Wösten et al.*, 1998) and is implemented in SWAP. The analytical $\theta(h)$ function proposed by Van Genuchten (1980) reads:

$$\boldsymbol{q}(h) = \boldsymbol{q}_{\text{res}} + \frac{\boldsymbol{q}_{\text{sat}} - \boldsymbol{q}_{\text{res}}}{\left(1+\left|\boldsymbol{a}h\right|^{n}\right)^{\frac{n-1}{n}}} \tag{2.15}$$

where θ_{sat} is the saturated water content (cm^3 cm^{-3}), θ_{res} is the residual water content in the very dry range (cm^3 cm^{-3}), and α (cm^{-1}) and n (-) are empirical shape factors. Using the above

$\theta(h)$ relation and applying the theory on unsaturated hydraulic conductivity by *Mualem* (1976), *Van Genuchten* (1980) derived the following $K(\theta)$ function:

$$K(\boldsymbol{q}) = K_{\text{sat}} \left(\frac{\boldsymbol{q} - \boldsymbol{q}_{\text{res}}}{\boldsymbol{q}_{\text{sat}} - \boldsymbol{q}_{\text{res}}} \right)^l \left[1 - \left(1 - \left(\frac{\boldsymbol{q} - \boldsymbol{q}_{\text{res}}}{\boldsymbol{q}_{\text{sat}} - \boldsymbol{q}_{\text{res}}} \right)^{\frac{n}{n-1}} \right)^{\frac{n-1}{n}} \right]^2 \tag{2.16}$$

Van Genuchten et al. (1991) developed the program RETC to estimate the parameter values of this model from measured $\theta(h)$ and $K(\theta)$ data.

2.10   Drainage

In the saturated part of the soil column, a distinction is made between a drainage and a bottom flux (Fig. 2.5). The drainage flux refers to the groundwater flux to/from the local drainage system. The bottom flux refers to the water flux at the soil profile bottom, which in general is caused by regional groundwater flow. In many soil water flow models, the drainage flux and bottom flux are combined into the bottom flux. SWAP can be used in the same way, by omitting the drainage component. The feature of defining the local drainage flux separately, allows simulation of the interaction between surface water management and groundwater levels, the evaluation of drainage alternatives and the residence time of solutes in the saturated zone.

q_{drain} is a lateral flux in the saturated zone for *local drainage* flow

q_{bot} is a vertical flux at the bottom of the soil profile for *regional groundwater* flow
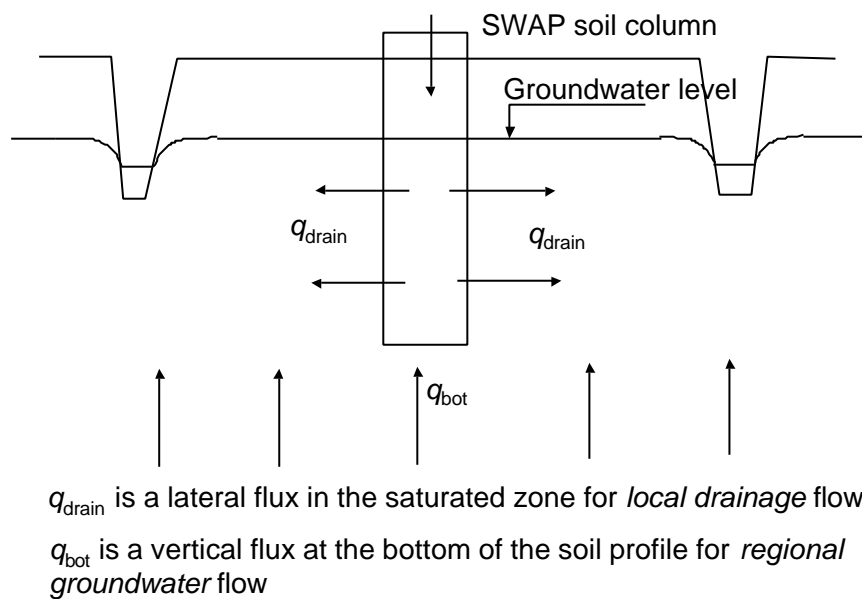
Figure 2.5 Schematization of local drainage and regional bottom flux in SWAP.

Three methods can be used to calculate the drainage flux density q_{drain} (cm d^{-1}):
1) A linear relation between groundwater level ϕ_{gwl} (cm) and q_{drain}:

$$q_{\text{drain}} = \frac{\boldsymbol{f}_{\text{gwl}} - \boldsymbol{f}_{\text{drain}}}{\boldsymbol{g}_{\text{drain}}} \tag{2.17}$$

Sub-irrigation | 0 | Drainage

$$tg = \frac{g_1 \cdot g_2 \cdot g_3}{g_1 + g_2 + g_3}$$

$\phi_{drain,3}$

$$tg = \frac{g_1 \cdot g_2}{g_1 + g_2}$$

$\phi_{drain,2}$

$tg = g_1$

Groundwater height

$\phi_{drain,1}$

$tg = g_{inf}$
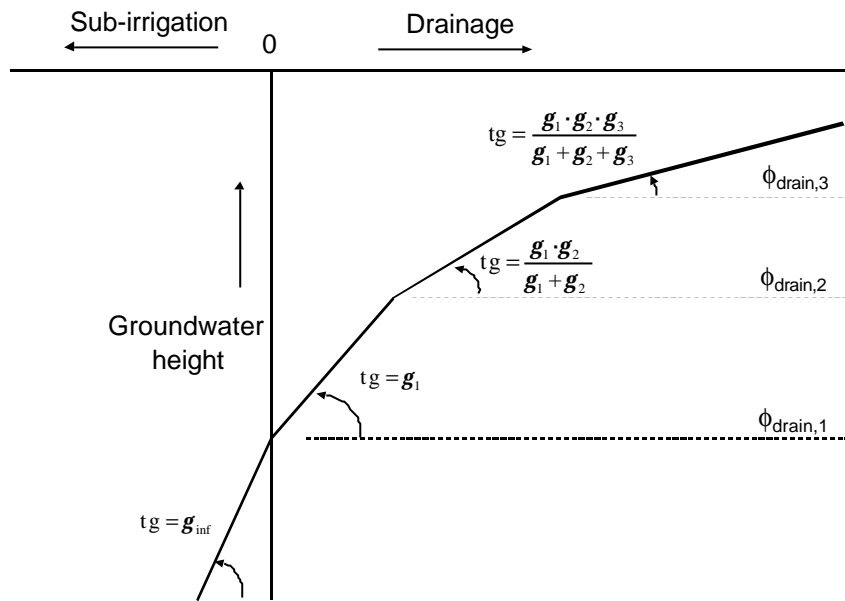
Figure 2.6 Drainage or sub-irrigation flux as function of groundwater height, drainage level ϕ, and drainage or sub-irrigation resistance γ.

where ϕ_{drain} is the drain level (cm) and γ_{drain} is the drainage resistance (d). Simultaneous drainage fluxes to various drainage levels can be calculated, which are superimposed to derive the total drainage flux (Fig. 2.6).

2) A tabular relation between groundwater level and drainage flux. This option is useful in case of drainage media at various levels, which cause a decreasing drainage resistance when the groundwater level increases. This situation gives a similar shape of the relation between groundwater level and drainage flux as depicted in Fig. 2.6, but at this option no separate drainage levels and resistances need to be distinguished.

3) Analytical drainage equations of Hooghoudt and Ernst. These equations have been extensively described by *Ritzema* (1994) and the drainage situations are depicted in Fig. 2.7.

Schematization	Soil profile	Drain position	Theory
	homogeneous	on top of impervious layer	Hooghoudt Donnan
	homogeneous	above impervious layer	Hooghoudt with equi- valent depth
K_{top} / K_{bot}	two layers	at interface of the two soil layers	Hooghoudt
K_{top} / K_{bot}	two layers $(K_{top} < K_{bot})$	in bottom layer	Ernst
K_{top} / K_{bot}	two layers $(K_{top} < K_{bot})$	in top layer	Ernst

Figure 2.7 Five field drainage conditions with analytical drainage flux equations as considered in SWAP (after *Ritzema*, 1994).

2.11 Bottom boundary condition

In the unsaturated zone water flow and solute transport occur mainly in the vertical direction. Once in the saturated zone, water starts to move in a three dimensional pattern, following the prevailing hydraulic head gradients. Therefore the bottom boundary of the one-dimensional SWAP is either the unsaturated zone or in the upper part of the saturated zone (Fig. 2.5) where the transition takes place to three-dimensional groundwater flow.

The following options are offered to prescribe the bottom boundary condition:
1) specify the groundwater level or soil water pressure head as function of time;
2) specify the bottom flux as function of time;
3) specify the bottom flux as function of groundwater level.
Measurements of groundwater levels are relatively easy and often used during model calibration with experimental data. However, when alternative scenario's have to be simulated, in most cases the groundwater levels will change, and therefore can not be prescribed anymore. Prescribed bottom fluxes are attractive, as fixed bottom fluxes may increase the accuracy of simulated soil moisture profiles and solute leaching. Unfortunately, efforts to develop reliable and practical instruments to measure soil water fluxes in situ, failed until now. Situations in which the bottom flux can be prescribed occur when a soil layer with a low permeability is present in the subsoil, or when the seepage flux is more or less constant and known. When the groundwater level is relatively deep, we may assume a zero gradient of the soil water pressure head at the bottom of the soil profile, so called *free drainage*. Application of Darcy's law gives for such a case:

$$q = -K(h)\left(\frac{\partial h}{\partial z}+1\right) = -K(h)(0+1) = -K(h) \tag{2.18}$$

In case of lysimeter experiments where *free outflow* occurs at the lysimeter bottom, SWAP will assume zero flow as long as $h \leq 0$ at the lysimeter bottom. As soon as h at the lysimeter bottom tends to become larger than zero, SWAP will fix h at zero and calculate the bottom flux.

2.12 Surface water management

At sub-regional level the interaction between soil water balance, crop growth and surface water management can be simulated (*Van Bakel*, 1986; *Massop et al.*, 1994). The surface water system can be partitioned in maximally five channel classes, each defined by its bed level, bed width, side-slope and spacing (Fig. 2.8). In each channel, except from the primary channel, the surface water has the same level, which is either input or calculated from the sub-regional water balance. Drainage to each channel order is calculated with the corresponding drainage resistances. Also sub-irrigation from the channels may be calculated when the surface water level rises above the groundwater level. To control the surface water level, a fixed or automatic weir can be selected. The SWAP user may specify surface water target levels, maximum mean groundwater levels, maximum soil water pressure heads and the minimum air volumes in the soil. During simulation SWAP will select the highest surface water level for which all specified criteria are met.
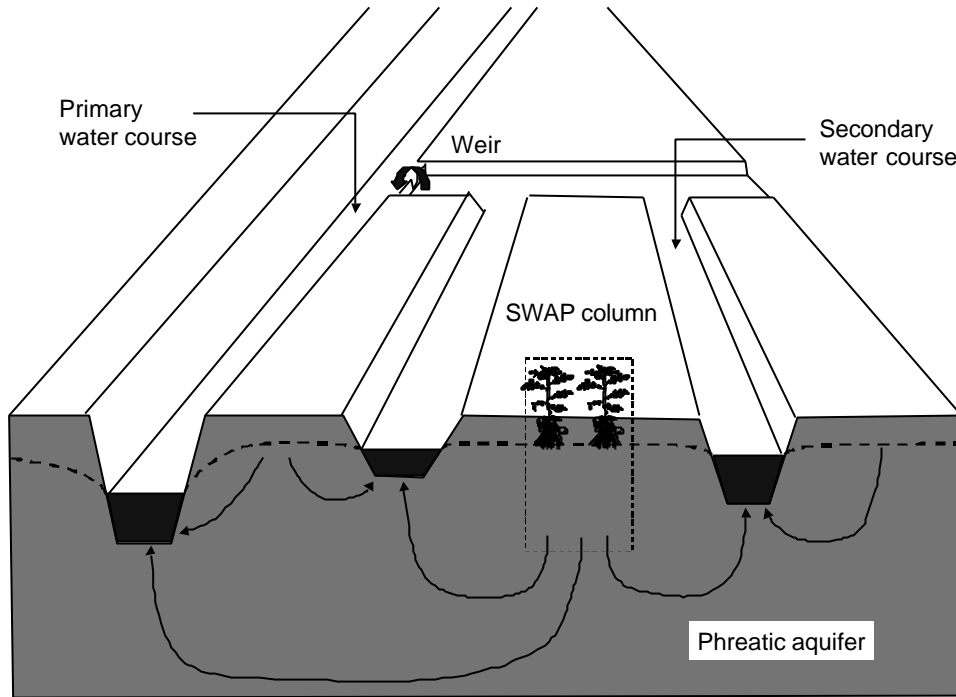
Figure 2.8 Schematization of the surface water system and interaction through groundwater with the SWAP column.

2.13   Solute transport

2.13.1   Transport processes

The three main solute transport mechanisms in soil water are diffusion, convection and dispersion. *Diffusion* is solute transport which is caused solely by a solute gradient. Thermal motion of the solute molecules within the soil solution, causes a net transport of molecules from high to low concentrations, similar to diffusive transport of gas molecules in air. The solute flux density J_{dif} (g cm^{-2} d^{-1}) is generally described by Fick's first law:

$$J_{dif} = -\boldsymbol{q} D_{dif} \frac{\partial c}{\partial z} \tag{2.19}$$

where D_{dif} is the diffusion coefficient (cm^2 d^{-1}) and c is the solute concentration in soil water (g cm^{-3}). D_{dif} is very sensitive to the actual soil water content, as it strongly affects the solute transport path and the effective cross-sectional transport area. In SWAP we employ the relation proposed by *Millington and Quirk* (1961):

$$D_{dif} = D_w \frac{\boldsymbol{q}^{7/3}}{\boldsymbol{f}_{por}^2} \tag{2.20}$$

with D_w the solute diffusion coefficient in free water (cm^2 d^{-1}) and ϕ_{por} the soil porosity (cm^3 cm^{-3}).

The bulk transport of solutes occurs when solutes are carried along with the moving soil water. The mean flux of this transport is called the *convective* flux density, J_{con} (g cm^{-2} d^{-1}), and can be calculated from the average soil water flux density q:

$$J_{con} = q\,c \tag{2.21}$$

17

When describing water flow, we usually consider only the Darcy flux q (cm d^{-1}), which is averaged over a certain cross section. In case of solute transport, we need to consider as well the water velocity variation between pores of different size and geometry and also the water velocity variation inside a pore itself. The variety of water velocities cause some solutes to advance faster than the average solute front, and other solutes slower. The overall effect will be that steep solute fronts tend to smoothen or to disperse. Solutes seem to flow from high to low concentrations, similar to diffusion. If the time required for solutes to mix in the transverse direction is small, compared to the time required for solutes to move in the flow direction by mean convection, the *dispersion* flux density J_{dis} (g cm^{-2} d^{-1}) is proportional to the solute gradient (*Bear*, 1972):

$$J_{dif} = -\boldsymbol{q} D_{dis} \frac{\partial c}{\partial z} \tag{2.22}$$

with D_{dis} (cm^2 d^{-1}) being the dispersion coefficient. Under laminar flow conditions, D_{dis} itself is proportional to the pore water velocity v ($= q/\theta$ cm d^{-1}) (*Bolt*, 1979):

$$D_{dis} = L_{dis} |v| \tag{2.23}$$

with L_{dis} the dispersion length (cm), which depends on the scale over which the water flux and solute convection are averaged. Typical values of L_{dis} are 0.5 - 2.0 cm in packed laboratory columns and 5-20 cm in the field, although they can be considerably larger in regional groundwater transport (*Jury et al.*, 1991). Unless water is flowing very slowly through repacked soil, the dispersion flux is usually much larger than the diffusion flux.

The total solute flux density J (g cm^{-2} d^{-1}) is therefore described by the sum:

$$J = J_{dif} + J_{con} + J_{dis} = q\,c - \boldsymbol{q}(D_{dif} + D_{dis})\frac{\partial c}{\partial z} \tag{2.24}$$

2.13.2 Transport equation

By considering conservation of mass in an elementary volume, we may derive the continuity equation for solute transport:

$$\frac{\partial X}{\partial t} = -\frac{\partial J}{\partial z} - S_s \tag{2.25}$$

where X is the total solute concentration in the soil system (g cm^{-3}) and S_s is the solute sink term, accounting for decomposition and uptake by roots (g cm^{-3} d^{-1}).

The solutes may be dissolved in soil water and/or may be adsorbed to organic matter or to clay minerals:

$$X = \boldsymbol{q}\,c + \boldsymbol{r}_b Q \tag{2.26}$$

with ρ_b being the dry soil bulk density (g cm^{-3}) and Q the amount adsorbed (g g^{-1}). The adsorption isotherm describes the amount of solutes adsorbed in equilibrium with the dissolved concentration c. In SWAP we assume instantaneous equilibrium between c and Q and use the non-linear Freundlich equation, which is a flexible function applicable to many organic and inorganic solutes. It turns out that the mobile-immobile concept, as applied in SWAP, also allows the transfer of solutes from the dissolved state to the adsorbed state and

vice versa at a certain rate (*Van Genuchten and Wagenet*, 1989; Chapter 6 this thesis). Freundlich adsorption can be written as:

$$Q = K_f \, c_{ref} \left(\frac{c}{c_{ref}} \right)^{N_f}$$

(2.27)

with K_f the Freundlich coefficient (cm^3 g^{-1}), N_f is the Freundlich exponent (-), and c_{ref} is a reference solute concentration (g cm^{-3}), which is used to make N_f dimensionless.

The solute sink term S_s accounts for first order transformation and proportional root uptake:

$$S_s = \boldsymbol{m}(\boldsymbol{q}c + \boldsymbol{r}_b Q) + K_r S_a c$$

(2.28)

where μ is the first order rate coefficient of transformation (d^{-1}), K_r is the root uptake preference factor (-), and S_a is the root water extraction rate (d^{-1}). The transformation rates of the dissolved and adsorbed solutes are assumed to be equal. K_r accounts for positive or negative selection of solute ions relative to the amount of solutes present in soil water extracted by the roots.

The transformation rate coefficient is affected by soil temperature, water content and depth. Analogous to *Boesten and Van der Linden* (1991), SWAP calculates μ from:

$$\boldsymbol{m} = f_T f_{\boldsymbol{q}} f_z \, \boldsymbol{m}_{ref}$$

(2.29)

in which f_T is a soil temperature factor (-), f_θ and f_z are reduction factors (-) accounting for the effect of soil water content and soil depth, and μ_{ref} (d^{-1}) is μ at reference conditions (e.g. soil from the plough layer at 20 °C and at soil water pressure head $h = -100$ cm).

Combination of Eqs. 2.24, 2.25, 2.26 and 2.28 yields the transport equation applied in SWAP which is valid for dynamic, one-dimensional, convective-dispersive mass transport, including non-linear adsorption, linear decay and proportional root uptake in unsaturated/saturated soil (*Van Genuchten and Cleary*, 1979; *Nielsen et al.*, 1986; *Boesten and Van der Linden*, 1991):

$$\frac{\partial(\boldsymbol{q}c + \boldsymbol{r}_b Q)}{\partial t} = -\frac{\partial qc}{\partial z} + \frac{\partial\left(\boldsymbol{q}\left(D_{dif} + D_{dis}\right)\dfrac{\partial c}{\partial z}\right)}{\partial z} - \boldsymbol{m}(\boldsymbol{q}c + \boldsymbol{r}_b Q) - K_r Sc$$

(2.30)

An explicit, central finite difference scheme is used to solve Eq. 2.30 (*Van Dam et al.*, 1997):

$$\frac{\boldsymbol{q}_i^{j+1}c_i^{j+1} + \boldsymbol{r}_b Q_i^{j+1} - \boldsymbol{q}_i^j c_i^j - \boldsymbol{r}_b Q_i^j}{\Delta t^j} =$$

$$\frac{q_{i-\frac{1}{2}}^j c_{i-\frac{1}{2}}^j - q_{i+\frac{1}{2}}^j c_{i+\frac{1}{2}}^j}{\Delta z_i} + \frac{1}{\Delta z_i}\left[\frac{q_{i-\frac{1}{2}}^j D_{i-\frac{1}{2}}^j \left(c_{i-1}^j - c_i^j\right)}{\Delta z_u} - \frac{q_{i+\frac{1}{2}}^j D_{i+\frac{1}{2}}^j \left(c_i^j - c_{i+1}^j\right)}{\Delta z_\ell} \right] -$$

$$\boldsymbol{m}_i^j \left(q_i^j c_i^j + \boldsymbol{r}_b Q_i^j\right) - K_r S_i^j c_i^j$$

(2.31)

where $D\ (= D_{dif} + D_{dis})$ is the overall dispersion coefficient (cm^2 d^{-1}); the superscript j denotes the time level, subscript i the node number and subscripts $i-\frac{1}{2}$ and $i+\frac{1}{2}$ refer to linearly interpolated values at the upper and lower compartment boundary, respectively. All the nodes, including the top and bottom node, are in the center of the soil compartments, with $\Delta z_u = z_{i-1} - z_i$, $\Delta z_\ell = z_i - z_{i+1}$, and Δz_i the compartment thickness (cm) (see Fig. 5.1). Compared to

an implicit, iterative scheme, above explicit scheme has the advantage that incorporation of non-linear adsorption, mobile/immobile concepts, and other non-linear processes is relatively easy. In order to ensure stability of the explicit scheme, the time step $\Delta t^{\,j}$ should meet the criterium (*Van Genuchten and Wierenga*, 1974):

$$\Delta t^{\,j} \leq \frac{\Delta z_i^2 \boldsymbol{q}_i^{\,j}}{2D_i^{\,j}}$$

(2.32)

2.13.3 Saturated zone

In the saturated zone, prevailing hydraulic head gradients will induce a three-dimensional water flow and solute transport pattern. A strict deterministic approach would require coupling of an one-dimensional agrohydrological model with a two- or three-dimensional model for the saturated zone. In many situations this is not feasible due to limitations of data, time, computer resources or experience. Also the required accuracy of the analysis might not justify such a detailed approach. For those situations with SWAP a simplified approach can be followed to calculate the transport of solutes to drains or ditches. *Ernst* (1973) and *Van Ommen* (1985) showed that the breakthrough curve of a field with fully penetrating drainage canals, is identical to the breakthrough curve of a reservoir with complete mixing (Fig. 2.9). This is also valid if linear adsorption and first order transformation take place (*Van Ommen*, 1985). Linear adsorption might be described by:

$$Q = k_{\text{ads}} c_{\text{gr}}$$

(2.33)

where k_{ads} is the linear adsorption coefficient in the saturated zone (cm^3 g^{-1}) and c_{gr} is the average solute concentration in the groundwater (g cm^{-3}). Numerical analysis by *Duffy and Lee* (1992) showed that dispersion in the saturated zone has only a minor effect for $L_{\text{drain}}/d_{\text{aquif}}$ ≥ 10, where L_{drain} is the distance between the drainage canals (cm) and d_{aquif} the thickness of the aquifer (cm). Generally $L_{\text{drain}}/d_{\text{aquif}}$ will be larger than 10, therefore dispersion can be ignored.

In order to derive the breakthrough curve, we will use the similarity between breakthrough curves of drained fields and mixed reservoirs (Fig. 2.9). Starting point is the solute transport equation of the unsaturated zone, Eq. 2.30. Replacement of non-linear adsorption by linear adsorption, and omittance of dispersion and root water uptake, results in the mass balance equation of the saturated zone:

$$\frac{\partial \left(\boldsymbol{q}_{\text{sat}} c_{\text{gr}} + \boldsymbol{r}_{\text{b}} k_{\text{ads}} c_{\text{gr}} \right)}{\partial t} = \frac{q_{\text{drain}} \left(c_{\text{in}} - c_{\text{gr}} \right)}{d_{\text{aquif}}} - \boldsymbol{m}_{\text{gr}} \left(\boldsymbol{q}_{\text{sat}} c_{\text{gr}} + \boldsymbol{r}_{\text{b}} k_{\text{ads}} c_{\text{gr}} \right)$$

(2.34)

where θ_{sat} is the saturated water content (cm^3 cm^{-3}), q_{drain} is the drainage flux density (cm d^{-1}), c_{in} is the solute concentration of water percolating from the unsaturated zone (g cm^{-3}) and μ_{gr} is the first order rate coefficient for transformation in the saturated zone (d^{-1}). Eq. 2.34 applies to a drainage situation ($q_{\text{drain}} > 0$). In case of sub-irrigation ($q_{\text{drain}} < 0$), SWAP assumes the solute concentration of the infiltrating water from the drainage system to be negligable, which transforms Eq. 2.34 to:

$$\frac{\partial \left(\boldsymbol{q}_{\text{sat}} c_{\text{gr}} + \boldsymbol{r}_{\text{b}} k_{\text{ads}} c_{\text{gr}} \right)}{\partial t} = \frac{q_{\text{drain}} c_{\text{gr}}}{d_{\text{aquif}}} - \boldsymbol{m}_{\text{gr}} \left(\boldsymbol{q}_{\text{sat}} c_{\text{gr}} + \boldsymbol{r}_{\text{b}} k_{\text{ads}} c_{\text{gr}} \right)$$

(2.35)
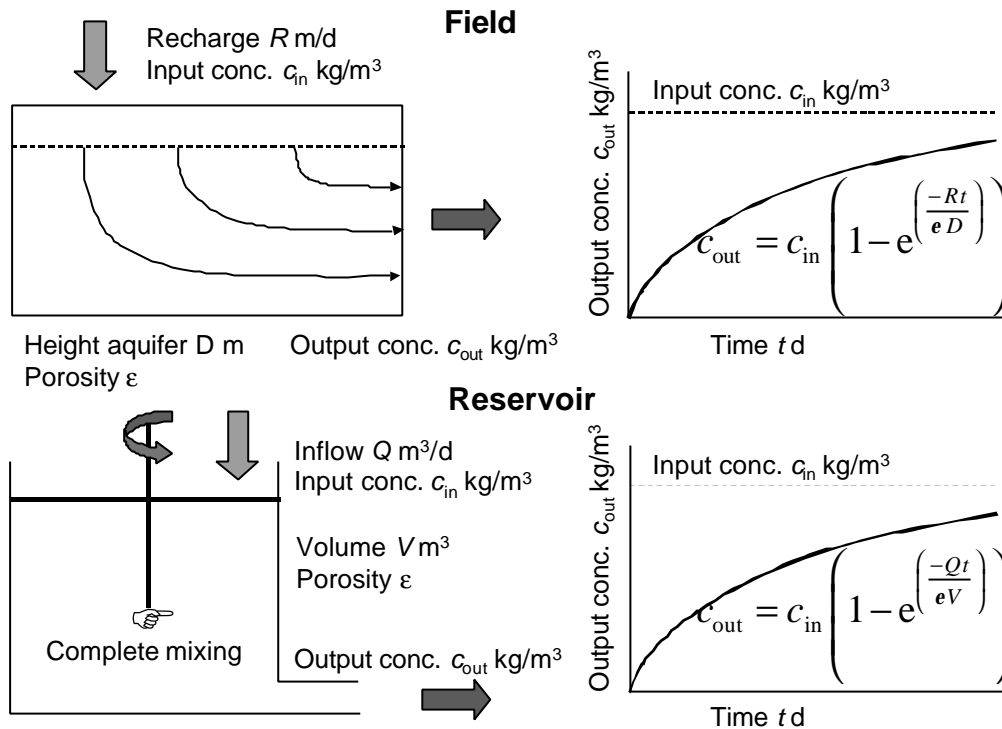
Figure 2.9 Similarity of solute breakthrough curves at fields with fully penetrating drains and reservoirs with complete mixing.

The mixed reservoir approach applies to an homogeneous aquifer and field drainage at one level. In case of heterogeneous groundwater flow or multi-level drainage, SWAP distributes the drainage fluxes in the saturated zone according to the relative transmissivities (*Rijtema et al.*, 1999) and solves the convection-dispersion equation (Eq. 2.30) with an extra sink/source term for lateral drainage/sub-irrigation in the saturated part of the soil column.

2.13.4 Advanced solute transport

The solute transport processes incorporated in SWAP permit the simulation of ordinary pesticide and salt transport, including the effect of salinity on crop growth. In case of advanced pesticide transport, including volatilization and kinetic adsorption, SWAP can be used in combination with the model PESTLA (*Van den Berg and Boesten*, 1998) and PEARL (*Leistra et al.*, 2000; *Tiktak et al.*, 2000). For nutrient transport (nitrogen and phosphorus), SWAP can be used in combination with the model ANIMO (*Rijtema et al.*, 1997; *Kroes and Roelsma*, 1998).

Solute transport processes for which currently no SWAP options exist, are :
- Transport of non-mixing or immiscible fluids (e.g. oil and water)
- Chemical equilibria of various solutes (e.g. between Na^+, Ca^{2+} and Mg^{2+})
- Chemical and biological chain reactions (e.g. mineralization)

2.14   Heat flow

2.14.1   General

Soil temperature affects many physical, chemical and biological processes in the top soil, for instance the surface energy balance, soil hydraulic properties, decomposition rate of solutes and growth rate of roots. Currently SWAP uses the soil temperatures only to adjust the solute decomposition rate, but other temperature relations may readily be included.

Commonly, heat flow by radiation, convection and conduction is modeled by incorporating these three processes into a conduction type equation. According to *De Vries* (1975), the rate of heat transfer by water vapour diffusion is small and proportional to the temperature gradient. Therefore, such diffusion might be taken into account by slightly increasing the soil thermal diffusivity. This approach is followed in SWAP as well. Apparent thermal properties rather than real thermal properties are assumed to account for both conductive and non-conductive heat flow.

The one-dimensional soil heat flux density, q_{heat} (J cm^{-2} d^{-1}), is described as:

$$q_{heat} = -\lambda_{heat} \frac{\partial T}{\partial z}$$

(2.36)

where λ_{heat} is the thermal conductivity (J cm^{-1} K^{-1} d^{-1}) and T is the soil temperature (K).

Conservation of energy results in:

$$C_{heat} \frac{\partial T}{\partial t} = -\frac{\partial q_{heat}}{\partial z}$$

(2.37)

where C_{heat} is the soil heat capacity (J cm^{-3} K^{-1}).

Combination of Eq. 2.36 and 2.37 yields the differential equation for soil heat flow:

$$C_{heat} \frac{\partial T}{\partial t} = \frac{\partial \left(\lambda_{heat} \frac{\partial T}{\partial t} \right)}{\partial z}$$

(2.38)

In SWAP an analytical or numerical solution of Eq. 2.38 can be selected.

2.14.2   Analytical solution

If the values of λ and C_h are considered to be constant with depth and in time, the soil thermal diffusivity D_{heat} (cm^2 d^{-1}) can be defined as:

$$D_{heat} = \frac{\lambda_{heat}}{C_{heat}}$$

(2.39)

and Eq. 2.38 simplifies to:

$$\frac{\partial T}{\partial t} = D_{heat} \frac{\partial^2 T}{\partial z^2}$$

(2.40)

This partial differential equation can be solved for simple boundary conditions, assuming D_{heat} constant or very simple functions for D_{heat} (*Van Wijk*, 1966; *Feddes*, 1971; *Jury et al.*,

1991). A commonly used top boundary condition is a sinusoidally varying soil surface temperature during the year:

$$T(0,t) = T_{\text{mean}} + T_{\text{ampl}} \sin\left(\tfrac{1}{2}\boldsymbol{p} + \boldsymbol{w}(t - t_{\text{max}})\right) \tag{2.41}$$

where T_{mean} is the mean yearly temperature (K), T_{ampl} is the wave amplitude (K), $\omega = 2\pi / \tau$ is the angular frequency, where τ is the period of the wave (365 d), t is the time (d) starting January 1st and t_{max} equals t when the temperature reaches its maximum. In case of a semi-infinite soil profile with constant D_{heat} and subject to the top boundary condition according to Eq. 2.41, the solution to Eq. 2.40 is:

$$T(z,t) = T_{\text{mean}} + T_{\text{ampl}}\, e^{\frac{z}{d_{\text{temp}}}} \sin\left(\tfrac{1}{2}\boldsymbol{p} + \boldsymbol{w}(t - t_{\text{max}}) + \frac{z}{d_{\text{temp}}} \right) \tag{2.42}$$

where d_{temp} is the damping depth (cm), which equals:

$$d_{\text{temp}} = \sqrt{\frac{2 D_{\text{heat}}}{\boldsymbol{w}}} \tag{2.43}$$

2.14.3 Numerical solution

In reality, C_{heat} and λ_{heat} depend on the soil moisture content and vary with time and depth. Also the soil surface temperature will deviate from a sinus wave. Therefore, higher accuracy can be reached by numerical solution of the heat flow equation (*Wesseling*, 1985). In SWAP a fully implicit finite difference scheme is employed (*Van Dam et al.*, 1997), in which Eq. 2.38 is written as:

$$C_i^{j+1}\left(T_i^{j+1} - T_i^j\right) = \frac{\Delta t^j}{\Delta z_i}\left[\boldsymbol{l}_{i-\frac{1}{2}}^{i+\frac{1}{2}} \frac{T_{i-1}^{j+1} - T_i^{j+1}}{\Delta z_u} - \boldsymbol{l}_{i+\frac{1}{2}}^{i+\frac{1}{2}} \frac{T_i^{j+1} - T_{i+1}^{j+1}}{\Delta z_\ell} \right] \tag{2.44}$$

where superscript j denotes the time level, subscript i is the node number, $\Delta z_u = z_{i+1} - z_i$ and $\Delta z_\ell = z_i - z_{i+1}$ (Fig. 5.1).

Both C_{heat} and λ_{heat} depend on the soil's composition. The volumetric heat capacity C_{heat} is calculated as weighted mean of the heat capacities of the individual components (*De Vries*, 1963):

$$C_{\text{heat}} = f_{\text{sand}} C_{\text{sand}} + f_{\text{clay}} C_{\text{clay}} + f_{\text{organic}} C_{\text{organic}} + \boldsymbol{q} C_{\text{water}} + f_{\text{air}} C_{\text{air}} \tag{2.45}$$

where f and C on the right hand side are respectively the volume fraction (cm^3 cm^{-3}) and volumetric heat capacity (J cm^{-3} K^{-1}) of each component.

In field conditions the variation of λ_{heat} is much greater than of C_{heat}. From wet to dry, C_{heat} may undergo a threefold or fourfold change, whereas the corresponding change in λ_{heat} may be hundredfold or more. Another complicating factor is that, unlike heat capacity, thermal conductivity is sensitive not merely to the volume composition of a soil but also to the sizes, shapes, and spatial arrangements of the soil particles (*Hillel*, 1980). SWAP employs the method of *De Vries* (1975) as applied by *Ten Berge* (1986) to calculate the thermal conductivity. A clear description of this method is given in *Ashby et al.* (1996).

At the soil surface the daily average air temperature T_{avg} is used as boundary condition. At the bottom of the soil profile SWAP assumes $q_{heat} = 0.0$. Application of Eq. 2.44 to each node and including the boundary conditions at the top and bottom of the soil profile, results in a tri-diagonal system of equations (*Van Dam et al.*, 1997). The coefficients C_{heat} and λ_{heat} are hardly affected by the temperature, which makes the system of equations linear and allows a direct solution without iteration. SWAP solves the equations with the *LU*-decomposition method for tridiagonal systems (*Press et al.*, 1989).

2.15   Similar media scaling

In many applied hydrological problems we deal with spatial variability of soil, vegetation and lower boundary condition. Spatial variability effects on the water and solute balance might be analysed by running the model at various locations. An alternative approach is to differentiate between sub-areas with different sequences of soil horizons, and find an equivalent uniform porous medium for either each horizon or the total soil profile (*Feddes et al.*, 1993a). Depending on the chosen scale of the fields, with the equivalent porous medium a certain amount of the natural heterogeneity will be lost (*Wösten*, 1990).

As the flow and transport processes in the unsaturated zone are strongly non-linear, in general the mean input of soil hydraulic functions will deviate from the areal mean water and solute balance. Therefore non-linear scaling techniques need to be used to derive 'effective' soil hydraulic properties, which can be used to simulate the area-average water balance. For example, in case of the Hupsel catchment (650 ha), the average water regime could closely be simulated with 'effective' soil hydraulic functions (*Hopmans and Stricker*, 1989; *Feddes et al.*, 1993a). As shown by *Kim* (1995), in semi-humid climates effective soil hydraulic functions may give a good approximation of the area-average water balance. However in arid climates, runoff and fast percolation complicate the use of 'effective' soil hydraulic functions (*Kim*, 1995).

Another way to quantify the effect of spatial heterogeneity is to determine first the stochastic distribution of the soil hydraulic functions in an area and next to perform a large number of SWAP simulations with input data derived from this stochastic distribution. These so-called Monte Carlo simulations will result in a stochastic distribution of water and solute balance components (*Hopmans and Stricker*, 1989). Alternatively, the stochastic distribution of soil hydraulic properties may be dealt with by writing Richards' equation (Eq. 2.14) in a perturbated form (e.g. *Mishra et al.*, 1990). *Miller and Miller* (1956) proposed the similar media scaling method to investigate the effect of field spatial heterogeneity of soil hydraulic properties, which method is used in SWAP.

Assuming geometrically similar media, *Miller and Miller* (1956) showed that the variability in both the $\theta(h)$ and $K(\theta)$ relationships can be described by just one dimensionless scale factor ρ (Fig. 2.10). The scale factor ρ_i at a certain location i is equal to:
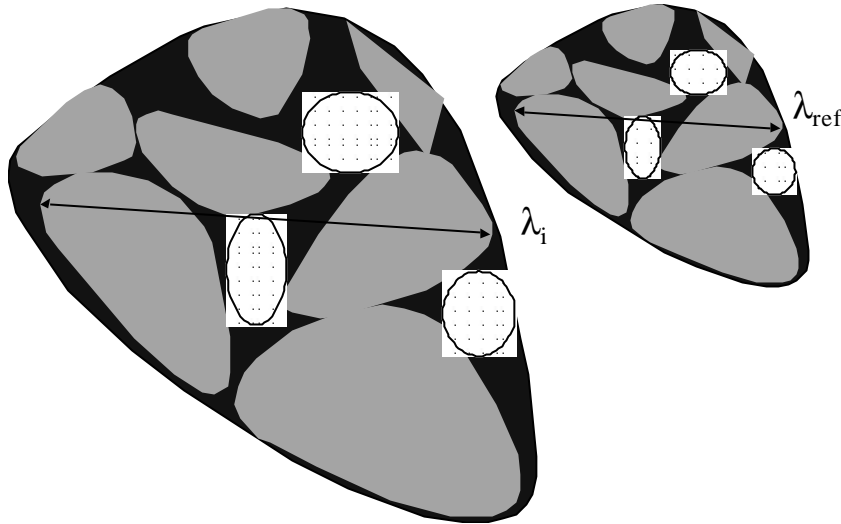
Figure 2.10 Characteristic lengths λ in geometrically similar media.

$$r_i = \frac{l_i}{l_{ref}} \tag{2.46}$$

where λ_i is the characteristic length at location i and λ_{ref} is the characteristic length of a reference soil. Then, applying the theory of capillary retention, the pressure head h_i at a given water content is related to the corresponding pressure head h_{ref} according to:

$$h_i = \frac{h_{ref}}{r_i} \tag{2.47}$$

Using Poiseuille's law, the hydraulic conductivity K_i at any location i at a given water content can be related to the corresponding hydraulic conductivity K_{ref} as:

$$K_i = r_i^2 K_{ref} \tag{2.48}$$

Natural soils will to some degree deviate from geometrically similar media. This is clear when we consider the saturated water content. If the similar media concept would apply strictly, the saturated water content should be the same for all soils. We know this is not the case. *Jury et al.* (1987) point out that due to dissimilarity, scaling of different soil properties, e.g. *h* and *K*, might result in different statistical properties of each scale factor's distribution. *Youngs and Price* (1981) measured microscopic characteristic lengths for porous materials ranging from glass beads and washed sands to sieved arable soils. They concluded that even for dissimilar soils the scaling concept is a good approximation.

In order to derive scale factors ρ_i and their statistical distribution, one should have $\theta(h)$ and $K(\theta)$ data of a series of soil samples. *Clausnitzer et al.* (1992) developed an efficient program for scaling $\theta(h)$ and $K(\theta)$ data of a series of soil samples. In their scaling approach, first a mean curve is fit to all the data available. Because natural soils don't have identical porosities, *h* and *K* are written as functions of the relative saturation θ/θ_{sat} rather than as functions of the volumetric water content θ. In the second step, the corresponding set of scale factors is calculated for each soil sample. The scaled hydraulic data ($h_i \rho_i$ and K_i / ρ_i^2, respectively) coalesce and allow an improved calculation of the mean curve. Therefore in the

next step a new mean curve is fitted through the scaled hydraulic data, after which the scale factors are determined again. These steps are repeated until both the mean curve and the scale factors converge. Finally the stochastic distribution of the scale factors (generally log-normal), its mean and standard deviation are calculated. The program of *Clausnitzer et al.* (1992) allows for separate as well as simultaneous scaling of $\theta(h)$ and $K(\theta)$.

In order to apply the scaling method with SWAP, the user should give as input the Mualem - Van Genuchten parameters that describe the reference curve, and a set of scale factors. For each scale factor, SWAP will generate the soil hydraulic functions and calculate the water and solute balance for the specified boundary conditions.

2.16   SWAP interface

SWAP can be used with or without graphical user interface. Researchers and more experienced SWAP users might prefer to work without the graphical user interface, as in- and output files are accessible faster and ASCII output data can be imported in personal graphical packages. Also changes to the program code which affect model input or output, require less effort without the graphical user interface. Use of SWAP with the plain ASCII in- and output files is documented by *Kroes et al.*, (1999).

The graphical user interface (*Huygen et al.*, 2000), written in Delphi, facilitates data input and analysis of simulation results. For instance at the input side, the format of weather data can be changed easily, soil hydraulic functions can be generated from soil texture, time dependent input data can be viewed to check consistency, and depending on earlier selected options, not relevant input data are hided. At the output side, soil profile data on water content, solute concentration and temperatures can be compared graphically between dates or scenario's, water and solute balances can be viewed graphically and the correlation between a large number of water, solute, heat and plant growth variables can be examined.

3. Inverse method to determine soil hydraulic functions

from laboratory outflow experiments[2]

3.1 Introduction

Unsaturated flow through rigid soils and other porous media is generally described by Richards' equation (Eq. 2.14). The solution of this equation requires knowledge of the soil hydraulic functions, $\theta(h)$ and $K(h)$, in which θ is the volumetric water content, h is the soil water pressure head and K is the unsaturated hydraulic conductivity. Currently there exist many laboratory and field methods to determine the highly non-linear relations between these quantities (Table 3.1 and 3.2). However, most methods require restrictive initial and boundary conditions and apply to a limited range, which makes determination of the soil hydraulic functions time consuming and expensive.

Table 3.1 Laboratory measurement methods of the retention function $\theta(h)$.

Method	Range (cm)	Reference
Sandbox apparatus	$-200 < h < 0$	*Klute* (1986)
Pressure cell	$-1000 < h < 0$	*Kool et al.* (1985a)
Pressure plate	$-20.000 < h < -1000$	*Klute* (1986)
Vapour equilibration	$h < -100000$	*Koorevaar et al.* (1983)

Table 3.2 Laboratory measurement methods of the unsaturated hydraulic conductivity function $K(h)$.

Method	Range (cm)	Reference
Suction cell	$-100 < h < 0$	*Klute and Dirksen* (1986)
Crust method	$-100 < h < 0$	*Bouma et al.* (1983)
Drip infiltrometer	$-100 < h < 0$	*Dirksen* (1991)
Evaporation method	$-800 < h < 0$	*Wendroth et al.* (1993)
Pressure cell	$-1000 < h < 0$	*Van Dam et al.* (1994)
Sorptivity method	$-1000 < h < 0$	*Dirksen* (1979)
Hot air method	$-10000 < h < -100$	*Van Grinsven et al.* (1985)
Centrifuge method	$-1000 < h < 0$	*Nimmo et al.* (1987)
Spray method	$-250 < h < 0$	*Dirksen and Matula* (1994)

An already long existing laboratory test is the One-step outflow (OSO) method. Different analytical methods have been developed to determine the soil water diffusivity function directly from these experiments (*Gardner*, 1956,1962; *Doering*, 1965; *Gupta et al.*, 1974; *Passioura*, 1976; *Valiantzas et al.*, 1988). To solve the non-linear flow equation analytically, simplifying assumptions had to be made, like a constant soil water diffusivity throughout the soil core at any time (*Gardner*, 1962) or a constant gradient $\partial\theta / \partial t$ (*Passioura*, 1976). In order to increase

---

the accuracy and efficiency *Kool et al.* (1985a) introduced the inverse method for OSO experiments. The inverse method employes a numerical model, which requires no simplifying assumptions for the analysis, while available information of the soil hydraulic functions can be incorporated in the optimization process. Under certain conditions, the retention and hydraulic conductivity function could be estimated simultaneously over a pressure head range from zero to -1000 cm. However, although coupling of the OSO with the inverse method was well received, many laboratories applying this method experienced problems with uniqueness of the parameter estimates (*Van Dam et al.*, 1990b).

Further evaluation of OSO in combination with inverse modeling, raised several points of consideration. Outflow experiments starting from saturation show non-uniform flow. This was clearly demonstrated by *Hopmans et al.* (1992), who during OSO experiments with initially saturated soil samples applied X-ray tomography. Preferential flow violates the uniform Darcian flow concept, which is the basis of Richards' equation in the numerical model. Furthermore, OSO experiments do not reflect realistic field situations. At the early stage of the experiment large pressure gradients and high fluxes might occur, resulting in rapid drying of wet soil. Under field conditions, large pressure gradients and high fluxes only occur during rapid wetting of a dry soil, just the opposite process. A flow experiment which deviates so much from field flow conditions, might result in non-representative parameter values. *Van Dam et al.* (1992) applied the OSO procedure to four soils (loess, sand, silt loam and loam) and compared the estimated hydraulic conductivity functions with results of other measurement techniques applied to the same soils. They showed that severe non-uniqueness problems occurred if only outflow observations were used in the optimization process. Reliable estimates of the unsaturated hydraulic conductivity function could only be achieved if the objective function contained soil water retention data in addition to outflow data. *Toorman et al.* (1992) analyzed the response surface of the objective function, which included various combinations of soil water pressure head, water content and outflow data. They concluded that additional measurements of the soil water pressure head in the soil sample improved the parameter estimation technique. These considerations stimulated investigation of the Multi-step outflow (MSO) method, which uses smaller air pressure increments to induce drainage of the soil core.

In this chapter the OSO and MSO approaches for estimating the soil hydraulic functions through inverse modeling are compared. Special attention will be paid to the uniqueness of the solutions, the number of parameters that can be estimated and the averaging of an ensemble of soil hydraulic functions.

3.2   Laboratory outflow method

An undisturbed soil sample is placed in a Tempe pressure cell on top of a ceramic plate and gradually saturated from below (Fig. 3.1). The outflow experiment is started by increasing the air pressure at the top of the sample. This induces downward unsaturated flow in the soil sample, with the ceramic plate remaining saturated. The applied air pressure and the cumulative outflow of water are recorded at discrete times.
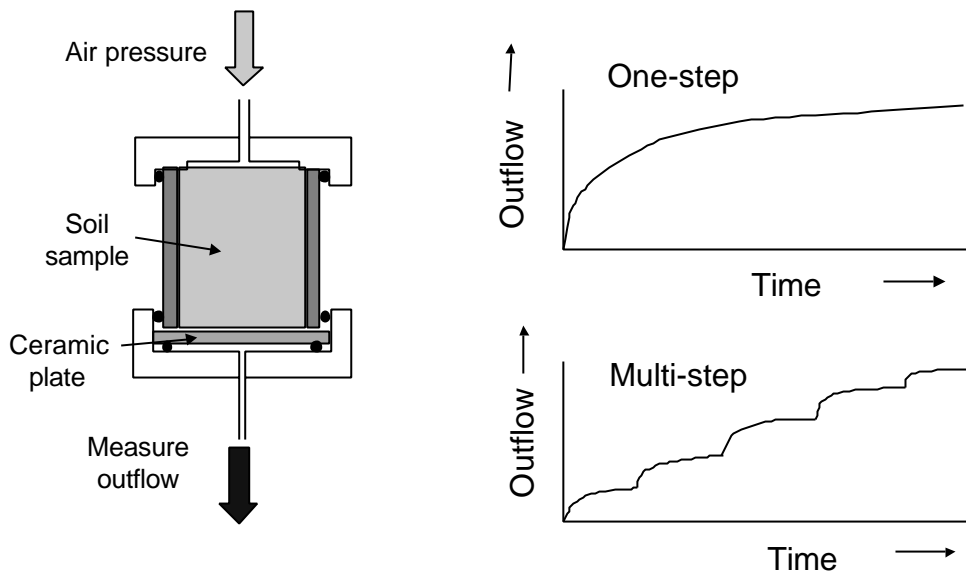
Figure 3.1 Cross section of the Tempe pressure cell and cumulative outflow versus time for One-step and Multi-step outflow experiments.

In the OSO procedure a single, large air pressure increment is used to drain a saturated soil sample at once, while in the MSO procedure several smaller pressure increments are applied. At MSO, the first applied pressure after saturation should be larger than the soil air entry value, in order to create unsaturated conditions throughout the soil sample, which reduces the risk of non-uniform flow during the outflow experiment (*Hopmans et al.*, 1992). This pressure is maintained until equilibrium is reached and serves as initial condition of the actual outflow experiment. The water content after the first step might be added to the objective function in order to achieve a good fit of the retention function in the very wet range. Simulations with prior estimates of the soil hydraulic functions are useful to determine the size of the pressure steps which result in equal outflow increments. The time interval between subsequent pressures steps in MSO is flexible, as the numerical analysis is able to handle a dynamic process. Most likely, the optimization results will be better if the soil water is closer to steady state before the next pressure step is applied. Except for fine textured soils, time intervals of one day appear to be sufficient. We did compare time steps of one hour and one day in case of medium textured, 5.1 cm high soil samples. Hourly intervals were insufficient, whereas the results for daily intervals were good (*Van Dam et al.*, 1990b).

The numerical model solves Richards' equation for unsaturated flow in a rigid porous medium (Eq. 2.14) with the following initial and boundary conditions for the outflow experiments (Fig. 3.1):

$$h = h(0, z) \qquad t = 0 \qquad 0 \le z \le L$$

$$\frac{\partial h}{\partial z} = -1 \qquad t > 0 \qquad z = L \qquad\qquad (3.1)$$

$$h = h(t,0) - h_{\text{air}}(t) \quad t > 0 \qquad z = 0$$

In Eq. 3.1, $h(0,z)$ represents the initial ($t = 0$) pressure head distribution (cm), L is the total height (cm) of the soil sample and the ceramic plate, $h_{\text{air}}(t)$ is the applied air pressure (cm water column) and $z = 0$ corresponds to the ceramic plate bottom. The soil hydraulic functions $\theta(h)$ and $K(\theta)$ are described by analytical functions of Van Genuchten and Mualem (Eqs. 2.15 and 2.16). The six parameters in these analytical functions will be referred to as MG parameters.

Applying boundary conditions according to Eq. 3.1, the cumulative outflow $Q_{\text{cal}}(t_i,\boldsymbol{b})$ is calculated at prescribed times t_i and as function of the vector with fitting MG parameters, $\boldsymbol{b}$, which are the only unknowns. The objective function $\Phi(\boldsymbol{b})$ quantifies the difference between $Q_{\text{cal}}(t_i,\boldsymbol{b})$ and observed cumulative outflow $Q_{\text{obs}}(t_i)$ and between predicted and measured soil water retention data ($\theta_{\text{cal}}(h_i,\boldsymbol{b})$ and $\theta_{\text{obs}}(h_i)$, respectively). A commonly used expression for $\Phi(\boldsymbol{b})$ is weighted least squares, as defined by:

$$\Phi(\boldsymbol{b}) = \sum_{i=1}^{N_1} \left\{ w_i \left[Q_{\text{obs}}(t_i) - Q_{\text{cal}}(t_i,\boldsymbol{b}) \right] \right\}^2$$
$$+ \sum_{i=1}^{N_2} \left\{ W_1 v_i \left[\boldsymbol{q}_{\text{obs}}(h_i) - \boldsymbol{q}_{\text{cal}}(h_i,\boldsymbol{b}) \right] \right\}^2 \qquad (3.2)$$

where w_i and v_i are weighting factors to account for differences in measurement accuracy, N_1 and N_2 are the number of observations of $Q_{\text{obs}}(t_i)$ and $\theta_{\text{obs}}(h_i)$, respectively, and W_1 is a normalization factor for measurement units and order of magnitude:

$$W_1 = \frac{\displaystyle\sum_{i=1}^{N_1} \frac{Q_{\text{obs}}(t_i)}{N_1}}{\displaystyle\sum_{i=1}^{N_2} \frac{\boldsymbol{q}_{\text{obs}}(h_i)}{N_2}} \qquad (3.3)$$

In this study $\Phi(\boldsymbol{b})$ contained outflow data only and the outflow measurements were assumed to have equal accuracy, which results in the ordinary least squares criterium :

$$\Phi(\boldsymbol{b}) = \sum_{i=1}^{N_1} \left[Q_{\text{obs}}(t_i) - Q_{\text{cal}}(t_i,\boldsymbol{b}) \right]^2 \qquad (3.4)$$

The used numerical model MULTISTEP is derived from the program ONESTEP (*Kool et al.*, 1985b; *Van Dam et al.*, 1992). The main modifications made to ONESTEP were a variable exponent λ in Mualem's expression of $K(h)$, a time dependent bottom boundary condition and an option to fix the retention function while fitting all parameters of Mualem's hydraulic conductivity function.

The optimization method is based on the Levenberg-Marquardt technique (*Kool and Parker*, 1988). This algorithm computes derivatives of $\Phi(\boldsymbol{b})$ with respect to each optimized parameter and initially descends along the steepest gradient, which makes the algorithm sensitive to

local minima. Therefore different sets of initial estimates were used to verify the location of the global minimum.

3.3   Experiments

Twenty soil sample cores with a volume of 100 cm^3 (5.0 cm diameter and 5.1 cm high) were collected from a loam soil (Typic Fluvaquent) at approximately 60 cm soil depth near Colijnsplaat in The Netherlands. To minimize soil disturbance, the samples were taken manually using a sample ring holder. In the laboratory, the samples were placed in pressure cells on top of 5.7-mm thick, high flow ceramic plates ($K_{sat} \approx 0.010$ cm h^{-1}). The rubber rings, which are used to prevent air and water leakage (Fig. 3.1), were not greased. Earlier experiments showed that traces of grease may seriously affect the saturated hydraulic conductivity (K_{sat}) of the ceramic plate, and thus the optimization results. Instead, we used flexible, thin rubber rings. The samples were saturated with distilled water, supplemented with 0.01 M CaCl$_2$, in order to prevent clay dispersion. In a five week period the equilibrium outflow of the samples was determined using five air pressure increments, corresponding to air pressures h_{air} of 20, 60, 140, 250 and 1000 cm. These data served as a verification of the results of the MSO and OSO experiments.

Next, the samples were resaturated, after which an air pressure of 30 cm was applied. When equilibrium was reached, the MSO experiment was started by increasing the air pressure to 60, 140, 250, 500 and 1000 cm with daily intervals. The timing of the outflow measurements was such that the shape of the outflow curve could be reproduced well, thereby using approximately seven outflow measurements for each pressure step.

After equilibrium at $h_{air} = 1000$ cm, the samples were resaturated again and brought back to a soil water pressure head of -30 cm, after which the OSO experiment was started. In a single pressure step, h_{air} was increased from 30 to 1000 cm. The outflow was measured for 48 hours, with the last outflow observation corresponding to about 50 percent of the equilibrium outflow (17 cm^3), which represented approximately 50 percent of the water available between θ_{res} and θ_{sat} (36 cm^3). Thus the conditions of the OSO experiment satisfied the minimal outflow requirements indicated by *Kool et al.* (1985a).

Finally, the soil samples were removed from the pressure cells and the water content was determined by drying in an oven for one day at 105 °C. Subsamples were used to determine the water content at $h_{air} = 16000$ cm in a pressure chamber. The K_{sat} of each ceramic plate was determined by measuring the outflow rate of water-filled cores, after application of an air pressure of 150 cm. We checked the water balance after each resaturation. The water loss was negligible, except for two soil samples which were excluded from further analysis. At the remaining 18 samples, the mean and standard deviation of the water balance error between resaturations were -1.03 and 0.89 cm^3, respectively. The outflow was determined from burette readings with a maximum error of 0.1 cm^3.

For this particular soil, inclusion of θ at $h = -30$ cm in the objective function did not significantly affect the optimized parameter values. Therefore, the used objective function contained outflow data only (Eq. 3.4). The MG parameters α, n, K_{sat} and λ were optimized while θ_{sat} was fixed to its measured value. The value of θ_{res} of the loam soil was assumed to be zero. In case of MSO, the near-equilibrium outflow data at the successive pressure steps can be used to estimate the initial parameters of the retention function for the inverse procedure. Since this is not possible for the OSO approach, the initial estimates for both MSO and OSO optimizations were derived from earlier experiments with a soil of similar texture and structure ($\alpha = 0.0185$ cm^{-1}, $n = 1.25$, $K_{sat} = 0.5$ cm h^{1} and $\lambda = 0.5$). The optimizations were repeated with other initial parameter estimates, corresponding to a coarser ($\alpha = 0.0278$ cm^{-1}, $n = 1.66$, K_{sat} and λ not changed) and to a finer ($\alpha = 0.0056$ cm^{-1}, $n = 1.12$, K_{sat} and λ not changed) soil texture.

3.4   Results and discussion

Figure 3.2 shows the measured outflow data for both the OSO and MSO experiments. Although the soil horizon during sampling was considered to be homogeneous, the outflow curves show large variability. The outflow curves of the individual samples are smooth for the OSO experiments, but change abruptly in case of MSO experiments when the applied pressure is increased. The final cumulative outflow after two days at the OSO experiments ranged from 5.4 to 9.3 cm^3. In the MSO experiments the last pressure of 1000 cm was maintained for 10 days. At this time still no equilibrium was reached and the cumulative outflow ranged from 10.2 to 14.5 cm^3. In Fig. 3.3 typical optimized retention functions are compared with the equilibrium soil water retention data. *The OSO technique overestimated water contents compared to equilibrium $\theta(h)$ data*, especially in the dry range. This occurred for all 18 samples. The optimized parameters using the *MSO data corresponded much better with the equilibrium $\theta(h)$-data*. The equilibrium θ-values at $h = -1000$ and -16000 cm were still
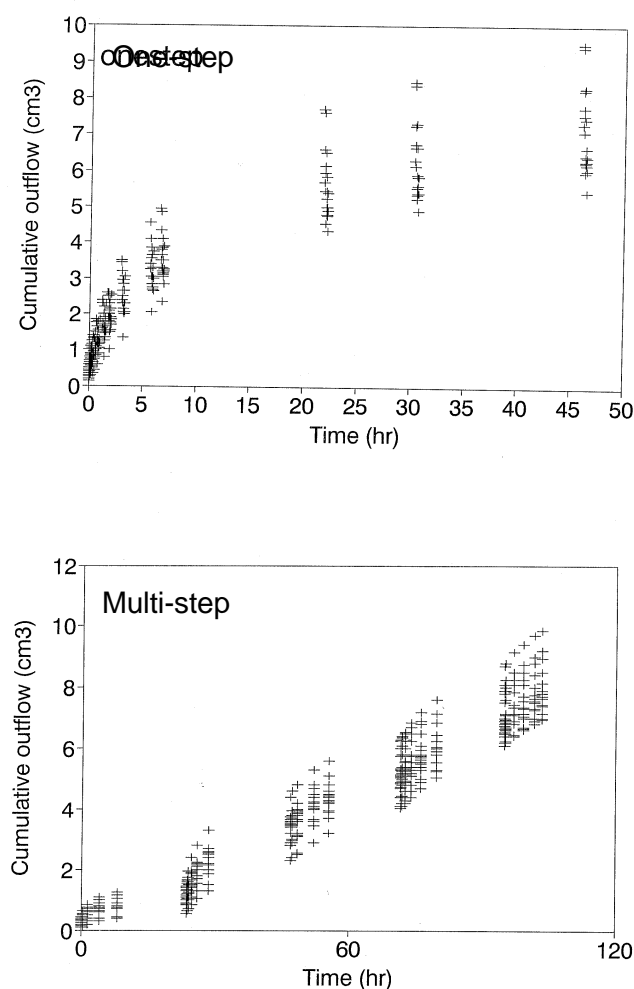
Figure 3.2 Cumulative outflow as function of time for 18 samples at the One-step outflow and the Multi-step outflow experiment.

2 volume percent higher than those of the MSO experiment. Overestimation of θ in the pressure chamber may occur, when the drying soil looses contact with the ceramic plate. The

optimization results of the OSO approach did depend on the initial parameter estimates. *In case of the MSO approach, optimizations with the three different initial parameter estimates converged all to the same optimized parameter set.* This indicates in case of MSO the presence of a distinct global minimum, which can be found with a derivative-based optimization algorithm.
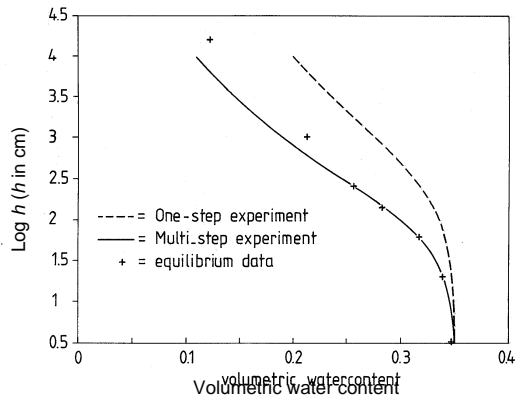
Figure 3.3 Optimized retention function for a typical soil sample. Equilibrium data and the estimated curves from the One-step and the Multi-step experiment are shown.

The optimization algorithm minimizes the residuals $(Q_{obs}(t) - Q_{cal}(t,b))$. The observed outflow $Q_{obs}(t)$ contains measurement errors such as the reading error of the burette, while the calculated outflow $Q_{cal}(t,b)$ includes model errors. The model errors might be structural, as caused by invalid assumptions in the flow equation or by too rigid expressions of the soil hydraulic functions, or incidental as caused by errors in initial and boundary conditions or in the remaining model input parameters. In contrast to measurement errors, model errors are difficult to quantify. In case of relatively small model errors, the residuals should be comparable to measurement errors. In the MSO experiments the mean standard deviation (*SD*) of the residuals was 0.16 cm^3, while the *SD* of burette reading errors was 0.06 cm^3. As more measurements errors are likely, we may conclude that *measurement and model errors were of the same order of magnitude.*
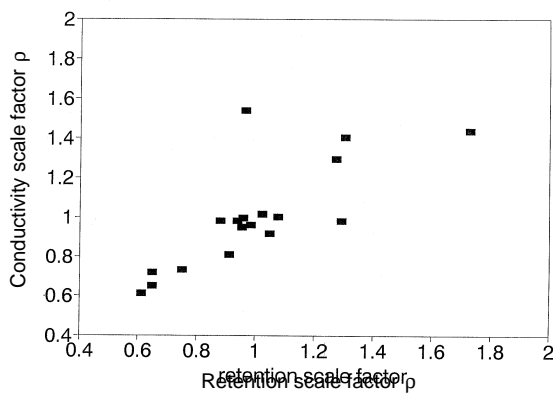
Figure 3.4 Scale factors for retention and conductivity data for 18 samples of a loam soil.

The laboratory outflow method can easily be applied simultaneously to a series of soil samples, which facilitates studies on the spatial variability of soil hydraulic functions. Different methods exist to determine mean soil hydraulic functions from an ensemble. The scaling approach, as described in Chapter 2, yields a reference curve and a set of scale factors (ρ) which relates each individual sample to the reference curve. Figure 3.4 compares the scale factors as estimated with the scaling program of *Clausnitzer et al.* (1992), using $\theta(h)$ and $K(\theta)$ data separately. The distributions of retention and conductivity scale factors were relatively close, so we used the scale factors based on simultaneous scaling of $\theta(h)$ and $K(\theta)$ data.

Alternatively, mean hydraulic functions can be obtained by simple arithmetic averaging of θ and log K as function of h. In a third approach, the mean soil hydraulic functions were obtained by a

single parameter optimization, using the the arithmetic-averaged outflow data in the objective function. Figure 3.5 shows good agreement between the reference curve as obtained from scaling with the mean curves derived either by averaging optimized soil hydraulic functions or by optimization of mean outflow data. *All three methods result in approximately the same mean soil hydraulic functions.*
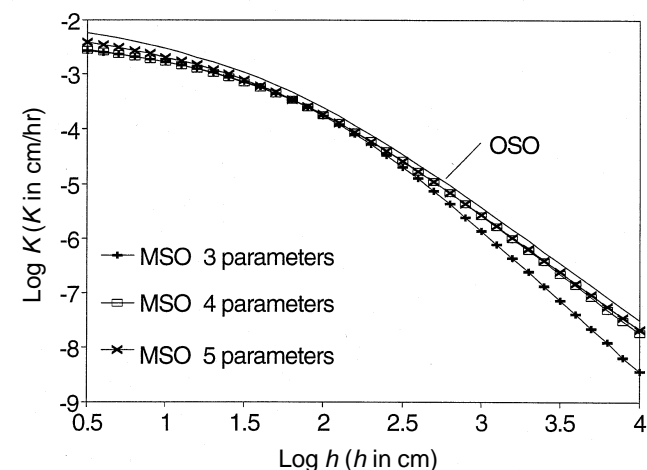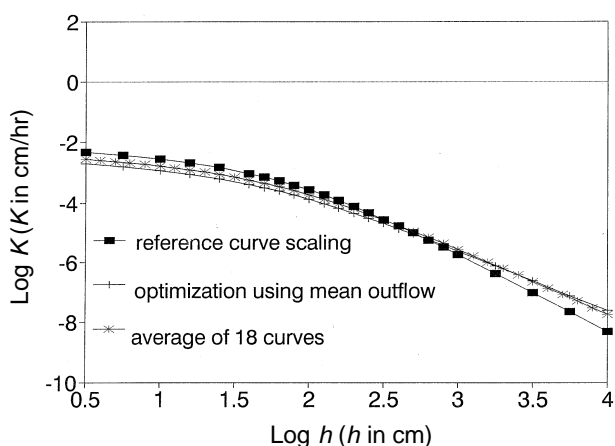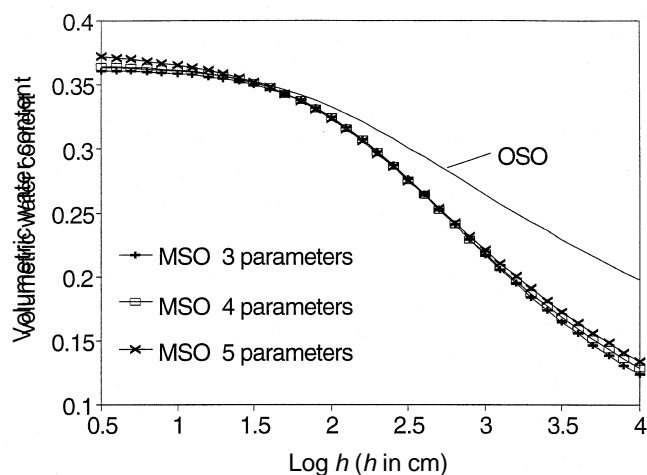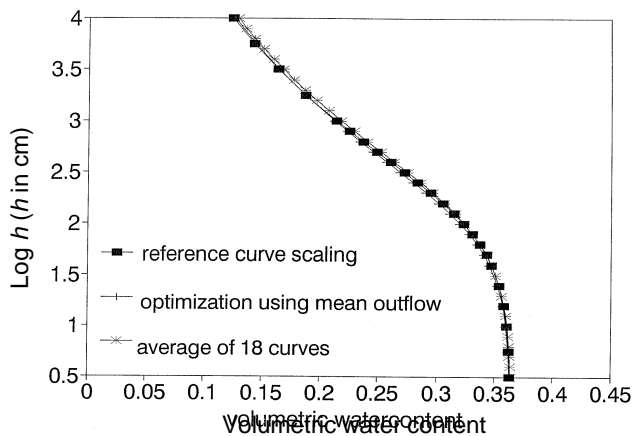
Figure 3.5 Mean soil hydraulic functions obtained with three methods: scaling, averaging optimized curves and optimizing mean outflow data.

Figure 3.6 Mean soil hydraulic functions for the One-step experiment (OSO) using four fitting parameters, and the Multi-step experiment (MSO) using three, four or five optimized parameters.

The MG parameter θ_{sat} is easily obtained during the experiment, while θ_{res} can be measured in a pressure chamber or estimated by pedo-transfer functions (*Wösten et al.*, 1998). Optimization of θ_{res} is not recommended, as the maximum suction applied in outflow experiments is approximately 1000 cm, while θ_{res} refers to higher suctions. Therefore an optimized θ_{res} will be largely based on extrapolation, making $\theta(h)$ ambiguous for very dry conditions. Still 3 or 4 parameters of the MG model are unknown, depending on whether K_{sat} is measured independently or is viewed as a fitting parameter. Using the MSO method, we checked the effect of the number of optimized parameters by repeating the optimizations with 3 (α, n and K_{sat}) and 5 (α, n, θ_{sat}, K_{sat} and λ) fitting parameters on all 18 samples. The mean curves were derived by

averaging θ and log K as function of h. The results are depicted in Fig. 3.6, together with the mean soil hydraulic functions of the OSO experiment. In the dry range, OSO overestimates θ considerably as compared to equilibrium and MSO data. Despite the large deviation of mean $\theta(h)$, mean $K(h)$ is only slightly overestimated by OSO. In case of MSO experiments, optimization with 5 parameters resulted in a mean optimized θ_s value of 0.381 cm^3 cm^{-3}, which is slightly more than the mean measured value (0.365 cm^3 cm^{-3}). Optimization with 5 parameters influenced $K(h)$ only between saturation and $h = -30$ cm, which is outside the experimental range. In the drier range $-1000 < h < -30$ cm, the mean retention functions were not affected by the number of optimized parameters. However, fixation of λ to 0.5 affected the prediction of the mean $K(h)$ function (Fig. 3.6; 3 parameters). Apparently, λ is needed to provide more flexibility for $K(h)$ in the MG model. Application of the simultaneous scaling algorithm showed that the variability, as indicated by the standard deviation of ln(ρ), was approximately equal for the optimizations of MSO experiments with 4 and 5 parameters. The relatively small deviations between mean soil hydraulic curves for the parameter sets (α, n, K_{sat} and λ) and (α, n, θ_{sat}, K_{sat} and λ) and the equal variability in the series of 18 samples, indicate that *the MG model is flexible enough when the 4 parameter set (α, n, K_s and λ) is optimized.*

Although the sample population is relatively small ($n = 18$), fractile diagrams indicated a small preference for a lognormal distribution of scale factors ρ rather than a normal distribution. For the MSO experiment with 4 optimized parameters, the mean and standard deviation of ln(ρ) were -0.037 and 0.278, respectively. Accordingly, the 95-percent confidence region of the soil hydraulic function was bounded by $\rho = 0.553$ and $\rho = 1.680$. Figure 3.7 shows this confidence region for both soil hydraulic functions.

Figure 3.7 Reference soil hydraulic functions and the 95% confidence region as determined by simultaneous scaling of 18 samples of a loam soil.

3.5   Conclusions

The outflow method illustrates some distinct advantages of the inverse modeling approach. Numerical models are flexible in initial and boundary conditions, and are able to solve the flow equation without simplifications. Those experimental conditions can be selected that are representative for the application considered. Furthermore, because of the information contained in Richards' equation and the physically based shape of the soil hydraulic functions, less

measurements are needed as compared to steady state methods. Also, any information can be used in the objective function, including initial estimates of the parameter values. Moreover, the inverse technique provides information on the accuracy of the estimated parameters.

In case of laboratory outflow experiments in combination with inverse modeling, MSO experiments have theoretical as well as practical advantages above OSO experiments. The soil water fluxes and hydraulic head gradients during the experiment are more comparable to natural situations. Time is saved that is needed at OSO experiments to determine equilibrium $\theta(h)$ data. Our laboratory experiments showed that the outflow data of MSO contain sufficient information for unique estimates of the soil hydraulic functions, using initial estimates derived from the outflow experiment itself. Although we did present here only the results of a loam soil, experiments with other soils show that MSO experiments are generally well-posed for sandy to medium textured soils. Special attention should be paid to soils that exhibit shrinkage at lower water contents due to a high clay or organic matter content. During the experiment such soils may loose contact with the ceramic plate, which severely affects the outflow and optimization results.

Three methods were used to determine mean soil hydraulic functions from a series of MSO experiments: (1) similar media scaling, (2) arithmetic averaging of θ and log K as function of h, and (3) optimization of arithmetic averaged outflow data. For the investigated loam soil and using 18 soil samples, the three methods resulted in comparable soil hydraulic functions.

Regarding the number of fitting parameters, fixation of the MG parameter λ negatively affects the optimization of the $K(h)$ function. As the MSO experiments apply to unsaturated conditions, which contain limited information of the saturated hydraulic conductivity, we advice to measure K_{sat} independently if the soil hydraulic functions are used in simulations with both saturated and unsaturated conditions. As the parameters θ_{res} and θ_{sat} can be determined relatively easily, this leaves the parameters α, n, and λ to be estimated from MSO data.

4. Prior analysis of inverse, field scale experiments

to select observations and fitting parameters[3]

4.1 Introduction

Numerical simulation models are important tools in environmental research and policy analysis. Unfortunately, a serious limitation of current model applications is the availability of accurate input parameters. Measurements which are needed to determine the input parameters are expensive and time consuming, both in the laboratory and in the field. However, the rapid increase of processor calculation speed and the development of effective optimization algorithms created the possibility to determine model input parameters by inverse techniques.

Inverse modeling techniques are relatively cheap and quick compared to traditional experiments. They require no simplifying assumptions in the flow and transport equations, as these equations are solved numerically. Numerical procedures allow for arbitrary initial and boundary conditions, which offers the possibility to design experiments according to the intended applications of particular models. In general, inverse modeling techniques require less measurements than traditional methods. Also, errors in fixed model parameters and the physical-mathematical concept are compensated by the optimized parameters. The objective function may include any prior information of the parameters, so available information can be employed optimally. Another important advantage of inverse modeling is that the accuracy of fitting parameters can be estimated.

However, the inverse modeling technique has also its drawbacks. By using functional relationships to allow parameter fitting, the flexibility of the measured relationships will be limited compared to extensive tabular relations. Further, the estimated parameters are less objective, as they will include not only measurement errors but also model errors, like differences between adopted and actual boundary conditions of the experiment, errors in fixed model parameters, or errors in the physical-mathematical model concept. The limited number of observations in time and space might miss essential features of the modeled system. Furthermore, experiences show that with inverse problems often non-uniqueness occurs.

Inverse modeling techniques are frequently used in groundwater flow problems (*Yeh*, 1986; *Carrera and Neuman*, 1986; *Knopman and Vos*, 1988; *McLaughlin and Townley*, 1996; *Hill et al.*, 1998; *Olsthoorn*, 1998). In groundwater, research focuses for a large part on conditions of well-posedness of the inverse problem, as in many applications the number of unknown parameters is large and the information content of the measurements limited. Also in the vadose zone inverse modeling techniques are increasingly used to determine model

---

[3] *Adapted from Van Dam, J.C., and P.J.J.F. Torfs, 2000. Prior analysis of inverse, field scale experiments to select observations and fitting parameters. Submitted to Water Resources Research.*

input parameters. Compared to groundwater, generally in the vadose zone the number of parameters is less and the number of observations more, which is favorable for unique and accurate parameter estimates. Inverse modeling techniques were first used with laboratory experiments, such as One-step or Multi-step type outflow experiments (*Kool et al.*, 1985a; *Van Dam et al.*, 1992, 1994; *Eching and Hopmans*, 1993) and evaporation experiments (*Ciollaro and Romano*, 1995; *Santini et al.*, 1995; *Šimunek et al.*, 1998a). Application of inverse methods to field plot experiments such as infiltration-drainage experiments (*Dane and Hruska*, 1983; *Kool and Parker*, 1988; *Zijlstra and Dane*, 1996; *Abbaspour et al.*, 1999), disc infiltrometers (*Šimunek and Van Genuchten*, 1996, 1997), extraction methods (*Inoue et al.*, 1998), and cone permeameters (*Šimunek et al.*, 1999) showed the high potential of the inverse technique. Although applications to field plots are more complex than applications to laboratory set-ups due to soil heterogeneity and uncertainty associated with the boundary conditions (*Šimunek et al.*, 1999), well-posed inverse field experiments are feasible.

Many applications of agro- and ecohydrological models are at field scale level, where flow and transport processes can be described in a rather physical way, as weather conditions, vegetation type, soil characteristics, drainage situation and cultivation scheme are well defined. For regional analysis, simulations at field scale level may form the basic unit to be combined with geographic information systems. The accuracy of model predictions at field scale level will increase, if the inverse problem is applied at the same level. However, field experiments to collect data for model calibration are expensive and not all the data are suitable for parameter fitting. Proper setup of the measurement scheme, in the sense of both type and time of observations, may save effort and avoid inaccurate parameter estimates.

One method to select proper measurements, is by calculating the sensitivity of measurements to fitting parameter values, as was shown by *Kool and Parker*, (1988) for an infiltration and drainage experiment and by *Hill et al.* (1998) for groundwater flow. In this way proper times of the measurements can be determined. Also relatively insensitive parameters can be distinguished which should be measured separately or fitted with narrow constraints. However, these type of sensitivity analysis gives no answer to the question which type of data should be measured, as measurement errors differ among data types. Also, the method does not take into account correlation between fitting parameters. Moreover such a sensitivity analysis gives no information on the accuracy of fitting parameters and model prediction.

Alternatively, using optional measurement schemes and fitting parameter sets, *calculated confidence intervals of fitting parameters may indicate which type of data at which place and time need to be measured and which parameters can be optimized with a given data set.* Confidence intervals may be calculated in various ways. A robust, but computationally intensive method is the generation of contour plots (*Toorman et al.*, 1992; *Gribb*, 1996). An important disadvantage of this method is that at each contour plot only two parameters can be studied. Alternative methods derive analytical covariance matrices for all the fitting parameters. The calculations can be based on a linear approximation of the objective function near its minimum (*Carrera and Neuman*, 1986; *Kool and Parker*, 1988; *Kuczera and*

Mroczkowski, 1998) or on non-linear algorithms (*Bates*, 1992; *Finsterle and Pruess*, 1995, *Christensen and Cooley*, 1999). In general non-linear algorithms require substantial more computational effort than linear algorithms. Recent studies show that in case of well-posed inverse problems, linear algorithms provide a good approximation of the parameter covariance matrix (*Kuczera and Mroczkowski*, 1998; *Christensen and Cooley*, 1999).

Table 4.1 Coefficient of variation (*CV*) and correlation matrix of estimated soil hydraulic function parameters using *One-step* outflow data corrupted with normally distributed, uncorrelated observation errors.

Parameter	*CV*	Correlation coefficient			
α	0.489	1.000	....	....	....
n	0.029	-0.998	1.000	....	....
K_{sat}	0.790	0.999	-0.997	1.000	....
λ	0.193	-0.924	0.937	-0.908	1.000

Table 4.2 Coefficient of variation (*CV*) and correlation matrix of estimated soil hydraulic function parameters using *Multi-step* outflow data corrupted with normally distributed, uncorrelated observation errors.

Parameter	*CV*	Correlation coefficient			
α	0.039	1.000	....	....	....
n	0.004	-0.882	1.000	....	....
K_{sat}	0.091	-0.535	0.2153	1.000	....
λ	0.173	-0.879	0.7700	0.775	1.000

The idea to analyse more closely the parameter covariance matrix prior to experiments originated from our laboratory outflow experiments. *Kool et al.* (1985) and *Parker et al.* (1985) introduced the inverse procedure to determine simultaneously the retention function and unsaturated hydraulic conductivity function from the so-called One-step outflow experiment (Chapter 3). Their method was much more efficient than other methods to measure the soil hydraulic functions and was therefore adopted quickly by other soil physical laboratories. In many cases however, the proposed One-step outflow experiment resulted in non-uniqueness of the inverse problem (*Toorman et al.*, 1992; *Eching et al.*, 1994; *Van Dam et al.*, 1992, 1994). A simple change in the experimental setup, namely gradually increasing the air pressure instead of one big increase (Fig. 3.1), showed much better correspondence to independent measurements (*Van Dam et al.*, 1994). The improvement of the latter procedure, called Multi-step outflow, was also *predicted by prior analysis of the coefficient of variation and the correlation matrix of optimized parameters*. We generated series of One-step and Multi-step outflow data, which were corrupted with measurement errors showing a normal distribution and independence. The inverse procedure was applied to both data sets and the coefficient of variation, *CV*, and correlation matrix of optimized parameters calculated. The results are listed in Table 4.1 and 4.2. In case of Multi-step outflow experiments, the *CV* values and the correlation among fitting parameters were much less, resulting in more effective optimization and higher accuracy of the optimized parameters. These results of prior

analysis with artificial data were confirmed in the inverse analysis using laboratory data (Chapter 3). If the parameter covariance matrix is useful to determine the appropriate experimental procedure of laboratory outflow experiments, it might also be useful to determine the appropriate observation and parameter set for other inverse experiments, like field experiments at cultivated soils. This may reduce the labour and financial effort needed to conduct field experiments and avoid the risk for ill-posed inverse problems in posterior analysis.

In this chapter, we calculate the covariance matrix of field-scale water flow parameters using a linear approximation of the objective function near its minimum. We investigate the appropriateness of the linear approximation with a Monte Carlo simulation. Next we use the parameter covariance matrix to select the parameter set that can be optimized, and to analyse how the accuracy of the inversely estimated parameters is affected by crop growth, tracer application, measurement type and measurement timing. The merit of this study lies in the application of the inverse methodology to field-scale experiments of vadose zone flow and transport and exploration of a practical, prior analysis method to improve measurement schemes.

4.2   Method

4.2.1   SWAP
The model SWAP is used to simulate water flow and solute transport in relation to crop development in a hypothetical field with ordinary, natural boundary conditions. The applied features of SWAP are described in Chapter 2.

4.2.2   PEST
PEST (Parameter ESTimation) is a non-linear parameter estimation program which can relatively easy be linked via templates to any model (*Doherthy et al.*, 1995). PEST runs the particular model, compares the model results with target values (e.g. observations), adjusts selected parameters using an optimization algorithm, and runs the model again (Fig. 4.1). This will continue until the differences between the model results and observations, or the number of iterations, meet a preset criterion.

An objective function quantifies the differences between model results and observations. If observation errors follow a multivariate normal distribution with zero mean, no correlation, and constant variance for each measurement type, maximization of the probability of reproducing the observed data leads to the weighted least squares objective function Φ (-) (*Bard*, 1974; *Kool and Parker*, 1988; *Press et al.*, 1989; *Doherty et al.*, 1995):

$$\Phi(\boldsymbol{b}) = \sum_{j=1}^{m} \left[\sum_{i=1}^{n_j} \left(\frac{y_j^*(t_i) - y_j(t_i, \boldsymbol{b})}{w_j} \right)^2 \right] \tag{4.5}$$

where $\boldsymbol{b}$ is the vector with fitting parameters, $y_j^*(t_i)$ denotes the observation of type j at time t_i, $y_j(t_i, \boldsymbol{b})$ is the corresponding model prediction, and w_j is the weighting factor. In case of
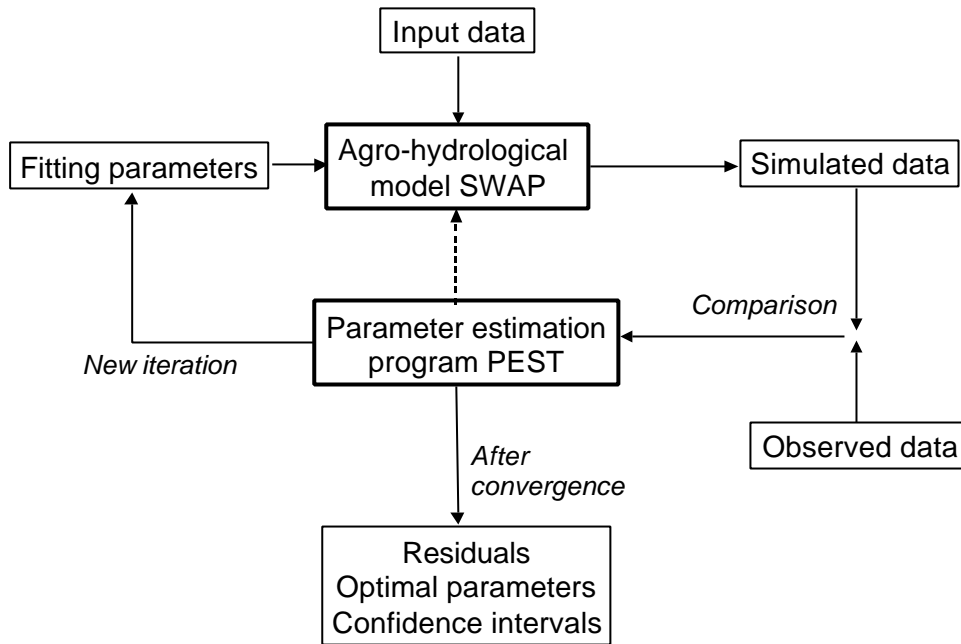
Figure 4.1 Communication between simulation model SWAP and optimization model PEST.

random observation errors only, according to maximum likelihood the weighting factor w_j should be equal to the standard deviation of the observation error of observation type j. The use of the standard deviation as weighting factor also effectively accounts for measurement unit differences between observation types, and is adopted by PEST.

Inverse problems in which more computation intensive simulation models are used, require an efficient optimization algorithm to arrive at the optimal parameter set with a limited number of model calls. The optimization algorithm used by PEST is derived from Gauss-Marquardt-Levenberg, which starts with searching mainly along the steepest gradient of the objective function surface and gradually switches to a direction based on a second order approximation of the objective function surface (*Marquardt*, 1963; *Press et al.*, 1989; *Doherthy et al.*, 1995). Experiences in soil water flow modeling show that the Gauss-Marquardt-Levenberg method is very efficient in optimization, in the sense of a minimum amount of model calls (*Cooley*, 1985; *Clausnitzer and Hopmans*, 1995; *Finsterle and Pruess*, 1995; *Olsthoorn*, 1998). In case of a large number of parameters compared to the number and quality of observations, which is often true for groundwater inversion problems, the response surface of the objective function may not show a dominant global minimum, but instead a scatter of local, equally sized minima. In such a case, the Gauss-Marquardt-Levenberg optimization search may end up in a local minimum, due to its initial descending along the steepest gradient and its switching to a second order approximation of the objective function surface near a minimum. In vadose zone inversion problems, the number of parameters is relatively small as compared to the number and quality of observations, which reduces the risk of local minima considerably. Also the PEST program partly circumvents local minima, by evaluating the objective function with a number of Marquardt values (*Doherthy et al.*, 1995). Still it is recommended to repeat optimization runs with different initial parameter values, in order to check the uniqueness of the results.

4.2.3 Parameter covariance matrix

Although not true for the unsaturated zone, we may assume a linear response of the objective function to the fitting parameters, in order to derive a first order approximation of the parameter covariance matrix $\boldsymbol{C}$ (see Appendix A):

$$C(\hat{\boldsymbol{b}}) = \frac{\Phi(\hat{\boldsymbol{b}})}{\boldsymbol{n}}(\boldsymbol{J}^{\mathrm{T}}\boldsymbol{Q}\boldsymbol{J})^{-1} \tag{4.6}$$

where $\hat{\boldsymbol{b}}$ is the vector with fitted parameter values, $\boldsymbol{J}$ is the derivative matrix $J_{kp} = \partial y_k /\partial b_p$, with k and p indices for the measurement and fitting parameter, respectively, $\boldsymbol{Q}$ is the diagonal weighing matrix with elements $Q_{k,k} = w_j^{-2}$ according to Eq. 4.1, and ν is the number of degrees of freedom (*Kool and Parker*, 1988). In the derivation of Eq. 4.2, it is assumed that the residuals, $(y_j^*(t_i) - y_j(t_i, \boldsymbol{b}))$, follow a normal distribution and are uncorrelated (Appendix A). The standard deviation σ_p of fitting parameter b_p follows directly from the parameter covariance matrix:

$$\boldsymbol{s}_p = \sqrt{C_{pp}} \tag{4.7}$$

The optimized parameters follow a Student's t distribution, thus the parameter confidence regions can be calculated by (*Kool and Parker*, 1988):

$$\Pr\left(\hat{b}_p - \boldsymbol{t}\boldsymbol{s}_p \leq b_p \leq \hat{b}_p + \boldsymbol{t}\boldsymbol{s}_p\right) = \boldsymbol{g} \tag{4.8}$$

where $\hat{b}_p$ and b_p are the fitted and true values of parameter b_p, respectively, and τ is the value of Student's t distribution for confidence levels γ and ν degrees of freedom. The parameter correlation matrix $\boldsymbol{A}$ is derived by dividing the elements of $\boldsymbol{C}$ with the standard deviations of the corresponding fitting parameters:

$$A_{ij} = \frac{C_{ij}}{\boldsymbol{s}_i\boldsymbol{s}_j} \tag{4.9}$$

The coefficient of variation CV_p of fitting parameter b_p, is then calculated as:

$$CV_p = \frac{\boldsymbol{s}_p}{\hat{b}_p} \tag{4.10}$$

4.3 Theoretical field experiment

The envisaged field experiment is conducted at a drained loamy soil cultivated with maize (Fig. 4.2). An important reason to select a drained field is that recharge and solute leaching can be measured with drains at field scale level, which are important results of agro-hydrological models for many applications. One of the experimental options is to apply a tracer. As tracers are usually leached during the winter period, the one year experimental period starts in autumn at October 1. The maize cropping period lasts from May 1 until September 30. We used the daily weather data near Wageningen of the ordinary meteorological period October 1, 1992 until September 30, 1993. The daily potential evapotranspiration rate was calculated with the Penman-Monteith equation (Eq. 2.1), assuming a minimum crop diffusion resistance r_{crop} of 70 s m^{-1}. Daily rainfall intensities were input, as runoff was not expected.

Experimental period 1 October 1992 - 30 September 1993

Maize crop from 1 May until 30 September

Optional: application bromide tracer 500 (μg cm^{-2}) at 1 October 1992

-0.40

Top soil loam

-0.80

Sub soil loam

Subsurface drains

8.0 m

-1.20

Impermeable clay
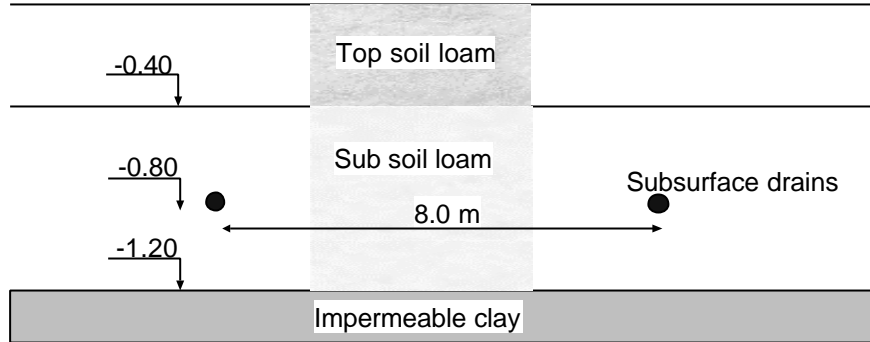
Figure 4.2 Soil profile and boundary conditions of the adopted experimental field.

The soil hydraulic functions were described with the Mualem - van Genuchten equations (Eq. 2.15 and 2.16). The used parameter values (Table 4.3) apply to a loamy soil and were derived from a national Dutch soil data base (*Wösten et al.*, 1994). The drains were located at 0.80 m depth, were spaced 8 m apart, and had an entry resistance γ_{entr} of 20 d. At 1.20 m depth, an impermeable layer confined the phreatic aquifer. In such a drainage situation, we may define the drainage resistance γ_{drain} (see Eq. 2.17) as:

$$\gamma_{drain} = \frac{L^2_{drain}}{4K_{drain}\left(\gamma_{gwl} - \gamma_{drain}\right)} + \gamma_{entr} \tag{4.7}$$

where L_{drain} is the drain spacing (cm), K_{drain} is the horizontal saturated hydraulic conductivity of the subsoil (cm d^{-1}), and γ_{entr} is the hydraulic entrance resistance at the drains (d).

Table 4.3 Parameters describing soil hydraulic functions of the first and second soil layer.

Soil layer	α (cm^{-1})	n (-)	θ_{sat} (cm^3 cm^{-3})	θ_{res} (cm^3 cm^{-3})	K_{sat} (cm d^{-1})	λ (-)
1 (0 - 40 cm)	0.0194	1.250	0.40	0.00	14.1	-0.802
2 (40-120 cm)	0.0136	1.342	0.47	0.00	9.08	-0.803

Figure 4.3 shows the resulting water flux at the soil surface (effective precipitation minus actual evapotranspiration) and the simulated groundwater levels. The water flux at the soil surface ranged from 7 mm upward to 26 mm d^{-1} downward, which is a moderate range. The groundwater level occurred during the winter period only, and did reach a highest level of $z = -29$ cm. In the scenarios with the tracer, the tracer was applied on October 1 by spraying 5 mm with a concentration of 1000 μg cm^{-3}. At the considered field conditions, solute diffusion is much less than solute dispersion, therefore solute diffusion was neglected. The dispersion
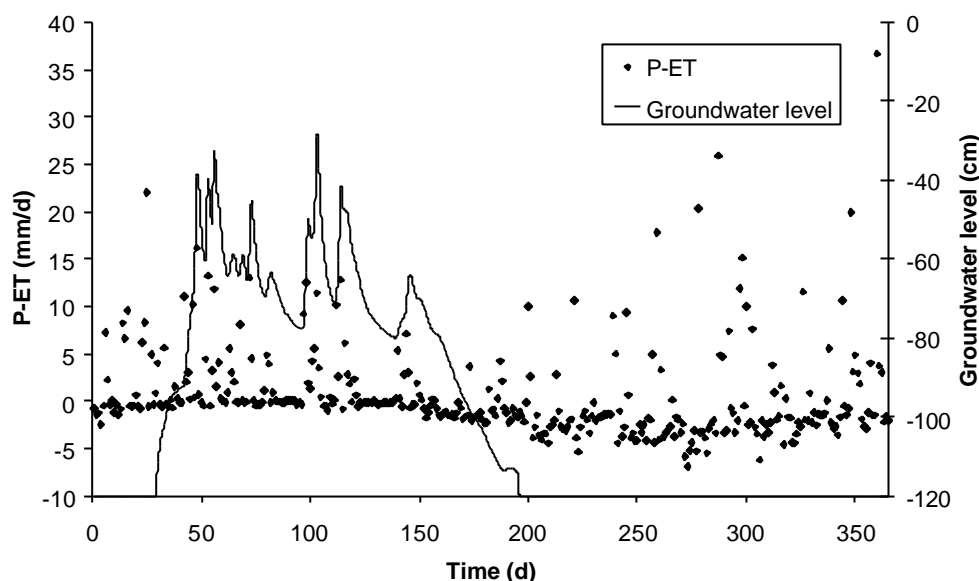
Figure 4.3 Input water flux at the soil surface (P-ET) and SWAP simulated groundwater levels for the reference situation.

coefficient was calculated with Eq. 2.23, assuming a field dispersion length of 5 cm. Adsorption, decomposition and root uptake of the tracer were assumed to be negligible.

The observations for the reference inverse problem consisted of weekly values of the volumetric water content and pressure head at 0.175 m depth and the drain discharge rate. The range of measured water contents and pressure heads depends on the measurement depth. More close to the soil surface, the range gets wider due to larger fluctuations. Figure 4.4 shows the simulated weekly values of the pressure head and the drainage flux. The weekly pressure head values at 0.175 m depth show the range $-531 < h < -9$ cm, which is within the tensiometer range and compares well to the ordinary range of $-1000 < h < 0$ cm in case of laboratory evaporation or outflow experiments (Table 3.1 and 3.2). The drainage flux only occurs during 14 weeks, when the groundwater level is above the impervious layer, and shows rather rapid fluctuations between 0 and 5.5 mm d^{-1}. Field scale measurement of the drainage rate is relatively easy in a drained field. Because of spatial variability, field scale values of soil water content and pressure head require averaging of measurements at various locations in the field. The observation data for the inverse problem were derived by forward simulation and adding an observation error, which was normally distributed with a constant variance per observation type and without correlation between observations. The observation error standard deviations amounted 0.01 cm^3 cm^{-3} for soil water contents, 3 cm for pressure heads, and 1.0 mm d^{-1} for drainage rates. However, the objective function weights the residuals by dividing with the observation standard deviation, according to Eq. 4.1. In this way, *the magnitude of the adopted observation error standard deviations does not affect the optimization results,* which makes the prior procedure more robust.
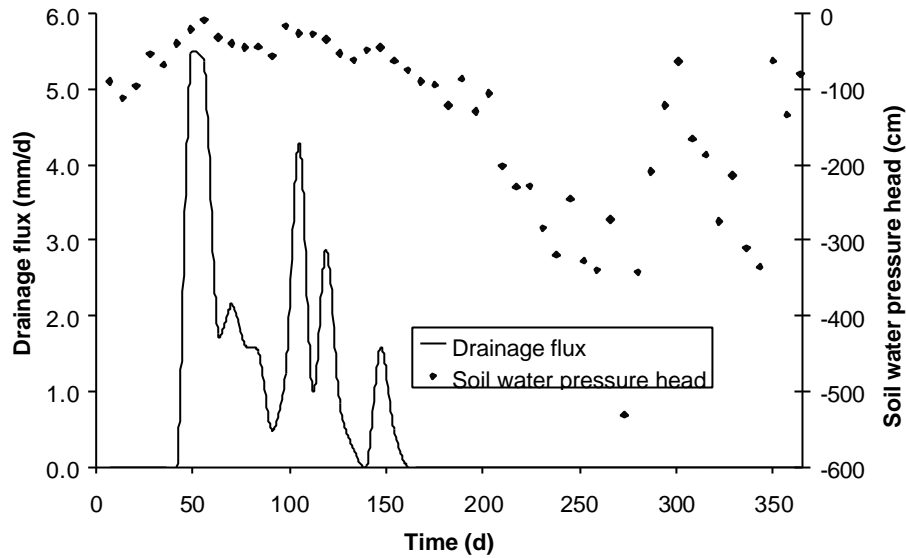
Figure 4.4 SWAP simulated drainage flux and soil water pressure head at 17.5 cm depth in case of the reference situation.

We did select the following four parameters for optimization: the crop resistance, r_{crop}, the soil texture scale factor of the top soil, ρ_{sca}, the saturated water content of the top soil, θ_{sat}, and the saturated hydraulic conductivity of the subsoil, K_{sat}. The number of fitting parameters was limited in order to achieve a well-posed inverse problem (*Yeh and Soon*, 1981; *Mishra and Parker*, 1989). The above mentioned four parameters were selected on the basis of their independent contribution to soil water flow processes and on general lack of information on their values. Relative errors of evapotranspiration rate are magnified in soil water percolation fluxes, therefore the crop diffusion resistance was fitted. A central role in soil water movement is played by the soil hydraulic functions. We choose to optimize the scale factor and saturated water content of the top soil, rather than optimizing each parameter of the Mualem-Van Genuchten model. In many applications basic information of the soil texture or soil hydraulic functions is available. In such cases, optimization of the scale factor and saturated water content is probably sufficient to derive suitable soil hydraulic functions. Regarding the drainage situation, with subsurface drains the spacing and depth can easily be measured. The average saturated hydraulic conductivity of the subsoil is however more difficult to measure, and was therefore selected as fitting parameter. Alternatively, the overall drainage resistance γ_{drain}, as used in Eq. 2.17, could have been optimized. The parameter γ_{drain} integrates the effects of drain spacing, drain depth, average saturated hydraulic conductivity of the subsoil, and drain entrance resistance.

The first order approximation of the confidence region assumes a linear variation of the objective function with the parameters near the optimum parameter set (see Appendix A). Because of the non-linearity of vadose zone flow processes, this is only valid if the parameter confidence regions are relatively small. In order to check the linearity assumption at this application, we did employ a Monte Carlo simulation (Fig. 4.5). We generated n observation sets by adding different observation error sets to the simulated observations for the reference
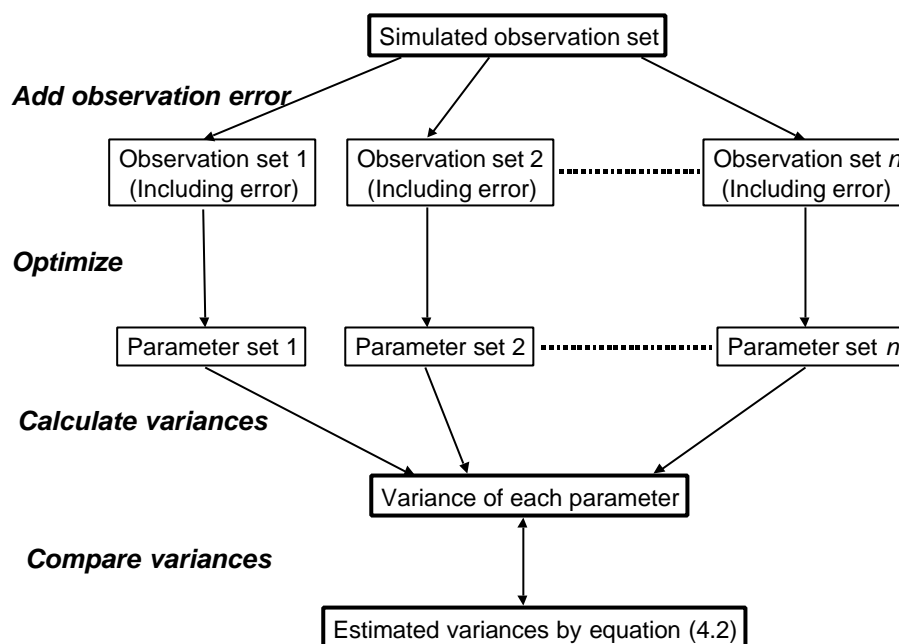
Figure 4.5 Check confidence intervals with Monte Carlo analysis (after *Press et al.*, 1989).

situation. Next we determined at each observation set the optimum parameters and calculated the variances of each set of *n* optimum parameters. These variances were compared with the variances as predicted by the first order approximation, given by Eq. 4.2.

The following scenarios were simulated and used for prior analysis:
1. Reference situation (as defined above);
2. Reference situation without maize cultivation;
3. Reference situation with short, intensive measurement periods, instead of weekly measurements;
4. Reference situation with application of a tracer;
5. Reference situation with estimation of all parameters that describe the top soil hydraulic functions.

In case of bare soil (Scenario 2), less fitting parameters were left, as the crop factor was not needed. In general at inverse problems, less fitting parameters result in lower coefficients of variation. However, removal of the crop will also affect the water dynamics and thus the observations. Crops are more effective in extracting water from the soil than atmospheric air at the soil surface, resulting in larger ranges of water content at cultivated soils. Larger ranges are favorable for parameter estimation.

In Scenario 3, the measurement timing was changed. Weekly measurement might be easy to schedule, but may lack essential features of the soil water dynamics which are needed to optimize the relevant parameters accurately. In this scenario, the same amount of measurements (3 times 52) was concentrated in periods during which the hydrological conditions were most transient. With respect to water contents and pressure heads of the top soil, 4 periods of 13 days were selected. Each period included a wet and a dry period. With

respect to drainage rates, 2 periods of 26 days were selected. The first period coincided with the drainage rate increase in autumn, and the second period with the drainage rate recession in spring.

At Scenario 4, a tracer was applied at the beginning of the experimental period. Tracers provide information of the residence time of soil water, which may result in more accurate estimates of the water flow parameters. However, in order to simulate tracer transport also the field scale dispersivity length needs to be determined, which increases the number of fitting parameters. The tracer concentration was measured weekly at 0.175 m depth, and in addition, in case of drainage, in the drainage water.

In Scenario 5 more parameters were fitted. In the reference simulation, the soil hydraulic functions of the top soil were estimated by two parameters: θ_{sat} and ρ_{sca}. Instead of these two parameters, the parameters α, n, θ_{sat} and K_{sat} of the top soil hydraulic functions were estimated in this scenario, which increased the total number of fitting parameters from four to six.

4.4   Simulation results

4.4.1   Reference situation

The yearly water balance of the reference simulation is shown in Fig. 4.6. Due to favorable soil moisture conditions, actual crop transpiration (25.0 cm) is almost potential (25.3 cm). The relatively long fallow period (October 1 – April 30) causes soil evaporation (33.5 cm) to be the main loss term in the water balance. Net drainage in this ordinary meteorological year amounts to 21.7 cm. In case of the tracer application, Fig. 4.7 shows the simulated yearly solute balance. One year after the tracer application of 500 μg cm^{-2}, only 136 μg cm^{-2} has leached to the drains and the remaining amount of 364 μg cm^{-2} is still in the soil profile.
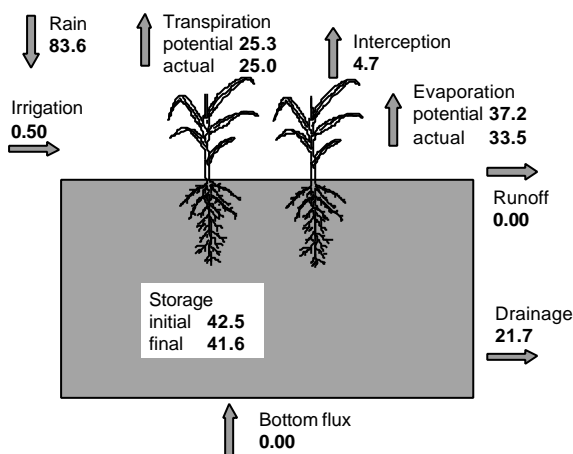
Figure 4.6 Simulated *water* balance (cm) of period 1/10/92 until 1/10/1993 for the *Reference* situation.
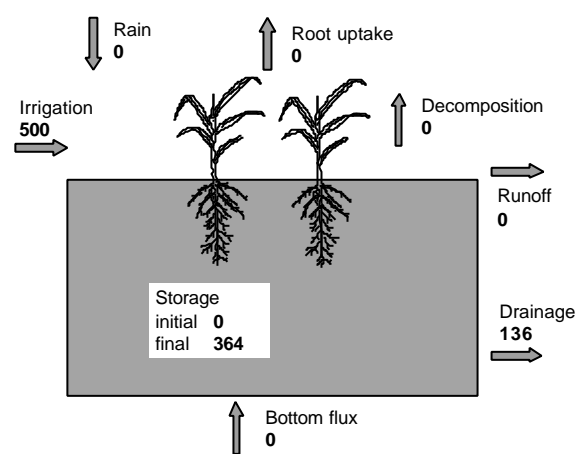
Figure 4.7 Simulated *solute* balance (μg cm^{-2}) of period 1/10/92 until 1/10/1993 for the *Reference* situation.

Optimization of the reference situation was started with various initial parameter values. *In a broad range of initial values, PEST converged to the same optimal parameters,* showing the uniqueness of the solution. Table 4.4 shows the coefficient of variation *CV* and the correlation matrix of the fitting parameters, based on Eq. 4.2. *The correlations are low* (less than 0.425), which is required for accurate parameter estimates. Therefore also the *CV* values are relatively low. The saturated hydraulic conductivity of the subsoil, K_{drain}, shows the largest *CV* value (0.112). The low parameter correlations and *CV* values made this problem suitable for further prior analysis.

Table 4.4 Coefficient of variation (*CV*) and correlation matrix resulting from a typical optimization at the reference situation.

Parameter	Mean	*CV*	Correlation coefficient			
r_{crop} (s m^{-1})	70.0	0.007	1.000	....	....	....
ρ_{sca} (-)	1.00	0.059	-0.421	1.000	....	....
θ_{sat} (-)	0.40	0.010	-0.070	0.425	1.000	....
K_{drain} (cm d^{-1})	25.0	0.112	0.119	0.082	0.104	1.000

4.4.2   Accuracy first order approximation

Table 4.5 shows parameter *CV* values as calculated using the Monte Carlo analysis ($n = 40$) and using the first order approximation (mean of 40 samples) . The parameter *CV* values of both methods correspond well, which is attributed to the relatively small parameter standard deviations. This shows that, at such field scale agro-hydrological experiments, *in case of ordinary measurement errors and a limited number of weakly correlated fitting parameters, the confidence regions can be efficiently calculated with the first order approximation.*

Table 4.5 Coefficient of variation *CV* of estimated parameters as calculated by the first order approximation and a Monte Carlo simulation.

Parameter	Method	
	First order	Monte Carlo
r_{crop}	0.007	0.008
ρ_{sca}	0.053	0.063
θ_{sat}	0.008	0.010
K_{drain}	0.163	0.158

4.4.3   Result of scenario analysis

Table 4.6 lists the *CV* values of the optimized parameters at each scenario. In case of bare soil (Scenario 2) the *CV* values remain more or less the same as in the reference situation. In this case the *positive effect of less fitting parameters is compensated by the negative effect of a smaller measurement range*. This means that both cultivated and bare soils can be used in the inverse experiment.

Table 4.6 Coefficient of variation *CV* of optimized parameters for 7 scenarios, which are described in the text.

Parameter	Scenario				
	1	2	3	4	5
r_{crop}	0.007	-	0.009	0.008	0.011
ρ_{sca}	0.059	0.055	0.047	0.005	-
θ_{sat}	0.010	0.008	0.010	0.006	0.012
K_{drain}	0.112	0.116	0.030	0.007	0.116
L_{dis}	-	-	-	0.012	-
α	-	-	-	-	0.051
n	-	-	-	-	0.005
K_{sat}	-	-	-	-	0.134

Collecting measurements in periods with rapidly changing and extreme hydrological conditions (Scenario 3), increases the accuracy of K_{drain}, of which the *CV* decreases from 0.112 to 0.030. The accuracy of the other parameters remains more or less the same. Accurate determination of the internal drainage of a soil profile is important for water balance calculations, so appropriate measurement timing seems worthwhile.

When the tracer is added (Scenario 4), the *CV* of K_{drain} decreases from 0.112 to 0.007, which is a major improvement. Also the *CV* of the dispersivity length L_{dis} (0.012) is low, which means that the dispersion coefficient D_{dis} can be determined accurately. The results show that *simultaneous optimization of water flow and solute transport parameters is beneficial*, rather than first optimization of water flow parameters, and afterwards optimization of solute transport parameters. This became also clear in a study by *Mishra and Parker* (1989).

In Scenario 5 more parameters of the top soil hydraulic functions (four instead of two) are fitted. The *CV* values of K_{drain} and K_{sat} are relatively large (0.116 and 0.134, respectively), but the confidence regions of the fitted parameters are still acceptable for most applications. This means that we *might include more fitting parameters of the soil hydraulic functions than two*, or, alternatively, fit in addition to K_{drain} more hydraulic parameters of the subsoil.

4.5 Conclusions

Prior analysis of fitting parameter *CV* values is an effective method to determine the most informative type and timing of measurements and the proper fitting parameter set. In case of too large *CV* values, either the measurement scheme should be changed, or the parameters with too large *CV*, which often show a large correlation with other fitting parameters, should be determined separately.

When the *CV* values of fitting parameter are relatively small, the first order approximation provides a good estimation of the parameter *CV* values in a typical agrohydrological simulation as described in this Chapter. Recently, *Kuczera and Mroczkowski* (1998) arrived

at the same conclusion in case of a conceptual catchment model with different data types and *Christensen and Cooley* (1999) in case of a groundwater flow model. Various non-linear estimation techniques exist, but they are more useful in posterior analysis. Monte Carlo analysis can be effectively used to check the accuracy of the first order approximation. In case of inverse problems that are not well-posed, the first order approximation generally results in large correlations and high *CV* values of the fitting parameters. When this occurs, the measurement scheme or the fitting parameter set should be changed.

In the procedure used, the standard deviation of the observation error is applied both to generate the random error and to weigh the residuals. The result is that the adopted standard deviations of the observation errors have no effect on the calculated *CV* values, which makes the prior analysis more robust. In prior analysis, the combination of model structure, fitting parameter set, and observation set, determine the calculated *CV* values.

In case of regular measurements at ordinary field conditions, four to eight hydrological parameters could be estimated uniquely with low correlations and *CV* values. The inclusion of a crop, a tracer and measurement at periods with extreme and transient conditions, improved the fitting parameter accuracy. In the presented example, daily rainfall intensities were used as input to the model, which results in less dynamic change of the observations than occurs in the field. If the measurement interval allows the use of actual rainfall intensities, either more accurate parameter estimates can be achieved or the duration of field experiments can be shorter.

Our ultimate goal is not to derive the parameter confidence intervals, but the accuracy of our model prediction, which is reflected in the magnitude of the residuals. Without model errors, as in prior analysis, the distribution of the residuals is more or less equal to the adopted distribution of the measurement errors. Therefore, in prior analysis smaller adopted measurement errors will directly result in more accurate model predictions. In model applications with the optimized parameters, model errors due to process simplifications and deviations of fixed system parameters and boundary conditions, are probably predominant. Unfortunately, model errors can not be revealed in prior analysis. To detect model errors, real observations are needed. For the same reason, prior analysis can not be used to select the proper model among a set of alternative models. However, the discussed prior analysis seems a practical and powerful method to design such a measurement scheme, that in the posterior analysis the inverse problem is well-posed and allows detection of model errors or selection of best-performing models.

5. Numerical simulation of infiltration, evaporation and shallow groundwater levels with Richards' equation[4]

5.1 Introduction

Soil water fluxes in the vadose zone have a dominant influence on the hydrological cycle, nutrient and pesticide leaching to groundwater, energy transport near the soil surface and plant growth. The equations describing water behaviour in the top soil should be solved numerically, because of soil heterogeneity, non-linearity of soil physical properties, non-uniform root water uptake, rapid changing boundary conditions, and complex interactions.

Water flow in the vadose zone is predominantly vertical, and can generally be simulated as one-dimensional flow (*Romano et al.*, 1998). By running the one-dimensional model at various locations, the horizontal variability of meteorological conditions, crop characteristics, soil properties and drainage conditions can be accommodated and hence regional water and solute balances can be determined (*Bresler and Dagan*, 1983; *Hopmans and Stricker*, 1989).

Richards' equation for variably saturated soil water flow (Eq. 2.14) has a clear physical basis. Therefore this equation is generally applicable and can be used for fundamental research and scenario analysis. Soil hydraulic data which are collected at a great number of soil physical laboratories (*Leij et al.*, 1996; *Bruand et al.*, 1996; *Wösten et al.*, 1998) further enhance the applicability of Richards' equation. However, the numerical solution of Richards' equation is still a subject of research. The equation is difficult to solve, because of its parabolic form in combination with the strong non-linearity of the soil hydraulic functions which relate water content, soil water pressure head and hydraulic conductivity. Also the sudden changes of moisture conditions near the soil surface, causing steep wetting fronts in dry soils, or steep drying fronts in wet soils, may pose problems. The result is that calculated soil water fluxes may depend largely on the structure of the numerical scheme and the applied time and space steps (*Van Genuchten*, 1982; *Milly*, 1985; *Celia et al.*, 1990; *Warrick*, 1991; *Zaidel and Russo*, 1992; *Baker*, 1995; *Pan et al.*, 1996; *Miller et al.*, 1998; *Romano et al.*, 1998).

Another reason why research continues to improve the numerical solution of Richards' equation, is the large computation time needed to achieve accurate solutions for heterogeneous soils with abruptly changing wetness conditions (*Ross*, 1990; *Pan and Wierenga*, 1995; *Miller et al.*, 1998; *Berg*, 1999). Despite the rapid advance of computation speed for personal computers, the computation time may still be excessive for long term simulations, in regional studies or in case of parameter optimization.

In this Chapter a versatile new numerical scheme is presented which is able to solve the one-dimensional Richards' equation with an accurate mass balance and which converges rapidly to the theoretically correct solution. The numerical scheme is able to handle accurately short

---

[4] *Adapted from Van Dam, J.C., and R.A. Feddes, 2000. Numerical simulation of infiltration, evaporation and shallow groundwater levels with Richards' equation. J. Hydrol., in press.*

duration infiltration and runoff during intensive rain showers, while maintaining acceptable computation times for long year simulations. Moreover, the scheme is relatively easy to implement. Special attention will be paid to the procedure with respect to the top boundary condition, which is important for situations with ponded water layers or fluctuating groundwater levels close to the soil surface. Experiences with the numerical scheme and top boundary procedure have been obtained by many applications of the agrohydrological models SWATRE (*Feddes et al.*, 1978; *Belmans et al.*, 1983), SWACROP (*Kabat et al.*, 1992), and SWAP (*Van Dam et al.*, 1997; *Groen*, 1997; *Smets et al.*, 1997). We will describe the new numerical scheme and the top boundary condition procedure and show the scheme performance for extreme events of infiltration, soil evaporation and rapidly fluctuating groundwater levels close to the soil surface.

5.2   Model

5.2.1   Discretization of flow equation

Both finite difference and finite element methods are used to solve Richards' equation for variably saturated soil (*Feddes et al.*, 1988; *Celia et al.*, 1990; *Pan et al.*, 1996). In two- and three-dimensional flow domains, finite elements are advantageous at irregular geometries. In one dimension finite difference is advantageous because it needs no mass lumping to prevent oscillations (*Van Genuchten*, 1982; *Pan et al.*, 1996), and is more easy to conceive and to implement in numerical routines.

A popular method to solve Richards' equation has been the implicit, finite difference scheme with explicit linearization of hydraulic conductivity K, differential water capacity C, and root water extraction S, as described by *Haverkamp et al.* (1977) and *Belmans et al.* (1983):

$$\frac{h_i^{j+1} - h_i^j}{\Delta t^j} = \frac{K_{i-\frac{1}{2}}^j \left(\frac{\Delta h_{i-\frac{1}{2}}^{j+1}}{\Delta z_u} + 1 \right) - K_{i+\frac{1}{2}}^j \left(\frac{\Delta h_{i+\frac{1}{2}}^{j+1}}{\Delta z_\ell} + 1 \right)}{C_i^j \Delta z_i} - \frac{S_i^j}{C_i^j} \tag{5.1}$$

where subscript i is the node number (increasing downward), superscript j is the time level, and $\Delta t^j = t^{j+1} - t^j$. All the nodes, including the top and bottom node, are in the center of the soil compartments, with $\Delta z_u = z_{i-1} - z_i$, $\Delta z_\ell = z_i - z_{i+1}$, and Δz_i the compartment thickness (cm) (see Fig. 5.1). The spatial averages of K were calculated as geometrical means. The values of K, C and S were taken at the old time level j (explicit linearization), which made it possible to calculate the new pressure heads h_i^{j+1} simultaneously without iteration.

Three adaptations to above scheme were implemented to arrive at the new scheme that is currently applied in SWAP. The first adaptation is the handling of the differential water capacity C. In Eq. 5.1, C is present in the denominator of a fraction. As C equals zero in the saturated zone, the right hand side of Eq. 5.1 is not defined in the saturated zone, which limits the numerical scheme to the unsaturated zone. The saturated zone and fluctuations of the groundwater table had therefore to be modelled separately (*Belmans et al.*, 1983). The numerical scheme in the present SWAP has been modified in such a way that only
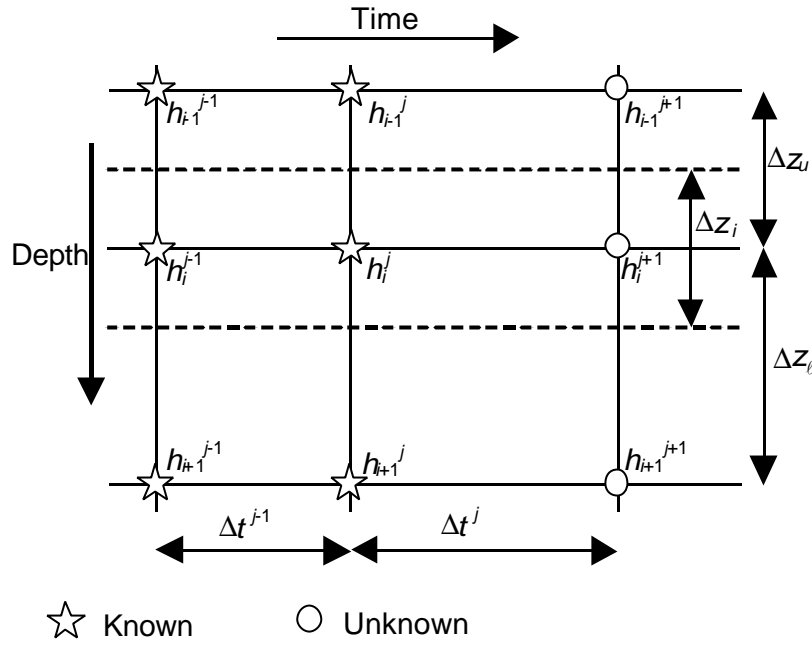
Figure 5.1 Spatial and temporal discretization used to solve Richards' equation.

multiplication with *C* occurs. Hence *the flow equation can be solved for the unsaturated and saturated zone simultaneously*, which is a big advantage.

The second adaptation concerns the temporal averaging of the *C* term. Because of the high non-linearity of *C*, averaging during a time step may result in serious mass balance errors when highly transient conditions are simulated. A simple but effective adaptation was made in SWAP, based on suggestions by *Milly* (1985) and further elaborated upon by *Celia et al.* (1990). Instead of applying during a time step

$$\boldsymbol{q}_i^{j+1} - \boldsymbol{q}_i^{j} = C_i^{j+\frac{1}{2}}\left(h_i^{j+1} - h_i^{j} \right) \tag{5.2}$$

where $C_i^{j+\frac{1}{2}}$ denotes some kind of average water capacity during the time step, which is generally unknown, we may use *the water content estimate at the new time level*, $\theta_i^{j+1,p-1}$, in the iterative solution:

$$\boldsymbol{q}_i^{j+1} - \boldsymbol{q}_i^{j} = C_i^{j+1,p-1}\left(h_i^{j+1,p} - h_i^{j+1,p-1} \right) + \boldsymbol{q}_i^{j+1,p-1} - \boldsymbol{q}_i^{j} \tag{5.3}$$

where superscript *p* is the iteration level and $C_i^{j+1,p-1}$ is the water capacity evaluated at the pressure head value of the last iteration, $h_i^{j+1,p-1}$. At convergence the term ($h_i^{j+1,p}$ - $h_i^{j+1,p-1}$) will be small, which eliminates effectively remaining inaccuracies in the evaluation of *C*. *Implementation of Eq. 5.3 requires an iterative solution of the equation matrix, but it results in a perfect water balance.*

The third adaptation concerns averaging of the hydraulic conductivity *K* between the nodes. *Haverkamp and Vauclin* (1979), *Belmans et al.* (1983) and *Hornung and Messing* (1983) proposed to use the geometric mean. In their simulations the geometric mean increased the accuracy of calculated fluxes and caused the fluxes to be less sensitive to changes in nodal

distance. However, the geometric mean has serious disadvantages too. When simulating infiltration in dry soils or high evaporation from wet soils, the geometric mean severely underestimates the water fluxes (*Warrick*, 1991) and may cause convergence problems of the iterative scheme due to steepening of the wetting front (*Zaidel and Russo*, 1992). Other researchers proposed to use the harmonic mean of K or various kind of weighted averages (*Warrick*, 1991; *Zaidel and Russo*, 1992; *Desbarats*, 1995; *Baker*, 1995; *Romano et al.*, 1998). In SWAP we selected instead *the arithmetic mean*, which will be argued in detail in the section of Simulation Results.

The implicit, finite difference scheme of Eq. 5.1, including the three adaptions, results in the following discretization of Richards' equation, as implemented in SWAP:

$$C_i^{j+1,p-1}\left(h_i^{j+1,p} - h_i^{j+1,p-1}\right) + q_i^{j+1,p-1} - q_i^j =$$

$$\frac{\Delta t^j}{\Delta z_i}\left[K_{i-\frac{1}{2}}^j\left(\frac{h_{i-1}^{j+1,p} - h_i^{j+1,p}}{\Delta z_u}\right) + K_{i-\frac{1}{2}}^j - K_{i+\frac{1}{2}}^j\left(\frac{h_i^{j+1,p} - h_{i+1}^{j+1,p}}{\Delta z_\ell}\right) - K_{i+\frac{1}{2}}^j\right] - \Delta t^j S_i^j \qquad (5.4)$$

In Eq. 5.4, K and S are still evaluated at the old time level j, as this decreases the number of iterations and provides an accurate solution at ordinary time steps of $10^{-6} < \Delta t^j < 0.2$ d. Calculations with SWAP show that in order to simulate infiltration and evaporation accurately, the distance between the nodes near the soil surface should be in the order of cm's. This advocates the *use of a variable node spacing* in the soil profile. Application of Eq. 5.4 to each node, including the prevailing boundary conditions, results in a tri-diagonal system of equations which can be solved efficiently (*Press et al.*, 1989). Appendix B lists the equations for the top, intermediate and bottom nodes, both for head and flux type boundary conditions. The numerical solution of the equation matrix renders the soil water pressure heads in the unsaturated and saturated zone simultaneously. Starting in the saturated zone, the phreatic groundwater table is simply found at $h = 0$. Also perched water tables, which may form above less conductive layers in the soil profile, are determined in this way.

The convergence criterion used to be a maximum pressure head difference $|h_i^{j+1,p} - h_i^{j+1,p-1}|$ in the iterative solution of Eq. 5.4. *Huang et al.* (1996) proposed to use the *water content difference* $|\theta_i^{j+1,p} - \theta_i^{j+1,p-1}|$ instead. The advantage of a criterion based on θ is that the criterion is more sensitive in pressure head ranges with a large differential soil water capacity, while it allows less iterations at low h-values, where soil water fluxes are minor but large steps of pressure head may occur. *Huang et al.* (1996) showed the higher efficiency of the θ-criterion for a large number of infiltration problems. Moreover, the θ-criterion was found to be more robust when the soil hydraulic characteristics are extremely non-linear. This θ-criterion was implemented in SWAP in 1994 and our experiences thus far are very positive. Simulations are performed in less time, without sacrificing mass balance accuracy. An extra criterion is needed for saturated conditions, where θ remains constant. At nodes in the saturated zone, the convergence criterion switches to maximum pressure head differences between iterations, $|h_i^{j+1,p} - h_i^{j+1,p-1}|$.

The variable, optimal time step should minimize the computational effort of a simulation. The number of iterations needed to reach convergence in the former time step, N_{it}, can effectively be used to derive the optimal time step (*Kool and Van Genuchten,* 1991). In case of a large number of iterations, many calculations are needed to reach convergence, and the time step is too large. In case of a small number of iterations, much less calculations are needed for convergence, and the time step can be increased. We therefore apply presently the following criteria :

$N_{it} < 2$: multiply the time step with a factor 1.25

$2 \leq N_{it} \leq 4$: keep the time step the same

$N_{it} > 4$: divide the time step by a factor 1.25

SWAP determines the actual time step using above criteria in combination with an initial time step, times at which a significant change of precipitation intensity occurs, times for output, and specified minimum and maximum time steps. If after 6 iterations no convergence is reached in the numerical solution of Richards' equation, the time step is divided by 3, and the iterative solution of Richards' equation starts again. This may continue until the minimum time step is reached.

5.2.2 Top boundary condition

At moderate weather and soil wetness conditions, the soil top boundary condition is flux-controlled. In case of very wet weather or soil conditions, water may collect on the soil surface, after which the hydraulic head of the ponding water starts to govern the infiltration flux. In case of prolonged dry weather or soil conditions, the soil water pressure head at the soil surface becomes equal to the air humidity and starts to govern the soil evaporation flux.

An appropriate procedure for the top boundary conditions during the iterative solution of Richards' equation may determine the success or failure of a numerical scheme. The soil water pressure heads may change very rapidly near the soil surface. For instance in case of irrigation or rainfall after a dry period, the soil water pressure head may increase in a few minutes from -10^6 to 0 cm. Also when saturated soils become unsaturated, the pressure head distribution near the soil surface changes rapidly because of the small differential water capacity near saturation of most soils. Moreover, the top boundary condition may switch from head-controlled to flux-controlled and vice versa during the iterative solution of Richards' equation.

At flux-controlled conditions, we may define the soil surface flux density q_{sur} (cm d^{-1}), and at head-controlled conditions the soil surface pressure head h_{sur} (cm). Soil water fluxes are considered positive when they are directed upward. Figure 5.2 shows the decision procedure developed by the present author and currently used in SWAP. Criterion <1> considers if the soil column is saturated. If so, Criterion <2> determines whether at the end of the time step, the soil column is still saturated or becomes unsaturated. The inflow Q_{in} (cm) during the time step is calculated as:

$$Q_{in} = \left(q_{bot} - q_{top} - q_{root} - q_{drain} \right) \Delta t^{j} \tag{5.5}$$
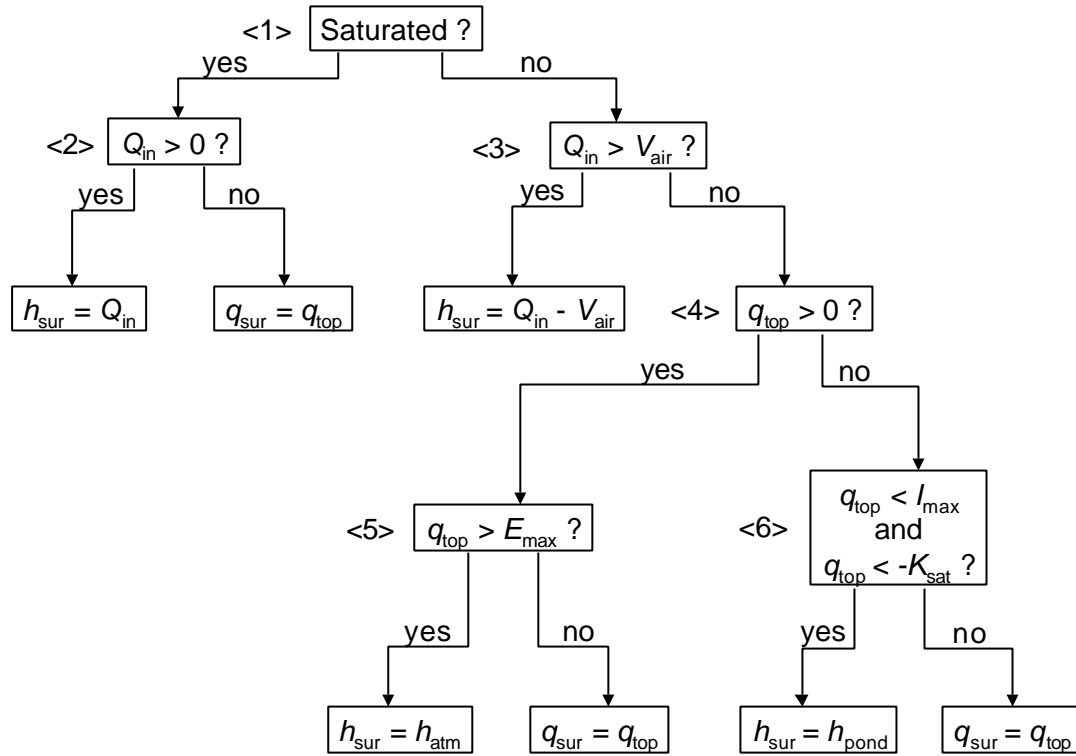
Figure 5.2 Procedure to select head (h_{sur}) or flux (q_{sur}) top boundary condition. The variables are explained in the text.

where q_{bot} is the flux density at the soil profile bottom (cm d^{-1}), q_{top} the potential flux density at the soil surface (cm d^{-1}), q_{root} the water flux density extracted by roots (cm d^{-1}), and q_{drain} the lateral flux density to drains or ditches (cm d^{-1}). The potential flux density at the soil surface q_{top} follows from:

$$q_{top} = q_{eva} - q_{prec} - q_{irrig} - \frac{h_{pond}}{\Delta t^{j}} \qquad \text{with} \qquad q_{top} \geq I_{max} \qquad (5.6)$$

where q_{eva} is the actual soil evaporation (cm d^{-1}), q_{prec} is the precipitation rate at the soil surface (cm d^{-1}), q_{irrig} is the applied irrigation flux density (cm d^{-1}), h_{pond} is the height of water ponding on the soil surface at the old time level t^{j} (cm), and I_{max} is the maximum soil water flux density at the soil surface. The last term at the right hand side of Eq. 5.6 equals the maximum amount of infiltration due to ponded water. I_{max} (cm d^{-1}) is calculated according to Darcy as:

$$I_{max} = K_{\frac{1}{2}} \left(\frac{h_{pond} - h_1^{j+1,p-1} - z_1}{z_1} \right) \qquad (5.7)$$

where the subscript 1 refers to the node in the center of the first compartment, and $K_{\frac{1}{2}}$ is the average hydraulic conductivity between the soil surface and z_1.

If inflow Q_{in} is positive, during the time step more water will enter than leave the soil profile (Criterion 2). In that case the soil profile remains saturated and a head condition applies, which is equal to Q_{in}. By defining q_{top} according to Eq. 5.6, Q_{in} includes ponding water amounts from earlier time steps. If inflow Q_{in} is negative, the soil profile becomes unsaturated and a flux condition applies, which is equal to q_{top}.

When the soil column is unsaturated, Criterion <3> determines whether the soil column will remain unsaturated or will become saturated during the time step. The symbol V_{air} (cm) denotes the air volume in the soil profile, which follows from the difference between saturated and actual water contents. If the soil becomes saturated ($Q_{in} > V_{air}$), a head condition applies, which is equal to Q_{in} - V_{air}. If the soil remains unsaturated ($Q_{in} < V_{air}$), Criterion <4> distinguishes between evaporation ($q_{top} > 0$) and infiltration ($q_{top} \leq 0$). In case of evaporation, the maximum flux density is limited to the maximum flux density according to Darcy, E_{max} (cm d^{-1}):

$$E_{max} = K_{\frac{1}{2}} \left(\frac{h_{atm} - h_1^{j+1,p-1} - z_1}{z_1} \right) \tag{5.8}$$

with h_{atm} the soil water pressure head in equilibrium with the prevailing air humidity (cm). If $q_{top} > E_{max}$ a head condition applies with $h_{sur} = h_{atm}$, else the flux condition $q_{sur} = q_{top}$ applies (Criterion 5).

In case of infiltration, a head-controlled condition applies, if the potential flux density q_{top} exceeds the maximum infiltration rate I_{max} as well as the saturated hydraulic conductivity K_{sat} (Criterion <6>). The extra condition of $q_{top} < -K_{sat}$ stabilizes the iterative procedure, as I_{max} according to Eq. 5.7 is only a first order approximation.

During the iterative procedure of calculating $h_i^{j+1,p}$, the top boundary condition is updated at each iteration p. Appendix B describes how the flux- and head-type boundary conditions are imposed at the first compartment.

5.3   Numerical experiment

The performance of this numerical scheme will be shown for three illustrative, extreme conditions at bare soils of sand and clay:

1 Intensive rain at a dry soil. The rainfall rate was 1000 mm d^{-1} during 0.1 day. The initial conditions were very dry, with $\theta = 0.1$ for sand and $h = -16000$ cm for clay. The infiltration capacity of both soils will be exceeded during the storm and the main part of the rainfall becomes runoff.

2 High evaporation at a wet soil. The potential evaporation amounted 5 mm d^{-1}, the initial h was -200 cm for both soils. After some time the maximum soil water flux starts to limit the evaporation rate.

3 Groundwater levels fluctuating near soil surface. At 2 consecutive days intensive rain storms of 40 mm with a duration of 0.1 d occurred on both soils with the initial groundwater level at 20 cm below the soil surface. No runoff was allowed, so precipitation in excess of the infiltration rate accumulated on top of the soil profile. During the storm, the groundwater level rose above soil surface. After the storm, the groundwater level gradually descended below soil surface. To achieve this, at the bottom of the soil profile ($z = -40$ cm) a constant downward flux density of 40 mm d^{-1} was adopted. The drainage amount of the total day was thus equal to the amount of rainfall during one storm.

The soil hydraulic functions $\theta(h)$ and $K(\theta)$ were described by the Mualem-Van Genuchten model (Eqs. 2.15 and 2.16). The input parameters were derived from a national Dutch soil catalogue (*Wösten et al.*, 1994) and are listed in Table 5.1. For both soils the hydraulic functions are strongly non-linear. The sand is well-sorted and loses water quickly in the pressure head range $-200 < h < -20$ cm. The clay soil shows a sharp drop of the hydraulic conductivity K below saturation. At saturation, K equals 15.50 cm d^{-1}, while at $h = -1$ cm, K has decreased to 0.73 cm d^{-1} already. As soon as $h < 0$, water is extracted from the macro pores present in the clay and K decreases sharply to the hydraulic conductivity of the clay matrix.

Table 5.1. Mualem-Van Genuchten parameters of the soils considered.

Soil	α (cm^{-1})	n (-)	θ_{res} (-)	θ_{sat} (-)	K_{sat} (cm d^{-1})	λ (-)
Sand	0.0249	1.507	0.01	0.43	17.5	-0.140
Clay	0.0532	1.081	0.00	0.55	15.5	-8.823

In all three cases we varied the nodal distance from 0.1 to 5 cm and applied both arithmetic and geometric averaging of K, as summarized in Table 5.2 (simulations S1-S4). At simulation S5, only the first 5 compartments have a thickness of 1 cm, the remaining compartments are 5 cm thick. The deviations due to discretization were also compared to the effects of hysteresis and spatial variability on soil water fluxes. For hysteresis (S6) the scaling concept as applied by *Scott et al.* (1983) and *Kool and Parker* (1987) was used (see Chapter 6). The main wetting branch was described by the parameter set (α_{wet}, n, θ_{res} and θ_{sat}) with $\alpha_{wet} = 2\alpha$ (Table 5.1). For spatial variability (S7) the similar media concept of *Miller and Miller* (1956), as described in Chapter 2, was followed. *Hopmans and Stricker* (1989) derived the distribution of scale factors of a 650 ha catchment with sandy soils in The Netherlands (Hupselse Beek). In this distribution, a scale factor of 2.25 corresponds to a 95 % soil, e.g. 5 % of the soils in the area have a more coarse texture. This scale factor was used for both the sand and the clay soil.

Table 5.2. Nodal distance, method of K-averaging and remarks of the simulations performed. For all simulations the minimum time step was 10^{-6} d, the maximum time step 0.2 d and the convergence criterium $|\theta_i^{j+1,p} - \theta_i^{j+1,p-1}| < 0.0001$. The reference simulation is denoted R.

Simulation	Nodal distance (cm)	Averaging K	Remarks
R	0.1	arithmetic + geometric	-
S1	1	arithmetic	-
S2	1	geometric	-
S3	5	arithmetic	-
S4	5	geometric	-
S5	1 and 5	arithmetic	upper 5 nodes $\Delta z_i = 1$ cm, others $\Delta z_i = 5$ cm
S6	1	arithmetic	hysteresis ($\alpha_{wet} = 2\alpha$)
S7	1	arithmetic	scaling (coarse 95%)

Theoretical solutions of Richards' equation are needed to evaluate the accuracy of the numerical scheme. Unfortunately, at the specified top boundary conditions the Richards' equation in combination with the Mualem-van Genuchten model for the soil hydraulic functions cannot be solved analytically. However, we may derive the theoretically correct solution by the numerical model itself. *By decreasing the nodal distance in combination with a strict convergence criterion, the hydraulic gradient and the average K will converge to the theoretical value. Whatever method of K-averaging is used, simulations converge to the same solution.* This was confirmed in the simulations considered. The reference solution R as listed in Table 5.2 is derived for a nodal distance $\Delta z_i = 0.1$ cm and a convergence criterion of $|\theta_i^{j+1,p}$ - $\theta_i^{j+1,p-1}| < 0.0001$. Smaller nodal distances and a more strict convergence criterion hardly affected the simulated soil water fluxes . In case of the fine temporal ($\Delta t^j \approx 10^{-6}$ d) and spatial discretization ($\Delta z_i \approx 0.1$ cm), the mass balance showed no accumulation of rounding-off errors in the numerical calculations. An independent check of the reference solution R was performed by using the detailed finite element model HYSWASOR (*Dirksen et al.*, 1993) with the same small nodal distances. Both SWAP and HYSWASOR showed the same reference solution R.

Note that adopting a more strict convergence criterion without decreasing the spatial discretization, is insufficient to derive the reference solution R. Although a very strict convergence criterion may result in a perfect mass balance due to Eq. 5.3, a large nodal distance will still cause the calculated Darcy fluxes to deviate from the theoretical Darcy fluxes (*Milly*, 1985; *Warrick*, 1991). The difference is caused by the linear approximation of the hydraulic head gradient $\partial(h + z) / \partial z$ and by the approximation of the spatial average *K* between the nodes.

5.4   Simulation results

Tables 5.3 and 5.4 show the simulated amounts of infiltration and evaporation for both the sand and the clay. We will discuss the results of the sandy soil, as the differences between the simulations are more pronounced at this soil. However the simulations S1-S7 show the same trend for the sand and clay soil.

Table 5.3. Cumulative infiltration (mm) of the simulations listed in Table 5.2 for the simulation *infiltration under intensive rain* .

Simulation	Sand	Clay
R	39	21
S1	40	23
S2	37	18
S3	47	30
S4	27	13
S5	42	24
S6	32	21
S7	94	79

Table 5.4. Cumulative evaporation (mm) of the simulations listed in Table 5.2 for the simulation *high evaporation demand*.

Simulation	Sand	Clay
R	11	12
S1	11	12
S2	4	11
S3	18	19
S4	1	12
S5	11	12
S6	11	12
S7	7	14

5.4.1 Intensive rain at a dry soil

At the reference case R, until t = 0.008 d, the hydraulic head gradient at the soil surface is large enough to absorb the high rain flux density of 1000 mm d^{-1}, as shown in Figure 5.3. At t = 0.008 d, h at the soil surface becomes zero and the flux condition is replaced by a head condition (h_{sur} = 0.0 cm). Gradually the infiltration rate declines, ultimately to the value of K_s = 175 mm d^{-1}. The total amount of infiltration is 39 mm out of 100 mm of rainfall (Table 5.3), the remaining amount is runoff. In general, use of arithmetic averages results in larger hydraulic conductivities and thus larger soil water fluxes than use of geometric averages. In case of Δz_i = 5 cm, arithmetic averages of K seriously overestimate the infiltration rate (S3: 47 mm) while geometric averages seriously underestimate the infiltration rate (S4: 27 mm). The very steep wetting front due to low geometric K-averages causes infiltration rate oscillations at S2 and S4. These oscillations gradually decrease when smaller nodal distances are used, but convergence to the final solution is relatively slow (Figure 5.3). Harmonic means (not shown here) underestimate the mean K at the wetting front and the infiltration rate even more than the geometric mean. However, *in case of arithmetic averages with $Dz_i = 1$ cm (S1), the calculated infiltration rate is close to that of the reference simulation R.*
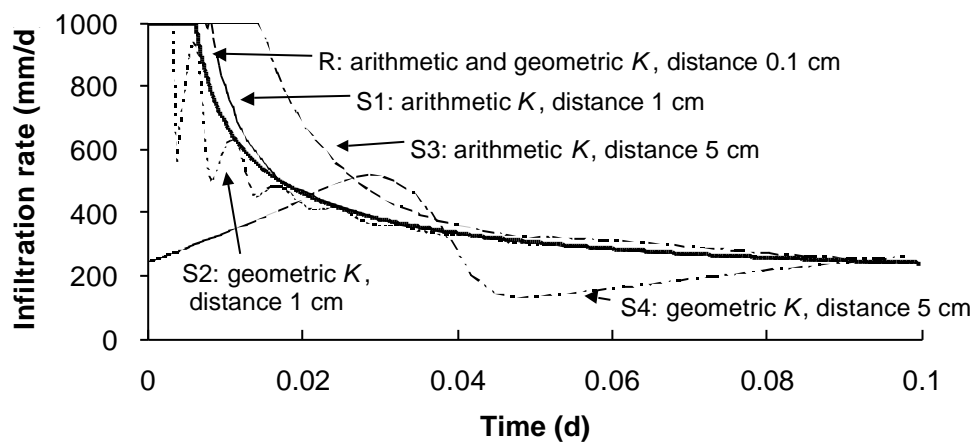
Figure 5.3 Infiltration rate of sand for simulations R and S1-S4 (Table 5.2) in case of *intensive rain at a dry soil*, showing the effect of nodal distance and K-averaging.

To obtain proper results, the nodal distance needs only to be smaller near the soil surface, as is shown for S5. Although only the first 5 compartments have $\Delta z_i = 1$ cm, the cumulative infiltration is 42 mm, compared to 39 mm for reference R (Table 5.3). The infiltration curve of S5 is very close to that of S1 in Figure 5.3. In case of hysteresis (S6), the infiltration decreases from 40 to 32 mm. If we change the soil texture to a 95 % coarse sand (S7), 94 mm infiltrates in stead of 40 mm! Thus the deviations due to the numerical discretization at $\Delta z_i = 1$ cm and with arithmetic averages of K, are considerably less than the deviations caused by hysteresis and horizontal spatial variability of soil hydraulic functions.

5.4.2 High evaporation at a wet soil

Figure 5.4 shows the simulated actual evaporation rate of sand for R and S1-S4. At the reference case R, initially the potential soil water flux is large enough to meet the potential soil evaporation rate ($q_{sur} = 5$ mm d^{-1}). At $t = 1.1$ d the upper boundary condition changes from flux- to head-controlled ($h_{sur} = h_{atm}$) and the evaporation rate gradually decreases. After 5 days, the cumulative actual evaporation amounts 11 mm (Table 5.4), while the cumulative potential evaporation equals 25 mm. The nodal distance and the type of K-averaging has a large effect on the evaporation rate. Similar to infiltration, geometric averaging underestimates the soil water flux, while arithmetic averaging overestimates the soil water flux. Choosing a nodal distance of 1 cm, results in (see Table 5.4) a cumulative evaporation of 11 mm for arithmetic averaging (S1) and of 4 mm for geometric averaging (S2), compared to 11 mm for the reference (R). The low evaporation in case of geometric averaging is caused by the low conductivity for the sand at $h_{atm} = -1377$ m. Also when Δz_i is decreased to 0.1 cm, cumulative evaporation for the geometric mean still equals 4 mm, compared to 11 mm for arithmetic mean. In this case no convergence was achieved between geometric and arithmetic averaging, which we attribute to the very low conductivity of sand at pressure heads near h_{atm}. Harmonic means of K underestimate the evaporation rate even more severely than geometric means. Increase of the nodal distance at larger soil depth is allowed, as simulation S5 gives the same results as S1.
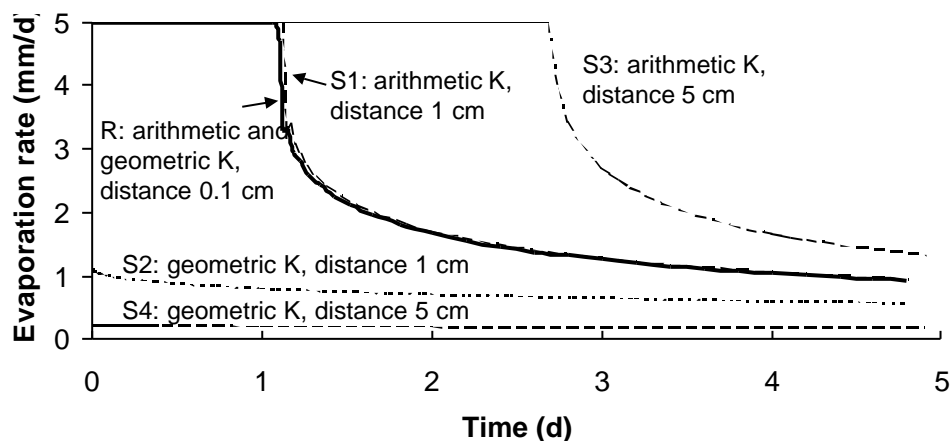
Figure 5.4 Evaporation rate of sand for simulations R and S1-S4 (Table 5.2) in case of *high evaporation at a wet soil*, showing the effect of nodal distance and *K*-averaging.

Hysteresis (S6) hardly affects the evaporation process. Under conditions of spatial variability (S7), the 95 % coarse sand evaporates 7 mm in stead of 11 mm. Hysteresis and spatial variability thus affect evaporation fluxes relatively less than infiltration fluxes. However the effects of hysteresis and spatial variability on simulated evaporation fluxes are larger than the effects of numerical discretization using $\Delta z_i = 1$ cm and arithmetic averages of K.

5.4.3   Groundwater levels fluctuating near soil surface

Heavy rain (40 mm in 0.1 d) is simulated at a sandy soil with initial groundwater level at 20 cm depth. Figure 5.5 shows the initial infiltration rate for $0 < t < 0.04$ day. The way of averaging K and the nodal distance near the surface (S1 - S4) had a minor effect on the infiltration rate. At $t = 0.003$ d, I_{max} becomes less than 400 mm/d. Therefore at the upper boundary the flux-type condition ($q_{sur} = 400$ mm/d) is replaced by a head-type condition ($h_{sur} = Q_{in}$). At $t = 0.014$ d, the soil profile becomes saturated and the infiltration rate declines sharply to the flux density at the soil profile bottom (40 mm d^1). Also hysteresis (S6) had hardly effect on the infiltration pattern, in contrast to the 95% coarse soil (S7). At S7 the infiltration rate is maximal until $t = 0.024$ d, when the soil is almost saturated. Starting in both cases from hydrostatic equilibrium with groundwater level at 20 cm depth, more water is needed to saturate the more coarse soil.
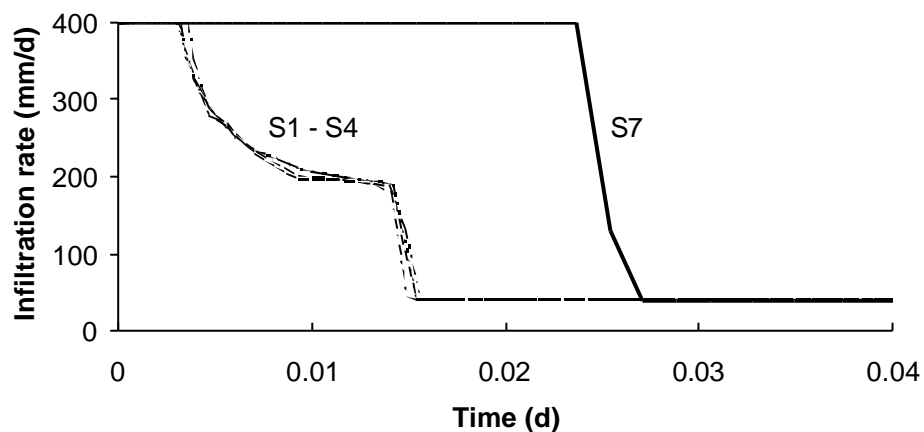
Figure 5.5 Infiltration rate of sand for simulations S1-S4 and S7 (Table 5.2) in case of *groundwater levels fluctuating near soil surface*, showing the effect of nodal distance, *K*-averaging and soil texture.

Figure 5.6 shows the groundwater level and infiltration rate of S1 and S7 for the total period of 2 days. The 2 rain showers of 40 mm occur at $0.0 < t < 0.1$ d and $1.0 < t < 1.1$ d. At t = 0.91 (S1) and 0.77 d (S7) the ponded water of the first shower has infiltrated into the sand soil. The numerical scheme solved the rapid pressure head change at the transition from saturated to unsaturated conditions without problems. At the end of the first day, the groundwater levels return gradually to their original level. In case of the more coarse sand (S7), the groundwater level rises more slowly and the ponding height is less as more water can be stored in the soil profile (Figure 5.6). The second day shows the same pattern.
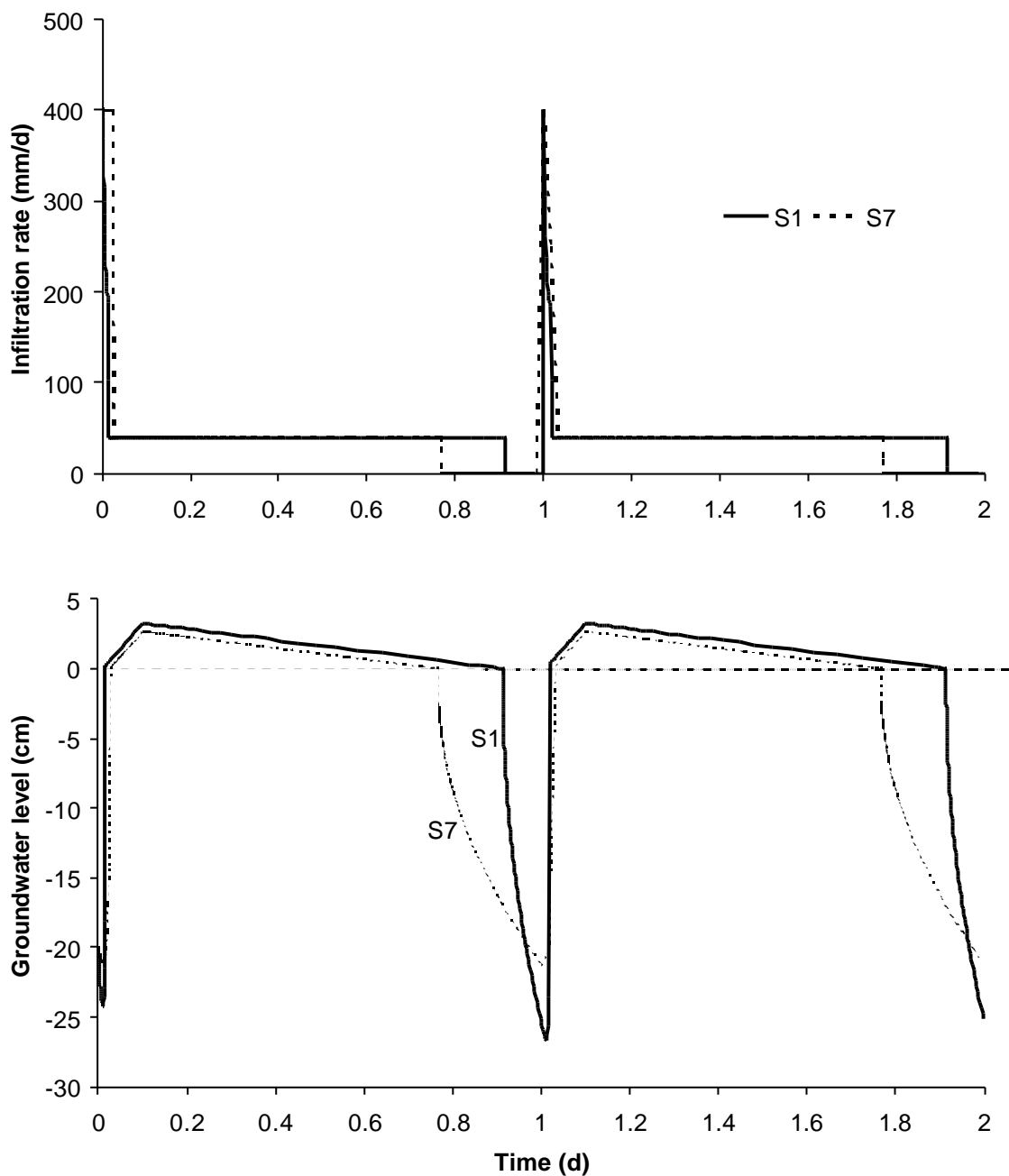
Figure 5.6 Infiltration rate and groundwater level of sand for simulations S1 and S7 (Table 5.2) in case of *groundwater levels fluctuating near soil surface*, showing the effect of soil texture.

At the clay soil a similar pattern can be shown. The water balance was closed for all simulations. The simulations illustrate that in case of shallow fluctuating groundwater levels, the transition from unsaturated to saturated soil profile and vice versa, and from flux controlled to head controlled and vice versa, is correctly simulated under extreme field conditions. Former numerical schemes failed to provide reliable results in the shown cases.

5.5   Concluding remarks

Reliable numerical schemes of Richards' equation are needed in order to use numerical soil water flow models in research and policy analysis routinely. In this paper an implicit, finite difference scheme is discussed, which applies simultaneously to the unsaturated and saturated zone and which is relatively easy to comprehend and implement in numerical models. The convergence criteria, in combination with the iterative solution of the capacity term as suggested by *Milly* (1985) and *Celia et al.* (1990) result in a closed water balance.

The simulation results show that nodal distances of 5 cm or more may seriously over- or underestimate infiltration and evaporation fluxes at the soil surface in case of arithmetic and geometric averages of the hydraulic conductivity. In two-dimensional problems we tend to work with relatively large grid sizes, which may have a large influence on the calculated boundary fluxes, especially at the soil surface.

At fine nodal grid, spatial averaging of *K* with arithmetic means performs better than geometric means. This supports the use of arithmetic averages in commonly applied finite element numerical schemes (*Kool and Van Genuchten*, 1991; *Šimunek et al.*, 1996, 1998b). However, the soil water fluxes near the soil surface will only be accurate when a nodal distance of about 1 cm is used.

When using nodal distances $\leq$ 1 cm as well as arithmetic averages of *K*, the effects of numerical discretization in extreme infiltration and evaporation events are less than typical effects of hysteresis and spatial variability. This suggests that in one-dimension further improvement of the numerical discretization schemes with various kind of weighting functions for *K* is less important than the incorporation of hysteresis and spatial variability of the soil hydraulic functions.

Romano et al. (1998) show that inaccuracies due to *K*-averaging may also occur at sharp texture transitions within the soil profile. Refinement of the nodal grid near these texture transitions with the described scheme, or application of the algorithm presented by *Romano et al.* (1998), may improve the simulation results near these transitions.

A proper procedure for the top boundary condition during the iterative solution of Richards' equation may determine the success or failure of a numerical scheme when simulating field conditions. The discussed procedure allows to calculate accurately infiltration and runoff, reduced soil evaporation and transitions from saturated to unsaturated soil and vice versa. In this paper three illustrative cases with extreme field conditions are discussed at which former numerical schemes failed. Recently, *Miller et al.* (1998) described a test case with sudden ponding of water on a relatively dry soil, which poses problems to many currently used numerical schemes of Richards' equation. We simulated this test case with the presented numerical scheme and encountered no problems.

The calculation time should be small if a large number of simulations are performed, e.g. at long term simulations, in regional studies or in case of parameter optimization. The run of an ordinary year with SWAP using an ordinary PC (Pentium 200 MMX PC) takes about 15 seconds. Further reduction of the calculation time might be achieved by transformation of the soil water pressure head (*Pan and Wierenga*, 1995) or by Hermite spline interpolation of discretized soil hydraulic functions (*Miller et al.*, 1998).

6. Simulation of water and solute movement in hysteretic and water repellent soils[5]

6.1   Introduction

Richards' equation is very useful to analyse soil water fluxes in variably saturated soils. Current numerical schemes are able to solve this equation with strongly non-linear soil hydraulic functions and at rapidly changing boundary conditions, as discussed in Chapter 5. However, still some factors may complicate straight-forward application of Richards' equation to field soils. Among these factors are hysteresis of the soil hydraulic functions, and preferential flow due to water repellency.

Hysteresis of the soil hydraulic functions occurs mainly in the relation between soil water content θ and soil water pressure head h. The relation between soil hydraulic conductivity K and θ is more uniquely defined (*Topp*, 1969; *Vachaud and Tony*, 1971). Because of hysteresis in the $\theta(h)$ relation, also the $K(h)$ relation shows hysteresis. The occurrence of various θ at the same h, is caused by variations of the pore diameter (inkbottle effect), differences in radii of advancing and receding meniscus, entrapped air and swelling/shrinking processes (*Hillel*, 1980). Gradual desorption of an initially saturated soil sample gives the main drying curve, while slow absorption of an initially dry sample results in the main wetting curve (Fig. 6.1). In the field partly wetting and drying occurs in numerous cycles, resulting in so-called drying and wetting scanning curves lying between the main drying and the main wetting curve (*Dirksen et al.*, 1993). In simulation practice, often only the main drying curve is used to describe the $\theta(h)$ relation. This is mainly due to the time and costs involved in measurement of the complete $\theta(h)$ relationship, including the main wetting, the main drying and the scanning curves, especially in the dry range. For instance, a generally applied soil hydraulic data base in The Netherlands, known as the Staring series (*Wösten et al.*, 1994), contains only $\theta(h)$ data of the main drying curve. Nevertheless, it is obvious that the simulation of infiltration events with the main drying curve can be inaccurate. *Kaluarachchi and Parker* (1987) showed that during infiltration the type of boundary condition at the soil surface determines the effect of hysteresis. A head-type boundary condition at the soil surface has more influence than a flux-type boundary condition. *Dirksen* (1987) could not explain his detailed experimental data on root water uptake in saline conditions without taking into account hysteresis. *Hopmans et al.* (1991) showed in case of trickle and furrow irrigation that hysteresis affects the water balance, although these effects were overwhelmed by spatial variability of the soil hydraulic functions.

---

[5] *Adapted from (1) Van Dam, J.C., J.M.H. Hendrickx, H.C. van Ommen, M.H. Bannink, M.Th. van Genuchten, and L.W. Dekker, 1990. Water and solute movement in a coarse-textured water repellent field soil. J. Hydrol., 120, 359-379. (2) Van Dam, J.C., J.H.M. Wösten, and A. Nemes, 1996. Unsaturated soil water movement in hysteretic and water repellent field soils. J. Hydrol., 184, 153-173.*
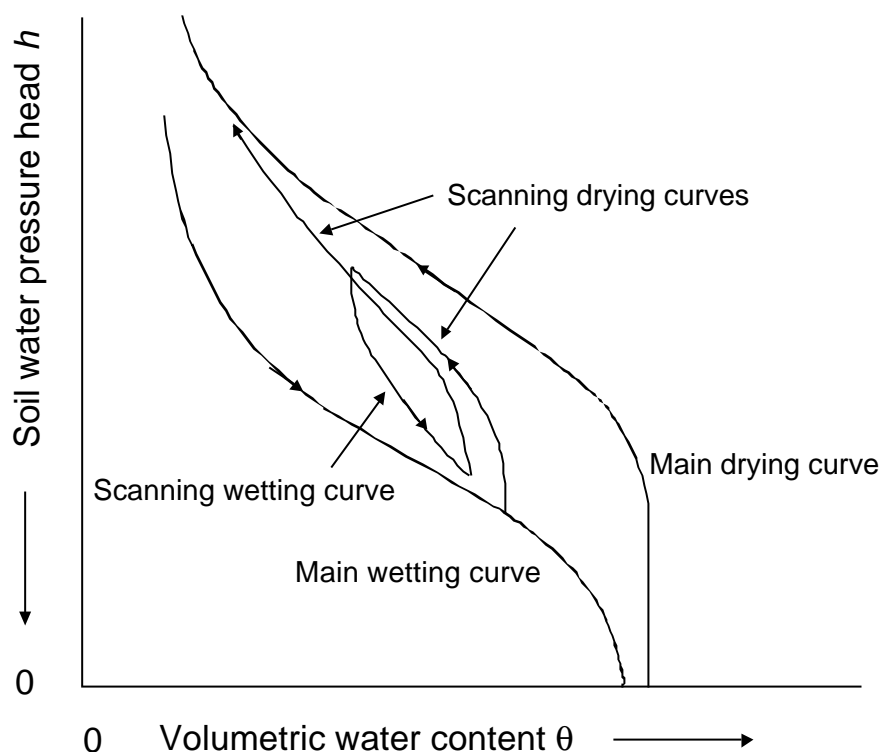
Figure 6.1 Water retention function with hysteresis, showing the main wetting, main drying and scanning curves.

To circumvent the tedious laboratory analysis, empirical hysteresis models with a limited number of parameters have been developed. *Jaynes* (1984) compared four of these models, which use the main wetting and main drying curve to generate scanning curves. None of the models was consistently better than the others for simulating primary wetting or drying curves for three test soils. Also each model performed equally well when used as part of a numerical model for simulating hysteretic flow. *Scott et al.* (1983) derived scanning curves by rescaling the main wetting or the main drying curve to the actual water content. Among others, *Kool and Parker* (1987) obtained acceptable results with Scott's method in the case of eight soils. The scaling method of Scott has been implemented into SWAP.

Another factor which may complicate application of Richards' equation, is water repellency. Water repellent field soils can be found in many parts of the world under a variety of climatic conditions (*DeBano*, 1981; *Dekker et al.*, 1999). For example, water drop penetration time tests of the former Dutch Soil Survey Institute revealed that more than 75% of the agricultural top soils in The Netherlands are moderately to extremely water repellent, whereas more than 95% of the top soils in nature reserves exhibit strong to extreme water repellency (*Dekker and Ritsema*, 1994). Water repellency is attributed to organic coatings of soil particles, to organic matter and to specific micro flora. Numerous laboratory and field studies have been conducted to investigate the physics of fluid flow in water repellent soils (e.g. *Jamison*, 1945; *Meeuwig*, 1971; *DeBano*, 1981; *Letey et al.*, 1975; *Burch et al.*, 1989; *Hendrickx et al.*, 1993; *Ritsema et al.*, 1993; *Larsson et al.*, 1999). These indicate that infiltration rates into water repellent soils can be considerably lower than those into wettable soils, and that wetting patterns in water repellent

soils can be quite irregular and incomplete. The studies also suggest that water repellency has its greatest effect in relatively dry soils. As a result of water repellency, water often flows through these soils in preferential paths or 'fingers'. Fingers have also been observed when water percolates from a fine-textured into a coarse textured layer, in the case of low rainfall intensity, or when the air pressure increases ahead of the infiltration front (*Raats*, 1973; *Hillel*, 1987). Among others, the fingering process was studied in the laboratory by *Hill and Parlange* (1972), *White et al*. (1977), *Diment and Watson* (1985), *De Rooij* (1996), *Whang et al*. (1998a), *Carrilo et al*. (1999), *De Jong et al*. (1999) and *Schoen et al*. (1999); and in the field by *Starr et al*. (1978), *Flury et al*. (1994), *Dekker* (1998), and *Ritsema* (1998). Theoretical analyses were attempted by *Raats* (1973), *Philip* (1975), *Parlange and Hill* (1976), *Diment and Watson* (1983), *Glass et al*. (1989), *Liu et al*. (1994), *Whang et al*. (1998b) and *Nguyen et al*. (1999).

Preferential flow obviously affects the leaching of nutrients, salts and pesticides, as the soil water flow bypasses large soil volumes. This might be simulated with a dual-porosity model as has been used for macropores in structured soils (*Gerke and Van Genuchten*, 1993; *Saxena et al*., 1994). However, the water exchange between the two domains in the case of water repellent soils is difficult to simulate. Field observations show a time dependent preferential flow path volume (*Ritsema and Dekker*, 1994), which can not be included in ordinary dual-porosity models. Also, dual-porosity models require twice as many soil physical parameters as single porosity models.

Another approach is to divide the soil into mobile and immobile parts, whose volumes may vary with time. A constant mobile-immobile concept has been used to explain accelerated breakthrough in the case of steady state solute transport (*De Smedt and Wierenga*, 1979; *Van Genuchten and Wagenet*, 1989). *Saxena et al*. (1994) applied successfully the dual-porosity concept to lysimeters with structured soil, and the mobile-immobile concept to lysimeters with unstructured soil, in order to interpret transient tracer breakthrough experiments. Because of its versatility, the mobile-immobile concept has been implemented into the SWAP model.

In this Chapter we will describe the concepts for hysteresis and water repellency which are implemented in SWAP. Next these concepts are applied to experiments on transient soil water flow and bromide transport in two hysteretic and water repellent, sandy field soils.

6.2   Concepts

6.2.1   Hysteresis

The main drying and main wetting curve should be measured in the laboratory and are described analytically with the Mualem-van Genuchten parameters (α, n, θ_{res}, θ_{sat}, K_{sat}, and λ) according to Eqs. 2.15 and 2.16. Some of the parameters describing the main wetting and main drying curve are related. We will assume θ_{res} and θ_{sat} to be equal for both curves. In general θ_{sat} will be somewhat less than porosity due to air entrapment under field conditions with intensive rainfall. Usually the $K(\theta)$ function shows only minor hysteresis effects. As Eq. 2.16 shows, this can be
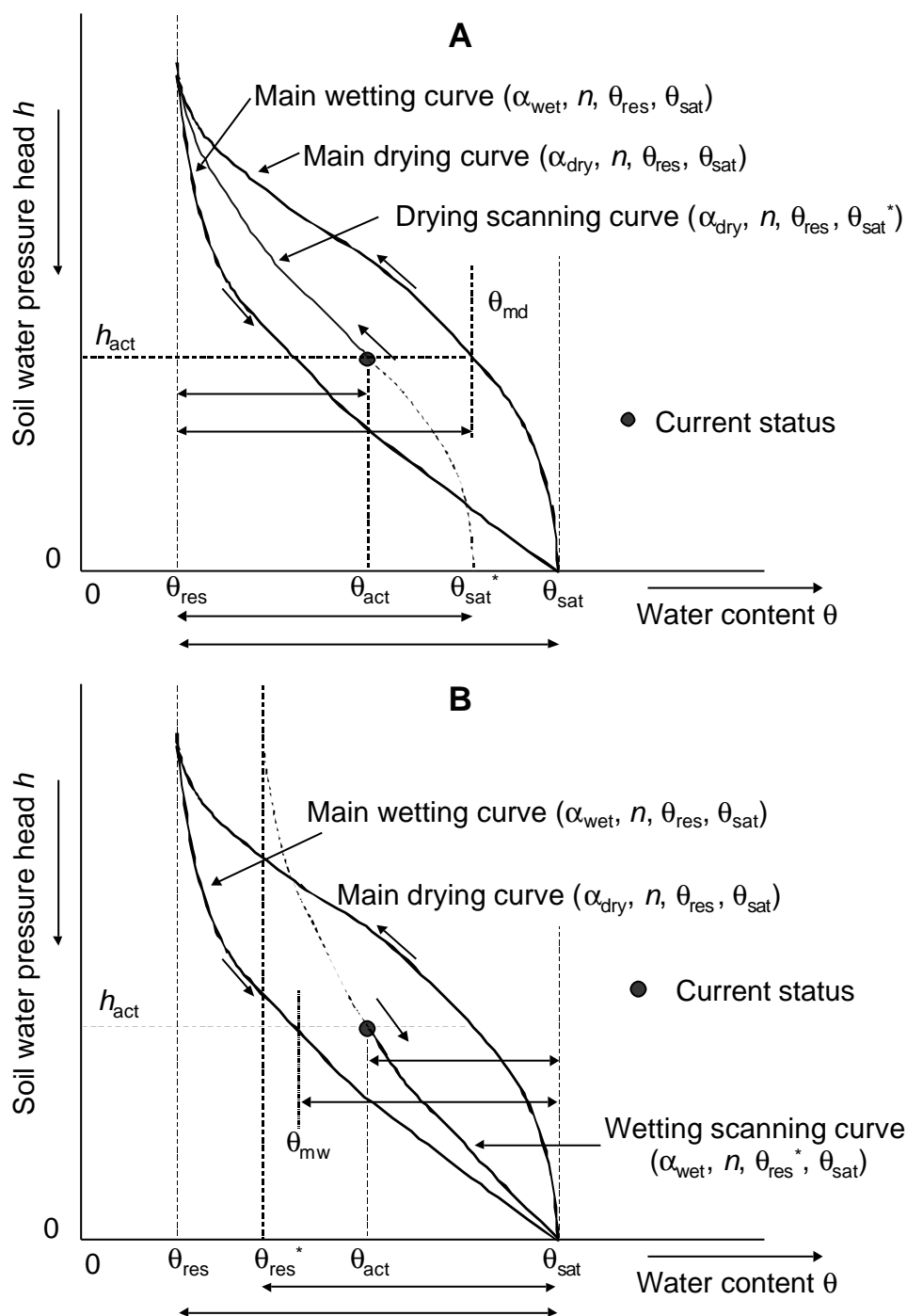
Figure 6.2 (A) Linear scaling of the main drying water retention curve in order to derive a drying scanning curve; (B) linear scaling of the main wetting water retention curve in order to derive a wetting scanning curve.

achieved by choosing for the main wetting and main drying curve a common value for n. Ultimately the two curves only differ in the parameter α, as depicted in Fig. 6.2.

The scanning curves are derived by linear scaling of either the main wetting or main drying curve, such that the scanning curve includes the current θ-h combination and approaches the main wetting curve in case of a wetting scanning curve and the main drying curve in case of a drying scanning curve. Fig. 6.2A shows the scaling principle in case of a drying scanning curve.

Based on its wetting and drying history, at a certain time and depth the soil shows an actual water content θ_{act} at the soil water pressure head h_{act}. The valid drying scanning curve should pass through the point (θ_{act}, h_{act}), and approach the main drying curve at smaller water contents. We may define θ_{md} as the water content of the main drying curve at h_{act}, and θ_{sat}^* as the saturated water content of the drying scanning curve. Linear scaling of the main drying curve with respect to the vertical axis $\theta = \theta_{res}$ gives (Fig. 6.2A):

$$\frac{\theta_{sat}^* - \theta_{res}}{\theta_{sat} - \theta_{res}} = \frac{\theta_{act} - \theta_{res}}{\theta_{md} - \theta_{res}} \quad \Rightarrow \quad \theta_{sat}^* = \theta_{res} + (\theta_{sat} - \theta_{res})\frac{\theta_{act} - \theta_{res}}{\theta_{md} - \theta_{res}} \tag{6.1}$$

The only unknown in Eq. 6.1 is θ_{sat}^*, which can be directly solved. The drying scanning curve is accordingly described with the parameters (α_{dry}, n, θ_{res}, θ_{sat}^*). As long as the soil keeps drying, this drying scanning curve is valid.

The opposite occurs when the soil gets wetter. Again we start from the arbitrary actual water content θ_{act} at the soil water pressure head h_{act}, and now define θ_{mw} as the water content of the main wetting curve at h_{act}, and θ_{res}^* as the residual water content of the wetting scanning curve. Linear scaling of the main wetting curve with respect to the vertical axis $\theta = \theta_{sat}$ gives (Fig. 6.2B):

$$\frac{\theta_{sat} - \theta_{res}^*}{\theta_{sat} - \theta_{res}} = \frac{\theta_{sat} - \theta_{act}}{\theta_{sat} - \theta_{mw}} \quad \Rightarrow \quad \theta_{res}^* = \theta_{sat} - (\theta_{sat} - \theta_{res})\frac{\theta_{sat} - \theta_{act}}{\theta_{sat} - \theta_{mw}} \tag{6.2}$$

From Eq. 6.2, θ_{res}^* can be directly solved. The wetting scanning curve is accordingly described with the parameters (α_{wet}, n, θ_{res}^*, θ_{sat}), and is valid as long as the soil keeps wetting. As the wetting-drying history is different at each soil depth, each node may show a different scanning curve. The unique $K(\theta)$ relation of a soil layer always follows from the parameter set (n, θ_{res}, θ_{sat}, K_{sat}, λ) according to Eq. 2.16.

6.2.2 Water repellency

Usually in the laboratory, when measuring the retention function and the hydraulic conductivity curve, soil samples are first brought to saturation, and during the experiment relatively long equilibrium times are allowed. These conditions suppress effects of water repellency. In the field, immobile soil domains may occur either as large, separate volumes (Fig. 6.3) or as numerous small volumes corresponding to less accessible pores. We will assume that the soil hydraulic functions as measured in the laboratory, $\theta_{lab}(h)$ and $K_{lab}(h)$, are valid in the mobile regions. A second assumption is that the water content in the immobile region, θ_{im} (cm^3 cm^{-3}) remains constant in time. Then the bulk field water retention function $\theta_{bulk}(h)$ can be calculated as (Fig. 6.3):

$$\theta_{bulk}(h) = F_{mob}\,\theta_{lab} + (1 - F_{mob})\theta_{im} \tag{6.3}$$

where F_{mob} equals the mobile fraction (cm^3 cm^{-3}) of the soil volume through which flow actually occurs. The factor F_{mob} can roughly be estimated by visual observation of dry and wet spots in the field shortly after precipitation, and more accurately with tracer colour tests, e.g. with iodide (*Van Ommen et al.*, 1989b) or Brilliant Blue (*Flury and Flühler*, 1995), with
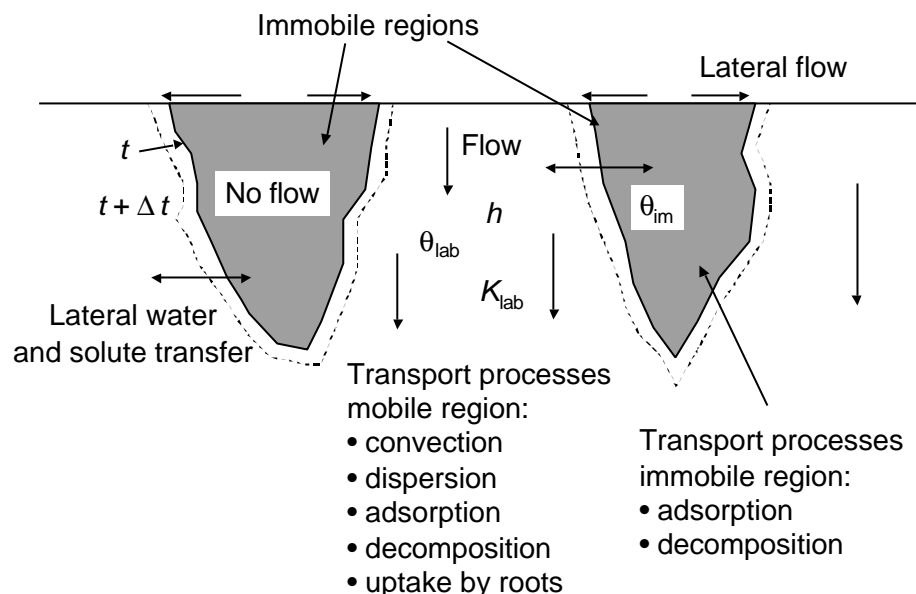
Figure 6.3 Schematization of mobile and immobile regions for flow and transport in water repellent soils.

a disc permeameter in combination with a tracer (*Clothier et al.*, 1992), with TDR transect measurements of water content (*Ritsema and Dekker*, 1994) or by model calibration (*Van Dam et al.*, 1990a).

Richards' equation only applies to the mobile region. Therefore the effective retention function, which is used to solve Richards' equation, follows simply from:

$$q(h) = F_{\text{mob}} q_{\text{lab}}(h) \tag{6.4}$$

We may assume that the soil texture and the unsaturated hydraulic conductivity curves of the mobile and immobile regions are identical. In that case the soil water flux density q at a certain gradient $\partial H/\partial z$ will be reduced by the factor F_{mob} due to the reduction in flow domain. Thus, the effective field conductivity curve $K(h)$ which should be used in the solution of Richards' equation, is related to $K_{\text{lab}}(h)$ measured in the laboratory as:

$$K(h) = F_{\text{mob}} K_{\text{lab}}(h) \tag{6.5}$$

In this way the acceleration of soil water flow due to a smaller flow volume is taken into account. The time needed for some lateral soil water flow at depths where F_{mob} either increases or decreases with depth, is neglected. This convergent or divergent flow would require a more complicated three-dimensional analysis, as e.g. performed by *De Rooij* (1996).

Field studies (*Ritsema and Dekker*, 1994) show that the mobile fraction F_{mob} varies in time. In general, when the soil becomes wetter, F_{mob} increases. We might include this feature by a linear relationship between log (-h) and F. Notice that when the immobile regions contain water, variation of F_{mob} with h induces exchange of water between the mobile and immobile soil volumes (Fig. 6.3). This exchange is included as an extra source term in the Richards' equation:

$$\frac{\partial \boldsymbol{q}}{\partial t} = \frac{\partial \left[K \left(\frac{\partial h}{\partial z} + 1 \right) \right]}{\partial z} - S_{\mathrm{a}} + \frac{\partial F_{\mathrm{mob}}}{\partial t} \boldsymbol{q}_{\mathrm{im}} \qquad (6.6)$$

where S_{a} is the root water extraction rate (d^{-1}) and the last term in the right hand side of Eq. 6.6 accounts for the water amount transferred (d^{-1}) from the immobile to the mobile region.

In case of reactive solutes, the mobile-immobile concept requires adjustment of the solute transport equation (*Van Dam et al.*, 1997). In this Chapter we will focus on conservative solutes only, for which solute transport Eq. 2.30, as applied to the fingers, reduces to:

$$\frac{\partial \boldsymbol{q} c}{\partial t} = -\frac{\partial (qc)}{\partial z} + \frac{\partial \left(\boldsymbol{q} D \frac{\partial c}{\partial z} \right)}{\partial z} \qquad (6.7)$$

6.2.3 Soil water flow as affected by hysteresis and water repellency

Pronounced effects of hysteresis and preferential flow occur in dry soils during and after infiltration events. To illustrate this, we simulated infiltration of 30 mm rain during one day into a dry soil ($h = -1000$ cm), with soil hydraulic data obtained from one of our experimental locations (Ouddorp). The simulations included a reference case, in which the main drying curve of the $\theta(h)$ relation is used, and cases in which hysteresis and preferential flow were included. Figure 6.4 shows the simulated water content profiles at the end of the day with precipitation. When hysteresis was included, the infiltration front became steeper and moved slower. Also subsequent days with redistribution taking place, showed a smaller rate of water movement compared to a simulation without hysteresis. *Youngs* (1958), and *Dane and Wierenga* (1975) have already shown that the redistribution after heavy infiltration is retarded due to hysteresis. This is favourable for vegetation as more water is retained in the root zone. Also in case of water harvesting, where large amounts of water are stored in the top layers, hysteresis decreases the percolation losses. We may explain the steeper infiltration front in the case of hysteresis by the smaller θ and thus smaller K at a given h compared to the reference case. This means that with hysteresis a larger gradient $\partial H / \partial z$ is needed to induce the same water flux (*Youngs and Poulovassilis*, 1976).

To demonstrate the effect of preferential flow, a simulation was performed with a constant mobile fraction $F_{\mathrm{mob}} = 0.60$ (Fig. 6.4). No water was assumed in the immobile parts, which means that the average initial water content is F_{mob} times smaller. Compared to the reference, the bulk water contents were lower and the infiltration front advanced faster. Probably the increase of water content and hydraulic conductivity in the fingers, where infiltrated water was concentrated, had more effect than the decrease of $K(h)$ due to the smaller, horizontal, flow cross-section according to Eq. 6.5.

We may conclude that hysteresis and preferential flow have opposite effects on the soil water fluxes. *Hysteresis retards soil water movement, while preferential flow enhances soil water movement.* Now we will investigate their effect at ordinary field conditions in The Netherlands.
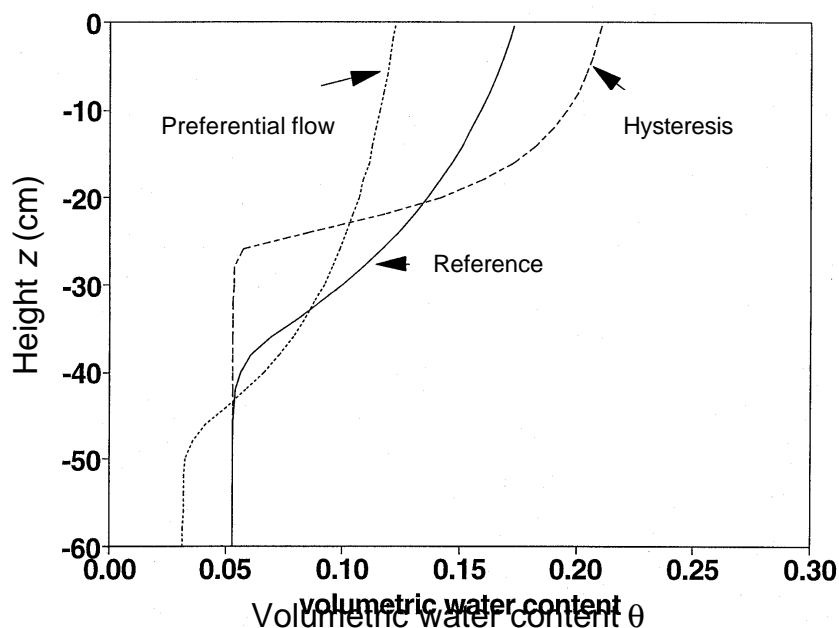
Figure 6.4 Effect of hysteresis and preferential flow (F_{mob} = 0.6) on simulated water content profiles after a day with 30 mm rain (initially h = -1000 cm; soil hydraulic properties of the water repellent top layer in Table 6.3).

6.3   Experiments

6.3.1   Field 1: Hupsel

This field is located in the watershed 'Hupselse Beek' in the eastern part of The Netherlands. The watershed comprises 650 ha and has been for 25 years an experimental area of the National Dutch Water Service. A soil survey of the area was made at a scale of 1 : 5000, with an average observation density of two borings per hectare. The mapping units occurring in the area represent major units of sandy soils in The Netherlands (*Wösten et al.*, 1985). The soil used in this study belongs to the dominant mapping unit of de Hupselse Beek and was classified as sandy, siliceous, mesic Typic Haplaquods (*Soil Survey Staff*, 1975). Four soil layers were distinguished, starting at depths 0, 15, 35 and 90 cm, respectively. Measurement with TDR sensors and visible inspection showed considerable variation of soil water contents in the top layer over a short horizontal distance. Earlier studies on water flow in this soil suggested effects of hysteresis and preferential flow (*Van Ommen et al.*, 1989a).

Two data sets from this field were used. The first data set comprised a 2-year period (1976-1977) and included neutron probe measurements each two weeks, daily on-site meteorological data (rain, net radiation, relative humidity, wind speed, air temperature) and daily groundwater levels. Among others, the data sets have been used by *Wösten et al.* (1990) to evaluate the accuracy of four methods to generate soil hydraulic functions. In general, the water storage in the upper 50 cm was well predicted. However, in the autumn following the very dry summer of

1976, the water storage in the upper 50 cm was systematically overestimated. *Wösten et al.* (1990) attributed the model overestimation to the omission of hysteresis in the used model.

The second data set comprises accurate water content measurements at four depths in a 77 days period starting August 1, 1993. In a transect of 1.8 m, 40 TDR sensors were installed at depths of 7, 20, 40, and 65 cm (10 sensors per depth) and measurements were made on days 16, 31, 37, 48, 54, 62, 68, and 77. As in the first data set, local, daily meteorological data and groundwater levels were measured (*Van den Eertwegh and Meinardi*, 1999). In addition, daily drainage outflow from horizontal pipe drains of this field were measured.

Undisturbed soil samples were taken to determine the soil hydraulic functions of each soil layer. The drying and wetting branch of the soil water curves in the range -600 < h < -5 cm were obtained by a modified hanging water column method. In this method a water column in a buret is connected to a porous plate which supports the soil sample. Different pressure heads are created by changing the distance between the water level in the buret and the middle of the soil sample in combination with different under-pressures in the air-filled section above the water level in the buret. First, the main drying branch of the water retention curve was determined by a step-wise decrease of the pressure head from -5 to -600 cm. Then, the wetting branch was determined by a step-wise increase of the pressure head from -600 to -5 cm. Water contents corresponding to pressure heads lower than -600 cm were obtained using a pressure plate apparatus (*Klute*, 1986). The hydraulic conductivity curves were measured with the column method for vertical saturated hydraulic conductivity (*Klute and Dirksen*, 1986), the crust method (*Bouma*, 1982; *Bouma et al.*, 1983) for hydraulic conductivities at -50 < h < 0 cm and the sorptivity method (*Dirksen*, 1979) for hydraulic conductivities at h < -50 cm.

6.3.2 Field 2: Ouddorp

This field is located near the village of Ouddorp in the south-western part of The Netherlands. The soil is sandy, of marine origin, and classified as Mesic Typic Psammaquent (*De Bakker*, 1979). The profile showed three horizons, at depth intervals of 0-32, 32-65 and 65-83 cm. Bromide tracer tests were carried out on two adjacent sites, one with a water repellent top layer, and one with a wettable top layer (*Hendrickx et al.*, 1988). The wettable top layer was calcareous with 5% clay and 2% organic matter content, while the water repellent top layer was not-calcareous and contained only 3% clay and 1.5% organic matter. The higher clay content of the wettable soil results from clay amendments about 40 years ago. The groundwater level of the two sites during the experiments fluctuated between depths of 0.4 and 1.2 m. At both sites, three identical plots of 6x2 m^2 were prepared.

On 12 November 1986, 1.25 mm KBr solution (11 g KBr l^1) was applied to the six plots. The solution was sprayed on the soil surface from a boom with six nozzles (Teejet 11002), spaced 0.33 m apart. The spraying pressure was 0.2 MPa and spraying height 0.3 m. Speed of walking during spraying was about 1 m s^{-1}. During spraying, samples were collected at twelve random locations along the borders of each plot to verify the amount and areal distribution of the applied
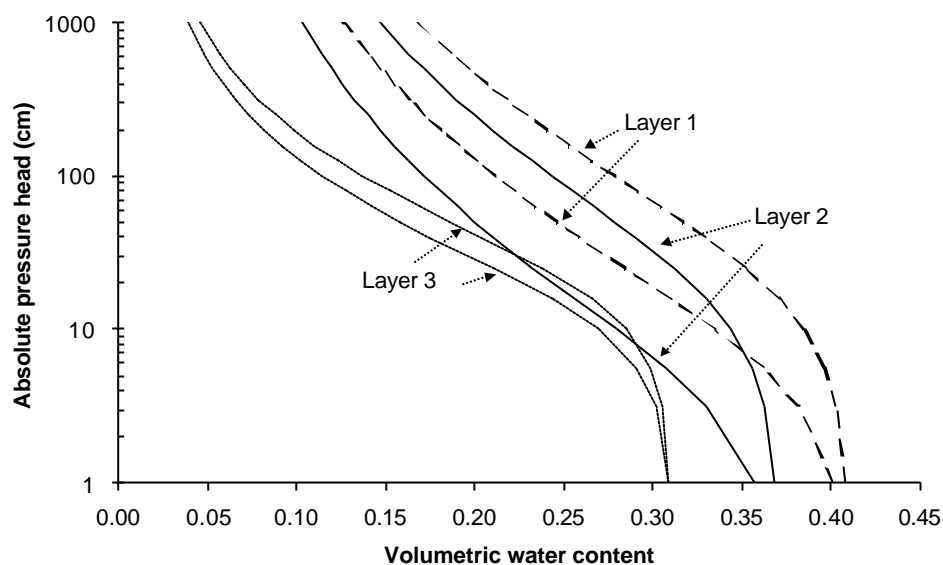
Figure 6.5 Fitted main wetting and drying water retention curves for 3 soil layers at Hupsel.

bromide pulse. The soil was sampled 12, 34 and 56 days after spraying, at which times samples were collected from five locations in each plot. The soil was sampled using a hollow cylinder that was driven mechanically into the soil. After removing the cover from the cylinder, the soil column was continuously sampled at 8 cm intervals (4-84 cm depth) with steel core cylinders (230 cm^3). These were emptied in a plastic jar and dried at 60 ℃. Next, 200 ml water was added to each jar and, after shaking for one hour, bromide was extracted by filtering through a membrane filter having a pore size of 0.45 μm. The extract passed the Baker-10 SPE system: a C18 reversed phase to exclude non-polar organic matter which may disturb the analysis. Finally, bromide concentrations in the extract were determined using ion chromatography (*Harmsen*, 1986).

Soil water retention curves were determined in the laboratory with the hanging water column method (-160 $< h <$ 0 cm). The unsaturated hydraulic conductivity was measured with the crust method in the range -65 $< h <$ -5 cm. Additional details of the soil and experimental procedures are given by *Hendrickx et al.* (1988) and *Ritsema et al.* (1993).

6.4   Results

6.4.1   Hupsel, data set 1

The measured main wetting and main drying water retention curves of the three layers were fitted to the Van Genuchten model. The parameterized curves are shown in Fig. 6.5. Hysteresis mainly occurred in layer 1 and 2 (until 35 cm depth). During 1976 and 1977 the measured groundwater levels fluctuated between -179 $< z <$ -35 cm. These measured groundwater levels were used as the lower boundary condition in the numerical model. Figure 6.6 shows the measured soil water storage in the top 50 cm for the years 1976 and 1977. During the dry summer of 1976, the water storage in the top 50 cm of the soil profile decreased from approximately 140 mm to 40 mm. During the growing period of 1977 (day 395 - 575), the water
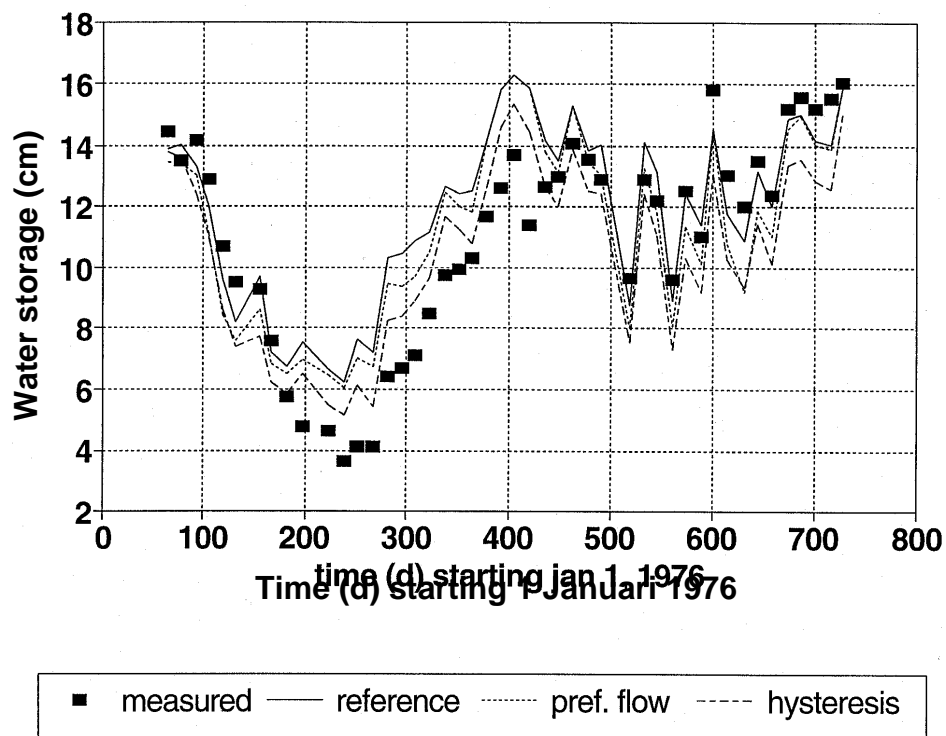
Figure 6.6 Measured and simulated water storage in the top 50 cm during 1976 and 1977 at Hupsel. The simulations include the reference and runs with preferential flow and hysteresis.

storage fluctuated only between 140 and 95 mm, because of the small water deficit during this growing period.

We simulated the soil water movement for the reference case (using the main drying curve of the water retention function) and subsequently added hysteresis and preferential flow (Fig. 6.6). In the reference case the simulated water storage in the top 50 cm corresponded fairly well with the measured water storage in 1977, but overestimated the measured water storage in the summer and autumn of the dry year 1976 ($170 < t < 450$ d). Table 6.1 shows the simulated water balances for both years. Whereas in 1976 net capillary rise was simulated (85 mm), in 1977 net drainage (150 mm) was computed.

The simulated water storage in case of hysteresis was less than in case of the reference. How is this related to the general reduction of soil water fluxes due to hysteresis, as discussed before? Starting with the same initial condition, higher soil water contents due to hysteresis occur during and shortly after infiltration events. However, during redistribution, when the soil water pressure heads gradually adjust to the pressure heads at the soil profile boundaries and the pressure heads due to root water extraction, the water storage in the case of hysteresis becomes smaller than in case of the reference. This is simply due to the fact that at a given pressure head, scanning curves have a smaller water content than the main drying curve. So, although during infiltration soil water fluxes are smaller in case of hysteresis, in the long run adjustment of the soil water pressure heads to those exerted on the system will result in less water storage! At infiltration
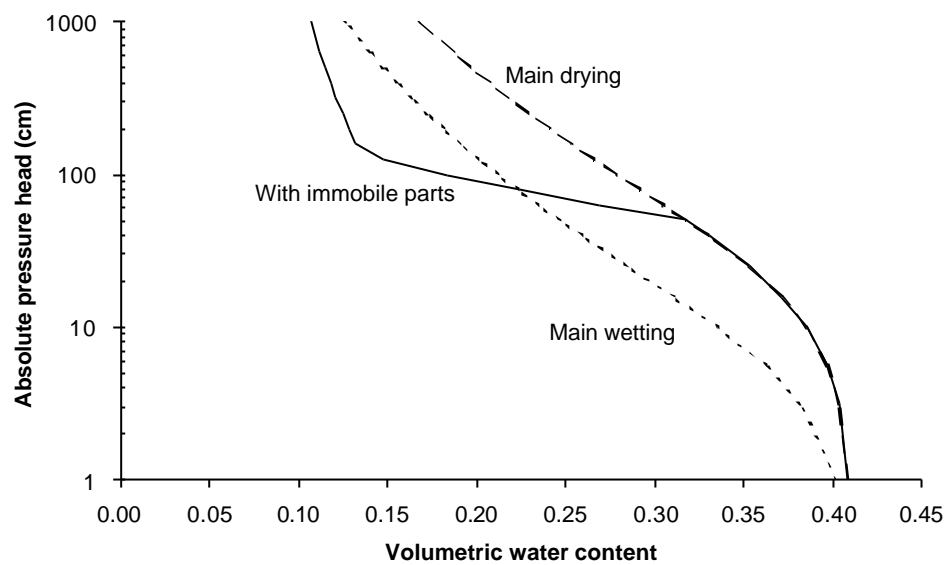
Figure 6.7 In case of top soil Hupsel, main wetting and main drying water retention curves, as well as the bulk retention curve including immobile regions (Eq. 6.4).

events, due to hysteresis not only extra water will be retained in the root zone because of the lower soil water fluxes, but also because of the lower initial soil water contents, which allow more increase of water storage. Figure 6.6 shows that inclusion of hysteresis clearly improved the simulation for the period $170 < t < 450$ d. However, in 1977 it performed slightly worse than the reference. Due to the lower water contents, actual transpiration and actual evaporation are slightly less, which increase the amount of percolation (Table 6.1).

In order to include preferential flow, the relation $F(h)$ had to be derived. We applied the inverse method on the second data set of this soil. This was simply done by comparing simulated soil water contents from the reference case with actually measured soil water contents, employing Eq. 6.3. We assumed $\theta_{im} = 0$. This resulted for the A1 horizon in a decrease of F_{mob} from 1.0 at $h = -50$ cm to 0.36 at $h = -125$ cm. Figure 6.7 shows the resulting retention function of the first layer. In the second and third layer no reduction of volumetric water contents due to preferential flow could be detected. Using these data, the preferential flow model performed in between the reference and the hysteresis simulation for both years (Fig. 6.6). As in case of hysteresis, the actual transpiration and evaporation decrease, while the percolation to the groundwater increases (Table 6.1).

Table 6.1 SWAP simulated water balance components (mm) of Hupsel, data set 1, during 1976 and 1977 for the reference (Ref), hysteresis (Hys) and preferential flow (Pref) simulation.

Water balance components	1976[a]			1977		
	Ref	Hys	Pref	Ref	Hys	Pref
Rain	390	390	390	789	789	789
Potential transpiration	575	575	575	500	500	500
Actual transpiration	430	404	415	493	472	488
Potential soil evaporation	125	125	125	103	103	103
Actual soil evaporation	83	80	66	103	103	103
Bottom flux (positive upward)	85	34	52	-150	-168	-157
Change storage (top 200 cm)	-38	-60	-39	43	46	41

[a] 1976 without first 60 days

6.4.2 Hupsel, data set 2

The measured groundwater levels varied between 33 and 102 cm below soil surface. Total rainfall amounted to 300 mm (maximum rainfall intensity of 37.2 mm/d) and total potential evapotranspiration amounted to 162 mm. Figure 6.8 shows the typical soil water content variability of the transect at days 16 and 77. In the top soil ($-15 < z < 0$ cm) at day 16 some wet fingers can be detected. In the subsoil the water content differences are less. During autumn with increasing net precipitation, the volumes with low water content decreased (day 77). Figure 6.9 shows the measured (mean, $N = 10$) and simulated water contents during the measurement period at 4 depths. At all depths the measured water contents increased rapidly after day 40. The simulated results for the reference case (main drying curve) reproduced the measurements closely, except for the top soil layer. Incorporation of hysteresis improved the calculated water contents of the top layer, although hysteresis slightly performed worse for the second layer ($-35 < z < -15$ cm). Also incorporation of preferential flow (in the top layer $F_{mob} = 1.0$ at $h = -50$ cm and $F_{mob} = 0.36$ at $h = -125$ cm) improved the result of the top soil layer. For the period considered preferential flow hardly affected the simulated water contents in the subsoil layers (Fig. 6.9).
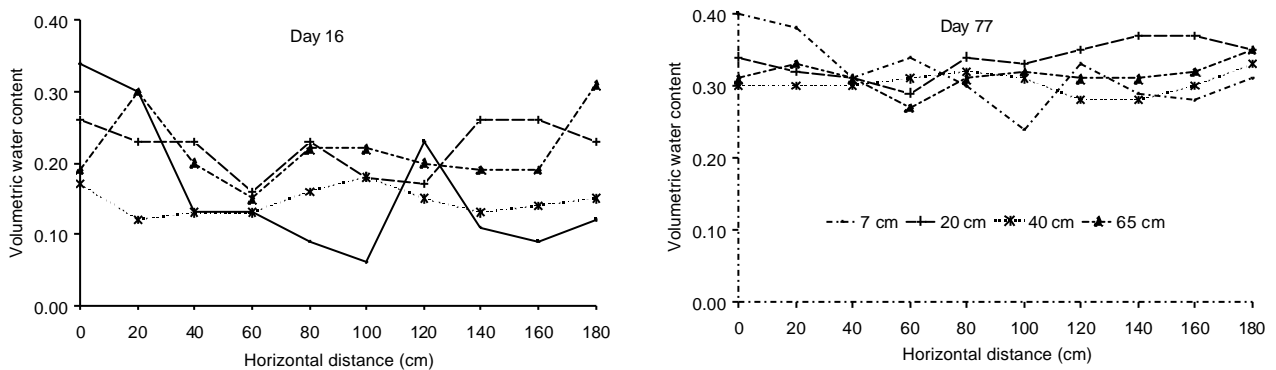
Figure 6.8 Soil water content measurements of 40 TDR probes at 4 depths in a transect of 180 cm at the start (day 17) and end (day 77) of the experimental period.
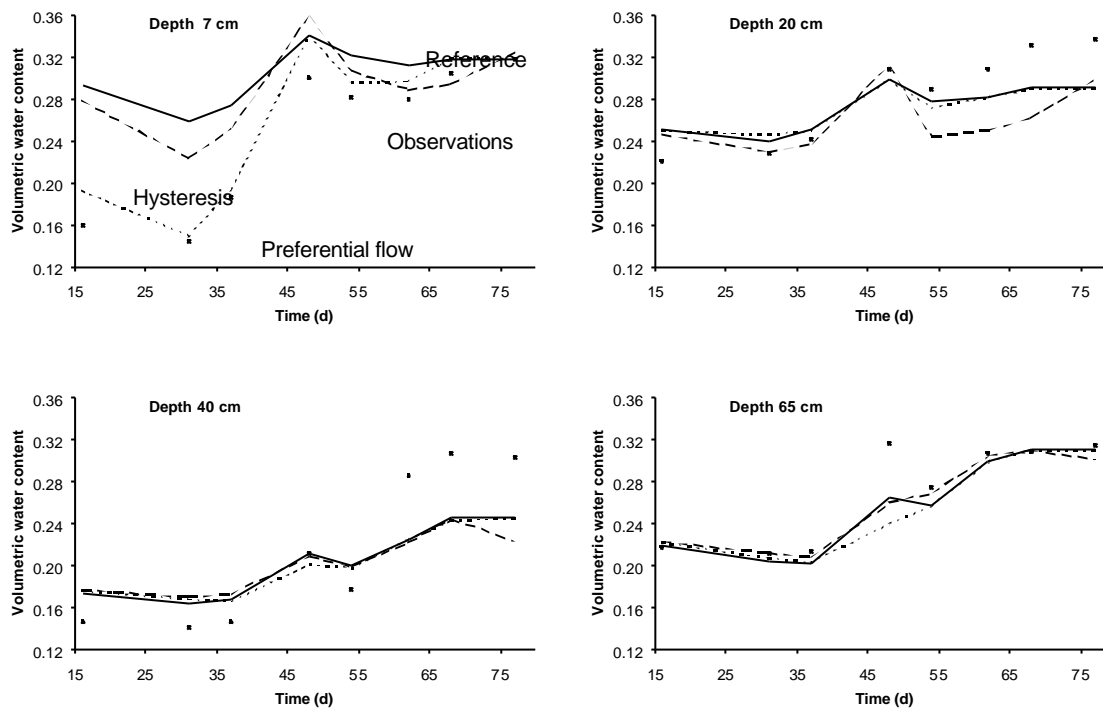
Figure 6.9 Measured (mean, $N = 10$) and simulated soil water contents, including the effects of hysteresis and preferential flow, at 4 depths during the experimental period.
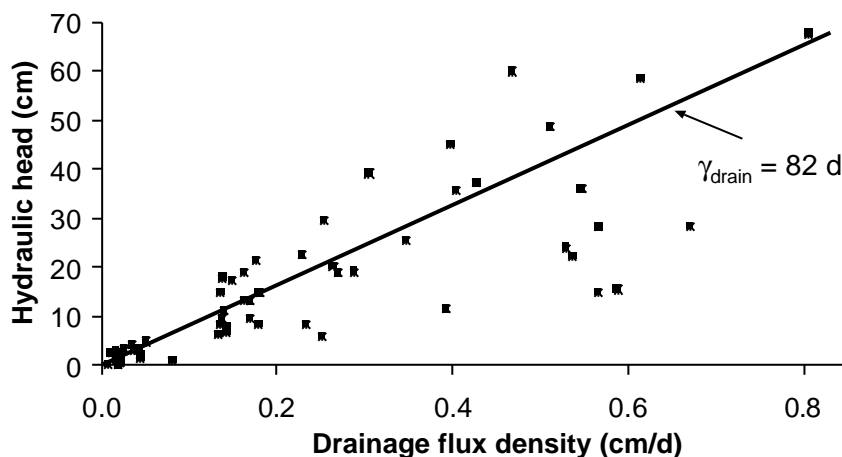
Figure 6.10 Measured drainage characteristic of the experimental field at Hupsel.

In the above simulations the daily measured groundwater levels were used as lower boundary condition in order to avoid disturbances due to uncertainties of the lower boundary fluxes. Combination of groundwater levels and field drainage data yielded a drainage characteristic with a resistance γ_{drain} of 82 d (Fig. 6.10). Figure 6.11 shows the measured groundwater levels. In autumn groundwater levels react rapidly with rainfall. The same figure shows the simulated groundwater levels using the drainage characteristic as lower boundary condition for the reference case. Although the simulated drainage (157 mm) closely reproduced the measured drainage (150 mm), simulated groundwater levels fluctuated less than the measured ones.
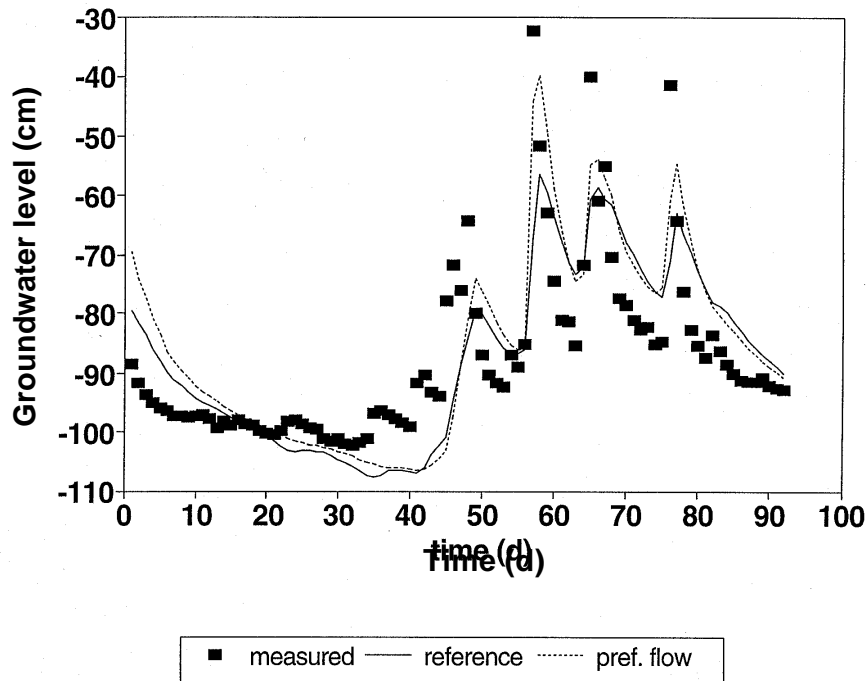
Figure 6.11 Measured and simulated groundwater levels at Hupsel. Two simulations are shown, the reference and a scenario with preferential flow ($F_{mob} = 0.60$, until $z = -65$ cm).

Inclusion of hysteresis hardly affected the result. Also inclusion of immobile flow regions, as derived from the soil water contents, showed a minor effect on the simulated groundwater levels. The high groundwater level peaks, which can be important for leaching of contaminants, could partly be reproduced using $F_{mob} = 0.60$ in the first 3 layers (to 65 cm depth), as shown in Fig. 6.11. The first high peak could not be reproduced, and might be caused by groundwater recharge from regional lateral groundwater flow in dry periods (*Van Ommen et al.*, 1989b). Further air entrapment, which is not accounted for in the model, may play an important role in the underestimation of groundwater level peaks.

6.4.3 Ouddorp

Total effective rainfall amounted to 184 mm, with maximum rainfall intensities of 21.6 mm d^{-1}. Groundwater levels increased gradually from $z = -87$ cm at the start to $z = -50$ cm at the end (Table 6.2). Figure 6.12 shows the measured soil water content profiles at the sampling dates. The water contents increased steadily during the experimental period. The surface layer of the water repellent soil contained ~5% less water than the surface soil of the wettable layer. Figure 6.13 shows the mean bromide concentrations measured on the three sampling dates. Observed peak concentrations in the water repellent soil were less than those in the wettable soil. The bromide tracer also reached the groundwater table earlier in the water repellent soil. After 12 days and 62 mm precipitation, solutes in the wettable soil had reached $z = -60$ cm, whereas in the water repellent soil already a mean concentration of ~20 mg l^{-1} was measured in the groundwater at $z = -80$ cm. Also some of the bromide remained close to the soil surface of the water repellent soil. Bromide recovery percentages for the two soils are listed in Table 6.2. Recovery percentages were always < 100%, especially for the wettable soil, indicating some

loss of bromide from the sampled region (until $z = -88$ cm), either in groundwater or perhaps some bromide uptake by the grass cover, which was more developed in the wettable soil.

Figures 6.14 show the laboratory measured retention functions. The $\theta(h)$ data of the water repellent and wettable soils differ mainly in the top layers, especially the wetting branches. This is particularly true near saturation, where water contents of the water repellent soil are 2-8% lower than those of the wettable soil. The parameters of the soil hydraulic functions (α, n, θ_{res}, θ_{sat}, K_{sat}, and λ) were estimated by means of a least-square optimization analysis with RETC (*Yates et al.*, 1992) using the original laboratory data. The results are listed in Table 6.3. Parameter α for the wetting curve is always much higher than α for the drying curve, indicating the presence of hysteresis. The measurements of the hydraulic conductivity at a certain h showed a large range of about two orders of magnitude. As the wet, sandy soil is relatively conductive (0.1 - 100 cm d^{-1}) compared to the moderate soil water fluxes (0 - 0.5 cm d^{-1}), the effect of inaccuracies in the hydraulic conductivity function on simulated soil water contents are minor compared to inaccuracies of the retention function.

Table 6.2 Effective precipitation (cumulative since start experiment), groundwater depths, and bromide recovery rates at three sampling dates.

Time (d)	Effective precipitation (mm)	Depth to groundwater (cm)		Recovery rate (%)	
		Wettable soil	Water-repellent soil	Wettable soil	Water repellent soil
12	61.8	83	73	70.3	91.3
34	93.3	78	68	70.0	97.6
56	184.0	57	50	70.8	68.5

Table 6.3 Parameters of the laboratory-measured unsaturated soil hydraulic functions.

	Wettable soil				Water repellent soil			
	Top layer		Second layer		Top layer		Second layer	
Parameter	Wet[1]	Dry[2]	Wet	Dry	Wet	Dry	Wet	Dry
θ_{res} (-)	0.01	0.01	0.01	0.02	0.01	0.01	0.01	0.02
θ_{sat} (-)	0.38	0.38	0.30	0.30	0.38	0.38	0.30	0.30
α (cm^{-1})	0.250	0.010	0.050	0.013	0.380	0.018	0.210	0.029
n (-)	1.3	1.9	2.0	7.0	1.3	1.9	1.7	2.3
λ (-)	-3.0	0.5	-0.5	2.0	-4.0	2.0	-3.0	2.0
K_{sat} (cm d^{-1})	1700	150	300	100	1500	160	300	300

(1) Wet = Wetting curve; (2) Dry = Drying curve
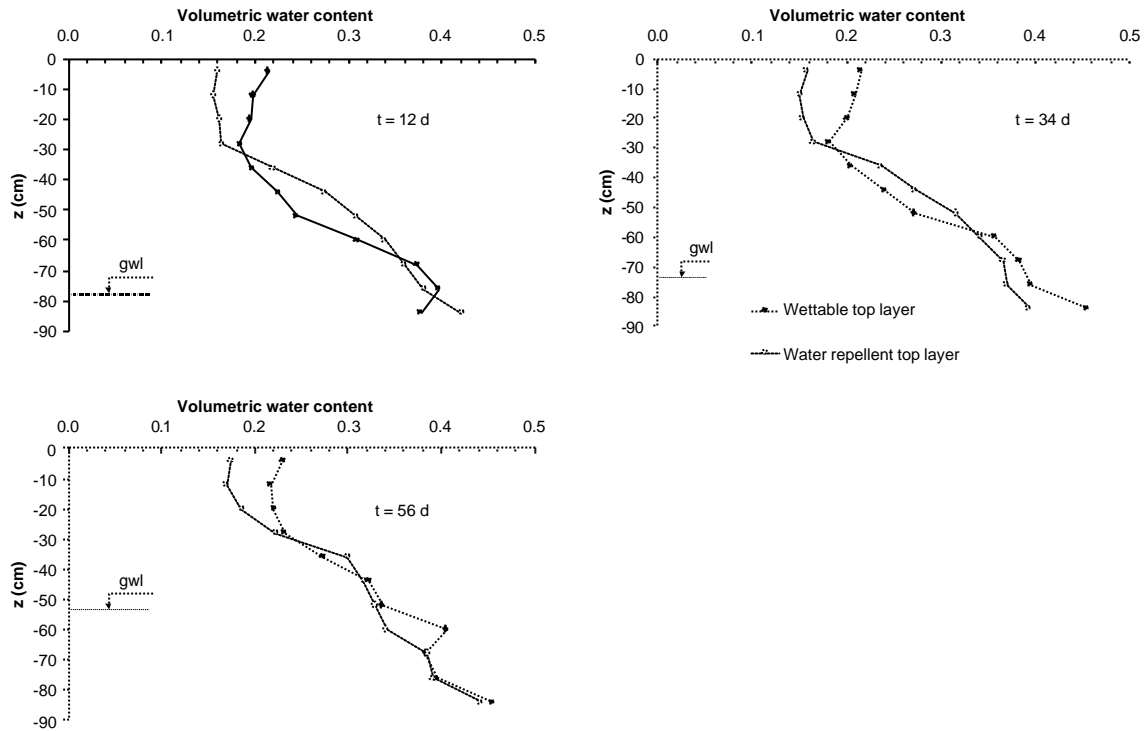
Figure 6.12 Measured *soil water contents* (arithmetic mean, $N = 15$) in the wettable and water repellent soils at three sampling dates.
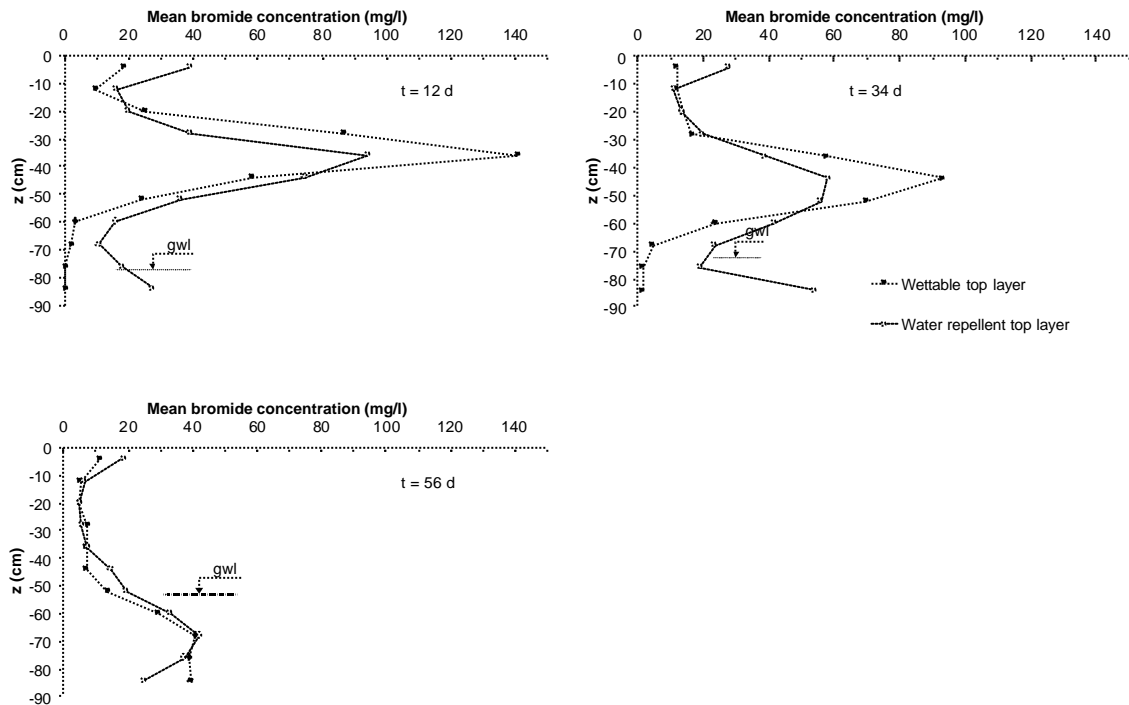
Figure 6.13 Measured *bromide concentrations* (arithmetic mean, $N = 15$) in the wettable and water repellent soils at three sampling dates.
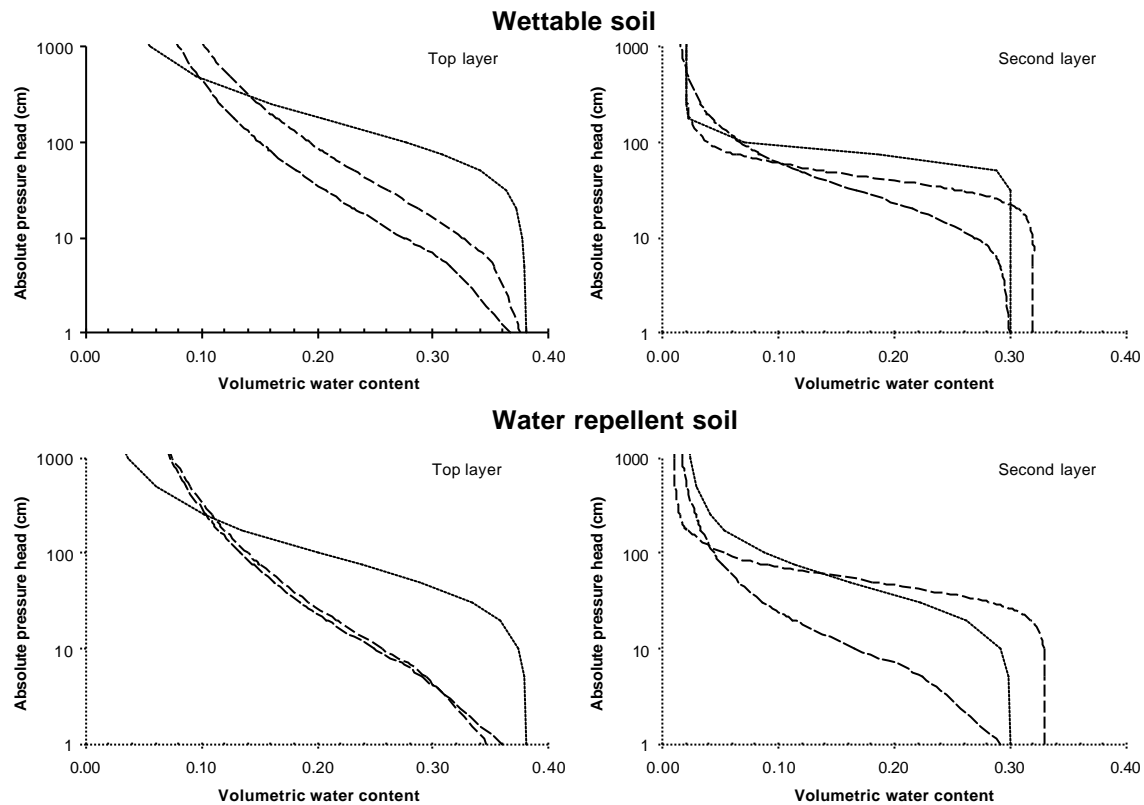
Figure 6.14 Laboratory measured main wetting and main drying curves and the fitted curve using field retention data, both of the wettable and water repellent soil.

Water flow and bromide transport were simulated, using effective rainfall fluxes as top boundary condition, and measured groundwater levels as bottom boundary condition. The goodness of fit between calculated and measured water contents and bromide concentrations was expressed in terms of relative efficiency, *RE* (*McCuen and Snyder*, 1986), which quantifies the improvement of the adopted model relative to a 'zero' model which gives only the average value in the entire profile:

$$RE = \frac{F_0 - F_1}{F_0}100\% \quad \text{with} \quad F_0 = \sum_{i=1}^{N}\left(\bar{u} - u_{i,\text{obs}}\right)^2 \quad \text{and} \quad F_1 = \sum_{i=1}^{N}\left(u_{i,\text{sim}} - u_{i,\text{obs}}\right)^2 \tag{6.8}$$

where $u_{i,\text{obs}}$ and $u_{i,\text{sim}}$ are the observed and simulated quantities and $\bar{u}$ is the mean value of N observations. Given an observation set, F_0 is constant, and *RE* is a linear function of F_1. When the simulation results exactly duplicate the measurements ($F_1 = 0$), *RE* = 100%. When the simulation produces the same sum of squared deviations as the zero model ($F_1 = F_0$), *RE* = 0%. When *RE* is negative, the simulation is even worse.

Table 6.4 Relative efficiencies, *RE* (%),of soil water content, for simulations using the main wetting curve, the main drying curve and the field optimized retention function.

Simulation	Wettable soil	Water repellent soil
Wetting curve	26.4	-68.9
Drying curve	-10.2	15.6
Optimization	81.7	89.1

First, soil water flow was simulated using the optimized hydraulic parameters of the main wetting and drying curves as given in Table 6.3. This effort did not yield satisfactory results for both the main wetting and main drying curve, as reflected by the low *RE* values depicted in Table 6.4. To improve the predictions, we estimated the soil hydraulic parameters with an inverse procedure (see Chapter 4), employing the field measured soil water content distributions. Of the first and second layer, we optimized the parameters α, n, λ, and K_s, and fixed the parameters θ_{res} and θ_{sat} to their measured values. The parameters of the measured wetting and drying curves (Table 6.3) were used as upper and lower limits. Results of the parameter optimization are listed in Table 6.5. The optimized soil hydraulic functions are also drawn in Fig. 6.14, and lie largely between the main drying and main wetting curve as determined in the laboratory. Table 6.5 also includes estimates for the hydraulic parameters of a third soil layer, consisting of mostly sandy material with locally thin allochtoneously eroded, disintegrated peat layers (*Hendrickx et al.*, 1988). This third layer causes the relatively high water contents at a depth of 65-85 cm (Fig. 6.12). Fig. 6.15 compares the measured and calculated soil water contents using the field-estimated soil hydraulic parameters. The relative efficiencies are now acceptable: 81.7 and 89.1% for the wettable and water repellent soils, respectively (Table 6.4). This suggests that *water flow is adequately simulated during the bromide tracer experiment, using field-optimized water retention functions to account for hysteresis*.

Table 6.5 Optimized values for the field-measured soil hydraulic and solute transport parameters.

Depth (cm)	Wettable soil			Water repellent soil		
	0 - 30	30 - 67	67 - 83	0 - 32	32 - 65	65 - 83
Soil hydraulic parameters						
θ_{res} (-)	0.01	0.02	0.02	0.01	0.01	0.04
θ_{sat} (-)	0.38	0.32	0.40	0.36	0.33	0.40
α (cm^{-1})	0.100	0.025	0.050	0.270	0.022	0.050
n (-)	1.3	4.0	2.8	1.3	3.5	3.0
λ (-)	-1.0	2.0	-1.0	-5.0	0.5	-1.0
K_{sat} (cm d^{-1})	1500	100	300	1000	80	100
Solute transport parameters						
L_{dis} (cm)	2	2	2	3	3	3
F_{mob} (-)	0.85	1.0	1.0	0.7	0.8	1.0

Although water contents were affected by the inclusion of either hysteresis or preferential flow, the water fluxes below the root zone were hardly affected. Figure 6.16 shows the daily simulated flux at 30 cm depth. In case of hysteresis, the fluxes are about two days later, and are slightly smaller. In case of preferential flow due to water repellency, the fluxes are almost identical to the reference case. Probably at the relatively wet, sandy soil with moderate soil water fluxes, the higher conductivity inside the fingers compensates for the smaller cross-sectional area through which flow occurs.
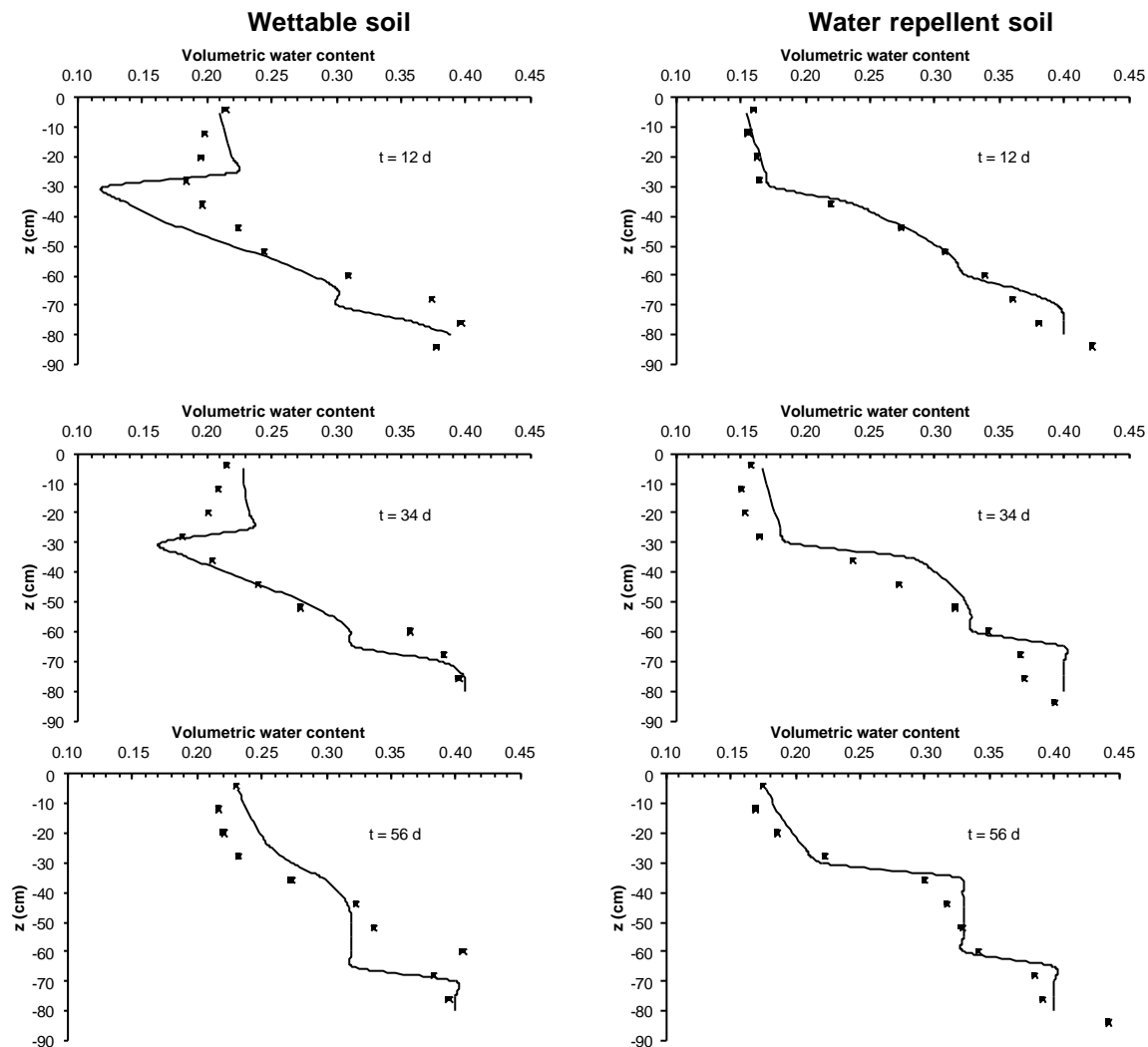
Figure 6.15 Comparison of measured (arithmetic mean, $N = 15$) and simulated water contents, using the fitted hydraulic parameters of Table 6.5, at three sampling dates.

After modeling the water flow, the solute dispersion length, L_{dis}, and the mobile fraction of the soil volume, F_{mob}, were estimated with the bromide concentrations. The measurements revealed relatively high bromide concentrations in the upper 10 cm of the profile during the entire experiment, especially for the water repellent soil (Fig. 6.13). We attribute this to delayed transport of bromide that was sprayed above stagnant (non-wettable) parts. We could not justify an impulse input and had to account somehow for the very slow release of bromide from the non-wettable to the wettable part of the surface soil. The gradual release was accounted for by assuming adsorption in the top 5 cm of the water repellent soil. Although in reality the process causing gradual release is complex and difficult to quantify, adsorption can be used to account macroscopically for solute retardation in the top soil.
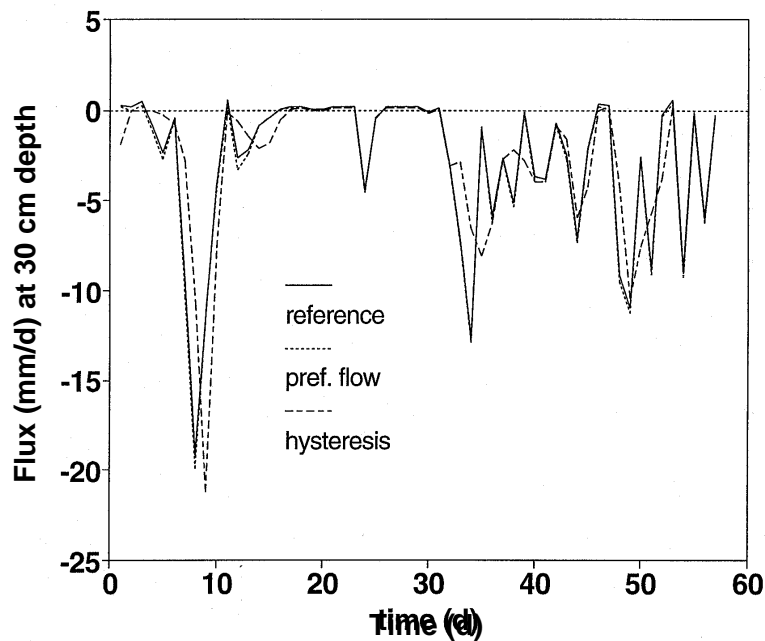
Figure 6.16 Effects of hysteresis and preferential flow on the simulated water flux at 30 cm depth (+ = upward) at Ouddorp.

The second and third field bromide sampling, showed concentration distributions at each depth which were often skewed with a few high concentrations. Because Shapiro-Wilk tests revealed that these skewed distributions were generally neither normally nor lognormally distributed, we decided to use the median bromide concentration per depth for parameter optimization. Table 6.5 lists the optimized transport parameters. The dispersivity L_{dis} for the wettable soil is 2 cm, and for the water repellent soil 3 cm, which is relatively low for field soils (e.g. *Biggar and Nielsen*, 1976; *Van Ommen et al.*, 1989a; *Jury et al.*, 1991). F_{mob} was estimated to be 0.85 for the wettable top layer, which was contrary to our expectations. A value for F_{mob} less than 1.0 may be caused by some slight water-repellency of the top layer (*Hendrickx et al.*, 1988). At the water repellent plots, in the first layer $F_{mob} = 0.7$ and in the second layer $F_{mob} = 0.8$. In the wet subsoil at $z < -65$ cm, $F_{mob} = 1.0$. Figure 6.17 shows the close fit between measured and calculated bromide concentrations, especially at $t = 34$ d. The rather good fit is also reflected by the relatively high *RE* values (72 and 82%) for the wettable and water repellent soils (Table 6.6). The observed solute front in the water repellent soil at $t = 55$ days stays behind the calculated front. This is probably caused by horizontal flow induced by thin less-permeable peat lenses at 60-90 cm below the soil surface. Table 6.6 shows that, in case of the water repellent, hysteretic soil, *the omission of either water repellency or hysteresis, decreases the relative efficiency of the simulation dramaticly*, whether the arithmetic mean or median bromide concentrations are used.
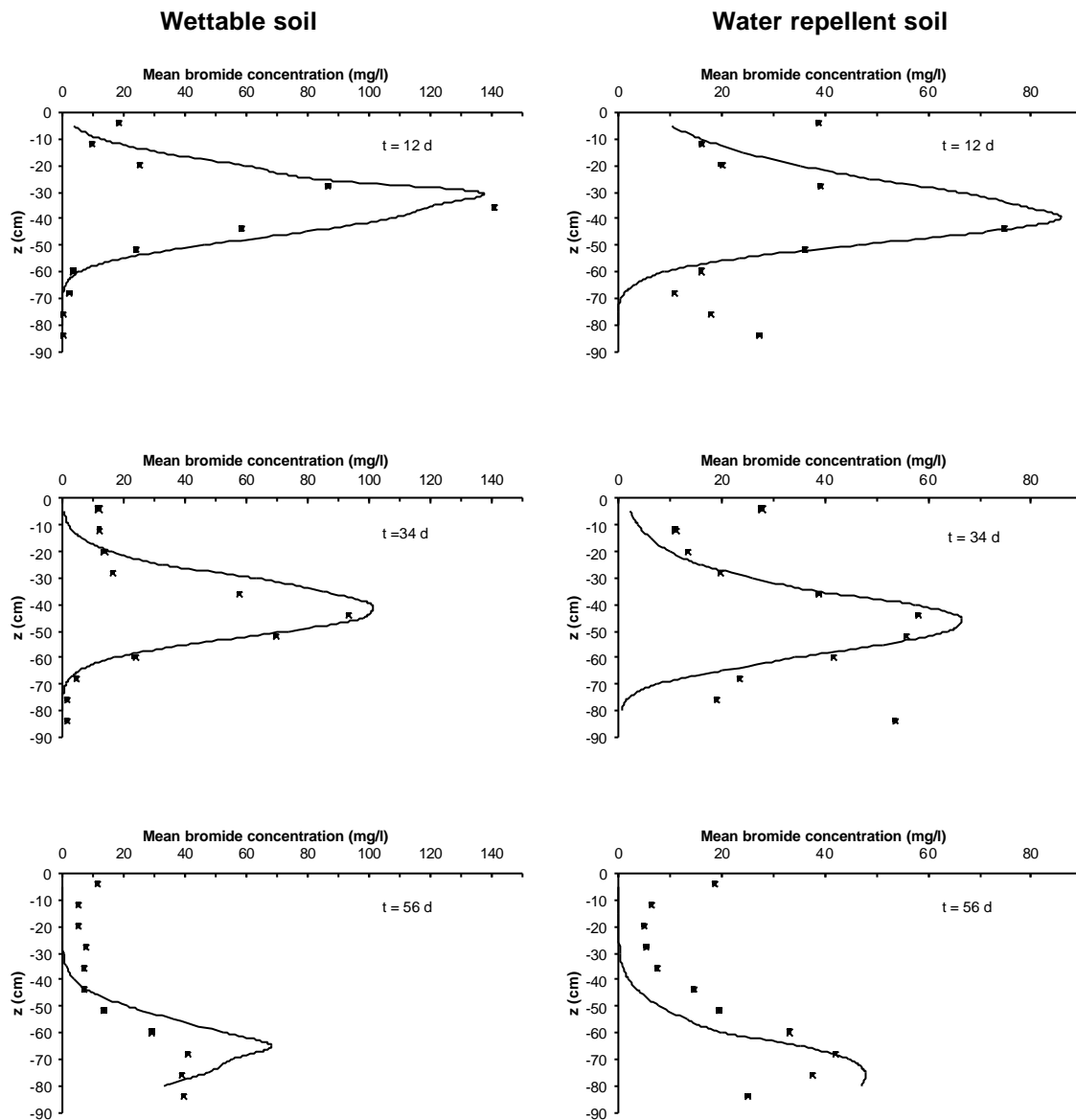
Figure 6.17 Comparison of measured (arithmetic mean, $N = 15$) and simulated bromide concentrations, using the fitted hydraulic and transport parameters of Table 6.5.

Table 6.6 Relative efficiencies, RE (%), for simulation of bromide concentrations, showing the effect of water repellency and hysteresis.

	Wettable soil			Water-repellent soil		
Simulation	Median ($N = 15$)	Mean[1] ($N = 15$)	Simulation	Median ($N = 15$)	Mean[1] ($N = 13$)	Mean[1] ($N = 15$)
$F_{mob} = 1.00$	48.3	50.9	Field-optimization	82.1	89.0	57.8
$F_{mob} = 0.85$	72.3	79.9	$F_{mob} = 1.00$	-112.7	-91.8	-196.8
$F_{mob} = 0.70$	63.1	77.8	Wetting curve	-136.2	-70.8	-110.0
			Drying curve	46.1	44.4	-2.0

(1) Arithmetic mean

6.5   Advanced model concept for water repellent soils

Internationally, an impressive research effort is undertaken to unravel the secrets of preferential flow at both laboratory and lysimeter scale. Still, practical concepts to simulate field scale, transient solute leaching in water repellent soils, are limited. Until better concepts become available, the discussed F_{mob} concept can be a useful tool to improve leaching studies in non-structured water repellent soils. One more advanced concept, which is currently evaluated with SWAP, is mainly based on the work of *Ritsema et al.* (1993) and *Selker et al.* (1996), and is illustrated in Fig. 6.18.
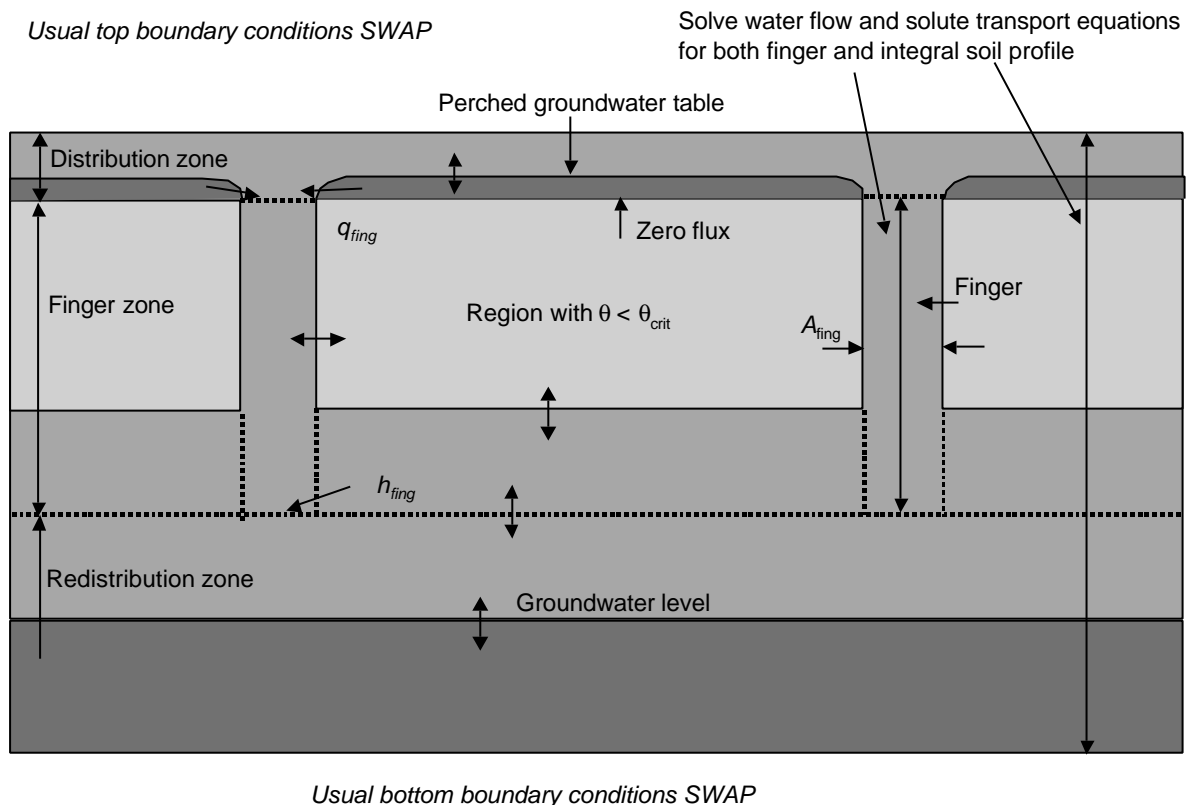
Figure 6.18 Extended concept of water flow in a soil profile with a water repellent zone.

The soil profile contains a distribution zone were lateral flow may occur towards the fingers, a finger zone, and a redistribution zone in which the fingers again merge. The following assumptions are made:

- As long as the water content in the layer below the distribution zone is higher than the critical soil water content ($\theta > \theta_{crit}$), the discussed flow and transport equations (Eqs. 2.14 and 2.30) apply to the entire soil profile.
- When the water content in the zone below the distribution zone becomes lower than the critical water content ($\theta < \theta_{crit}$), at the bottom of the distribution zone a zero flux condition is valid. This may result in a perched groundwater table in the distribution zone, which creates a lateral soil water flux towards the fingers.

- The relative cross-sectional area of the fingers, A_{fing} (cm^2 cm^{-2}), is equal to (*Selker et al.*, 1996):

$$A_{\text{fing}} = \sqrt{\frac{q_{\text{fing,max}}}{K_{\text{sat}}}} \tag{6.9}$$

  where $q_{\text{fing,max}}$ is the maximum flux density (cm d^{-1}) at the top of the fingers after they were created, and K_{sat} the saturated hydraulic conductivity (cm d^{-1}) in the finger zone. In this way at $q_{\text{fing,max}}$ nearly saturated conditions are created in the fingers. When in due course q_{fing} decreases, A_{fing} remains constant, and thus the water content in the finger becomes smaller.

- Lateral diffusion of water from the fingers towards the surrounding water repellent soil will be limited due to hysteresis and water repellency, and is neglected.

- Inside the fingers Richards' equation applies, with a flux condition ($q = q_{\text{fing}}$) at the top, and a head condition ($h = h_{\text{fing}}$) at the bottom. Solute movement inside the fingers can be described with the general transport equation (Eq. 2.30), taking into account the finger volume.

- The Richards' equation and solute transport equation can be solved for the remaining soil profile (Fig. 6.18), when we take into account at the bottom of the distribution zone a zero flux condition if $\theta < \theta_{\text{crit}}$ and a possible lateral flux towards the fingers, in the finger zone possible changes of the cross section and length of the fingers, and at the top of the redistribution zone a flux from the fingers.

- The root water extraction rate $S_a(z)$ inside and outside the finger may be different due to different soil water pressure heads. SWAP calculates $S_a(z)$ inside and outside the finger separately, using the root density π_{root} and the prevailing soil water pressure heads h, as discussed in Chapter 2.

- The fingers will disappear if:
  - due to soil water flow or root water extraction, the water content inside the fingers becomes less than the critical water content;
  - due to increasing groundwater levels, the water content below the distribution zone becomes larger than the critical water content;
  - due to extreme lateral fluxes towards the fingers, the cross-sectional area of the fingers becomes larger than a defined maximum.

This concept enables us to simulate effects of water repellency on the water- and solute balance and to analyse its sensitivity to factors as rainfall intensity, thickness of distribution zone, critical water content, saturated hydraulic conductivity of water repellent layer, height of redistribution zone, and groundwater level fluctuations. The flexible boundary conditions of SWAP allow this analysis for entire growing seasons. Currently the concept is evaluated, using data of tracer experiments at water repellent field soils.

6.6 Discussion and conclusions

For hysteresis of the soil hydraulic functions we incorporated Scott's scaling method into SWAP. This method requires only the measured main drying and main wetting water retention curves to generate the scanning curves. The mobile-immobile concept for transient flow in water

repellent soils, as implemented into SWAP, requires a function $F_{mob}(h)$. The parameter F_{mob} has a clear physical meaning, which facilitates measurement at field conditions.

In general, hysteresis retards water movement, while preferential flow enhances water movement. This directly affects the residence time of water and solutes in the unsaturated zone. In the simulated field conditions, hysteresis slightly decreased the water storage in the root zone. The slow increase of the water storage in the root zone after a dry year could better be predicted by including hysteresis. However, under field conditions hysteresis hardly affected the soil water fluxes to the groundwater level, and could not account for observed groundwater peaks after large rainfall events. In the field experiments considered in this study, no ponding occurred and thus flux-type boundary conditions apply. This is generally the case in The Netherlands with its mild climate and relatively permeable soils. *Kaluarachchi and Parker* (1987) showed that a head-type boundary condition at the soil surface has a larger affect on simulated soil water fluxes than a flux-type boundary condition. Thus in runoff situations, hysteresis will have a larger effect on the simulation results. Also we may expect hysteresis to affect percolation in irrigated fields, where ponding occurs and intensive wetting and drying alternate continuously.

Adjustment of the soil hydraulic functions with the preferential flow concept slightly improved the simulated soil water contents. The effect of the factor F_{mob} on the soil water fluxes, however, is marginal for the experiments considered. This is probably due to compensation of the higher water contents in the fingers by the smaller horizontal flow cross section in temperate conditions. In the field experiments, the soil water fluxes were dictated by the net rainfall, actual evapotranspiration and the relatively shallow groundwater levels. However, during infiltration events in dry soils, as shown in Fig. 6.4, or in soils with deep water table levels, soil water fluxes are more affected. The relative insensitivity of soil water fluxes to preferential flow under temperate conditions implies that determination of preferential flow from water balance measurements under these conditions is difficult (*Luxmoore*, 1991). Simulation with laboratory measured soil hydraulic functions might compare well to measured soil water fluxes in the field or lysimeter, while the actual flow takes place through fingers. If we are interested in soil water fluxes only, the laboratory measured functions suffice. However, for leaching of nutrients and pesticides the residence time in the unsaturated zone is important, and this time is considerably reduced in case of preferential flow, as shown for the Ouddorp experiment. The leaching of bromide to groundwater at this experiment was much better predicted when the F_{mob} concept was included.

Until better concepts become available, the F_{mob} concept can be a useful tool to improve leaching studies in non-structured, water repellent soils. Also a more advanced concept has been presented which has been implemented into SWAP and is currently applied to tracer experiments at water repellent field soils.

7. Simulation of water and solute movement in a cracked clay soil[6]

7.1   Introduction

Shrinkage cracks may have a large impact on water flow and solute transport through the vadose zone and should be included in generally applied agrohydrologic models like SWAP. Empirical models incorporating the bypass through cracks in a simplified way can be calibrated for specific soil samples or fields. However, because of their empirical character, the use of these models for predictive purposes is limited. Models that simulate the general physical processes are more reliable for use in scenario studies. Unfortunately, detailed simulation of the physical transport processes in cracked clay soils is not feasible, as the chaotic and dynamic morphology of each location would require a huge amount of data. We may therefore search for some systematic behaviour on a larger scale, in the same way as Darcy's law incorporates complicated, unpredictable pore geometry at a scale where a continuum of water, solid material and air applies. In experimental fields with cracked clay, various locations show at the same soil depth a large variability of water contents and solute concentrations (*Beven and Germann*, 1982; *Bronswijk et al.*, 1995). Instead of trying to describe water flow and solute transport at the various locations, the field average behaviour might be more easy to catch in a model. In order to make the model suitable for process and scenario analysis, concepts should be used that are generally applicable, thus physically based. Furthermore, model calibration requires a limited number of parameters, and preferably parameters that can be measured directly in the field.

Hoogmoed and Bouma (1980) developed one of the earliest numerical models for infiltration into a cracked clay soil. Rainfall in excess of the maximum infiltration rate, ponded on the soil surface, until a specified threshold value of the ponding height was reached. Thereafter, the excess rainfall amounts would flow into the cracks. In the cracks, horizontal adsorption at each nodal depth was calculated by a numerical routine which solved horizontal water adsorption by an initially dry soil. Water that was not adsorbed laterally in the crack, was considered as drainage. Their model did not include solute transport.

Germann and Beven (1985) described infiltration into the soil matrix at the soil surface by Philip's sorptivity concept. Flow in the macropores was approached by kinematic wave theory, which requires three parameters for calibration. The model assumes a uniform macropore system, and describes water flow only.

The MACRO model (*Jarvis*, 1994; *Andreu et al.*, 1994) is widely used to simulate water flow and solute transport in aggregated soils. In the model two domains are distinguished, one with macropores, and one with micropores. At the top boundary, the amount of water flowing into the macropore domain is simulated by an accurate solution of Richards' equation in the micropore domain, which generates the runoff. In the macropores, water flow is calculated by

assuming unit hydraulic gradient. Water adsorption from the macropore domain to the micropore domain is calculated with a diffusion type of equation. The macropores are continuous until the bottom of the soil profile. Solute transport is considered to be convective-dispersive in the micropore domain and solely convective in the macropore domain. The mass transfer between both domains is given by a combination of diffusion and convection. At the top boundary, a mixing layer is used to calculate the solute amounts routed to the macropores during heavy rainfall or irrigation.

Gerke and Van Genuchten (1993) developed a dual porosity model, in which Richards' equation and convection-dispersion equation are solved in both domains. One domain may represent the soil matrix and the other domain the soil fractures. Although crack flow probably not obeys Darcy's law, the soil hydraulic properties of the crack might be adjusted such that crack flow can be modeled with Richards' equation. The water exchange between the fracture and matrix at each node depends on the pressure head difference and a transfer coefficient. The solute exchange between both domains at each node is written as the sum of convection and diffusion/dispersion. The relative volumes of matrix and fracture are assumed to be constant in depth and time.

Zurmühl and Durner (1996) developed an approach for modeling water and solute transport in a bi-porous soil. The retention function is constructed by superposition of two Van Genuchten-type of retention functions. In this way they can describe the high non-linearity of the hydraulic conductivity function near saturation, which is typical for bi-porous soils. In this modeling approach, however, the small pores at any depth should be filled before water does flow into the large pores. This means that bypass flow, which hardly affects the water content of the micropores, cannot be modeled. In order to account for preferential solute transport, the authors employ the convection-dispersion equation, modified for an immobile water fraction which is a function of the total water content.

In this Chapter the shrinkage characteristic will be used to describe the swelling and shrinking of a clay soil, including its crack volume and crack depth. Water flow and solute transport are described with basic physics, employing ordinary numerical procedures. The model concept was developed to simulate the field average behaviour of a field with cracks, rather than the flow and transport at a single plot. The model will be applied to an extensive field experiment, which was performed and described by *Bronswijk et al.* (1995).

7.2   Model description

7.2.1   Basic theory of cracking clay

A shrinkage characteristic describes the relation between the amount of pores, as expressed by the void ratio, and the amount of water, as expressed by the moisture ratio (*Bronswijk*, 1988). The void ratio e (cm^3 cm^{-3}) is defined as:

$$e = \frac{V_p}{V_s} \qquad (7.1)$$

and the moisture ratio ν (cm^3 cm^{-3}) as:

$$\boldsymbol{n} = \frac{V_{\text{w}}}{V_{\text{s}}}$$ (7.2)

where V_{p} is the total pore volume (cm^3 cm^{-3}) either filled with air or water, V_{w} the water volume (cm^3 cm^{-3}) and V_{s} the solid volume (cm^3 cm^{-3}). Figure 7.1 shows a typical shrinkage characteristic. Four stages can be distinguished (*Stroosnijder*, 1975; *Bronswijk*, 1988):

1) Structural shrinkage. When saturated soils dry, large water filled pores may be emptied. As a result, aggregates can get a somewhat denser packing. On the whole, the volume changes in this shrinkage phase are negligible, but water losses can be considerable.

2) Normal shrinkage. Volume decrease of clay aggregates is equal to moisture loss. The aggregates remain fully saturated.

3) Residual shrinkage. Upon drying the volume of the aggregates still decreases, but moisture loss is greater than volume decrease. Air enters the pores of the aggregates.

4) Zero shrinkage. The soil particles reached their densest configuration. Upon further moisture extraction, the volume of the aggregates remains constant. Moisture loss is equal to air volume increase of the aggregates. Rigid soils, like sands, only show this stage.
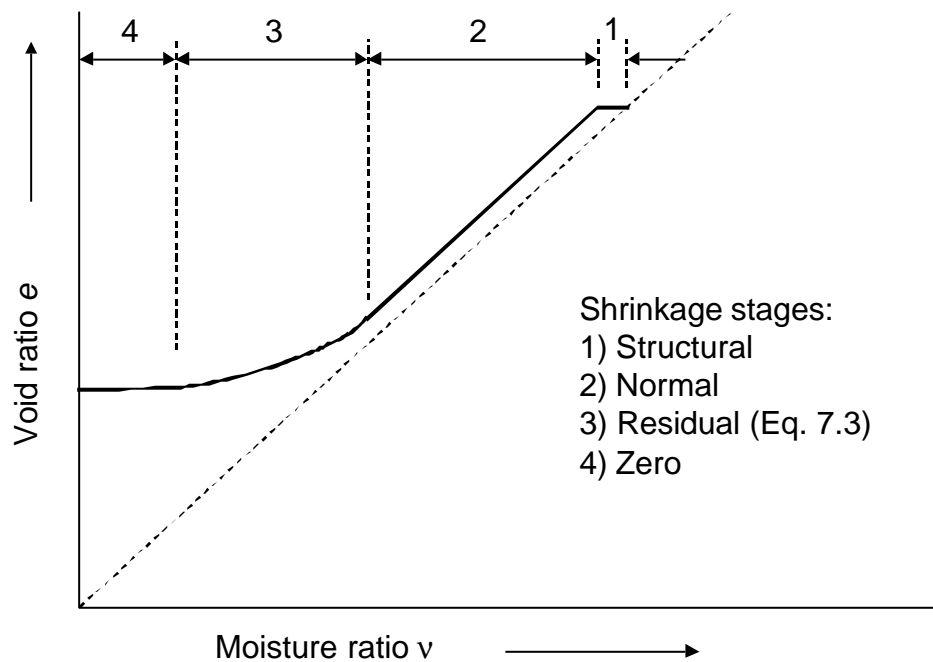
Figure 7.1 Void ratio e as function of moisture ratio ν, showing the four stages of a typical shrinkage characteristic (after *Bronswijk*, 1988).

To facilitate input and data analysis in SWAP, an exponential relationship is employed for the residual shrinkage stage (*Kim*, 1992):

$$e = \boldsymbol{a}_{\text{sh}} \mathrm{e}^{-\boldsymbol{b}_{\text{sh}}\boldsymbol{n}} + \boldsymbol{g}_{\text{sh}}\boldsymbol{n}$$ (7.3)

with α_{sh}, β_{sh}, and γ_{sh} dimensionless, empirical parameters. *Yule and Ritchie* (1980a, 1980b) described shrinkage characteristics of eight Texas Vertisols, using small and large cores. *Bronswijk and Evers-Vermeer* (1990) described shrinkage characteristics of seven clay soils in The Netherlands. *Garnier et al.* (1997) propose a simple evaporation experiment to

determine simultaneously the moisture retention curve, hydraulic conductivity function and shrinkage characteristic.

The shrinkage characteristic enables us to calculate the crack volume and depth. Imagine a soil cube with sides z (cm) and volume $V = z^3$ (cm^3). In case of isotropic shrinkage of volume ΔV (cm^3) we may derive:

$$V = z^3, \quad V - \Delta V = (z - \Delta z)^3 \quad \text{and} \quad \Delta V = z^3 - (z - \Delta z)^3 \tag{7.4}$$

with Δz the change of each side length (cm). Therefore:

$$1 - \frac{\Delta V}{V} = \left(1 - \frac{\Delta z}{z}\right)^3 \tag{7.5}$$

In the case of one-dimensional subsidence without cracking, the following relation applies:

$$1 - \frac{\Delta V}{V} = \left(1 - \frac{\Delta z_{\text{ver}}}{z}\right)^1 \tag{7.6}$$

where Δz_{ver} is the vertical subsidence (cm). In a study on pedogenetically unripened soils, *Rijniersce* (1983) called the exponent in Eqs. 7.5 and 7.6 the geometry factor r_s. This results in a general relation between volume change ΔV and subsidence Δz_{ver} of a clay soil volume:

$$1 - \frac{\Delta V}{V} = \left(1 - \frac{\Delta z_{\text{ver}}}{z}\right)^{r_s} \tag{7.7}$$

In case of three-dimensional isotropic shrinkage, $r_s = 3$. When cracking dominates subsidence $r_s > 3$, when subsidence dominates cracking $1 < r_s < 3$. In case of subsidence only, $r_s = 1$.
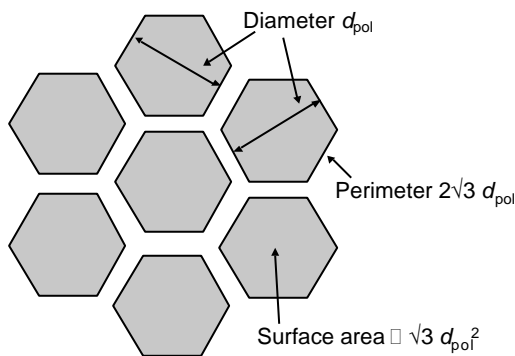
Figure 7.2 Geometry of soil matrix hexagons at a cracked clay soil.

In order to calculate the lateral infiltration rate of water collected in cracks, we need to derive the vertical crack wall area. Consider a crack pattern of hexagons with diameter d_{pol} (cm) as depicted in Fig. 7.2. We may derive that per unit depth the relative area of the vertical crack walls with respect to the horizontal surface area, $A_{\text{wall,rel}}$ (cm^2 cm^{-2}), equals:

$$A_{\text{wall,rel}} = \frac{2\sqrt{3}\, d_{\text{pol}}}{\tfrac{1}{2}\sqrt{3}\, d_{\text{pol}}^2} = \frac{4}{d_{\text{pol}}} \tag{7.8}$$

The matrix and crack infiltration at a given rainfall intensity P can be calculated as (*Bronswijk*, 1988):

$$\begin{aligned} P < I_{\text{max}}: \quad & I_m = A_m P \\ & I_c = A_c P \\ P > I_{\text{max}}: \quad & I_m = A_m I_{\text{max}} \\ & I_c = A_m (P - I_{\text{max}}) + A_c P \end{aligned} \tag{7.9}$$

with P the rainfall intensity (cm d^{-1}), I_{max} the maximum infiltration rate of the soil matrix (cm d^{-1}), I_m the infiltration rate into the soil matrix (cm d^{-1}), I_c infiltration rate into the cracks (cm d^{-1}), and A_m and A_c relative areas of soil matrix and cracks, respectively (cm^2 cm^{-2}).

7.2.2 Water flow concept

Figure 7.3 shows the concept of water flow in a cracked clay soil as implemented in SWAP. Precipitation in excess of the infiltration rate flows as runoff to the cracks, as described by Eq. 7.9. The time needed for ponding water to flow on the soil surface to the cracks is probably negligable. A small time delay can be created by defining a threshold ponding height, which should be reached before runoff to the cracks starts. The maximum infiltration rate I_{max} is derived from an accurate solution of Richards' equation near the soil surface (see Chapter 5). In order to do so, the nodal spacing near the soil surface should not exceed 1 cm, and the saturated hydraulic conductivity K_{sat} should be determined for the clay matrix without cracks. Actual rainfall rates should be used, as daily rainfall rates underestimate seriously runoff amounts to the cracks.
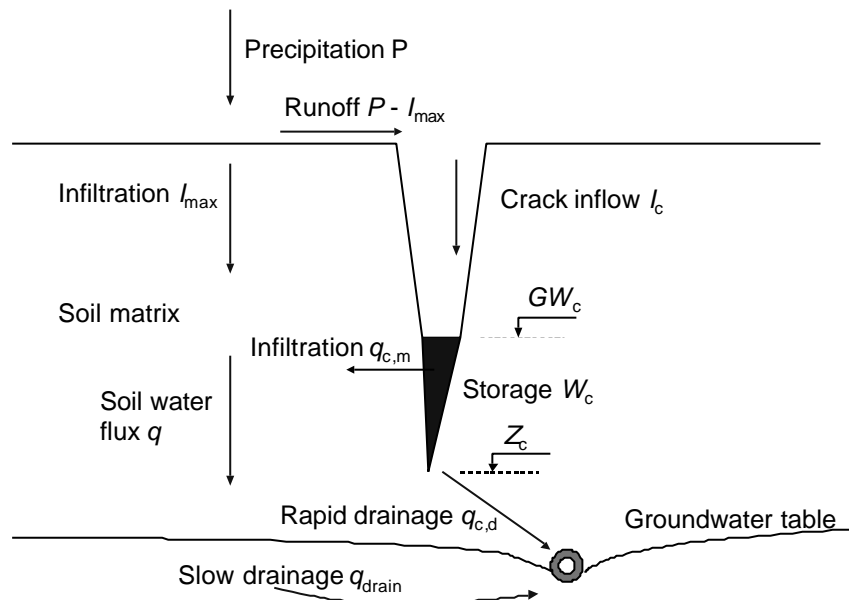
Figure 7.3 Concept of water flow in a cracked clay soil as applied in SWAP. The variables are explained in the text.

Using the shrinkage characteristic and the actual water contents, the following steps are made to derive the amount of shrinkage ΔV, subsidence Δz_{ver} and relative, horizontal crack area A_c (cm^2 cm^{-2}) at a certain soil depth or node i:

1) Solid volume $V_s = 1.0 - \theta_{sat}$, where θ_{sat} is saturated water content (cm^3 cm^{-3}) of the considered soil layer;
2) Moisture ratio $v = \theta_i / V_s$, with the water content θ_i (cm^3 cm^{-3}) of node i, following from the solution of the Richards' equation at this time step;
3) Calculate void ratio e from the specified shrinkage characteristic $e(v)$;
4) Total pore volume $V_p = e\, V_s$;
5) Shrinkage soil volume with respect to maximum soil volume $\Delta V = \theta_{sat} - V_p$; vertical subsidence Δz_{ver} follows from Eq. 7.7;

6) Volume vertical crack $V_c = \Delta V - 1.0 \, \Delta z_{ver}$ (cm^3 cm^{-3});

7) Relative horizontal crack area $A_c = 1.0 \, V_c / (1.0 - \Delta z_v)$ (cm^2 cm^{-2}).

In this procedure the water contents of the soil matrix are not adjusted for the shrinkage itself, which will change the vertical and horizontal co-ordinates. A study by *Peerboom* (1987) showed that the effects of these co-ordinate changes on simulated water contents and soil water movement inside the clay matrix are minor, while the numerical coding of this correction is substantial. Therefore this correction has been skipped, which results in the above listed straightforward procedure.

According to the described theoretical shrinkage characteristic (Fig. 7.1), a crack volume would exist when $\theta_i < \theta_{sat}$. This would imply that as soon as the clay matrix is unsaturated ($h < 0$) cracks are formed. Field soils may deviate from this behaviour, showing crack bottoms higher and lower than the groundwater level. In the SWAP program we took this into account by calculating a crack volume if $\theta < \theta_{crit}$, where θ_{crit} is the critical water content for cracking derived from measurements. The concept of the shrinkage characteristic does not allow for the existance of cracks below the groundwater level ($\theta_{crit} \le \theta_{sat}$), which is maintained in the SWAP program. In this way the level of the crack bottom Z_c is calculated as function of time.

Water collected in the cracks, will either infiltrate laterally to the soil matrix or flow rapidly to nearby drains and/or ditches, as depicted in Fig. 7.3. The infiltration rate $q_{c,i}$ (cm d^{-1}) at node i can be derived straight from Darcy, if we assume a linear lateral pressure gradient in the soil matrix polygon and infiltration from each side:

$$q_{c,i} = -K(h_i) \frac{\partial H}{\partial x} = -6K(h_i) \frac{(h_i - h_{c,i})}{d_{pol}} \tag{7.10}$$

where K is the unsaturated hydraulic conductivity (cm d^{-1}), H the soil hydraulic head (cm), x the horizontal distance (cm), and h_i and $h_{c,i}$ are the nodal water pressure heads (cm) in the soil matrix and in the crack, respectively. The factor 6 accounts for water adsorption from all sides in the horizontal plane of the polygon. The water level in the cracks, GW_c (cm), can be calculated using the crack volume as function of depth as described earlier and the actual crack water storage. The total lateral infiltration rate, $q_{c,m}$ (cm d^{-1}), is derived by the summation (Fig. 7.3):

$$q_{c,m} = \sum_{z=Z_c}^{z=GW_c} q_{c,i} A_{wall,rel} \tag{7.11}$$

where Z_c is the crack depth (cm). The lateral infiltration rate is added as a source term $q_{c,i}/\Delta z_i$ to the Richards' equation for the water movement in the clay matrix:

$$\frac{\Delta q_i}{\Delta t} = \frac{\Delta}{\Delta z_i} \left[K(h_i) \left(\frac{\Delta h_i}{\Delta z_i} + 1 \right) \right] - S_a(h_i) + \frac{q_{c,i}}{\Delta z_i} \tag{7.12}$$

where S_a is the root water extraction rate (cm^3 cm^{-3} d^{-1}). Field observations show that in cracked clay fields, water may flow directly from the cracks to drains or ditches, without entering the soil matrix. *Hendriks et al.*, (1999) discussed an extensive concept for this so-called rapid drainage rate. In SWAP the rapid drainage rate, $q_{c,d}$ (cm d^{-1}), is calculated with

one calibration parameter, the mean residence time $T_{c,d}$ (d) of water in the cracks if only rapid drainage would occur:

$$q_{c,d} = \frac{W_c}{T_{c,d}} \tag{7.13}$$

where W_c is the crack water storage (cm). Finally the change of water storage in the cracks, ΔW_c (cm), follows from the balance (Fig. 7.3):

$$\Delta W_c = \left(I_c - q_{c,m} - q_{c,d} \right) \Delta t \tag{7.14}$$

Note that different from the earlier concept of *Hoogmoed and Bouma* (1980), water adsorption above the water level in the cracks is not included. *Bouma and Dekker* (1978) already concluded that the contact area between preferential flow and soil matrix forms only a small fraction of the total area available in the vertical ped surfaces. This complicates the calculation of horizontal adsorption. *Booltink and Bouma* (1993) applied the model with water adsorption to soil types ranging from loamy sand to clay and found that the lateral adsorption during bypass flow was always less than 1 percent. Therefore in current SWAP this lateral adsorption was not included.

7.2.3 Solute transport concept

The solutes that enter the cracks may originate from the precipitation directly falling into the cracks, or from runoff water when the soil matrix infiltration capacity is exceeded ($P > I_{max}$):

$$I_c c_{in} = A_m \left(P - I_{max} \right) c_{in} + A_c P c_{in} \tag{7.15}$$

with c_{in} the solute concentration of the precipitation or irrigation water (g cm^3). Field experiments show that water flowing along the crack walls, leaches solutes out of the soil matrix and transport them quickly to the subsoil. In the SWAP model, lateral solute transfer between soil matrix and water flowing down the cracks, $s_{lat,i}$ (g cm^{-2} d^{-1}), is calculated as:

$$s_{lat,i} = D_{lat} I_c \left(c_i - c_{in} \right) \Delta z_i \tag{7.16}$$

where D_{lat} is the lateral transfer coefficient (cm^{-1}) and c_i the solute concentration (g cm^3) in the soil matrix. D_{lat} is a function of the crack morphology and transmitting properties of the crack wall and has to be derived from field or laboratory measurements. The amount of solutes that enter the water reservoir in the cracks, $s_{c,in}$ (g cm^{-2} d^{-1}), equals:

$$s_{c,in} = I_c c_{in} + \sum_{z=GW_c}^{z=0} s_{lat,i} \tag{7.17}$$

In the crack water reservoir, the solutes are mixed. Part of the solutes will enter the soil matrix along the crack wall in contact with the water. Another part is transported with rapid drainage water directly to the drains and/or ditches (Fig. 7.3):

$$s_{c,out} = c_c \left(q_{c,m} + q_{c,d} \right) \tag{7.18}$$

with $s_{c,out}$ the total flux density of solutes leaving the crack reservoir (g cm^{-2} d^{-1}) and c_c the mean solute concentration in the crack reservoir (g cm^{-3}).

Change of solute storage in the cracks ΔS_c (g cm^{-2}) is calculated with the balance:

$$\Delta S_c = \left(s_{c,in} - s_{c,out} \right) \Delta t \tag{7.19}$$

In the soil matrix the ordinary solute transport equation (Eq. 2.30) is applied. The lateral diffused solute amounts due to water flowing down the cracks, $s_{\text{lat},i}$, and the adsorbed solutes from the water reservoir in the cracks, $q_{\text{c},i} c_{\text{c}}$, are added as a source term to Eq. 2.30.

7.3   Measurements at De Vlierd

Experimental farm De Vlierd is situated in the Riverine area in the central part of the Netherlands and has pasture in use for cattle grazing. Its soil can be classified as a very fine clayey, mixed illitic-montmorillonitic, mesic, Typic Fluvaquent (*Soil Survey Staff*, 1975). The soil clay content ranges from 51 to 60%, and the soil shows a pronounced soil structure. The site has tile drains with a length of 210 m, a depth of 0.95 m, and a spacing of 15 m.

On 26 September 1991, *Bronswijk et al.* (1995) applied bromide to an experimental field of 30x15 m by spraying 0.005 cm water with a concentration of 360 μg cm^{-3} KBr. Water content and bromide concentrations in the top meter of the soil were measured 6, 46, 209, 335 and 572 days after bromide application. On each sampling day, at 15 locations within the experimental field, steel cylinders of 1 m length and 8.8 cm inner diameter were pushed into and pulled out of the soil using a hydraulic crane. The soil columns were sectioned into pieces of 5 cm, of which the water content and bromide concentration was determined. Other on-site measurements included daily rainfall data, the shrinkage characteristic of each soil layer, groundwater levels, drainage fluxes (discontinuous), and bromide concentrations in ground- and drainage water (discontinuous).

Table 7.1 Measured soil water content and bromide concentration profiles (mean, N = 15) at 5 sampling days.

Depth (cm)	Water contents (cm^3 cm^{-3})					Bromide concentrations (μg cm^{-3})				
	Day 6	46	209	335	572	Day 6	46	209	335	572
2.5	0.423	0.575	0.467	0.441	0.624	80.2	41.1	13.0	17.7	9.8
7.5	0.263	0.467	0.473	0.333	0.507	7.8	7.2	3.5	5.9	7.9
12.5	0.281	0.443	0.472	0.348	0.490	6.6	5.5	2.9	4.2	6.6
17.5	0.297	0.419	0.483	0.351	0.506	6.3	4.4	2.8	4.3	5.7
22.5	0.300	0.443	0.458	0.372	0.480	6.4	4.8	2.4	3.1	3.3
27.5	0.330	0.436	0.451	0.381	0.470	7.5	4.8	2.6	2.6	2.4
32.5	0.347	0.435	0.450	0.393	0.454	8.1	4.7	3.1	1.9	1.6
37.5	0.373	0.436	0.449	0.422	0.450	10.9	6.5	3.7	1.9	1.3
42.5	0.404	0.421	0.468	0.438	0.465	13.9	8.4	4.6	1.8	1.2
47.5	0.428	0.449	0.475	0.452	0.479	16.8	9.9	5.7	1.9	1.2
52.5	0.448	0.435	0.481	0.462	0.477	18.8	11.2	7.3	2.1	1.4
57.5	0.472	0.459	0.501	0.469	0.492	18.3	11.4	8.2	2.6	1.3
62.5	0.481	0.481	0.509	0.479	0.500	13.5	11.6	9.3	4.4	1.9
67.5	0.489	0.504	0.524	0.492	0.505	10.4	13.5	14.9	6.0	1.5
72.5	0.486	0.494	0.519	0.496	0.516	7.4	12.4	16.2	6.7	1.6
77.5	0.495	0.504	0.512	0.478	0.519	5.7	12.7	16.4	7.8	1.7
82.5	0.486	0.524	0.510	0.487	0.494	4.3	12.8	17.1	7.3	2.2
87.5	0.487	0.515	0.521	0.478	0.518	3.7	12.1	15.4	7.1	2.0
92.5	0.460	0.509	0.536	0.506	0.509	2.6	6.5	18.0	8.8	2.0
97.5	0.501	0.511	0.496	0.516	0.497	2.4	6.0	6.3	12.4	2.1

In order to determine the shrinkage characteristic, clods were briefly immersed in SARAN-F310 resin (resin to solvent ratio 1:5 on weight base) and allowed to dry in the laboratory. The applied SARAN coating is very elastic, impermeable to water and permeable to water vapor. As the clod dry and shrink, the elastic coating remains tightly fitted around the clods. By repeated weighing and under water weighing, both weight and volume of the clod can be determined at different stages of shrinkage in a non-destructive way. After two to four weeks, weight losses became negligible. Finally the SARAN-coated clods were oven dried in order to measure final dry volume and dry weight (*Bronswijk and Evers-Vermeer*, 1990). Detailed description of the other experimental procedures were given by *Bronswijk et al.* (1995).

In this study the focus is on the average flow and transport at the experimental field. Therefore, at each sampling date the average water content and bromide concentrations of the 15 soil columns for each depth will be considered, which are listed in Table 7.1. When the bromide was applied, the soil was very dry. At day 6, soil water contents at depth 5-35 cm still range between 0.263 and 0.347. The effect of rainfall surplus in winter time (day 209 and 572) and rainfall shortage in summer time (day 335) are clearly visible in water content fluctuations at 10-40 cm depth. Below 60 cm depth, the water content variations are relatively small. On day 4, 20 mm rain fell in about 7 hour. This caused the relative high bromide concentrations of 10-19 μg cm^{-3} at depth 35-70 cm on day 6. During the whole experimental period bromide was retained in the top soil, while concentrations at 5-35 cm depth were relatively low. The bromide wave in the subsoil is clearly visible. After 572 days, 75% of the bromide amount applied was leached out of the soil top meter.

7.4   Model input

In the reference simulation without cracks, SWAP model input consisted of rainfall rate, potential evapotranspiration rate, crop rooting depth, root water uptake reduction function, soil hydraulic functions, drainage rate as function of groundwater level, bromide application, and solute dispersion coefficient. In the simulation with cracks, additional model input consisted of shrinkage characteristic, diameter soil matrix polygon, solute transfer coefficient, and mean residence time of rapid drainage water.

Reference evapotranspiration data were measured at weather station Herwijnen, which is assumed to be representative for experimental farm De Vlierd. Daily rainfall amounts were measured near the research field. Actual rainfall intensities are needed, which were derived by dividing the daily rainfall amounts by daily rain duration. Grass rooting depth was assumed to be 40 cm throughout the experimental period. Reduction of root water uptake at either too dry or too wet conditions was described according to Fig. 2.3. For the grass canopy, we assumed no water extraction if $h > -15$ cm or $h < -8000$ cm, maximum root water extraction ($\alpha_{rw} = 1.0$) at $-25 < h < -500$ cm, and a linear increase/decline of α_{rw} in the ranges $-15 < h < -25$ cm and $-500 < h < -8000$ cm. The soil hydraulic functions $\theta(h)$ and $K(\theta)$ were derived from soil texture, using a Dutch database (*Wösten et al.*, 1994). The functions were analytically described according to Eq. 2.15 and 2.16, and their parameters are listed in Table 7.2. The bottom boundary condition could be described with a linear relation between

groundwater level and drainage rate, according to Eq. 2.17. Simultaneous measurements of drainage rate and groundwater level indicated a drainage resistance, γ_{drain}, of 44 d. The solute dispersion coefficient in the clay matrix was calculated using a dispersion length L_{dis} of 10 cm, which accommodates biopores and small cracks (*Jury et al.*, 1991). In principle for each soil layer a different shrinkage characteristic might be defined. As the differences between the measured shrinkage characteristics of the various layers were small, we conducted the analysis with one shrinkage characteristic for the entire profile, being described according to Eq. 7.3 by $\alpha_{sh} = 0.32$, $\beta_{sh} = -1.11$, and $\gamma_{sh} = 0.036$. The diameter of the soil polygons d_{pol} in the subsoil was estimated at 25 cm.

Table 7.2 Van Genuchten (1980) parameters describing soil hydraulic functions of first and second soil layer.

Soil layer	α (cm^{-1})	n (-)	θ_{sat} (cm^3 cm^{-3})	θ_{res} (cm^3 cm^{-3})	K_{sat} (cm d^{-1})	λ (-)
First (0-30 cm)	0.0532	1.08	0.55	0.00	1.00	-8.82
Second (30-150 cm)	0.0171	1.11	0.53	0.00	3.32	-4.64

Still three parameters had to be derived from calibration by the field-scale measurements:
−   The top soil saturated hydraulic conductivity, K_{sat}, which controls runoff and was calibrated using the measured water content profiles, resulting in $K_{sat} = 1.0$ cm d^{-1};
−   The solute transfer coefficient, D_{lat}, which was calibrated using the measured bromide concentration profiles and bromide leaching fluxes, resulting in $D_{lat} = 0.25$ cm^{-1};
−   The mean residence time for rapid drainage, $T_{c,d}$, which was calibrated using the drainage fluxes and bromide leaching fluxes, resulting in $T_{c,d} = 20$ d.

7.5   Simulation results

In all simulation results that will be shown, the mass balances were accurate, with a maximum closure error for water of 0.15 cm y^{-1}, and for bromide of 0.20 µg cm^{-2} y^{-1}. Figures 7.4 and 7.5 show the simulated water content and bromide profiles *when cracks are not taken into account*. In that case the measured relative low soil water contents at 10-40 cm depth, which are due to water bypass, are not reproduced. The calculated bromide wave shows the characteristic shape of the convection-dispersion equation and deviates strongly from the measured concentrations. Extensive calibration could not improve the simulation results. Simulated bromide leaching below 100 cm depth is much slower than measured (Table 7.3). For instance, after 335 days, a bromide leaching of 710 µg cm^{-2} was measured, while only 61 µg cm^{-2} was simulated. It is clear that for this field cracks significantly affect water flow as well as solute transport and should therefore be taken into account during simulation.

Figure 7.6 shows the measured and simulated water content profiles *when cracks are included*. The dryness of the soil at 10-40 cm depth due to bypass flow is much better reproduced, although the simulated water content gradients at 0-10 cm depth are less steep as measured. The seasonal changes of water storage are well reproduced.

Figure 7.4 Measured (mean, $N = 15$) and simulated soil water content profiles at the 5 sampling days; the simulations were performed assuming *no cracks.*

Figure 7.5 Measured (mean, $N = 15$) and simulated bromide concentration profiles at the 5 sampling days; the simulations were performed assuming *no cracks*.

Table 7.3 Measured and simulated bromide leaching ($\mu g \ cm^{-2}$) below 100 cm soil depth as function of time. The simulation variants are explained in the text.

Measurements or simulation variant	Day number				
	6	46	209	335	572
Measured	0	190	360	710	900
No cracks	0	0	58	61	479
Reference simulation	**54**	**140**	**453**	**533**	**976**
Daily rainfall intensities	28	46	292	437	873
Soil texture	151	222	515	582	971
Saturated hydraulic conductivity top soil	19	96	351	496	927
Shrinkage characteristic	54	139	453	533	973
Diameter soil polygon	25	59	382	429	923
Lateral solute transfer	59	152	477	559	990
Crack depth	67	176	316	404	837
Rapid drainage	102	256	546	656	1022
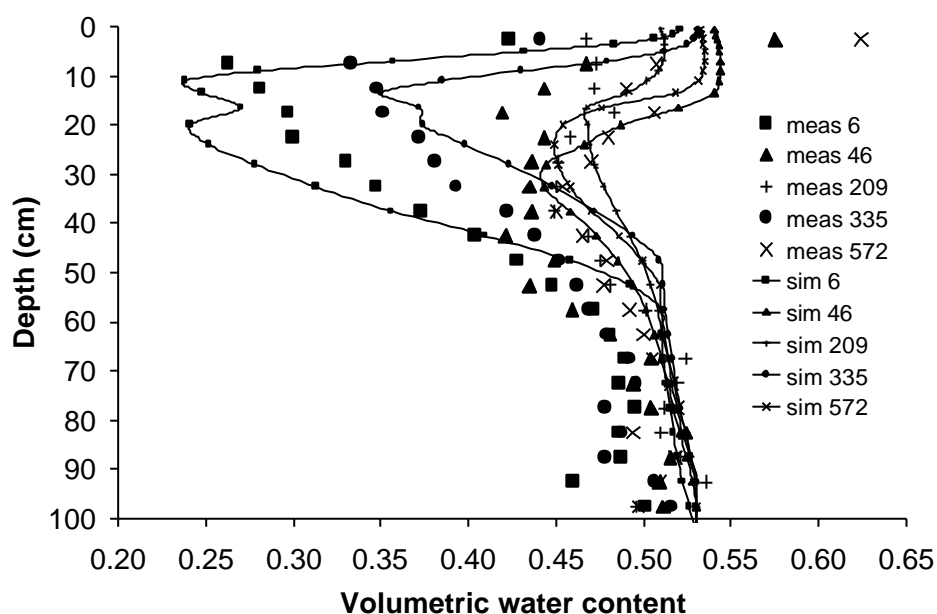
Figure 7.6 Measured (mean, $N = 15$) and simulated water content profiles at the 5 sampling days; the simulations were performed assuming *cracks*.

Figure 7.7 shows the measured and simulated groundwater levels. The range and dynamics of the simulated groundwater levels correspond well to the measurements. Figure 7.7 also shows the simulated crack bottom and water level in the crack. Only during short time intervals of 1-3 wet days, no cracks are present. The rainfall surplus in the winter period (day number 40-200 and 410-550) results in simulated crack depths of circa 20 cm, while during dry periods in summer the simulated crack depths increase to 85 cm. The water depth in the crack generally ranges between 0 and 5 cm, with some exceptional high values up to 25 cm. Figure 7.8 shows the measured and simulated drainage rates. The measurements are not complete, which makes the comparison not conclusive. The measured drainage rates at days 215 and 350 are not reproduced by the model. In the remaining part, the range of the predicted
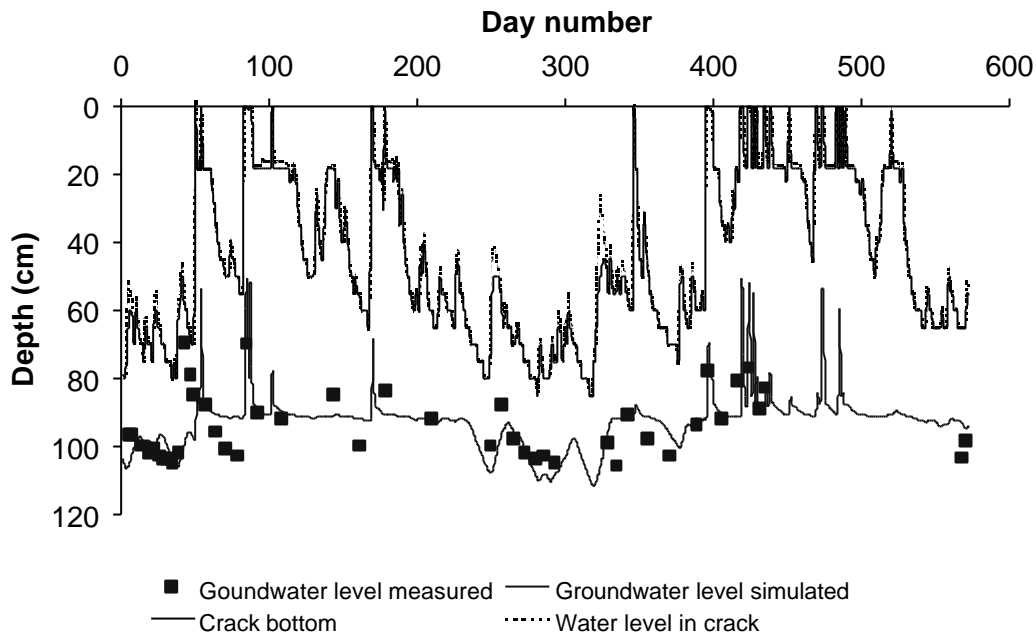
Figure 7.7 Measured and simulated groundwater levels during the experimental period; also the simulated crack bottom Z_c and water level in the crack GW_c are shown.

drainage rates is okay. Overall, this water flux simulation seems accurate enough to form a sound basis for bromide transport simulation.

Figure 7.9 shows the measured and simulated bromide profiles when cracks are included. At day 6, the measurements show bromide concentrations of 10-18 μg cm^{-3} at 35-70 cm depth, while the model predicts bromide concentrations of 10-35 μg cm^{-3} at 40-80 cm depth. Thus during the first 6 days, the model overestimates both the amount of bromide leached from the top soil and the depth at which the bromide is absorbed. At day 46, measurements indicate that the largest bromide concentrations occur at 50-90 cm depth, with concentrations ranging from 11.0 to 13.5 μg cm^{-3}. At this date, the model predicts the peak to occur at 65 cm, with a bromide concentrations of 35 μg cm^{-3}. At day 209, the predicted bromide concentrations are quite close to the measured values. The measurements show high bromide concentrations in the top soil until the last sampling date. The model does not reproduce this bromide retardation in the top soil, but suggests relatively fast leaching from the top soil. At the first and second sampling date, the bromide concentrations in the groundwater at 80-100 cm depth are underestimated. At the later sampling dates (day 335 and 572) the measured concentrations in the shallow groundwater are lower than simulated. As Table 7.3 shows, the incorporation of cracks clearly improved the calculation of bromide amounts leached from the top 100 cm soil.
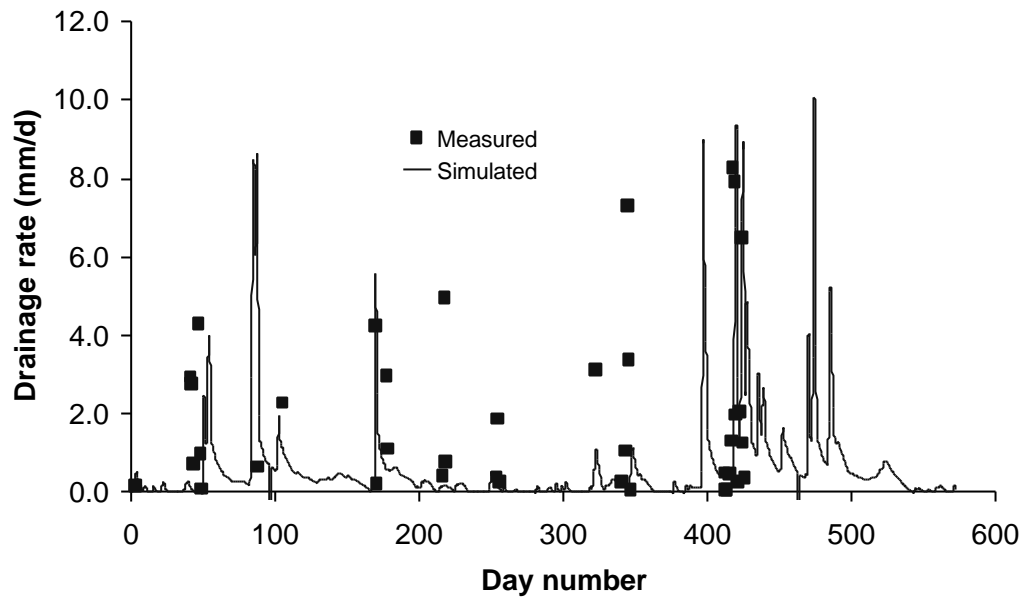
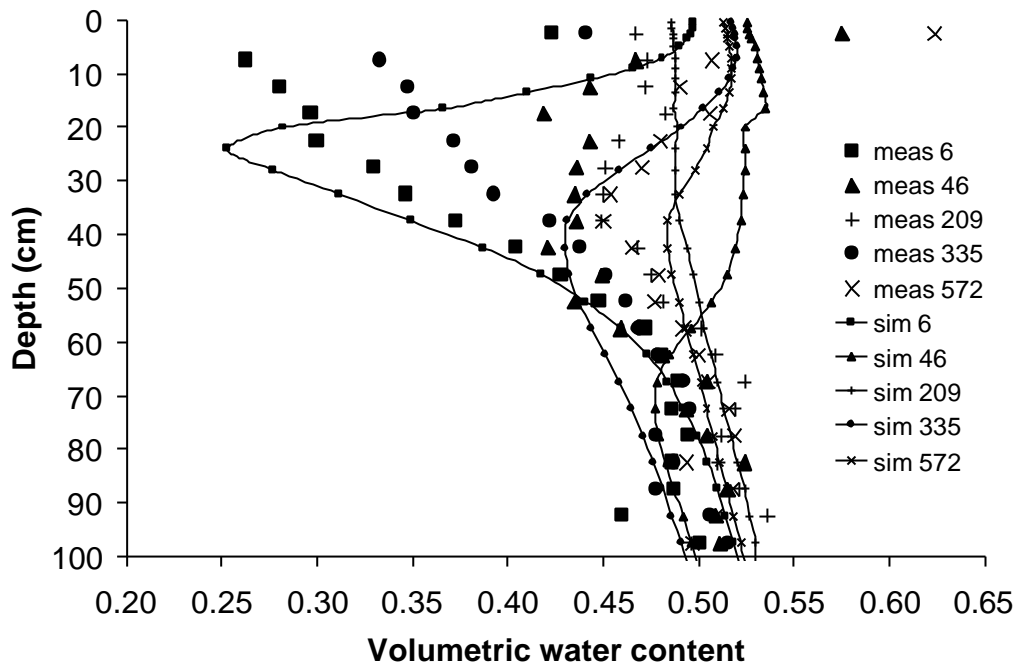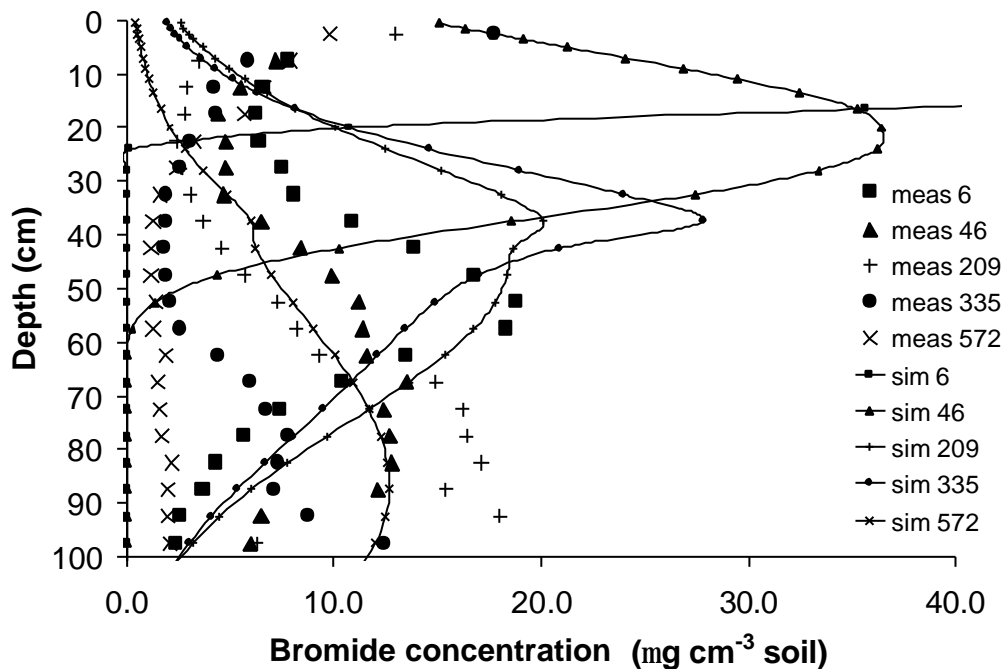**Figure 7.8** Measured and simulated drainage rate during the experimental period.
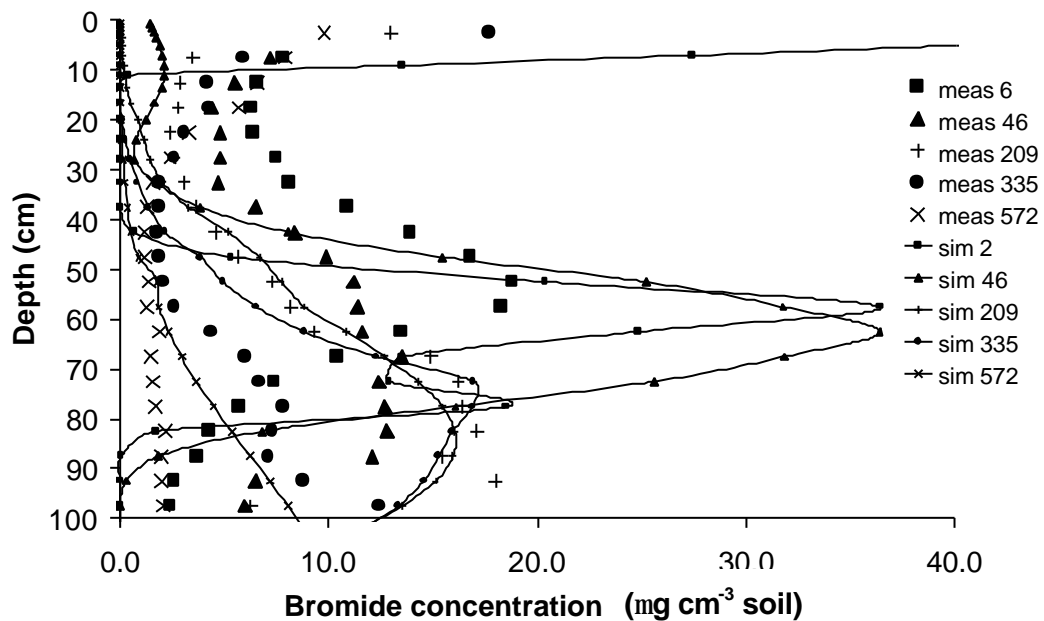
Figure 7.9 Measured (mean, $N = 15$) and simulated bromide concentration profiles at the 5 sampling days; the simulations were performed assuming *cracks*.

To determine the sensitivity of simulation results to input data and parameters, additional simulations were performed. One by one the following input data and parameters were changed:

- Rainfall intensities P from actual intensities to daily rainfall intensities;
- Soil hydraulic parameters from clay in the actual field to silty clay (*Soil Survey Staff*, 1975), with parameters $\alpha = 0.0243$ cm^{-1}, $n = 1.111$, $K_{sat} = 1.0$ cm d^{-1} and $\lambda = -5.395$ for the first soil layer, and $\alpha = 0.0095$ cm^{-1}, $n = 1.159$, $K_{sat} = 1.14$ cm d^{-1} and $\lambda = -4.171$ for the second soil layer (*Wösten et al.*, 1994);
- Saturated hydraulic conductivity of the top soil K_{sat} from 1.0 to 15.5 cm d^{-1};
- The shrinkage characteristic to those of a field with a less heavy texture, namely Dronten (*Bronswijk and Evers-Vermeer*, 1990), with parameters $\alpha_{sh} = 0.60$, $\beta_{sh} = -1.11$, and $\gamma_{sh} = -0.81$ according to Eq. 7.3;
- Diameter soil polygon d_{pol} from 25 to 15 cm;
- Solute transfer coefficient D_{lat} from 0.25 to 0.30 cm^{-1};
- Critical water content θ_{crit} below which cracks are present from 0.53 to 0.51 cm^3 cm^{-3} for the top soil and from 0.51 to 0.49 cm^3 cm^{-3} for the subsoil;
- Mean residence time of rapid drainage $T_{c,d}$ from 20 to 10 d.

The results with regard to bromide amounts leached from the top meter are listed in Table 7.3. Use of daily rainfall intensities, instead of actual rainfall intensities, results in serious underestimation of the bromide amount leached. Change of soil hydraulic parameters, except K_{sat} of the top soil, from clay to silty clay affects the leaching mainly in the initial period, until day 46. After this period the effect of soil hydraulic parameters is relatively low. The K_{sat} of the top soil directly affects the runoff and therefore has a large impact on the bromide amounts leached. The shrinkage characteristic affects mainly the crack area at the soil surface, while the bromide amounts leached are hardly affected. A smaller soil polygon diameter d_{pol} results in more rapid infiltration of water at the crack bottom, and thus in less bypass to surface water. This results in slightly lower bromide amounts leached. The solute transfer coefficient D_{lat} has a large impact on the bromide amounts leached. A smaller critical water content θ_{crit} for crack formation, results in more shallow cracks. As Table 7.3 indicates, at day 6 and 46 the bromide amounts leached increase. This is caused by the slower infiltration rate into the soil matrix at the crack bottom and thus more rapid drainage. At later stages, the more shallow crack bottom results in smaller bromide amounts leached. Decrease of the rapid drainage mean residence time $T_{c,d}$ strongly increases the bromide amounts leached, as expected. In summary, the *amounts of bromide leached are especially sensitive to the saturated hydraulic conductivity of the top layer*, *the solute transfer from the soil matrix to crack water flow and the rapid drainage mean residence time*, while the shrinkage characteristic and the soil hydraulic properties of the clay matrix show a low sensitivity.

7.6   Discussion

As illustrated by the simulation without cracks, the *Richards' and convection dispersion equation in one domain cannot mimic the average behaviour* of solute transport in the considered cracked clay soil. The bypass of solutes to depth 35-70 cm on day 6, and also the

water flow and solute transport dynamics during later stages, can not be reproduced by these equations, no matter how much calibration is applied.

Runoff to cracks can conveniently be simulated by accurate numerical solution of the Richards' equation in the clay matrix. Especially the saturated hydraulic conductivity K_{sat} and the actual rainfall intensities P determine for such cases the amount of runoff. *Use of daily rainfall intensities results in serious underestimation of the runoff amount to cracks.*

According to the discussed concept, water which infiltrates into the cracks collects instantaneously at the bottom of the crack. As shown by *Booltink and Bouma* (1993), lateral adsorption of water by vertical walls is relatively small (less than 1 percent), which makes the exact velocity of the bypassing water less important. *Booltink et al.* (1993) suggest that horizontal ped surfaces may adsorb much more water than vertical crack walls. Our simulations show that crack volumes are such large, that in general the bypass water can be stored in the lowest 5 cm of the crack (Fig. 7.7). Probably important for simulation purposes is *the distribution of cracks widths, orientations and depths, which cause water to infiltrate in the matrix at various depths*. As discussed by *German and Beven* (1985), this may result in dispersion of wetting and draining fronts and increased spreading of solutes. The main limitation of the current concept and probably main cause of deviations that still exist between simulated and measured bromide concentrations, is attributed to the use of one representative crack geometry. When in the future more detailed morphological data are available for field soils, the present concept might be extended with parameters that describe the crack depth distribution. *Hendriks et al.* (1999) did distinguish between a number of macropore domain, each with their own crack volume and depth, to simulate the internal catchment at various depths. However, with each additional macropore domain the number of calibration parameters increases.

Another reason for the discrepancy between measured and simulated bromide concentration is caused by the averaging of 15 soil columns to get the measured values. The bromide profiles show a large variation between the measured columns (*Bronswijk*, 1995), which upon averaging result in a large dispersion of the bromide concentrations.

The retardation of bromide in the top is caused by diffusion of the bromide into the top soil aggregates and highly depends on the weather conditions after tracer application. The exact amount of solute taken up by water flowing into the cracks is difficult to reproduce by deterministic models, although it may affect the simulated bromide concentrations to a large extent. In this study only one transfer parameter (D_{lat}) was used to quantify the amount taken up by bypassing water. A mixing layer, as described by *Jarvis* (1994) might improve the simulation of the tracer retardation in the top soil and gradual release of the tracer to bypassing water. In that case extra parameters are needed, e.g. the depth of the mixing layer.

The shrinkage characteristic is helpful to simulate crack volume, crack depth and horizontal area, but *simulated water flow and solute transport is not very sensitive to the actual*

shrinkage characteristic. A simplified concept, which indicates at which times the cracks are present and what their depths are, might provide similar results. To make this operational, presence of cracks and its depth should be related to easily derived soil properties as clay and soil moisture content, as suggested by *Yassoglou et al.*, (1994).

The presented model is parsimonious in the number of parameters and most of the parameters are physically based and relatively easy to obtain. The main fitting parameters still are the solute transfer coefficient of soil matrix to crack water flow, D_{lat}, and the rapid drainage mean residence time, $T_{c,d}$. As these parameters incorporate various factors, field experiments are needed to determine the range of these parameters.

Acknowledgements

8. SWAP applications to improve water management

8.1 Introduction

In recent years SWAP has been employed to explore alternative flow and transport concepts, to analyse laboratory and field experiments, and to evaluate management options with respect to field scale water and solute movement. Published, typical examples are given in Table 8.1. Further SWAP serves to generate soil water fluxes for the pesticide transport models PESTLA (*Van den Berg and Boesten*, 1998) and PEARL (*Leistra et al.*, 2000; *Tiktak et al.*, 2000), and the nutrient transport model ANIMO (*Kroes and Roelsma*, 1998). Also SWAP forms the land component of the detailed Soil-Vegetation-Atmosphere-Transfer (SVAT) model SWAPS (*Ashby et al.*, 1996).

Table 8.1 Recently published, typical agro- or ecohydrological studies which employed SWAP or its predecessor SWAP93.

Topic	References
Field scale water balance	*Clemente et al.* (1994); *Beekma et al.* (1995); *Qureshi and Hussain* (1996); *Bastiaanssen et al.* (1996a); *De Jong and Bootsma* (1997); *Abenney Mickson et al.* (1997); *Droogers et al.* (2000a); *Kroes et al.* (2000)
Evapotranspiration	*Feddes and Van Dam* (1999); *Droogers* (2000); *Van der Tol* (2000); *Droogers and Bastiaanssen* (2000)
Irrigation scheduling	*Jacucci et al.* (1995); *Bastiaanssen et al.* (1996b); *Van den Hoven* (1997); *Kuper* (1998); *De Groot and Hack-ten Broeke* (1999); *Droogers et al.* (2000b)
Plant growth as affected by water and/or salinity stress	*Van den Broek and Kabat* (1995); *Van der Neut et al.* (1995); *Tedeschi et al.* (1996); *Li et al.* (1999)
Field scale salinization	*Smets et al.* (1997); *Feddes and Van Dam* (1997); *Hamaker et al.* (1997); *Van Dam* (1997); *Prathapar et al.* (1997)
Groundwater fluctuations	*Knotters and Van Walsum* (1997); *Bierkens* (1998); *Knotters and De Gooijer* (1999); *Massop et al.* (2000)
Dynamic drainage criteria	*Sarwar* (2000)
Improvement of surface water management	*Massop et al.* (1994); *Spieksma et al.* (1996); *Bierkens et al.* (1999)
Pesticide and nutrient leaching to groundwater	*Groen* (1997); *Van de Veen et al.* (1997); *Hack-ten Broeke (2000)*
Soil water flow as affected by soil spatial heterogeneity	*Feddes et al.* (1993a); *Feddes et al.* (1993b); *Wösten et al.* (1995); *Finke et al.* (1996a); *Kabat et al.* (1997); *De Groot et al.* (1998); *Kelleners et al.* (1999)
Soil erosion	*Boers* (1994); *De Roo et al.* (1996)
Soil moisture indicators for natural vegetations	*Runhaar et al.* (1997); *Jansen et al.* (2000)
Sensitivity analysis	*Finke et al.* (1996b); *Wesseling et al.* (1998)

As illustration, in the next paragraphs SWAP calibration and application will be discussed for two studies, in which the present author was closely involved. In the last part of this Chapter expected future developments with regard to SWAP are highlighted.

8.2 Irrigation and salinization in a semi-arid region of Pakistan

8.2.1 Introduction

In ancient times, agriculture formed one of the main pillars of the wealthy Indus Valley Civilization. Also today, agriculture is one of the most important parts of Pakistan's economy. It employs almost 50% of the labour force and produces 25% of the gross national product. About 75% of the total cropped area in Pakistan is irrigated. Extensive irrigation in the provinces Punjab and Sind could be developed because of vast amounts of fresh water supplied by large rivers flowing from the Himalaya mountains. Today this irrigation system is one of the most extensive irrigation systems in the world. In the second half of the 19th century, the British introduced perennial irrigation to supply water both during the summer and winter season. The continuous irrigation supply caused a gradual rise of the groundwater table. Along the canals and in lower areas waterlogging started to hamper agricultural production (Fig. 8.1). At fields with shallow groundwater tables, capillary rise brought salts back into the root zone. Already in the beginning of this century, waterlogging and salinity posed such problems that remedial measures became necessary. Measures taken to lower the groundwater table were temporary closures of canals, lowering of canal levels, lining of canals, planting of eucalyptus trees, drainage by open surface, and recently, drainage by tile drains and groundwater extraction by tube wells.
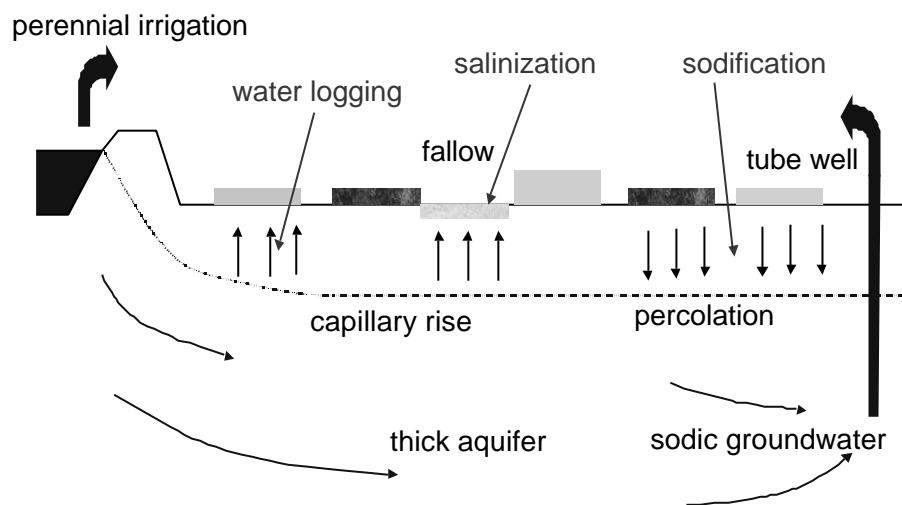
Figure 8.1 Side effects of perennial irrigation and irrigation by tube wells in Punjab, Pakistan.

Tubewells might be used to relieve the shortage of canal water, to lower the groundwater table, to leach saline/sodic soils, and to add flexibility in time and amount of irrigation. The Indus plain is underlain by deep deposits of unconsolidated sediments consisting of fine to medium sand. The high transmissivity of this aquifer favours the use of tubewells. Since 1959, as part of Salinity Control and Reclamation Projects (SCARP), 20.000 deep, public tubewells were constructed. Since 1980, shallow private tubewells became popular. *IWASRI* (1991) estimated that in 1985/1986, $11.0 \cdot 10^9$ m^3 of groundwater was extracted by public tube wells and $30.2 \cdot 10^9$ m^3 by private tube wells. Regarding its effect on waterlogging and salinization, *Kuper and van Waiijen* (1993) mention a survey among 200 farmers in 40 water

courses in the Fordwah and Azim distributaries in Punjab, which showed that over the period 1985-1992 the majority of the farmers observed a decrease in salinity levels. Some farmers were able to reduce salinity levels from 8 dS/m to 3 dS/m within 2-3 seasons. However, despite the clear advantages, also serious concerns exist of the long term effects of irrigation with tubewell water (*IWMI*, 1995). Groundwater with a high sodium content will be brought back in the root zone, which may detrimentally affect the soil structure, root water uptake and plant growth.

Since 1988, the International Water Management Institute (IWMI) has conducted integrated field research on inter-related aspects of irrigation, salinity and agricultural production (*Kuper*, 1998). The research was conducted on farmer's fields in order to capture the wide range of irrigation practices that are employed by farmers in response to the physical environment they have to face. From 1993 onwards, research efforts focused on the Chishtian Sub-Division in south-east Punjab, a 70,000 ha irrigation scheme, receiving it's surface irrigation water through the Fordwah Branch canal. Increased cropping intensities have prompted farmers to augment available canal water supplies by groundwater, pumped by over 4000 tube wells in the area (about 7 per 100 ha). Consequently, groundwater tables have dropped and waterlogging forms no problem anymore in Chishtian Sub-Division. The average electrical conductivity (*EC*) of all the tube wells amounts to 0.89 dS m^{-1}, with 90% of the tube wells showing an *EC* between 0 and 4 dS m^{-1}. The study area is located in the arid agro-ecological zone, with cotton and wheat being the dominant crops in the summer (June till December) and winter season (January till May) respectively. The soils are of alluvial and eolian origin, resulting in a mixture of silty to sandy deposits (*Smets et al.*, 1997).

8.2.2 Field experiments

Four farmer's fields of 0.4 ha each were monitored during three growing seasons in order to collect an extensive data set to calibrate and validate the SWAP model (cotton-wheat-cotton cycle from July '94 up to December '95). The four fields represent the predominant soils in the study area, ranging from loamy sand to silty clay loam. In Table 8.2, the soil type and availability of canal water and/or tube well water are indicated for the four fields. The farmers of field 1 and 2 have access to canal water and both own a tube well to supplement their canal water supplies. The farmers of field 3 and 4 do not have access to canal water, but have a shared ownership of a tube well. The quality of canal water is excellent with an *EC* of 0.2 dS m^{-1}. The farmers of field 1 and 2 use groundwater from various tube wells with an *EC* ranging from 0.8 to 1.6 dS m^{-1}. The farmers of field 3 and 4 use only water from one tube well, whose quality ranges from 0.75 to 1.3 dS m^{-1}. Irrigation regime and crop development was registered by IWMI field staff. Farmers irrigate their bounded fields by flooding, whereby in the case of cotton small beds and furrows are made. Wheat is grown in basins. In each field tensiometers were installed at eight depths (at 15, 30, 45, 60, 90, 120, 150 and 200 cm) and were read almost every other day. At the beginning of a growing season, in each field, 10 soil samples were taken at different depths and analyzed in the laboratory to determine the soil texture, soil water content and the *EC* of the saturated extract, *EC*$_e$. In the surrounding area of the sample fields, piezometers were frequently read and used to determine the groundwater levels of the four

fields. Meteorological data were derived from the nearest meteorological stations and precipitation was recorded with rain gauges near the sample fields. Precipitation is about 150-200 mm annually (*Smets et al., 1997*).

Table 8.2 Characteristics of the 4 sample fields: soil type, irrigation water origin and quantity during the data collection period of July 1994 - December 1995.

Field	Soil type	Canal water (%)	Tube well water (%)	Depth irrigation water (cm)
1	Loamy sand (LS)	75	25	396
2	Sandy loam (SL)	67	33	167
3	Loam to silty clay loam (L to SiCL)	-	100	159
4	Loam to silty loam (L to SiL)	-	100	150

8.2.3　SWAP simulations of field experiments

The water and salt balances of the four fields were simulated with the following input data (see Table 8.3 for input values):

- Daily reference evapotranspiration, as calculated with the CROPWAT model (*Smith*, 1992)
- Daily rainfall and irrigation data, including irrigation water quality
- Relations between volumetric water content, soil water pressure head and unsaturated hydraulic conductivity of each soil layer, as expressed by the Mualem - van Genuchten parameters
- Crop factors, soil cover and rooting depth of the crop during the growing season
- Limiting pressure heads and *EC* values, to determine reduction of root water extraction due to water and/or salinity stress (Fig. 2.3 and 2.4)
- Groundwater levels (if less than 3 m from soil surface)
- Initial soil water contents and salinity levels

After a period of one year, at 10 locations in each field the soil water pressure head, water content and electrical conductivity of the soil profile were measured. These measurements were compared to the SWAP simulations in order to evaluate the model performance.

The hydraulic conductivity is not homogeneous in a field, and more water will infiltrate in the higher conductive parts, especially in the case of basin irrigation. Also, non-uniform water distribution over a field or differences in soil surface level may result in heterogeneous infiltration, which leads at the field scale to more percolation. Although more water percolates, the lower salt concentration in the percolation water results in less salt leaching on field scale basis. Therefore, we simulated three cases:

- Uniform flow (field average)
- The mobile/immobile concept (preferential flow)
- An inhomogeneous distribution of irrigation water over the field (non uniform flow)

In case of the mobile/immobile concept, percolation of water and salts takes place in the mobile region, while the immobile region keeps part of the salts in the soil and delays the leaching (Chapter 6). In case of the inhomogeneous distribution of irrigation water, the irrigated field was divided in three rather arbitrary units: 0.375 part, receiving 67% of the irrigation water depth, 0.375 part receiving 100% and 0.25 part, receiving 150%. For conservative variables such as soil water content and EC_e, the weighted averages of the simulation results are compared with the measured data.

Table 8.3 General and field specific SWAP input data.

General								
Boesten parameter	$\beta = 0.90$ cm$^{1/2}$							
Crop factors	Cotton: 0.5 - 0.8 - 1.2 - 0.9 - 0.7; wheat : 0.4 - 0.8 -1.15 - 0.7 - 0.3							
Maximum rooting depth	Cotton: 140 cm; wheat: 110 cm							
Limiting pressure heads	h_1= -0.1 cm; h_2=-1.0 cm; h_{3h} =-500 cm; h_{3l} =-900 cm; h_4=-16000 cm							

Field specific	Field 1		Field 2		Field 3		Field 4	
	Layer 1	Layer 2	Layer 1	Layer 2	Layer 1	Layer 2	Layer 1	Layer 2
Depth of layer (cm)	0-140	140-315	0-125	125-290	0-105	105-210	0-105	105-210
Soil texture	LS	S	SL	LS	SiCL	LS	SiL	LS
Res. moisture content θ_{res}	0.01	0.02	0.045	0.02	0.05	0.02	0.045	0.02
Sat. moisture content θ_{sat}	0.33	0.35	0.33	0.35	0.39	0.35	0.38	0.35
Sat. hydr. cond. K_{sat} (cm d^{-1})	45.0	150.0	40.0	90.0	16.0	90.0	12.0	90.0
Shape parameter α (cm^{-1})	0.028	0.026	0.050	0.028	0.030	0.028	0.016	0.028
Shape parameter n	2.1	2.6	1.8	2.6	1.6	2.6	1.6	2.6
Shape parameter λ	0.0	1.0	-0.5	1.0	-1.0	1.0	-1.0	1.0
Groundwater table depth (cm)	-	280	-	250	-	free dr.	-	free dr.

Generally, the simulated pressure heads match quite well with the measured pressure heads. As a typical example, the measured and simulated pressure heads for the loamy sand (Field 1) are shown for field average and preferential flow in Fig. 8.2. The simulated pressure heads obtained with the preferential flow concept show more pronounced peaks and declines, since the water movement takes place in the mobile region only, causing a quicker wetting and drainage of the soil profile. The soil water content profiles are satisfactorily simulated by the model for all soil types. In Fig. 8.3 a typical example is given for the silty clay loam (Field 3). The width of the rectangles in Fig. 8.3 represent the augering inaccuracy of 5 cm depth, while the length of the rectangles represents twice the standard deviation of the measured soil water content of 10 samples. In case of the preferential flow concept, less water is stored in the total soil profile, since the soil water content in the immobile region is relatively low. For the non-uniform concept, less water is stored in the under-irrigated part of the field, which cannot be compensated by a higher moisture storage in the over-irrigated part, since field capacity is already reached and the surplus of water percolates. Therefore both the mobile/immobile concept and the non-uniform concept result on field-scale basis in lower soil water contents.
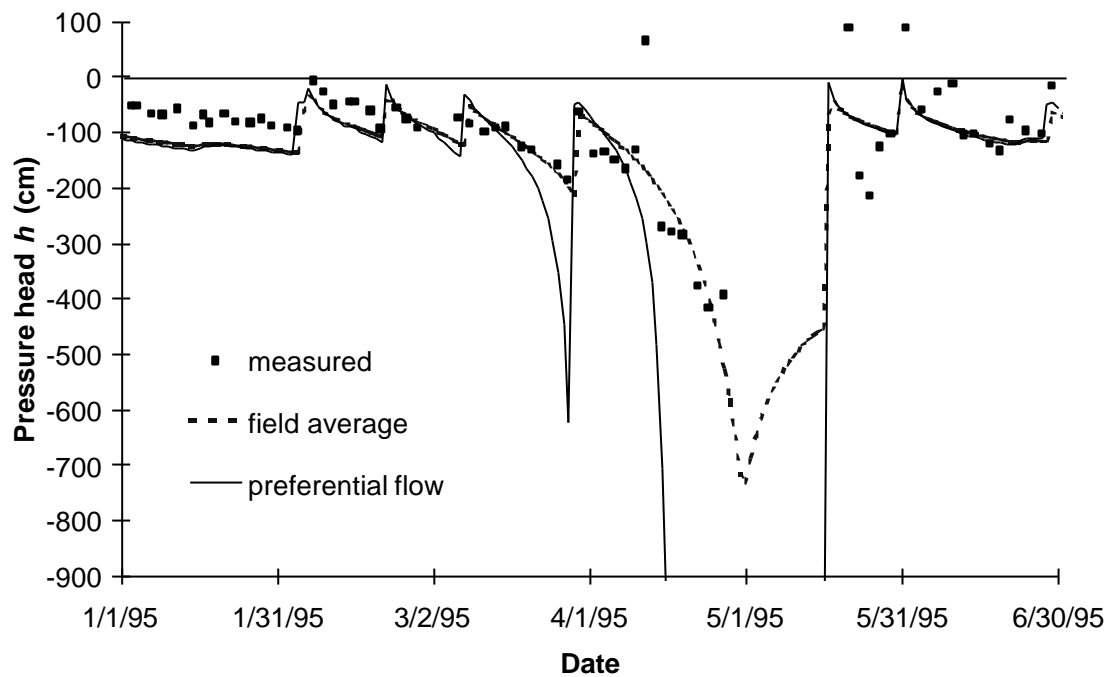
Figure 8.2 Measured and simulated soil water pressure heads (z = -60 cm) with the field average and preferential flow concept on the loamy sand soil (Field 1).
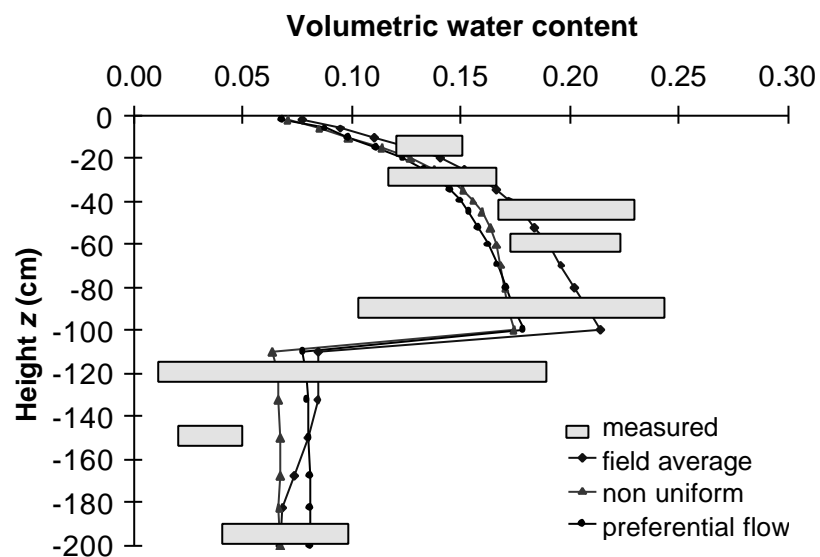
Figure 8.3 Measured and simulated volumetric water content profile with the field average, non uniform and preferential flow concept on the silty clay loam (Field 3).
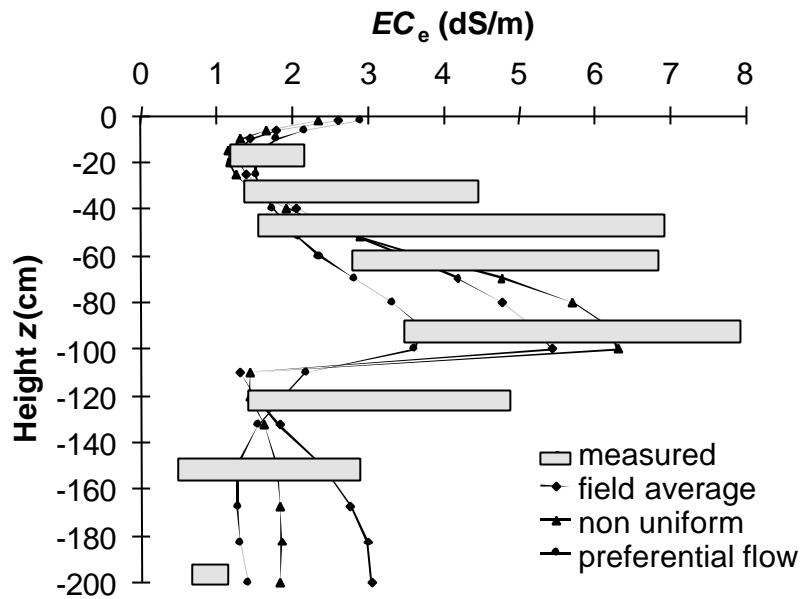
Figure 8.4 Measured and simulated EC_e profile with field average, non uniform and preferential flow concept on the sandy loam soil in July 1995(Field 2).

Figure 8.4 illustrates the EC_e profiles in the beginning of July 1995 for the sandy loam (Field 2). In general the model simulations show a more pronounced salinity profile than the measurements. This is probably caused by the fact that the measurements are averages of 10 locations, while the simulations mimic the salt transport at one, more or less representative spot. In case of non-uniform, less salts are leached to the groundwater, causing higher EC_e values in comparison to a field average simulation. Also in case of preferential flow less salts are leached. The salinity concentrations as depicted in Fig. 8.4 are still relatively low, as they depend largely on the assumed salinity concentrations in the immobile region.

In this case the simulations with preferential and non-uniform flow did not show enough improvement to be used in the sensitivity and scenario analysis. For these simulations the field average values were used, which is most straightforward and for our purpose accurate enough.

8.2.4 Sensitivity analysis
A sensitivity analysis has been performed to determine which input parameters have the largest effect on the simulation results. As one criteria, we used the relative transpiration T_a / T_p, where T_a is the cumulative actual crop transpiration and T_p the cumulative potential crop transpiration (cm). The relative transpiration can be related to the reduction of plant photosynthesis, and thus to reduction of crop yield (*De Wit et al.*, 1978). Another criteria is the relative salt storage change ΔS_p / $S_{p,0}$ where ΔS_p is the change in salt storage of the soil profile over a certain time span (g/m²) and $S_{p,0}$ is the initial salt storage of the soil profile (g/m²). This relative salt storage change is related to long term sustainable irrigation.

Table 8.4 Relative transpiration and relative salt storage change as function of various input parameters for the silty loam soil.

Scenario	Relative Transpiration	Rel. Salt Storage Change
	(T_a / T_p)	($\Delta S_p / S_{p,0}$)
Reference	0.93	0.14
Decrease of rooting depth (with 50%)	0.89	0.10
Decrease of crop factors (with 25%)	0.99	-0.48
Decrease of Boesten parameter (with 33%)	0.95	-0.15
Decrease of sat. water content (with 16%)	0.91	-0.02

Table 8.4 shows some of the results. Decrease of the rooting depth with 50 % has only a small effect on both criteria, suggesting that for the research area no accurate data of the rooting depth are required. The crop factor, however, has a large effect. Decrease of the crop factor with 25 %, increases the relative transpiration from 0.93 to 0.99, and decreases the salt storage change from 0.14 to -0.48. The effects of the soil evaporation parameter and the saturated water content, are in between the effects of rooting depth and crop factor.

8.2.5   One year simulations

Several one year irrigation management scenarios were simulated and compared with the simulation results of a Reference irrigation scenario, which is based on the recommended irrigation practices of the authorized Agricultural Department (see Table 8.5). The results of the scenario simulations are listed in Table 8.6. All scenarios except Tube-well included a pre-sowing irrigation with good quality canal water (EC_{iw} = 0.2 dS m^{-1}) in order to ensure proper plant germination. The initial salt storage of all scenarios was the same (1000 g m^2 in the top 2.1 m) in order to obtain comparable simulation results.

In the Reference scenario, the relative transpiration is very favorable, amounting 1.00 for the wheat and 0.99 for the cotton crop. The wheat crop is over-irrigated to a larger extent than the cotton crop, which is evident from the lower salts storage change during the wheat season.

In the Under-irrigation scenario, the irrigation amounts are decreased to 75% of the reference amounts. In this case the wheat crop water requirements are still met, but there is hardly any percolation and salt concentrations increase in the soil. During the cotton season, a considerable reduction in crop transpiration takes place (T_a / T_p = 0.85) and the salinization process intensifies ($\Delta S_p / S_{p,0}$ = 0.37).

In the Low frequency scenario, the total number of applications is reduced from 16 to 12, while the total amount of irrigation water is kept the same as in the Reference scenario. The simulation results show that the larger irrigation gifts cause more soil water percolation beyond the root zone, so less water can be extracted by the roots and more salts are leached. This phenomenon is not very pronounced on the silty loam soil (Table 8.6), but is significantly on permeable sandy soils with a smaller retention capacity. Managing the water

and salt balances by means of changing the irrigation interval is only effective in case there is a significant percolation component.

In the Tube-well scenario, irrigation at the beginning of the growing season is performed with tube-well water instead of canal water. The simulation results show after one year a clear increase of salinity level ($\Delta S_p / S_{p,0} = 0.44$), while crop transpiration is not yet reduced ($T_a / T_p = 0.99$). Still, a pre-sowing irrigation with canal water is preferred, since the germination stage is the most sensitive period of most crops with respect to salinity.

The Poor groundwater scenario simulates a situation where a farmer has access only to bad quality groundwater ($EC_{iw} = 3.0$ dS/m) by tube wells. The simulation results show a 66% increase of salinity in just one year, and crop salinity stress especially in the cotton season. The crop salinity stress will continue to increase in succeeding seasons.

Table 8.5 Description of the one year scenarios by water quantity (cm), water quality (dS/m) and irrigation application frequency (-).

	Wheat season						Cotton season					
	Quantity		Quality		Frequency		Quantity		Quality		Frequency	
Scenario	Pre	Other	Pre	Other	Pre	Other	Pre	Other	Pre	Other	Pre	Other
Reference	15.0	7.5	0.2	1.5	1	5	10.0	7.8	0.2	1.5	2	8
Under-irrigation	**10.0**	**5.6**	0.2	1.5	1	5	**7.5**	**5.9**	0.2	1.5	2	8
Low frequency	15.0	**12.5**	0.2	1.5	1	**3**	10.0	**10.4**	0.2	1.5	2	**6**
Tube-well	15.0	7.5	**1.5**	1.5	1	5	10.0	7.8	**1.5**	1.5	2	8
Poor groundw.	15.0	7.5	**3.0**	**3.0**	1	5	10.0	7.8	**3.0**	**3.0**	2	8

Table 8.6 Simulated relative transpiration (T_a / T_p) and relative salt storage change ($\Delta S / S_0$) during a period of one year in case of various scenarios at the silty loam soil.

	Wheat season		Cotton season		Total agricultural year	
Scenario	T_a / T_p	$\Delta S_p / S_{p,0}$	T_a / T_p	$\Delta S_p / S_{p,0}$	T_a / T_p	$\Delta S_p / S_{p,0}$
Reference	1.00	0.00	0.99	0.24	1.00	0.20
Under-Irrigation	0.98	0.26	0.85	0.37	0.89	0.73
Low frequency	0.99	-0.22	0.98	0.55	0.99	0.18
Tube-well	1.00	0.12	0.98	0.33	0.99	0.44
Poor groundw.	0.99	0.61	0.93	0.67	0.95	1.66

8.2.6 Ten year simulations

Long term scenarios of 10 year periods were performed for the 4 experimental fields in order to evaluate the sustainability of irrigation management options. The scenarios started from the previously discussed Reference scenario. We changed the irrigation depths and the irrigation water quality, while keeping all other variables the same (e.g. irrigation interval). Often, farmers do not have enough irrigation water at their disposal and crop water
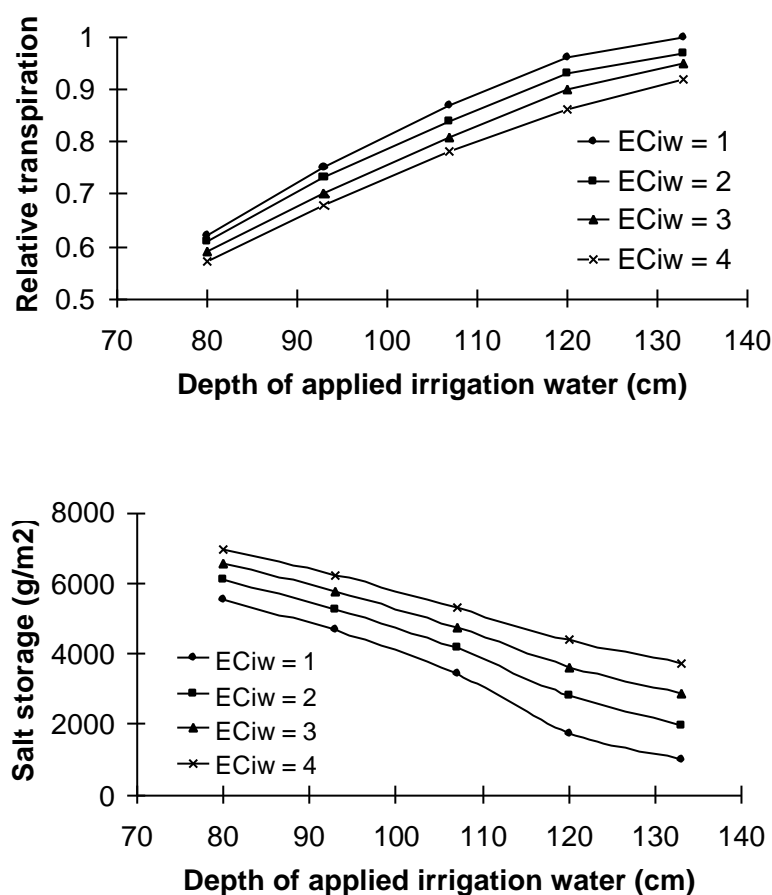
Figure 8.5 Relative transpiration and salt storage (top 210 cm) of a *silty loam soil* after a period of 10 years at different irrigation amounts and different water qualities.

requirements are not fully met. Therefore, five under-irrigation scenarios were performed, decreasing the application depths down to 60% of the reference application depths with 10% interval. As farmers are using more and more tube well water for irrigation, the irrigation water quality of the scenarios was varied from 1 to 4 dS/m (interval 1 dS/m).

After a few years, the salinization process reaches a certain equilibrium state with a constant salt storage: the amount of salts added to the soil equals the amount of salts leached from the soil. The equilibrium state is reached on sandy soils after two years and on loamy soils after four years. The results after a period of 10 years are shown, at which time equilibrium was reached. Figure 8.5 shows for the silty loam and different irrigation amounts, relative transpiration (T_a/T_p) and total salt amount in the soil profile. The decrease of T_a/T_p due to a poorer water quality of the irrigation water (from 1 to 4 dS/m) is approximately 8%, while the reduction of T_a/T_p due to under-irrigation (from 133 down to 80 cm) is 38% at the silty loam. The amount of salts in the soil (calculated up to a depth of 210 cm) increases with a higher electrical conductivity of the irrigation water, but is mostly affected by the extent of under-irrigation.
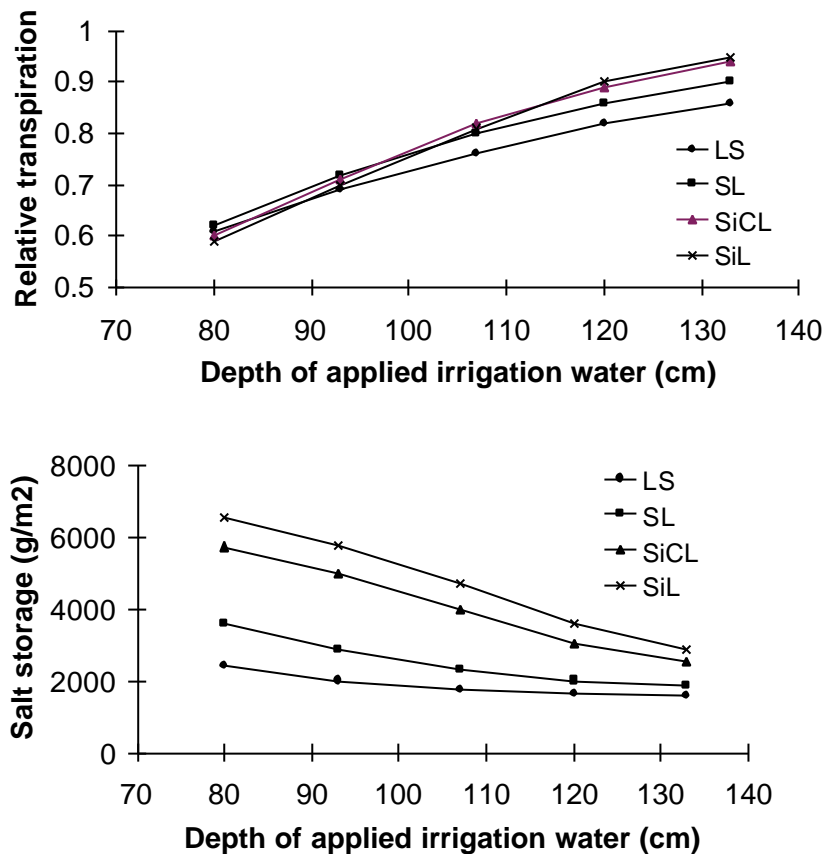
Figure 8.6 Relative transpiration and salt storage (top 210 cm) using water quality $EC_{iw} = 3$ dS m^{-1} after a period of 10 years at different irrigation amounts and *different soil textures* (LS - loamy sand; SL - sandy loam; SiCL - loam to silty clay loam; SiL loam to silty loam).

The salinization process takes place differently on sandy and loamy soils, which is shown in Fig. 8.6. Due to a lower hydraulic conductivity and higher retention capacity, resulting in less percolation, T_a/T_p is generally larger on a loamy soil compared to a sandy soil. The higher transpiration of the loamy soils means less leaching and higher salinization at these soils. Figure 8.6 also shows that the effect of soil texture on T_a/T_p becomes smaller if the amount of irrigation is reduced. In case of severe under-irrigation, all irrigation water will be transpired, regardless of soil texture!

Using the calibrated SWAP model for the 4 experimental fields, *Kuper* (1998) investigated the possibility to decrease salinization by changing current canal water distribution in the Chishtian Sub-Division. Alternative canal water distributions were calculated with an unsteady state hydraulic model linked to a regulation module, which captures the operational decisions of the irrigation agency. *Kuper* (1998) showed that a change of the operational rules at the main canal and of the outlet capacities in the secondary canals, may distribute the good quality irrigation water in such a way that salinization in potentially vulnerable areas is decreased.

8.2.7   Conclusions

From this study the following conclusions for the Chishtian area can be drawn:

- Non-uniform water infiltration and preferential flow results in more water loss and less salt leaching compared to field average flow
- Accurate data on crop factors and soil hydraulic functions are needed for reliable water and salt balances
- Stress due to water shortage is affecting plant growth more than stress due to high salinity
- The officially recommended irrigation amounts are sufficient to prevent serious salt stress on long term
- A field scale model as SWAP in combination with a hydraulic model for canal water distribution and linked to a regulation module which incorporates management decisions, is useful to design measures against salinization at regional level

8.3   Desalinization of island and plates in a former estuary of The Netherlands

8.3.1   Introduction

De Grevelingen is a former estuary of 13800 ha in the south-western part of The Netherlands. In 1971 a closing dam has been constructed, which eliminated the tidal water level differences. After dam closure, a constant lake water level has been maintained at -0.20 m New Amsterdam Level (NAL), and the lake has been flushed with seawater, keeping the salinity of the lake water closely to seawater concentrations (16 g l^{1}). Very soon saline pioneer vegetation settled on the bare islands and plates along the shore. Gradually the rainfall surplus leached the salts from the top soils of the islands and plates. After a number of years, the saline pioneer vegetation transformed to grass and bushes, with exception of a several hundreds meter wide strip next to the shore. In the past 29 years, a botanically very precious area developed in this strip with all kind of environmental transitions from salt to fresh, from wet to dry and from nutrient rich to nutrient poor. Birds intensively use the bare transition zone as breeding ground. However, nature organisations fear a further narrowing of the transition zone due to continuing leaching of salts. They recommended preservation or, if possible, enlargement of the transition zone by increasing the water level fluctuations in the Grevelingen lake, imitating the former tidal fluctuations. Various water management scenarios were proposed with different water levels in the winter and summer season. SWAP was used to analyse the effects of the five water management scenarios on the desalinization rate in the transition zone along the shore (*Van Dam*, 1997).

The water contents and salinity concentrations in the soils along the shore change rapidly. As an illustration, Fig. 8.7 shows the chloride concentration at three times of an ordinary year, simulated for a location with a soil surface level at +0.10 m NAL on the Flakkee South plates. At the end of June, the chloride concentration at the soil surface is 2 g l^{1}. At the beginning of July, the spot is flooded with saline lake water due to a strong wind driving up the lake water. Subsequently, the salinity concentration in the top soil increases above lake water concentration (16 g l^{1}) due to water extraction by soil evaporation and plant transpiration. At the end of August, the soil surface chloride concentration has reached values
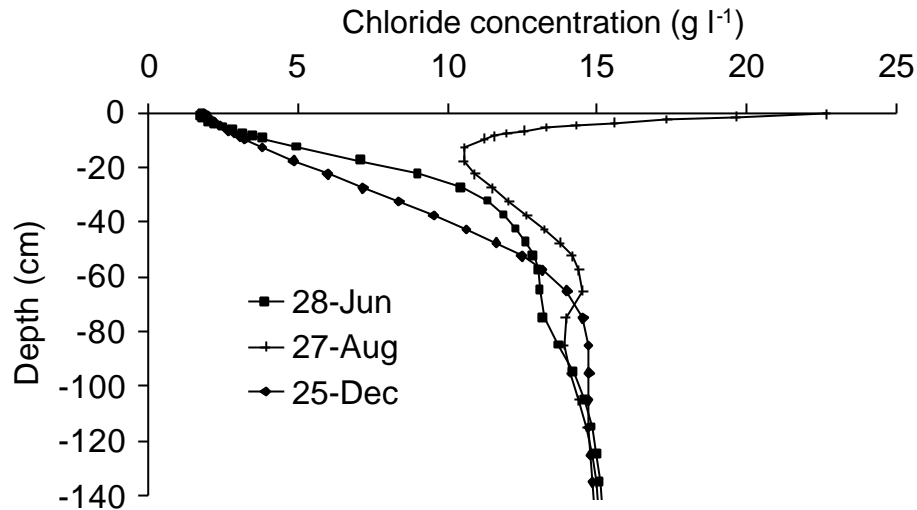
Figure 8.7 Simulated chloride concentration profiles at three dates in an ordinary year for a location with soil surface level +0.10 NAL at Flakkee South plates. At the beginning of July due to strong wind the plot is flooded with salty lake water.

as high as 23 g l^1. In the autumn months that follow, surplus rain water causes chloride dilution and leaching. The high salt concentrations in the top soil due to the flood in July, have totally disappeared at the end of the year. These simulated fluctuations were confirmed with measurements taken at a number of locations.

8.3.2   Model calibration

SWAP was calibrated by using groundwater level and soil salinity measurements during the period 1971 - 1996. Figure 8.8 shows measured and simulated groundwater levels for a location at Flakkee North plates in 1978. During the winter months, the groundwater level reached the soil surface, and most rain water flowed over the soil surface to the lake. In summer time, the groundwater levels decreased down to approximately 1 m below soil surface. Near day 170, a sudden increase of the groundwater level occurred, which probably was caused by a flood due to strong wind. Although the soil hydraulic functions had to be derived from general soil textural data, the range and dynamics of the simulated groundwater levels corresponded reasonably well to those of the measurements, as illustrated in Fig. 8.8.

Figure 8.9 shows the measured and simulated chloride concentrations at 1 m depth for three locations at Flakkee South plates. The three locations are part of a crossline perpendicularly to the coast, whereby location A is at 10 m from the shore, B at 180 m and C at 360 m. For location A, during the period 1974-1980 SWAP underestimates the chloride concentrations. This is probably caused by infiltration of salty runoff water from higher parts of the plates, which was not included in the simulations. In case of location B, the desalinization rate during the period 1971-1981 is reasonably reproduced. Only during the winter periods of 1974-1975 and 1975-1976, the chloride concentrations are underestimated. At location C the relative fast desalinization rate (from 16 g l^1 down to 0.1 g l^1 in 4 year) is properly reproduced by SWAP. Calibration of SWAP to the measured salinity levels showed that *chloride leaching is mainly affected by the level of the soil surface with respect to the lake,*
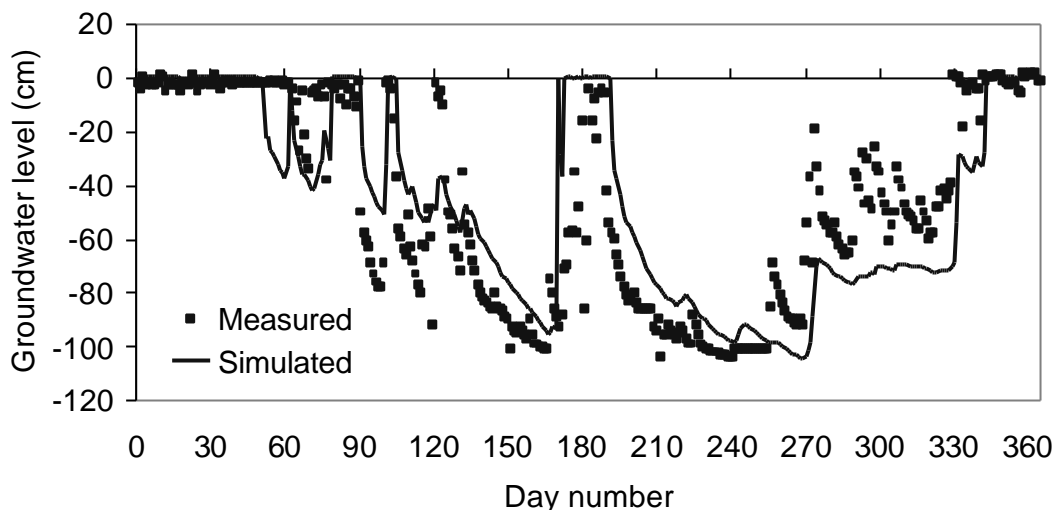
Figure 8.8 Measured and simulated groundwater levels in 1978 at location C3 of Flakkee North plates.
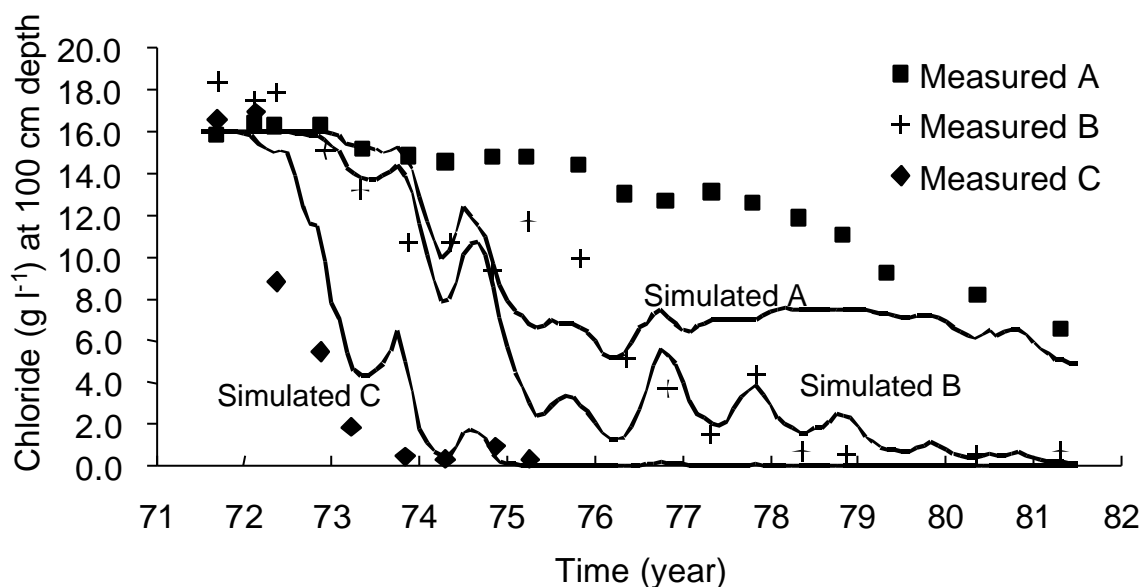
Figure 8.9 Measured and simulated chloride concentrations at 100 cm depth on Flakkee South plates at three locations (distance from shore: A - 10 m; B - 180 m; C - 360 m).

the drainage resistance of the subsoil, the vegetation cover and the number of floods during the summer season.

Validation was performed for other years and other locations. Differences between simulated and measured groundwater levels and chloride concentrations could be explained by spatial variation of soil physical properties and extra salinisation/leaching due to local differences of soil surface level. Fluctuations of groundwater levels, relative differences of chloride

concentrations in measured crosslines, and long term leaching rates, were satisfactorily reproduced by SWAP.

8.3.3   Scenario analysis

The calibrated model was used to simulate water flow and chloride transport along four cross-sections in the area during a 10-year period. The simulations started with the salinity concentrations of March 1997, and weather data were equal to those of the period 1980-1989. For future water levels in the Grevelingen lake, the following 5 scenarios were proposed:

1) Current water management, lake water level constant at -0.20 m NAL;
2) During the months February and September high lake water levels at 0.00 m NAL, during the remaining period at -0.20 m NAL;
3) During the months February and September high lake water levels at +0.20 m NAL, during the remaining period at -0.20 m NAL;
4) During the period September - March high lake water levels at -0.10 m NAL, during the remaining period at -0.30 NAL;
5) During the period September - March high lake water levels at 0.00 m NAL, during the remaining period at -0.20 NAL.
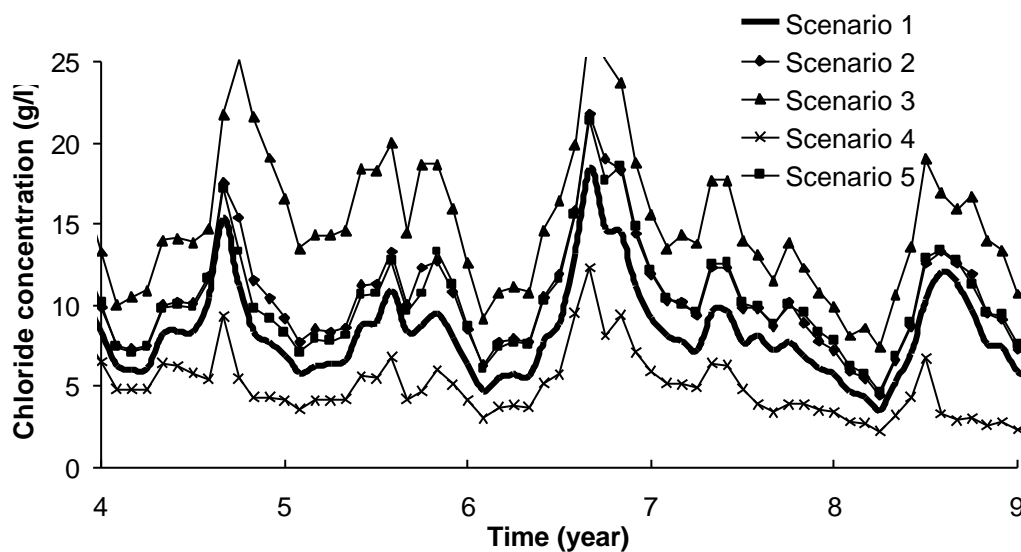
Figure 8.10 Simulated chloride concentrations at 0.30 m soil depth at a location with the soil surface at +0.20 NAL on Flakkee North plates for five water management scenarios, as explained in the text.

Starting with current chloride concentrations, after 4 - 9 years the effects of the different water management scenarios become clearly visible in the transition zone. Figure 8.10 shows the simulated chloride concentrations at 0.30 m soil depth for years 4 - 9 on Flakkee North plates at a location with soil surface level +0.20 m NAL. The salinity concentrations show clear seasonal fluctuations with the highest value in August and the lowest value in February. With respect to current management (Scenario 1), all proposed scenarios except Scenario 4 result in increased salinity concentrations, as desired. The simulation results indicate that

increase of water levels during the winter months is most effective to maintain high salinity levels in the transition zone. Most effective is Scenario 3, but the high lake water levels proposed in this scenario require substantial adaptations for harbour facilities and shore protection. Ultimately Scenario 5 was selected as the most desirable management option (*Van Dam*, 1997).

8.4   Expected model developments in the near future

With the rapid increase of computation power and software tools, 2- and 3-dimensional flow and transport models play an increasing role in both hydrological research and practice. Examples of currently available, physical based, users friendly models are HYDRUS2D (*Šimunek et al.*, 1996) and HYDROGEOCHEM (*Scientific Software Group*, 2000). Another rapidly developing and promising approach is formed by hydrological frameworks, which consist of independent, object oriented components that are combined for specific applications (*Otjens et al.*, 1999; *Groenendijk et al.*, 1999).

These developments are exciting and will certainly improve our understanding of variably saturated flow and transport in natural soils. However, the skill, data, and computation time required still limit the application range of multi-dimensional flow and transport models. In the author's view, the coming 5-10 years one-dimensional models such as SWAP, HYDRUS (*Šimunek et al.*, 1998) and WAVE (*Vanclooster et al.*, 1994) will still play an important role to explore new flow and transport concepts, to analyse laboratory and field experiments, to select viable, hydrological management options, to perform regional studies employing geographical information systems, and to illustrate transport processes for education and extension. We distribute the SWAP source code with the program through the Internet, and invite other research groups to indicate possible improvements. Concept developments that currently seem promising with SWAP, are:

- Improvement of evapotranspiration simulation (*Van der Tol*, 2000)
- Aeration/crop growth in soils with shallow groundwater levels (*Van der Neut et al.*, 1995)
- Moisture indicators for natural vegetations (*Jansen et al.*, 2000)
- Flow and transport in water repellent soils (*Ritsema et al.*, 2000)
- Flow and transport in cracked clay soils (*Van Dam*, 2000)
- Combination with ecological water quality models (*Van Delft and Kemmers*, 1998)
- Combination with regional groundwater flow models (*Massop et al.*, 2000)
- Effective and efficient calibration of SWAP (*Van Dam and Torfs*, 2000)
- Flow and transport in frozen soils (*Daanen*, 1997)

9. Summary and conclusions

In top soils, numerous interactive physical, chemical and biological processes occur which are essential for sustaining life. Many of these processes are directly affected by the amount of water residing in the soil. Therefore in many environmental studies, water and solute residence and movement in top soils are important elements. This thesis aims to contribute to three current trends in hydrological research. The first trend is a shift from analytical to numerical modeling, as only numerical models are able to mimic the close interaction between highly non-linear processes during rapidly changing boundary conditions, as occurs in top soils under natural conditions. The second trend is a shift in focus from uniform to heterogeneous soils. Cracks due to shrinkage and water repellent parts may have a large effect on water and solute movement, and should therefore be incorporated into experiment analysis and policy evaluation. The third trend concerns a shift from measurements in the laboratory to measurements in the field. In a time in which more and more non-destructive and stand-alone instruments for field measurements come available, and inverse modeling techniques get more and more reliable, field experiments become an attractive option to collect information of natural system parameters.

Chapter 2 starts with the basic demands that shaped the development of the agrohydrological model SWAP (Soil Water Atmosphere Plant) during the past 10 years. The interaction at the soil surface of water, solutes, heat and plant processes, requires simultaneous solution of the mathematical relationships describing water flow, solute transport, heat flow and plant growth. Regarding the spatial scale the focus should be on the field scale, as a field has clearly defined system characteristics, and a physical rather than an empirical description of flow and transport processes allows for all kind of scenario analysis. By locating the upper boundary of the system just above the canopy, and the lower boundary in the top of the groundwater system, the flow and transport equations could be kept one-dimensional, which reduces considerably the input effort and calculation time. Long year simulations with changing weather, crop and drainage conditions, should be accommodated, in order to investigate critical periods. SWAP employs the experiences gained with the model SWATR and its derivatives, and is designed for research, education and application. In the remaining part of Chapter 2, the main features and theoretical concepts of SWAP, as relevant for this thesis, are discussed.

A serious limitation of many model applications is the availability of reliable input parameters. With the rapid increase of processor computation speed and development of effective optimization algorithms, it became possible to determine input parameters by inverse modeling. In this technique, the simulation model is run with initial values of the unknown input parameters and the simulated results are compared to measurements. Next the input parameters are adjusted by searching techniques as Gauss-Marquardt-Levenberg, and the model is run again. This is repeated until the simulated results and the measurements match as closely as possible. Main advantages of inverse modeling are that they are relatively cheap and fast as compared to traditional laboratory and field experiments, require no simplifying assumptions in the flow and transport equations, allow for arbitrary initial and boundary conditions, incorporate errors of fixed model parameters and of the physical-

mathematical concept in the value of the optimized parameters, may include any prior information of the fitting parameters, and contain information of the accuracy of optimized parameters.

A typical and verifiable example of the inverse modeling technique are laboratory outflow experiments, as described in Chapter 3. In this experiment, a soil sample is placed in a pressure cell on top of a ceramic plate, and is saturated from below. By increasing the air pressure above the soil sample, downward, unsaturated flow in the soil sample is induced. The cumulative outflow as function of time is recorded, and is used to optimize the parameters describing the soil hydraulic functions. In the originally proposed method, one large increase of air pressure, equivalent to 500-1000 cm water pressure, was applied. This method was applied to four different soils, and compared to the results of independent measurements of the soil hydraulic functions. This showed that optimization using only data of cumulative outflow with time is insufficient, and results in non-unique and deviating fitting parameters. In case the cumulative outflow data were supplemented with retention data, which can be obtained in the same pressure cell, the results improved considerably. Next Chapter 3 describes outflow experiments of a loam soil in which the air pressure is increased in five steps (Multi-step), rather than one large step (One-step). The optimization results of Multi-step are compared to the results of One-step, and to independent retention data. It appeared that in case of Multi-step, the cumulative outflow data are sufficient for unique and reliable parameter estimates of the soil hydraulic functions. This became also clear in a prior analysis of the confidence regions of the optimized parameters, which were much smaller for Multi-step as compared to One-step.

Laboratory outflow experiments are often applied to a series of soil samples, in order to quantify effects of spatial variability of soil hydraulic functions on water and solute fluxes. In such cases always the question arises, which soil hydraulic functions are representative for the particular soil layer to which the series samples belong. Three averaging methods were applied to the 18 samples of the loam soil which had been used in the Multi-step outflow experiment: (1) similar media scaling, (2) arithmetic averaging of volumetric water content and the logarithm of hydraulic conductivity as function of soil water pressure head, and (3) optimization of arithmetic averaged, cumulative outflow data. In case of the investigated loam soil, all three methods resulted in comparable, average soil hydraulic functions.

The accuracy of field scale model predictions will increase, if the inverse problem is also applied to measurements at field level. Proper selection of measurement type and timing before the actual experiment takes place, may save financial effort and avoid inaccurate parameter estimates. To design the most informative measurement schedule, one may effectively use calculated confidence regions of fitting parameters in a prior analysis, as was illustrated in case of laboratory outflow experiments. In Chapter 4, a prior analysis is applied to a theoretical field experiment at a drained, loamy soil, cultivated with maize. The generated observations by SWAP consisted of weekly water contents and pressure heads in the root zone, drainage discharge rates and, optionally, tracer concentrations. Four parameters

(crop diffusion resistance, soil texture scaling factor, saturated water content of the top soil and saturated hydraulic conductivity of the subsoil) were selected for optimization. These parameters could be optimized by the program PEST with narrow confidence intervals, using the generated observations with normally distributed and non-correlated observation errors. In order to calculate the fitting parameter accuracy, the covariance matrix of the fitting parameters was calculated with a linear approximation of the objective function near its minimum. This method is very practical and sufficiently accurate, as was verified with a Monte Carlo simulation. The prior analysis showed that inclusion of a crop, a tracer and measurements at periods with extreme and rapidly changing hydrological conditions, improved the accuracy of the fitting parameters indeed. The discussed prior analysis is a practical and powerful method to select those type and timing of measurements that result in a well-posed inverse problem, and which may subsequently in a posterior analysis allow for detection of model errors or selection of best-performing models.

Analysis of water and solute movement in variably saturated soil systems would greatly benefit from an accurate and efficient numerical solution of Richards' flow equation. About 10 years ago, the mass balance problem has been solved by proper evaluation of the differential water capacity term. However, the soil water fluxes as calculated by various numerical schemes still deviate significantly due to differences in nodal spacing and spatial averaging of the hydraulic conductivity K. Chapter 5 discusses a versatile, implicit, backward finite difference scheme, which is relatively easy to implement in numerical models. Special attention is given to the selection of the proper top boundary condition during the iterative solution of the Richards' equation. The stability of the scheme is shown for two strongly non-linear soils at extreme events of infiltration, soil evaporation and rapidly fluctuating, shallow groundwater levels. For nodal distances of 5 cm, arithmetic means of K overestimate the soil water fluxes, while geometric means of K underestimate these fluxes. At smaller nodal distances, arithmetic means of K converge faster to the theoretical solution than geometric means. In case of nodal distances of 1 cm and arithmetic averages of K, errors due to numerical discretization are small compared to errors due to hysteresis and horizontal spatial variability of the soil hydraulic functions.

Both hysteresis of the soil hydraulic functions and preferential flow may affect water and solute movement in variably saturated soils. Hysteresis occurs mainly in the relation between soil water content and soil water pressure head. Gradual desorption of an initially saturated soil yields the main drying curve, while slow absorption of an initially dry sample results in the main wetting curve. In the field partly wetting and drying occurs in numerous cycles, resulting in so-called drying and wetting scanning curves which lie between the main drying and the main wetting curve. The author implemented in SWAP hysteresis according to a method, in which scanning curves are derived by rescaling the measured main wetting or main drying curve to the actual soil water content.

Many dry soils, under a variety of climates and vegetation, show to a certain extent water repellency. Infiltration rates into water repellent soils can be considerably lower than those into

wettable soils, and wetting patterns in water repellent soils are irregular and incomplete. In order to describe water flow and solute transport in such a soil with SWAP, we distinguished mobile regions, in which the Richards' equation for water flow and the convection-dispersion equation for solute transport apply, and immobile regions in which no convective flow or transport occurs. The volume of the mobile region may vary with depth, and also depends on the soil water pressure head in the mobile region. In the usual laboratory protocol for measuring soil hydraulic functions, water repellency is surpressed. Therefore laboratory soil hydraulic functions are assumed to be valid in the mobile regions. In field conditions, the mobile regions volume can roughly be estimated by visual observation of dry and wet spots of a soil profile shortly after precipitation, and more accurately with tracer colour tests, e.g. with iodide or Brilliant Blue, with a disc permeameter in combination with a tracer, with TDR transect measurements of water content, or through model calibration.

The concepts for hysteresis and water repellency were applied to data sets from two locations with hysteretic and water repellent soils. This showed that generally hysteresis retards soil water movement, while preferential flow enhances soil water movement. During infiltration events, simulations showed that due to hysteresis more water is retained in the root zone. However in field conditions, incorporation of hysteresis decreases the amount of simulated water storage, as at the same pressure head scanning curves have a lower volumetric water content than the usually applied main drying curve. For example the slow increase of water in the root zone occurring after a dry year could better be predicted by including hysteresis. Furthermore, it was shown that in fields with shallow groundwater levels and without ponding, soil water fluxes are marginally affected by hysteresis and could not account for the observed groundwater peaks occurring after large rainfall events.

Adjustment of the soil hydraulic functions with the mobile-immobile concept improved the simulated water contents as compared with measured data (Chapter 6). The effect of the immobile regions on the soil water fluxes, however, was marginal for the experiments considered. In the field conditions encountered, the soil water fluxes were governed by the net rainfall, actual evapotranspiration and the relatively shallow groundwater levels. The relative insensitivity of soil water fluxes to preferential flow under temperate conditions implies that determination of preferential flow from water balance measurements under these conditions is difficult. Rather than soil water fluxes, soil water contents were significantly affected by preferential flow. Also leaching of bromide to groundwater was much better predicted when the mobile-immobile concept was applied.

Single domain models may seriously underestimate leaching of nutrients and pesticides to groundwater in clay soils that contain shrinkage cracks. Various two-domain models have been developed, either empirically or physically based, which take into account the effects of cracks on water flow and solute transport. Chapter 7 discusses a model concept, which employs the clay shrinkage characteristic to derive crack volume and crack depth under transient field conditions. The concept has been developed to simulate field average behavior of a field with cracks, rather than flow and transport at a small plot. Water flow and solute

transport in the soil matrix and the cracks are described with basic physics, which allows for process and scenario analysis. The model concept has been implemented into SWAP, and was applied to a field experiment on a cracked clay soil, at which water flow and bromide transport were measured during 572 days. A single domain model was not able to mimic the field-average water flow and bromide transport. Incorporation of the crack concept improved considerably the simulation of water content and bromide leaching to the groundwater. Still deviations existed between the measured and simulated bromide concentration profiles. The model did not reproduce the observed bromide retardation in the top layer and the high bromide dispersion due to water infiltration at various soil depths. A sensitivity analysis showed that the amounts of bromide leached were especially sensitive to the saturated hydraulic conductivity of the top layer, the solute transfer from the soil matrix to crack water flow and the mean residence time of rapid drainage water. The shrinkage characteristic and the soil hydraulic properties of the clay matrix showed a low sensitivity.

Chapter 8 lists a number of recently published, typical agrohydrological studies in which SWAP has been employed. Two examples are more extensively described. The first one concerns sustainable irrigation in a semi-arid region of Punjab, Pakistan. As in the area the distribution of canal irrigation water is insufficient, farmers extract more and more groundwater for irrigation by private tube wells. Four fields with different water quantities and qualities were intensively monitored during three cropping seasons. SWAP has been calibrated to these fields, and was subsequently used for a sensitivity analysis and short and long term simulations. The sensitivity analysis showed that the simulated water and salt balance are most sensitive to the crop coefficients used for calculating potential transpiration and to the soil hydraulic functions. Also it showed that non-uniform water infiltration and preferential flow results in more water loss beyond the root zone and less salt leaching. The short term simulations indicated that currently plant growth is more limited by water shortage than by high salinity concentrations. The simulations over a period of 10 years showed that the officially recommended irrigation amounts are sufficient to prevent serious salt stress on long term.

The second example concerns desalinization of islands and plates in De Grevelingen, a former estuary in the south-western part of The Netherlands. After dam closure in 1971, a constant lake water level has been maintained, while the lake is kept salty by regular flushing with sea water. Due to the yearly rainfall surplus, the plates along the shore and the islands in the lake gradually desalinize. In the past 29 years, a botanically very diverse area along the lake shore developed with all kind of environmental transitions from salt to fresh, from wet to dry, and from nutrient rich to nutrient poor. However, due to continuing leaching of salts, a further narrowing of this transition zone is expected. Therefore alternative water management scenarios were proposed with larger fluctuations of the lake water level, which more or less imitate the previous tidal differences. SWAP has been used to analyse soil water movement and desalinization at four cross lines perpendicularly to the lake shore. Calibration of SWAP, using measured groundwater levels and salinity concentrations after dam closure, showed that desalinization is mainly affected by the level of the soil surface with respect to the water level

in the lake, the drainage resistance of the subsoil, the vegetation cover and the number of floods due to strong winds during the summer season. The salinity concentrations showed clear seasonal fluctuations with the highest value in August and the lowest value in February. Fluctuations of groundwater levels, relative differences of chloride concentrations in measured cross lines, and long term leaching rates, were satisfactorily reproduced by SWAP. The calibrated model was used to simulate water flow and chloride transport for 5 water management scenarios during a 10-year period. All proposed scenarios, except one, increased significantly the salinity levels in the transition zone as compared to the current situation. As most desalinization occurs with downward soil water flow during the winter months, increase of the lake water level during the winter months turned out to be the most effective.

Current developments with multi-dimensional, physically based models and integrated, hydrological frameworks, will further improve our analysis of water and solute movement in soils. However, because of their flexibility, accessibility and speed, the coming 5-10 years one-dimensional models as SWAP will keep to play an important role to explore new flow and transport concepts, to analyse laboratory and field experiments, to select viable, hydrological management options, to perform regional studies employing geographical information systems, and to illustrate transport processes for education and extension.

Samenvatting en conclusies

In bovengronden vinden talrijke interactieve natuurkundige, chemische en biologische processen plaats die essentieel zijn voor het in standhouden van leven. Veel van deze processen worden sterk beinvloed door de hoeveelheid water dat in de grond aanwezig is. Daarom vormen stroming van bodemvocht en transport van in bodemvocht opgeloste stoffen belangrijke elementen in veel milieustudies. Dit proefschrift heeft als doel bij te dragen aan drie actuele trends in hydrologisch onderzoek dat hierop betrekking heeft. De eerste trend is een verschuiving van analytische naar numerieke modellering, aangezien alleen numerieke modellen in staat zijn om de vele interacties na te bootsen tussen sterk niet-lineaire processen onder snel fluctuerende omstandigheden, zoals die voorkomen in bovengronden. De tweede trend is een verschuiving van homogene naar heterogene gronden. Krimpscheuren en waterafstotende delen kunnen een groot effect hebben op water- en stoffentransport en dienen daarom onderdeel te zijn van experimentele analyse en beleidsstudies. De derde trend heeft betrekking op een verschuiving van metingen in het laboratorium naar metingen in het veld. Aangezien steeds meer niet-destructieve en automatische meetinstrumenten beschikbaar komen voor veldmetingen en parameter-optimalisatietechnieken steeds betrouwbaarder worden, zijn veldexperimenten in combinatie met optimalisatietechnieken een aantrekkelijke mogelijkheid geworden om informatie te verzamelen over de eigenschappen van het natuurlijke systeem.

Hoofdstuk 2 begint met de uitgangspunten die gedurende de afgelopen 10 jaar vormgaven aan de onwikkeling van het agrohydrologische model SWAP (Soil Water Atmosphere Plant). De nauwe interactie in de bovengrond van water, opgeloste stoffen, warmte en vegetatie maakt het noodzakelijk de analytische vergelijkingen die waterstroming, stoffentransport, warmtestroming en vegetatiegroei beschrijven, gelijktijdig op te lossen. Wat betreft de ruimtelijke schaal ligt het accent op de veldschaal, aangezien velden duidelijk gedefinieerde systeemeigenschappen hebben en een fysische in plaats van empirische modelbeschrijving van stromings- en transportprocessen het mogelijk maakt allerlei ingrepen of buitengewone omstandigheden te analyseren. Door de bovenrand van het systeem net boven de vegetatie te leggen, en de onderrand bovenin het grondwatersysteem, kunnen de stromings- en transportprocessen ééndimensionaal gehouden worden, waardoor de hoeveelheid invoer en de rekentijd relatief gering zijn. Simulaties voor langjarige perioden met wisselende weer, vegetatie en drainage condities zijn noodzakelijk om kritische perioden te kunnen analyseren. SWAP diende voort te bouwen op de ervaringen met het model SWATR (Soil Water Actual Transpiration Rate) en van haar afgeleide modellen, en geschikt te zijn voor onderzoek, onderwijs en toepassing. In het resterende deel van Hoofdstuk 2 wordt aandacht geschonken aan de belangrijkste mogelijkheden en theoretische concepten van SWAP, zover die van belang zijn voor dit proefschrift.

Een belangrijke beperking van veel modeltoepassingen is het ontbreken van betrouwbare invoergegevens. Door de sterke toename van computerrekensnelheden en de ontwikkeling

van efficiënte rekentechnieken voor parameteroptimalisatie, zijn de mogelijkheden om invoerparameters vast te stellen met inverse modellering aanzienlijk uitgebreid. Bij deze techniek wordt een modelsimulatie uitgevoerd met initiële schattingen van de onbekende invoerparameters en de simulatieresultaten worden vergeleken met metingen. Vervolgens worden de invoerparameters aangepast met zoektechnieken als Gauss-Marquardt-Levenberg, en het model wordt opnieuw gedraaid. De procedure wordt herhaald tot de gesimuleerde en gemeten waarden zoveel mogelijk overeenstemmen. Belangrijke voordelen van inverse modellering zijn dat de hele procedure aanzienlijk goedkoper en sneller is dan die bij traditionele experimenten in het laboratorium of veld, er door de numerieke oplossing geen vereenvoudigingen nodig zijn van de stromings- en transportvergelijkingen, willekeurige initiële- en randvoorwaarden mogelijk zijn waardoor de experimentele omstandigheden heel flexibel zijn, fouten in vastgezette modelparameters of het modelconcept worden verdisconteerd in de waarden van de geoptimaliseerde parameters, alle bestaande informatie met betrekking tot de invoerparameters gebruikt kan worden, en 'last but not least' de nauwkeurigheid van de geoptimaliseerde parameters vastgesteld kan worden.

Een typisch en controleerbaar voorbeeld van inverse modellering zijn uitstromings-experimenten in het laboratorium, zoals beschreven in Hoofdstuk 3. In dit experiment wordt een ongestoord bodemmonster geplaatst in een drukcel op een keramische plaat en vervolgens verzadigd met water. Het experiment start door verhoging van de luchtdruk in de drukcel, waardoor een neerwaartse, onverzadigde waterstroming ontstaat in het bodemmonster. De cumulatieve uitstroming als functie van tijd wordt gemeten en wordt gebruikt voor optimalisatie van parameters die de bodemfysische functies (de relaties tussen bodemvochtgehalte, drukhoogte en hydraulische doorlatendheid) beschrijven. In de oorspronkelijke uitvoering werd één grote drukstap, overeenkomend met 500-1000 cm waterdruk, gebruikt. Deze methode is toegepast op vier verschillende grondsoorten en vergeleken met de resultaten van andere methoden voor het meten van de bodemfysische functies. Hieruit bleek dat optimalisatie met gebruik van alleen de cumulatieve uitstromingsgegevens onvoldoende is en leidt tot niet-unieke, afwijkende parameterwaarden. Wanneer de cumulatieve uitstromingsdata werden aangevuld met zogenaamde retentiedata (bodemvochtgehalte als functie van drukhoogte), die eenvoudig in dezelfde drukcel gemeten kunnen worden, verbeterde het resultaat aanzienlijk. Vervolgens beschrijft Hoofdstuk 3 uitstromingsexperimenten van een zavelgrond, waarbij de luchtdruk is verhoogd in vijf stappen (Multi-step) in plaats van één grote stap (One-step). De optimalisatieresultaten van Multi-step worden vergeleken met de resultaten van One-step en met afzonderlijke metingen van bodemvochtgehalte en drukhoogte. In geval van Multi-step bleken de cumulatieve uitstromingsdata voldoende te zijn voor unieke en betrouwbare parameterschattingen van de bodemfysische functies. Dit kwam ook naar voren in een vooranalyse van het betrouwbaarheidsinterval van de geoptimaliseerde parameters, welke voor Multi-step veel smaller was dan voor One-step.

Uitstromingsexperimenten in het laboratorium worden vaak toegepast op een serie bodemmonsters om effecten te berekenen van de ruimtelijke variatie van bodemfysische

functies op transport van water en opgeloste stoffen. Daarbij rijst veelal de vraag welke bodemfysische functies representatief zijn voor de bodemlaag waartoe de serie monsters behoort. Drie middelingsmethoden zijn toegepast op de 18 monsters van de zavelbodem die waren gebruikt in het Multi-step experiment: (1) schaling volgens geometrisch gelijkvormige media, (2) rekenkundige middeling van het volumetrisch vochtgehalte and de logaritme van de hydraulische doorlatendheid als functie van de drukhoogte, en (3) optimalisatie van rekenkundig gemiddelde, cumulatieve uitstromingsgegevens. Voor de onderzochte zavel-grond leidden alle drie middelingsmethoden tot vergelijkbare representatieve bodemfysische functies.

De nauwkeurigheid van modelvoorspellingen op veldschaal zullen toenemen als het inverse probleem ook wordt toegepast op veldschaal. Juiste selectie van het type metingen en de tijdstippen waarop gemeten moet worden tijdens het veldexperiment, kunnen veel geld besparen en onnauwkeurige parameterschattingen voorkomen. Voor het vaststellen van het meest informatieve meetschema, zijn betrouwbaarheidsintervallen van te schatten parameters, zoals berekend in een vooranalyse, zeer geschikt. Dit werd reeds duidelijk bij uitstromingsexperimenten in het laboratorium, waarbij Multi-step experimenten aanzienlijk smallere betrouwbaarheids-intervallen liet zien dan One-step experimenten. In Hoofdstuk 4 wordt zo'n vooranalyse met betrouwbaarheidsintervallen toegepast op een veldexperiment met gedraineerde zavelgrond waarop mais wordt verbouwd. Door SWAP zijn metingen gegenereerd, bestaande uit wekelijkse vochtgehalten en drukhoogten in de wortelzone, drainafvoeren en, facultatief, tracerconcentraties in het bodemprofiel en het drainagewater. Aan de gegenereerde metingen werden normaal verdeelde, ongecorreleerde meetfouten toegevoegd. Vier parameters (diffusieweerstand van het gewas, schaalfactor van bodemfysische functies, verzadigd vochtgehalte van de bovengrond en verzadigde hydraulische doorlatendheid van de ondergrond) werden geselecteerd voor optimalisatie. Deze parameters konden met smalle betrouwbaarheidsintervallen worden geoptimaliseerd door de combinatie SWAP-PEST (Parameter ESTimation, een flexibele schil voor parameter-optimalisatie). Bij de berekening van de betrouwbaarheidsintervallen werd de covariantie-matrix van de te optimaliseren parameters bepaald met een lineaire benadering van de doelfunctie rond het minimum. Deze benadering vraagt weinig rekenwerk en is voldoende nauwkeurig, zoals bleek uit verificatie met een Monte Carlo simulatie. Uit de vooranalyse bleek dat de nauwkeurigheid van de te optimaliseren parameters toeneemt als het experiment wordt uitgevoerd met een gewas en een tracer, en als de metingen plaatsvinden in perioden met extreme en veranderlijke hydrologische condities. De beschreven vooranalyse is een praktische en krachtige methode om het type en tijdstip van metingen zo te kiezen dat het inverse probleem goed gedefinieerd is. Na het uitvoeren van het experiment kunnen de metingen worden gebruikt om de onbekende parameters via inverse modellering vast te stellen, maar ook om modeltekortkomingen op te sporen of beter presterende modellen te selecteren.

Analyse van water- en stoffentransport in bovengronden is sterk gebaat bij een nauwkeurige en efficiënte numerieke oplossing van Richards stromingsvergelijking. Ongeveer 10 jaar

geleden is het waterbalansprobleem voor de numeriek oplossing van deze vergelijking opgelost door een verbeterde berekening van de differentiele watercapaciteitsterm. Echter, de bodemvochtfluxen zoals berekend door verschillende numerieke schema's kunnen nog sterk uiteenlopen door verschillen in compartimentsdikten en in ruimtelijke middeling van de hydraulische doorlatendheid K. Hoofdstuk 5 beschrijft een flexibel, impliciet, terugwaarts, eindig differentieschema dat relatief eenvoudig geïmplementeerd kan worden in numerieke modellen. Speciale aandacht wordt geschonken aan de selectie van de bovenrandvoorwaarde tijdens het iteratief oplossen van Richards stromingsvergelijking. De stabiliteit van het numerieke schema wordt geïllustreerd voor twee sterk niet-lineaire grondsoorten onder extreme omstandigheden van infiltratie, bodemverdamping en snel veranderende grondwaterstanden boven en onder maaiveld. Bij compartimentsdikten van 5 cm, worden de bodemvochtfluxen overschat bij rekenkundige middeling van K en onderschat bij geometrische middeling van K. Bij geringere compartimentsdikten convergeert het schema met rekenkundige middeling van K sneller tot de theoretisch juiste oplossing dan het schema met geometrische middeling van K. Bij compartimentsdikten van 1 cm en rekenkundige middeling van K zijn de afwijkingen door de numerieke discretisatie gering ten opzichte van andere onzekerheden, zoals hysterese in de waterretentiefunctie en horizontale ruimtelijke variabiliteit van bodemfysische functies.

Hysterese in de bodemfysische functies en preferente stroming door waterafstotendheid van grond kunnen een belangrijke invloed hebben op water- en stoffentransport in bovengronden. Hysterese komt voornamelijk voor in de relatie tussen bodemvochtgehalte en drukhoogte. Geleidelijke desorptie van initiëel verzadigde grond levert de hoofd-desorptiecurve, terwijl langzame adsorptie van initiëel droge grond resulteert in de hoofd-adsorptiecurve. In het veld komen adsorptie en desorptie voor in allerlei cycli, resulterend in zogenaamde adsorptie- en desorptie-scanningcurven die zich bevinden tussen de hoofd-adsorptiecurve en hoofd-desorptiecurve. In SWAP is hysterese geïmplementeerd volgens een methode waarbij de scanningcurven worden afgeleid door herschaling van de hoofd-adsorptiecurve of hoofd-desorptiecurve.

Onder invloed van allerlei klimaten en vegetaties vertonen veel droge gronden een zekere mate van waterafstotendheid. Infiltratiesnelheden in waterafstotende gronden kunnen aanzienlijk lager zijn dan die in bevochtigbare gronden en bevochtigingspatronen in waterafstotende gronden zijn onregelmatig en incompleet. Om waterstroming en stoffentransport in zulke gronden met SWAP te beschrijven, wordt onderscheid gemaakt tussen mobiele gedeelten, waarin de traditionele vergelijkingen voor waterstroming en stoffentransport gelden, en immobiele gedeelten waarin geen convectief transport van water en stoffen plaatsvindt. Het volume van het mobiele gedeelte kan variëren met de diepte en ook met de drukhoogte in het mobiele gedeelte. In het gangbare meetprotocol van bodemfysische functies wordt waterafstotendheid onderdrukt. Daarom worden de gangbaar gemeten bodemfysische functies geldig verondersteld in de mobiele gedeelten waarin geen waterafstotendheid voorkomt. In veldomstandigheden kan het volume van het mobiele gedeelte globaal worden geschat aan de hand van zichtbaar natte en droge plekken in een

136

bodemprofiel kort na neerslag. Meer nauwkeurig zijn experimenten met inerte kleurstoffen zoals jodide en Brilliant Blue, metingen met de zogenaamde disc-permeameter in combinatie met inerte kleurstoffen, profielmetingen met TDR (Time Domain Reflectrometry) sensoren en inverse modellering.

De beschreven concepten voor hysterese en waterafstotendheid zijn toegepast op gegevensbestanden van twee locaties met gronden die gevoelig zijn voor hysterese en waterafstotendheid. Aangetoond werd dat in het algemeen bodemvochtstroming wordt vertraagd door hysterese en versneld door preferente stroming. Simulaties lieten zien dat door hysterese de grond meer vocht vasthoudt na een relatief grote infiltratie. Echter, in normale veldomstandigheden leiden simulaties met hysterese tot een geringere vochtberging in de wortelzone, omdat bij een zekere drukhoogte scanningcurven een geringer vochtgehalte hebben dan de hoofd-desorptiecurve die anders gewoonlijk bij simulaties wordt gebruikt. Daardoor kon de langzame vochttoename van de wortelzone na een zeer droge zomer beter gesimuleerd worden door rekening te houden met hysterese. Verder bleek dat in velden met relatief geringe grondwaterstanden zonder wateraccumulatie op het maaiveld, de bodemvochtfluxen slechts in geringe mate worden beïnvloed door hysterese en dat hysterese geen verklaring vormt voor waargenomen grondwaterpieken na zware neerslag.

Aanpassing van de bodemfysische functies met het mobiel-immobiel concept verbeterde de gesimuleerde vochtgehalten in vergelijking met gemeten waarden (Hoofdstuk 6). Echter, het effect van immobiele gedeelten op gesimuleerde waterfluxen was gering voor de beschouwde experimenten. In de gemeten veldcondities werden de waterfluxen in de bodem bepaald door netto neerslag, actuele verdamping en de relatief ondiepe grondwaterstanden. De geringe gevoeligheid van bodemvochtfluxen voor preferente stroming bij gematigde condities betekent dat bij gematigde condities preferente stroming moeilijk afgeleid kan worden uit waterbalansmetingen. In tegenstelling tot bodemvochtfluxen, werden bodemvochtgehalten significant beïnvloed door preferente stroming als gevolg van waterafstotendheid. Ook de uitspoeling van bromide naar het grondwater werd veel beter voorspeld wanneer het mobiel-immobiel concept werd toegepast.

Modellen met één domein kunnen in kleigronden met krimpscheuren de uitspoeling van nutriënten en pesticiden naar grondwater sterk onderschatten. Verschillende fysische en empirische modellen met twee domeinen zijn ontwikkelt, die rekening houden met het effect van scheuren op waterstroming en stoffentransport. In Hoofdstuk 7 wordt een modelconcept beschreven, dat gebruik maakt van de krimpkarakteristiek van klei om het volume en de diepte van de scheuren te berekenen voor variabele veldcondities. Het concept is ontwikkelt om het gemiddelde gedrag van het veld te beschrijven, in plaats van stroming en transport op één locatie. De waterstroming en het stoffentransport in de bodemmatrix en de scheuren worden beschreven met elementaire bodemfysica, waardoor uitgebreide analyse van experimenten en scenarios mogelijk zijn. Het modelconcept is geïmplementeerd in SWAP en toegepast op een veldexperiment met gescheurde kleigrond, waar de waterstroming en het bromidetransport op veldschaal waren gemeten gedurende een periode van 572 dagen. SWAP

met gebruik van één domein was niet in staat de waterstroming en het bromidetransport gemiddeld voor het veld te simuleren. Toevoeging van het scheurconcept verbeterde de simulatie van vochtgehalten en bromideuitspoeling naar het grondwater aanzienlijk. Er bestaan echter nog steeds verschillen tussen gemeten en gesimuleerde bromideconcentraties. SWAP simuleerde niet het waargenomen achterblijven van bromide in de bovenste vijf centimeters en de grote dispersie van bromide door infiltratie van water via scheuren op verschillende diepten. Een gevoeligheidsanalyse liet zien dat uitspoeling van bromide vooral gevoelig is voor de verzadigde hydraulische doorlatendheid van de bovenlaag, de overdracht van stoffen tussen bodemmatrix en water dat langs de scheuren stroomt en de gemiddelde verblijftijd van water dat via de scheuren direct naar drains of sloten stroomt. De krimpkarakteristiek en de bodemfysische functies van de kleimatrix lieten slechts een geringe gevoeligheid zien.

Hoofdstuk 8 geeft een overzicht van recent gepubliceerde, typisch agrohydrologische studies die gebruik maakten van SWAP. Twee voorbeelden worden uitgebreid beschreven. De eerste heeft betrekking op duurzame irrigatie in een semi-aried gebied in de Punjab van Pakistan. In dit gebied is de aanvoer en verdeling van irrigatiewater onvoldoende, waardoor boeren méér en méér grondwater onttrekken voor irrigatie met behulp van eigen pompen. Vier velden met verschillende hoeveelheid en kwaliteit van irrigatiewater werden intensief gevolgd gedurende drie gewasseizoenen. SWAP is gecalibreerd op de metingen en vervolgens gebruikt voor een gevoeligheidsanalyse voor de korte en lange termijn. De gevoeligheidsanalyse liet zien dat de gesimuleerde water- en zoutbalansen vooral gevoelig zijn voor de verdampingsgewasfactor en de bodemfysische functies. Verder bleek dat heterogene waterinfiltratie en preferente stroming leiden to meer waterpercolatie uit de wortelzone en minder zoutuitspoeling. De simulaties voor de periode van 1 jaar gaven aan dat in de huidige situatie de gewasgroei meer belemmert wordt door watertekort dan door verzouting. De simulaties voor de periode van 10 jaar lieten zien dat de officiële richtlijnen voor irrigatie in het gebied voldoende zijn om negatieve gevolgen van verzouting voor gewasgroei ook op langere termijn te vermijden.

Het tweede voorbeeld heeft betrekking op ontzouting van de eilanden en slikken in De Grevelingen, een voormalige zeearm in het zuidwesten van ons land. Na de afsluiting door de Brouwersdam in 1971, wordt het waterniveau van het meer constant gehouden, terwijl het zoutgehalte op peil wordt gehouden door constante verversing met zeewater. Door het jaarlijkse neerslagoverschot vindt toch een geleidelijke ontzouting plaats in de bodems van de slikken langs de kust en de eilanden in het meer. Daardoor ontwikkelde zich in de afgelopen 29 jaar langs de oevers van het meer een botanisch zeer afwisselend milieu met allerlei overgangen van zout naar zoet, van nat naar droog en van nutriëntenrijk naar nutriëntenarm. Echter, de ontzouting gaat door en leidt tot het steeds smaller worden van deze waardevolle overgangszone. Daarom zijn alternatieven voor het waterbeheer van de Grevelingen voorgesteld met grotere variaties van het waterniveau, waarmee het vroegere getijdeverschil enigszins wordt nagebootst. SWAP is gebruikt om de waterbalans en ontzouting te analyseren in vier raaien loodrecht op de oever. Calibratie van SWAP, waarbij gebruik werd gemaakt van gemeten grondwaterstanden en zoutprofielen na afsluiting, liet zien dat de

ontzoutingssnelheid vooral bepaald wordt door de maaiveldshoogte ten opzichte van het meerpeil, de drainageweerstand van de ondergrond, de gewasbedekking en het aantal overstromingen door harde wind in het zomerseizoen. De zoutconcentraties vertonen grote seizoensmatige fluctuaties, met de hoogste waarden in de maand augustus en de laagste waarden in februari. De grondwaterstandsfluctuaties, relatieve verschillen in zoutprofielen van raaien loodrecht op de oever en langjarige ontzoutingssnelheden, werden naar tevredenheid gereproduceerd door SWAP. Het gecalibreerde model is gebruikt om de bodemvochtstroming en het zouttransport te simuleren voor 5 watermanagement scenario's en voor perioden van 10 jaar. Alle voorgestelde scenario's, met uitzondering van één, leiden tot significante verhoging van de zoutconcentraties in de overgangszone langs de oevers. Aangezien de meeste ontzouting plaatsvindt bij neerwaartse bodemvochtstroming in de wintermaanden, is verhoging van het waterniveau in de Grevelingen tijdens de wintermaanden het meest effectief.

Actuele ontwikkelingen met méérdimensionale, fysisch gebaseerde modellen en geïntegreerde hydrologische raamwerken, zullen onze analyse van waterstroming en stoffentransport in bodems verder verbeteren. Echter, vanwege hun flexibiliteit, toegankelijkheid en snelheid, zullen de komende 5-10 jaar ééndimensionale modellen als SWAP een belangrijke rol blijven spelen om nieuwe stromings- en transportconcepten te verkennen, laboratorium- en veldexperimenten te analyseren, geschikte watermanagement mogelijkheden te selecteren, regionale studies uit te voeren met gebruik van geografische informatiesystemen en transportprocessen te illustreren voor onderwijs en voorlichting.

References

Abbaspour, K.C., M. Sonnleitner, and R. Schulin, 1999. *Uncertainty in estimation of soil hydraulic parameters by inverse modeling: example lysimeter experiments.* Soil Sci. Soc. Am. J., 63: 501-509.

Abenney-Mickson, S., A. Yomota, and T. Miura, 1997. *Water balance of field plots planted with soybean and pumpkin.* Trans. ASAE, 40: 899-909.

Allen, R.G., L.S. Pereira, D. Raes, and M. Smith, 1998. *Crop evapotranspiration. Guidelines for computing crop water requirements.* Irrigation and Drainage Paper 56, FAO, Rome, Italy, 300 p.

Andreu, L., F. Moreno, N.J. Jarvis, and G. Vachaud, 1994. *Application of the model MACRO to water movement and salt leaching in drained and irrigated marsh soils, Marismas, Spain.* Agric. Water Manage., 25: 71-88.

Ashby, M., A.J. Dolman, P. Kabat, E.J. Moors and M.J. Ogink-Hendriks, 1996. *SWAPS version 1.0. Technical reference manual.* Technical document 42, Alterra Green World Research, Wageningen.

Bakel, P.J.T. van, 1986. *Planning, design and operation of surface water management systems; a case study.* PhD-thesis, Wageningen University, 118 p.

Baker, D.L., 1995. *Darcian weighted interblock conductivity means for vertical unsaturated flow.* Ground Water, 33: 385-390.

Bakker, H. de, 1979. *Major soils and soil regions in The Netherlands.* Pudoc, Wageningen, 203 p.

Bard, Y., 1974. *Nonlinear parameter estimation.* Academic Press, Orlando, Florida, 340 p.

Bastiaanssen, W.G.M., J. Huygen, J.K. Schakel, and B.J. van den Broek, 1996a. *Modelling the soil-water-crop-atmosphere system to improve agricultural water management in arid zones (SWATRE).* In 'Dutch experience in irrigation water management modelling', B.J. van den Broek (Ed.), Report 123, Alterra Green World Research, Wageningen, p. 13-30.

Bastiaanssen, W.G.M., R. Singh, and S. Kumar, 1996b. *Analysis and recommendations for integrated on-farm water management in Haryana, India: a model approach.* Report 118, Alterra Green World Research, Wageningen, 152 p.

Bates, B.C., 1992. *Improved methodology for parameter inference in nonlinear, hydrologic regression models.* Water Resour. Res., 28: 89-97.

Bear, J., 1972. *Dynamics of fluids in porous media.* Elsevier, Amsterdam.

Beekma, J., T.J. Kelleners, T.M. Boers, and Z.I. Raza, 1995. *Applications of SWATRE to evaluate drainage of an irrigated field in the Indus Plain, Pakistan.* In 'Crop-water-simulation models in practice.' Proc. ICID Congress 1993, The Hague, The Netherlands, p. 141-160.

Belmans, C., J.G. Wesseling and R.A. Feddes, 1983. *Simulation of the water balance of a cropped soil: SWATRE.* J. Hydrol., 63: 271-286.

Beltman, W.H.J., J.J.T.I. Boesten and S.E.A.T.M. van der Zee, 1995. *Analytical modelling of pesticide transport from the soil surface to a drinking water well.* J. Hydrol., 169: 209-228.

Berg, F. van den, and J.J.T.I. Boesten, 1998. *PEsticide Leaching and Accumulation model (PESTLA) version 3.4; description and user's guide.* Technical Document 43, Alterra Green World Research, Wageningen, 150 p.

Berg, P., 1999. *Long-term simulation of water movement in soils using mass-conserving procedures.* Adv. Water Resour., 22: 419-430.

Beven, K. and P. Germann, 1982. *Macropores and water flow in soils.* Water Resour. Res., 18: 1311-1325.

Bierkens, M.F.P., 1998. *Modeling water table fluctuations by means of a stochastic differential equation.* Water Resour. Res., 34: 2485-2499.

Bierkens, M.F.P., P.J.T. van Bakel, and J.G. Wesseling, 1999. *Comparison of two modes of surface water control using a soil water model and surface elevation data.* Geoderma, 89: 149-175.

References

Biggar, J.W. and D.R. Nielsen, 1976. *The spatial varability of the leaching characteristics of a field soil.* Water Resour. Res., 12: 78-84.

Black, T.A., W.R. Gardner and G.W. Thurtell, 1969. *The prediction of evaporation, drainage, and soil water storage for a bare soil.* Soil Sci. Soc. Am. J., 33: 655-660.

Boekhold, S., 1992. *Field scale behaviour of cadmium in soil.* PhD-thesis, Wageningen University, 181 p.

Boers, Th.M., 1994. *Rain water harvesting in arid and semi-arid zones.* PhD-thesis, Wageningen University, 133 p.

Boesten, J.J.T.I., 1986. *Behaviour of herbicides in soil : Simulation and experimental assessment.* PhD-thesis, Wageningen University, 263 p.

Boesten, J.J.T.I. and L. Stroosnijder, 1986. *Simple model for daily evaporation from fallow tilled soil under spring conditions in a temperate climate.* Neth. J. Agric. Sci., 34: 75-90.

Boesten, J.J.T.I. and A.M.A. van der Linden, 1991. *Modeling the influence of sorption and transformation on pesticide leaching and persistence.* J. Environ. Qual., 20: 425-435.

Bolt, G.H., 1979. *Movement of solutes in soils: principles of adsorption/exchange chromatography.* In 'Soil Chemistry B. Physico-Chemical Models', G.H. Bolt (Ed.), Elsevier, Amsterdam, p. 285-348.

Booltink, H.W.G., 1993. *Morphometric methods for simulation of water flow.* PhD-thesis, Wageningen University, 169 p.

Booltink, H.W.G. and J. Bouma, 1993. *Sensitivity analysis on processes affecting bypass flow.* Hydrol. Process., 7: 33-43.

Booltink, H.W.G., R. Hatano, and J. Bouma, 1993. *Measurement and simulation of bypass flow in a structured clay soil: a physico-morphological approach.* J. Hydrol., 148: 149-168.

Bouma, J. and L.W. Dekker, 1978. *A case study on infiltration into a dry clay soil. I. Morphological observations.* Geoderma, 20: 27-40.

Bouma, J., 1982. *Measuring the hydraulic conductivity of soil horizons with continuous macropores.* Soil Sci. Soc. Am. J., 46: 438-441.

Bouma, J., C. Belmans, L.W. Dekker and W.J.M. Jeurissen, 1983. *Assessing the suitability of soils with macropores for subsurface liquid waste disposal.* J. Environ. Qual., 12: 305-311.

Bouten, W., 1992. *Monitoring and modelling forest hydrological processes in support of acidification research.* PhD-thesis, University of Amsterdam, 218 p.

Braden, H., 1985. *Ein Energiehaushalts- und Verdunstungsmodell for Wasser und Stoffhaushaltsuntersuchungen landwirtschaftlich genutzer Einzugsgebiete.* Mittelungen Deutsche Bodenkundliche Geselschaft, 42: 294-299.

Brady, N.C., and R.R. Weil, 1996. *The nature and properties of soils.* 11th edition. Prentice-Hall, Upper Saddle River, New Jersey.

Bresler, E., and G. Dagan, 1983. *Unsaturated flow in spatially variable fields. 2. Application of water flow models to various fields.* Water Resour. Res., 19: 421-428.

Broek, B.J. van den, J.C. van Dam, J.A. Elbers, R.A. Feddes, J. Huygen, P. Kabat and J.G. Wesseling, 1994. *SWAP 1993, input instructions manual.* Report 45, Subdep. Water Resources, Wageningen University.

Broek, B.J. van den, and P. Kabat, 1995. *SWACROP: dynamic simulation model of soil water and crop yield applied to potatoes.* In 'Modeling and parameterization of the Soil-Plant-Atmospere System. A comparison of potato growth models', P. Kabat, B. Marshall, B.J. van den broek, J. Vos and H. van Keulen (Eds.), Wageningen Press, p. 299-334.

Bronswijk, J.J.B. 1988. *Modeling of water balance, cracking and subsidence of clay soils.* J. Hydrol., 97: 199-212.

Bronswijk, J.J.B. and J.J. Evers-Vermeer, 1990. *Shrinkage of Dutch clay soil aggregates.* Neth. J. of Agric. Sci., 38: 175-194.

Bronswijk, J.J.B., 1991. *Magnitude, modeling and significance of swelling and shrinkage processes in clay soils.* PhD-thesis, Wageningen University, 145 p.

Bronswijk, J.J.B., W. Hamminga and K. Oostindie, 1995. *Field-scale solute transport in a heavy clay soil.* Water Resour. Res., 31: 517-526.

Brooks, R.H., and A.T. Corey, 1964. *Hydraulic properties of porous media.* Hydrology paper 3, Colorado State University, 27 p.

Bruand, A., O. Duval, J.H.M. Wösten, and A. Lilly, 1996. *The use of pedotransfer functions in soil hydrology research in Europe.* Proc. workshop, 10-12 October 1996, Orleans, France, 211 p.

Burch, G.J., I.D. Moore, and J. Burns, 1989. *Soil hydrophobicity effects on infiltration and catchment runoff.* Hydr. Process., 3: 211-222.

Carrera J., and S. P. Neuman, 1986a. *Estimation of aquifer parameters under transient and steady state conditions : 1. Maximum Likelihood method incorporating prior information.* Water Resour. Res., 22: 199-210.

Carrera J., and S. P. Neuman, 1986b. *Estimation of aquifer parameters under transient and steady state conditions : 2. Uniqueness, stability and solution algorithms.* Water Resour. Res., 22: 211-227.

Carrilo, M.L.K., J. Letey and S.R. Yates, 1999. *Measurement of initial soil-water contact angle of water repellent soils.* Soil Sci. Soc. Am. J., 63: 433-436.

Carsel, R.F., and R.S. Parrish, 1988. *Developing joint probability distributions of soil water characteristics.* Water Resour. Res., 24: 755-769.

Celia, M.A., E.T. Bouloutas and R.L. Zarba, 1990. *A general mass-conservative numerical solution for the unsaturated flow equation.* Water Resour. Res., 26: 1483-1496.

Christensen, S., and R.L. Cooley, 1999. *Evaluation of prediction intervals for expressing uncertainties in groundwater flow model predictions.* Water Resour. Res., 35: 2627-2639.

Ciollaro, G., and N. Romano, 1995. *Spatial variability of the soil hydraulic properties of a vulcanic soil.* Geoderma, 65: 263-282.

Clausnitzer, V., J.W. Hopmans and D.R. Nielsen, 1992. *Simultaneous scaling of soil water retention and hydraulic conductivity curves.* Water Resour. Res., 28: 19-31.

Clausnitzer, V., and J.W. Hopmans, 1995. *LM-OPT : General purpose optimization code based on the Levenberg-Marquardt algorithm.* LAW Resources Paper 100032, Hydrol. Science, Dept. LAW, UC Davis, California, 16 p.

Clemente, R.S., R. de Jong, H.N. Hayhoe, W.D. Reynolds and M. Hares, 1994. *Testing and comparisons of three unsaturated soil water flow models.* Agric. Water Manage., 25: 135-152.

Clothier, B.E., M.B. Kirkham and J.E. McLean, 1992. *In situ measurement of the effective transport volume for solute moving through soil.* Soil Sci. Soc. Am. J., 56: 733-736.

Cooley, R.L., 1985. *A comparison of several methods of solving nonlinear regression groundwater flow problems.* Water Resour. Res., 21: 1525-1538.

Daanen, R., 1997. *Water flow and heat transport under frost and thaw conditions at an arable field soil with snow cover near Sjökulla, Finland.* MSc-thesis, Sub-department Water Resources, Wageningen University, 86 p.

Dam, J.C. van, J.M.H. Hendrickx, H.C. van Ommen, M.H. Bannink, M.Th. van Genuchten and L.W. Dekker, 1990a. *Water and solute movement in a coarse-textured water-repellent field soil.* J. Hydrol., 120: 359-379.

Dam, J.C. van, J.N.M. Stricker, and P. Droogers, 1990b. *From One-step to Multi-step. Determination of soil hydraulic functions by outflow experiments.* Report 7, Subdep. Water Resources, Wageningen University.

Dam, J.C. van, J.N.M. Stricker, and P. Droogers, 1992. *Evaluation of the inverse method for determining soil hydraulic functions from One-step outflow experiments.* Soil Sci. Soc. Am. J., 56: 1042-1050.

Dam, J.C. van, J.N.M. Stricker, and P. Droogers, 1994. *Inverse method to determine soil hydraulic functions from multi-step outflow experiments.* Soil Sci. Soc. Am. J., 58: 647-652.

Dam, J.C. van, J.H.M. Wösten, and A. Nemes, 1996. *Unsaturated soil water movement in hysteretic and water repellent soils.* J. Hydrol., 184: 153-173.

Dam, J.C. van, 1997. *Effects of water level changes in De Grevelingen on salinity concentrations along the shore.* Consultancy report, RIZA, Dep. Water Management, Lelystad, The Netherlands, 47 p. (in Dutch)

Dam, J.C. van, J. Huygen, J.G. Wesseling, R.A. Feddes, P. Kabat, P.E.V. van Walsum, P. Groenendijk and C.A. van Diepen, 1997. *Theory of SWAP version 2.0. Simulation of water flow, solute transport and plant growth in the Soil-Water-Atmosphere-Plant environment.* Report 71, Subdep. Water Resources, Wageningen University, Technical document 45, Alterra Green World Research, Wageningen.

Dam, J.C. van, 2000. *Simulation of field-scale water flow and bromide transport in a cracked clay soil.* Hydrol. Proces., 14: 1101-1117.

Dam, J.C. van, and R.A. Feddes, 2000. *Numerical simulation of infiltration, evaporation and shallow groundwater levels with the Richards' equation.* J. Hydrol., in press.

Dam, J.C. van, and P.J.J.F. Torfs, 2000. *Prior analysis of inverse, field scale experiments to select observations and fitting parameters.* Submitted to Water Resour. Res.

Dane, J.H., and P.J. Wierenga, 1975. *Effect of hysteresis on the prediction of infiltration, redistribution and drainage of water in a layered soil under transient flow conditions.* J. Hydrol., 25: 229-242.

Dane, J.H., and S. Hruska, 1983. *In-situ determination of soil hydraulic properties during drainage.* Soil Sci. Soc. Am. J., 47: 619-624.

Dekker, L.W. and C.J. Ritsema, 1994. *How water moves in a water repellent sandy soil. 1. Potential and actual water repellency.* Water Resour. Res., 30: 2507-2517.

Dekker, L.W., 1998. *Moisture variability resulting from water repellency in Dutch soils.* PhD-thesis Wageningen University, 240 p.

DeBano, L.F., 1981. *Water repellent soils: a state of the art.* Gen. Tech. Rep. PSW-46, Pacific Southwest For. Range Exp. Stn., 21 p.

Dekker, L.W., C.J. Ritsema, O. Wendroth, N. Jarvis, K. Oostindie, W. Pohl, M. Larsson, and J.P. Gaudet, 1999. *Moisture distributions and wetting rates of soils at experimental fields in the Netherlands, France, Sweden and Germany.* J. Hydrol., 215: 4-22.

Delft, S.P.J. van, and R.H. Kemmers, 1998. *Regulation of base composition by specific measures in wet fields with low nutrient availability and low-laying peat marshlands.* Pre-study: system description. Report 619, Alterra Green World Research, Wageningen, 63 p. (in Dutch)

Desbarats, A.J., 1995. *An interblock conductivity scheme for finite difference models of steady unsaturated flow in heterogeneous media.* Water Resour. Res., 31: 2883-2889.

Diment, G.A., and K.K. Watson, 1983. *Stability analysis of water movement in unsaturated porous materials: 2. Numerical studies.* Water Resour. Res., 19: 1002-1010.

Diment, G.A., and K.K. Watson, 1985. *Stability analysis of water movement in unsaturated porous materials: 3. Experimental studies.* Water Resour. Res., 21: 979-984.

Dirksen, C., 1979. *Flux-controlled sorptivity measurements to determine soil hydraulic property functions.* Soil Sci. Soc. Am. J., 43: 827-834.

Dirksen, C., 1987. *Water and salt transport in daily irrigated root zone.* Neth. J. Agric. Sci., 35: 395-406.

Dirksen, C., 1991. *Unsaturated hydraulic conductivity.* In 'Soil analysis, physical methods', K.A. Smith and C.E. Mullins (Eds.), Marcel Dekker, New York, p. 209-269.

Dirksen, C., J.B. Kool, P. Koorevaar and M.Th. van Genuchten, 1993. *Hyswasor: simulation model of hysteretic water and solute transport in the root zone.* In 'Water flow and solute transport in soils', D. Russo and G. Dagan (Eds.), Adv. Series in Agric. Science 20, Springer-Verlag, p. 99-122.

Dirksen, C. and S. Matula, 1994. *Automatic atomized water spray system for soil hydraulic conductivity measurements.* Soil Sci. Soc. Am. J., 58: 319-325.

Dirksen, C., 1999. *Soil physics measurements.* Catena Verlag, Reiskirchen, Germany, 154 p.

Doering, E.J., 1965. *Soil-water diffusivity by the one-step method.* Soil Sci., 99: 322-326.

Doherty, J., L. Brebber and P. Whyte, 1995. *PEST. Model independent parameter estimation.* Australian Centre for Tropical Freshwater Research, James Cooke University, Townsville, Australia, 140 p.

Doorenbos, J., and W.O. Pruitt, 1977. *Guidelines for predicting crop water requirements.* Irrigation and Drainage Paper 24, FAO, Rome, Italy.

Doorenbos, J., and A.H. Kassam, 1979. *Yield response to water.* FAO Irrigation and Drainage Paper 33, FAO, Rome, Italy.

Droogers, P., 1997. *Quantifying differences in soil structure induced by farm management.* PhD-thesis, Wageningen University, 134 p.

Droogers, P., 2000. *Estimating actual evapotranspiration using a detailed agro-hydrological model.* J. Hydrol., 229: 50-58.

Droogers, P., and W.G.M. Bastiaanssen, 2000. *Evapotranspiration in irrigation performance and water accounting frameworks: an assessment from combined hydrological and remote sensing modeling.* Submitted to J. Irrig. Drain. Eng.

Droogers, P., G. Kite, and H. Murray-Rust, 2000a. *Use of simulation models to evaluate irrigation performances including water productivity, risk and system analyses.* Submitted to Irrig. Sci.

Droogers, P., W.G.M. Bastiaanssen, M. Beyazgül, Y. Kayam, G.W. Kite, and H. Murray-Rust, 2000b. *Distributed agro-hydrological modeling of an irrigation system in western Turkey.* Agric. Water Manage., in press.

Duffy, C.J. and D.H. Lee, 1992. *Base flow response from nonpoint source contamination: simulated spatial variability in source, structure and initial condition.* Water Resour. Res., 28: 905-914.

Eching, S.O., and J.W. Hopmans, 1993. *Optimization of hydraulic functions from transient outflow and soil water pressure data.* Soil Sci. Soc. Am. J., 57: 1167-1175.

Eching, S.O., J.W. Hopmans, and O. Wendroth, 1994. *Unsaturated hydraulic conductivity from transient Multi-step outflow experiments.* Soil Sci. Soc. Am. J., 58: 687-695.

Eertwegh, G.A.P.H. van den, and C.R. Meinardi, 1999. *Water flow and nutrient transport in the catchment of 'De Hupselse Beek'.* Report 74, Subdep. Water Resources, Wageningen University, (in Dutch)

Ernst, L.F., 1973. *The determination of residence times in case of groundwater flow.* Report 755 ICW, now Alterra Green World Research, Wageningen.

Feddes, R.A., 1971. *Water, heat and crop growth.* PhD-thesis, Wageningen University, 184 p.

Feddes, R.A., P.J. Kowalik and H. Zaradny, 1978. *Simulation of field water use and crop yield.* Simulation Monographs, Pudoc, Wageningen, 189 p.

Feddes, R.A., 1987. *Crop factors in relation to Makking reference crop evapotranspiration.* In 'Evaporation and weather', Proc. and Information 39, TNO Committee on Hydrol. Research, p. 33-46.

Feddes, R.A., P. Kabat, P.J.T. van Bakel, J.J.B. Bronswijk and J. Halbertsma, 1988. *Modelling soil water dynamics in the unsaturated zone - state of the art.* J. Hydrol., 100: 69-111.

Feddes, R.A., G.H. de Rooij, J.C. van Dam, P. Kabat, P. Droogers, and J.N.M. Stricker, 1993a. *Estimation of regional effective soil hydraulic parameters by inverse modelling.* In 'Water flow and solute transport in soils: modelling and application', D. Russo and G. Dagan (Eds.), Springer Verlag, Berlin, p. 211-231.

Feddes, R.A., M. Menenti, P. Kabat, and W.G.M. Bastiaanssen, 1993b. *Is large scale inverse modelling of unsaturated flow with areal average evaporation and surface soil moisture as estimated from remote sensing feasible?* J. Hydrol., 143: 125-152.

Feddes, R.A., and J.C. van Dam, 1997. *Modelling of water flow and salt transport for irrigation management and drainage design.* In 'Water management, salinity and pollution control towards sustainable irrigation in the Meditterranean region', Int. Conf., Sept. 1997, Bari, Italy, p. 145-179.

Feddes, R.A., and J.C. van Dam, 1999. *Effects of plants on the upper boundary condition.* In 'Modeling of transport processes in soils', J. Feyen and K. Wiyo (Eds.), Proc. of Int. Workshop, Nov. 1999, Leuven, Belgium, p. 391-405.

Finke, P.A., 1992. *Spatial variability of soil structure and its impact on transport processes and some associated land qualities.* PhD-thesis, Wageningen University, 131 p.

Finke, P.A., J.H.M. Wösten, and J.G. Kroes, 1996a. *Comparing two approaches of characterizing soil map unit behaviour in solute transport.* Soil Sci. Soc. Am. J., 60: 200-205.

Finke, P.A., J.H.M. Wösten, and M.J.W. Jansen, 1996b. *Effects of uncertainty in major input variables on simulated soil behaviour.* Hydrol. Process., 10: 661-669.

Finsterle, S., and K. Pruess, 1995. *Solving the estimation-identification problem in two-phase modeling.* Water Resour. Res., 31: 913-924.

Flury, M., H. Flühler, W.A. Jury and J. Leuenberger, 1994. *Susceptibility of soils to preferential flow of water: a field study.* Water Resour. Res., 30: 1945-1954.

Flury, M. and H. Flühler, 1995. *Tracer characteristics of Brilliant Blue FCF.* Soil Sci. Soc. Am. J., 59: 22-27.

Gardner, W.R., 1956. *Calculation of capillary conductivity from pressure plate outflow data.* Soil Sci. Soc. Am. Proc., 20: 317-320.

Gardner, W.R., 1962. *More on the separation and solution of diffusion type equations.* Soil Sci. Soc. Am. Proc., 26: 404.

Garnier, P., Rieu, M., Boivin, P., Vauclin, M., and Baveye, P. 1997. *Determining the hydraulic properties of a swelling soil from a transient evaporation experiment.* Soil Sci. Soc. Am. J., 61: 1555-1563.

Gehrels, H., 1999. *Groundwater level fluctuations. Separation of natural from anthropogenic influences and determination of groundwater recharge in the Veluwe area, The Netherlands.* PhD-thesis, Vrije Universiteit Amsterdam, 267 p.

Genuchten, M.Th. van, and P.J. Wieringa, 1974. *Simulation of one-dimensional solute transfer in porous media.* Bull. 628, Agric. Exp. Stn., New Mexico State University, New Mexico.

Genuchten, M.Th. van, and R.W. Cleary, 1979. *Movement of solutes in soil : computer simulated and laboratory results.* In 'Soil Chemistry B, Physico-Chemical Models', G.H. Bolt (Ed.), Elsevier, Amsterdam, p. 349-386.

Genuchten, M.Th. van, 1980. *A closed form equation for predicting the hydraulic conductivity of unsaturated soils.* Soil Sci. Soc. Am. J., 44: 892-898.

Genuchten, M.Th. van, 1982. *A comparison of numerical solutions of the one-dimensional unsaturated-saturated flow and transport equations.* Adv. Water Resour., 5: 47-55.

Genuchten, M.Th. van, and R.J. Wagenet, 1989. *Two-site/two-region models for pesticide transport and degradation: Theoretical development and analytical solutions.* Soil Sci. Soc. Am. J., 53: 1303-1310.

Genuchten, M.Th. van, F.J. Leij, and S.R. Yates, 1991. *The RETC code for quantifying the hydraulic functions of unsaturated soils.* US Salinity Lab., Riverside, California.

Gerke, H.H. and M.Th van Genuchten, 1993. *A dual-porosity model for preferential movement of water and solutes in structured porous media.* Water Resour. Res., 29: 305-319.

Germann, P.F. and K. Beven, 1985. *Kinematic wave approximation to infiltration into soils with sorbing macropores.* Water Resour. Res., 21: 990-996.

Glass, R.J., J.Y. Parlange, and T.S. Steenhuis, 1989. *Wetting front instability, 1 Theoretical discussion and dimensional analysis.* Water Resour. Res., 25: 1187-1194.

Goudriaan, J., 1977. *Crop meteorology: a simulation study.* Simulation monographs, Pudoc, Wageningen.

Gribb, M.M., 1996. *Parameter estimation for determining hydraulic properties of a fine sand from transient flow measurements.* Water Resour. Res., 32: 1965-1974.

Grinsven, J.J.M. van, C. Dirksen and W. Bouten, 1985. *Evaluation of hot air method for measuring soil water diffusivity.* Soil Sci. Soc. Am. J., 49: 1093-1099.

Grinsven, J.J.M. van, 1988. *Impact of acid atmospheric deposition on soils : quantification of chemical and hydrologic processes.* PhD-thesis, Wageningen University, 213 p.

Groen, K.P., 1997. *Pesticide leaching in polders. Field and model studies on cracked clays and loamy sand.* PhD-thesis, Wageningen University, 296 p.

Groenendijk, P. and J.G. Kroes, 1997. *Modelling the nitrogen and phosphorus leaching to groundwater and surface water; ANIMO 3.5.* Report 144, Alterra Green World Research, Wageningen.

Groenendijk, P., M. van Elswijk, J. Huygen, J.G. Kroes, A.J. Otjens, M.F.R. Smit, A.A. Veldhuizen, and J.G. Wesseling, 1999. *MultiSwap: an application of the Integrated Framework Water Management.* Technical document 60, Alterra Green World Research, Wageningen, 82 p. (in Dutch)

Groot, W.J.M de., P.A. Finke, J. Oude Voshaar, M.J.D. Hack-ten Broeke, F. de Vries and Y. van Randen, 1998. *Soil schematisation. Upscaling by aggregation of soil information for model simulations at national and regional level.* Report 651, Alterra Green World Research, Wageningen, 62 p. (in Dutch)

Groot, W.J.M. de, and M.J.D. Hack-ten Broeke, 1999. *Verification of irrigation planning with the hydrological model SWAP2.0. Research results 1997.* Report 661, Alterra Green World Research, Wageningen, 80 p. (in Dutch)

Gupta, S.C., D.A. Farrell, and W.E. Larson, 1974. *Determining effective soil water diffusivities from one-step outflow experiments.* Soil Sci. Soc. Am. Proc., 38: 710-716.

Hack-ten Broeke, M.J.D., 2000. *Nitrate leaching from dairy farming on sandy soils. Case studies for experimental farm De Marke.* PhD-thesis, Wageningen University, 145 p.

Hamaker, P., W.H.B. Aarnink, and J.M.P.M. Peerboom, 1997. *Effects of reducing water supply and leaching of the area Voorne-West.* Report 435, Alterra Green World Research, Wageningen, 149 p. (in Dutch)

Harmsen, J., 1986. *Optimalisation of column choice, eluent preparation and detection by ion chromatography of inorganic anions.* Nota 1699, ILRI, Wageningen, 46 p.

Haverkamp, R., M. Vauclin, J. Touma, P.J. Wierenga and G. Vachaud, 1977. *A comparison of numerical simulation models for one-dimensional infiltration.* Soil Sci. Soc. Am. J., 41: 285-294.

Haverkamp, R., and M. Vauclin, 1979. *A note on estimating finite difference interblock hydraulic conductivity values for transient unsaturated flow problems.* Water Resour. Res., 15: 181-187.

Heinen, M., 1997. *Dynamics of water and nutrients in closed, recirculating cropping systems in glasshouse horticulture with special attention to lettuce grown in irrigated sand beds.* PhD-thesis, Wageningen University, 270 p.

Hendrickx, J.M.H., L.W. Dekker, E.J. van Zuilen, and O.H. Boersma, 1988. *Water and solute movement through a water repellent sand soil with grass cover.* In 'Validation of flow and transport models for the unsaturated zone', Proc. Conf. Ruidoso, New Mexico, p. 131-146.

Hendrickx, J.M.H., L.W. Dekker, and O.H. Boersma, 1993. *Unstable wetting fronts in water repellent soils.* J. Environ. Qual., 22: 109-118.

Hendriks, R.F.A., K. Oostindie, and P. Hamminga, 1999. *Simulation of bromide tracer and nitrogen transport in a cracked clay soil with the FLOCR/ANIMO model combination.* J. Hydrol., 215: 94-115.

Hijmans, R.J., I.M. Guiking-Lens and C.A. van Diepen, 1994. *User's guide for the WOFOST 6.0 crop growth simulation model.* Technical Document 12, Alterra Green World Research, Wageningen, 144 p.

Hill, D.E., and J.-Y. Parlange, 1972. *Wetting front instability in layered soils.* Soil Sci. Soc. Am. Proc., 36: 697-702.

Hill, M.C., R.L. Cooley, and D.W. Pollock, 1998. *A controlled experiment in ground water flow model calibration.* Ground Water, 36, 520-535.

Hillel, D., 1980. *Fundamentals of soil physics.* Academic Press, San Diego, California, 412 p.

Hillel, D., 1987. *Unstable flow in layered soils: a review.* Hydrol. Process., 1: 143-147.

Homaee, M., 1999. *Root water uptake under non-uniform transient salinity and water stress.* PhD-thesis, Wageningen University, The Netherlands, 173 p.

Hoogmoed, W.B., and Bouma, J. 1980. *A simulation model for predicting infiltration into a cracked clay soil.* Soil Sci. Soc. Am. J., 44: 458-461.

Hopmans, J.W., and J.N.M. Stricker, 1989. *Stochastic analysis of soil water regime in a watershed.* J. Hydrol., 105: 57-84.

Hopmans, J.W., K.C. Roy, and W.W. Wallender, 1991. *Irrigation water management and soil-water hysteresis - a computer modeling study with stochastic soil hydraulic properties.* Transactions of the ASAE, 34: 449-459.

Hopmans, J.W., T. Vogel, and P.D. Koblik, 1992. *X-ray tomography of soil water distribution in One-step outflow experiments.* Soil Sci. Soc. Am. J., 56: 355-362.

Hornung, U., and W. Messing, 1983. *Truncation errors in the numerical solution of horizontal diffusion in saturated/unsaturated media.* Adv. Water Resour., 6: 165-168.

Hoven, C.A. van den, 1997. *Regional water resources management in the Andean region with numerical models and satellite remote sensing.* Evaluation of user's oriented water application strategies in irrigation schems (Mendoza, Argentina) using a one-dimensional model of solute and unsaturated flow. Report 75.3, Alterra Green World Research, Wageningen, 113 p.

Hoyningen-Hüne, J. von, 1983. *Die Interzeption des Niederschlags in landwirtschaftlichen Beständen.* Schriftenreihe des DVWK 57: 1-53.

Huang, K., B.P Mohanty and M.Th. van Genuchten, 1996. *A new convergence criterion for the modified Picard iteration method to solve the variably saturated flow equation.* J. Hydrol., 178: 69-91.

Huygen, J., J.C. van Dam, and J.G. Kroes, 2000. *SWAP for Windows. Users manual.* Report, Alterra Green World Research, Wageningen.

Inoue, M., J. Šimunek, J.W. Hopmans, and V. Clausnitzer, 1998. *In-situ estimation of soil hydraulic functions using multistep soil water extraction technique.* Water Resour. Res., 34: 1035-1050.

IWASRI, 1991. *Control of waterlogging and salinity in Pakistan. A review of information and methods.* Publication 21, Lahore, Pakistan.

IWMI, 1995. *Salinity and sodicity research in Pakistan.* Proc. Workshop salinity and sodicity research, Feb. 1995, Lahore, Pakistan.

Jacucci et al., 1995. *HYDRA, a decision support model for irrigation water management.* In 'Crop-water-simulation models in practice.' Proc. ICID Congress 1993, The Hague, The Netherlands, p. 315-332.

Jamison, V.C., 1945. *The penetration of irrigation and rain water into sandy soils of central Florida.* Soil Sci. Soc. Am. Proc., 10: 25-29.

Jansen, P.C., J. Runhaar, J.P.M. Witte, and J.C. van Dam, 2000. *Wetness indication of grass vegetations in relation to the moisture status of soils.* Report 057, Alterra Green World Research, Wageningen, 59 p. (in Dutch)

Jarvis, N. 1994. *The MACRO model (version 3.1). Technical description and sample simulations.* Monograph, Reports and dissertations 19, Dep. of Soil Sciences, Uppsala, Sweden, 51 p.

Jaynes, D.B., 1984. *Comparison of soil water hysteresis models.* J. Hydrol., 75: 287-299.

Jong, R. de, and A. Bootsma, 1997. *Estimates of water deficits and surpluses during the growing season in Ontario using the SWATRE model.* Can. J. Soil Sci., 77: 285-294.

Jong, L.W. de, O.H. Jacobsen, and P. Moldrup, 1999. *Soil water repellency: effects of water content, temperature and particle size.* Soil Sci. Soc. Am., J., 63: 437-442.

Jury, W.A., 1982. *Simulation of solute transport using a transfer function mode.* Water Resour. Res., 18: 363-368.

Jury, W.A., D. Russo and G. Sposito, 1987. *The spatial variability of water and solute transport properties in unsaturated soil, II Scaling of water transport.* Hilgardia, 55: 33-56.

Jury, W.A., W.R. Gardner and W.H. Gardner, 1991. *Soil Physics.* Fifth edition, Wiley, New York, 330 p.

Kabat, P., B.J. van den Broek and R.A. Feddes, 1992. *SWACROP: A water management and crop production simulation model.* ICID Bulletin 92, vol. 41, no. 2: 61-84.

Kabat, P., R.W.A. Hutjes, and R.A. Feddes, 1997. *The scaling characteristics of soil parameters: from plot scale heterogeneity to subgrid parameterization.* J. Hydrol., 190: 363-396.

Kaluarachchi, J.J., and J.C. Parker, 1987. *Effects of hysteresis with air entrapment on water flow in the unsaturated zone.* Water Resour. Res., 23: 1967-1976.

Kelleners, T.J., J. Beekma, and M.R. Chaudhry, 1999. *Spatially variable soil hydraulic properties for simulation of field-scale solute transport in the unsaturated zone.* Geoderma, 92: 199-215.

Kim, D.J., 1992. *Characterization of swelling and shrinkage behaviour, hydraulic properties and modelling of water movement in a physically ripening marine clay soil.* PhD-thesis, Catholic University Leuven, Belgium, 169 p.

Kim, R., 1995. *The water budget of heterogeneous areas.* PhD-thesis, Wageningen University, 182 p.

Klute, A., 1986. *Water retention: laboratory methods.* In 'Methods of soil analysis; Part 1; Physical and Mineralogical methods', A. Klute (Ed.), Agronomy series n. 9, ASA and SSSA, Madison, Wisconsin, p. 635-662.

Klute, A., and C. Dirksen, 1986. *Hydraulic conductivity and diffusivity: laboratory methods.* In 'Methods of soil analysis; Part 1; Physical and Mineralogical methods', A. Klute (Ed.), Agronomy series n. 9, ASA and SSSA, Madison, Wisconsin, p. 687-734.

Knopman, D.S., and C.I. Voss, 1988. *Further comments on sensitivities, parameter estimation, and sampling design in one-dimensional analysis of solute transport in porous media.* Water Resour. Res., 24: 225-238.

Knotters, M., and P.E.V. van Walsum, 1997. *Estimating fluctuation quantities from time series of water-table depths using models with a stochastic component.* J. Hydrol., 197: 25-46.

Knotters, M., and J.G. de Gooijer, 1999. *TARSO modeling of water table depths.* Water Resour. Res., 35: 695-705.

Kool, J.B., J.C. Parker, and M.Th. van Genuchten, 1985a. *Determining soil hydraulic properties from One-step outflow experiments by parameter estimation: I. Theory and numerical studies.* Soil Sci. Soc. Am. J., 49: 1348-1354.

Kool, J.B., J.C. Parker, and M.Th. van Genuchten, 1985b. *Onestep: a nonlinear parameter estimation program for evaluating soil hydraulic properties from One-step outflow experiments.* Bulletin 85-3, Virginia Agricultural Experiment Station, Blacksburg, Virginia, 44 p.

Kool, J.B., and J.C. Parker, 1987. *Development and evaluation of closed form expressions for hysteretic soil hydraulic properties.* Water Resour. Res., 23: 105-114.

Kool, J.B., and J.C. Parker, 1988. *Analysis of the inverse problem for transient unsaturated flow.* Water Resour. Res., 24: 817-830.

Kool, J.B., and M.Th. van Genuchten, 1991. *HYDRUS, One-dimensional variably saturated flow and transport model including hysteresis and root water uptake.* Research Report 124, U.S. Salinity Laboratory, Riverside, California.

Koorevaar, P., G. Menelik and C. Dirksen, 1983. *Elements of soil physics.* Developments in Soil Science 13, Elsevier, Amsterdam, 223 p.

Kroes, J.G., and J. Roelsma, 1998. *User's Guide ANIMO 3.5; input instructions and technical programme description.* Technical Document 46, Alterra Green World Research, Wageningen.

Kroes, J.G., J.C. van Dam, J. Huygen, and R.W. Vervoort, 1999. *User's Guide of SWAP version 2.0. Simulation of water flow, solute transport and plant growth in the Soil-Water-Atmosphere-Plant environment.* Technical Document 48, Alterra Green World Research, Wageningen, Report 81, Department of Water Resources, Wageningen University, 127 p.

Kroes, J.G., P. Groenendijk, and J. Huygen, 1999. *Hydrology for STONE: calculations with SWAP 207d.* Tech. Doc. 57, Alterra Green World Research, Wageningen, 49 p. (in Dutch)

Kuczera, G., 1990. *Assessing hydrological nonlinearity using response surface plots.* J. Hydrol., 118: 143-161.

Kuczera, G., and M. Mroczkowski, 1998. *Assessment of hydrologic parameter uncertainty and the worth of multiresponse data.* Water Resour. Res., 34: 1481-1489.

Kuper, M., and E.G. van Waiijen, 1993. *Farmer irrigation practices and their impact on soil salinity in the Punjab, Pakistan: Is salinity here to stay?* IWMI internal programme review, Colombo, Sri Lanka.

Kuper, M., 1998. *Irrigation management strategies for improved salinity and sodicity control.* PhD thesis, Wageningen University, 238 p.

Laat, P.J.M. de, 1980. *Model for unsaturated flow above a shallow watertable applied to a regional sub-surface flow problem.* PhD-thesis, Wageningen University, 126 p.

Larsson, M.H., N.J. Jarvis, G. Torstensson, and R. Kasteel, 1999. *Quantifying the impact of preferential flow on solute transport to tile drains in a sandy field soil.* J. Hydrol., 215: 116-134.

Leij, F.J., W.J. Alves, M. Th. van Genuchten and J.R. Williams, 1996. *The UNSODA Unsaturated Soil Hydraulic Database. User's manual Version 1.0.* US Salinity Laboratory, Riverside, California.

Leistra, M., A.M.A. van der Linden, J.J.T.I. Boesten, A. Tiktak, and F. van den Berg, 2000. *PEARL model for pesticide behaviour and emissions in soil-plant systems.* Description of processes. Report 13, Alterra Green World Research, Wageningen.

Letey, J., J.F. Osborn, and N. Valoras, 1975. *Soil water repellency and the use of nonionic surfactants.* Contrib. 154, Calif. Water Res. Center, California.

Li, K.Y., J.B. Boisvert, and R. de Jong, 1999. *An exponential root water uptake model.* Can. J. Soil Sci., 79: 333-343.

Liu, Y., T.S. Steenhuis, and J.-Y Parlange, 1994. *Closed form solution of finger width in sandy soils at different water contents.* Water Resour. Res., 30: 949-952.

Luxmoore, R.J., 1991. *On preferential flow and its measurement.* In 'Preferential flow', Gish and Shirmohammadi (Eds.), Proc. Nat. Symp., Dec. 1991, Chicago, Illinois.

Maas, E.V., and G.J. Hoffman, 1977. *Crop salt tolerance-current assessment.* J. Irrig. and Drainage Div., 103: 115-134.

Maas, E.V., 1990. *Crop salt tolerance.* In 'Agricultural salinity assessment and management', K.K. Tanji (Ed.), ASCE Manuals and Reports on Engineering practice, no. 71, New York.

Marquardt, D.W., 1963. *An algorithm for least squares estimation of nonlinear parameters.* J. Soc. Ind. Appl. Math., 11: 431-441.

Massop, H.Th.L., J.M.P.M. Peerboom, and H.C. van Vessem, 1994. *Effects of measures to alleviate desiccation at rural estate 'De Wildenborch'.* Report 342, Alterra Green World Research, Wageningen, 128 p. (in Dutch)

Massop, H.T.H.L., T. Kroon, P.J.T. van Bakel, W.J. de Lange, A. van der Giessen, M.J.H. Pastoors, and J. Huygen, 2000. *Hydrology for STONE; schematization and parameterization.* Report 38, Serie Milieu Planbureau 9, Alterra Green World Research, Wageningen, 101 p. (in Dutch)

McCuen, R.H., and W.M. Snyder, 1986. *Hydrologic modeling. Statistical methods and applications.* Prentice Hall, Englewood Cliffs.

McLaughlin, and L. Townley, 1996. *A reassessment of the groundwater inverse problem.* Water Resour. Res., 32: 1131-1161.

Meeuwig, R.O., 1971. *Infiltration and water repellency in granitic soils.* Res. Pap. INT-111, USDA For. Serv., Ogden, Utah, 20 p.

Miller, E.E., and R.D. Miller, 1956. *Physical theory for capillary flow phenomena.* J. Appl. Phys., 27: 324-332.

Miller, C.T., G.W. Williams, C.T. Kelly, and M.D. Tocci, 1998. *Robust solution of Richards equation for nonuniform porous media.* Water Resour. Res., 34: 2599-2610.

Millington, R.J., and J.P. Quirk, 1961. *Permeability of porous solids.* Trans. Faraday Soc., 57: 1200-1207.

Milly, P.C.D., 1985. *A mass conservative procedure for time-stepping in models of unsaturated flow.* Adv. Water Resour., 8: 32-36.

Mishra, S., and J.C. Parker, 1989. *Parameter estimation for coupled unsaturated flow and transport.* Water Resour. Res., 25: 385-396.

Mishra, S., J.L. Zhu and J.C. Parker, 1990. *How effective are effective medium properties?* In 'ModelCARE 90: Calibration and reliability in groundwater modeling', IAHS Publ. 195, Proc. Conf., Sept. 1990, The Hague, The Netherlands.

Monteith, J.L., 1965. *Evaporation and the Environment.* In 'The state and movement of water in living organisms', G.E. Fogg (Ed.), Cambridge University Press, p. 205-234.

Monteith, J.L., 1981. *Evaporation and surface temperature.* Quarterly J. Royal Soc., 107: 1-27.

Mualem, Y., 1976. *A new model for predicting the hydraulic conductivity of unsaturated porous media.* Water Resour. Res., 12: 513-522.

Neut, D. van der, J.C. van Dam, and R.A. Feddes, 1995. *Effects of higher surface water levels in 'De Hoeksche Waard'. An evaluation of yield reductions of potatoes and sugar beets at 4 drainage depths during 42 years.* Report 48, Subdep. Water Resources, Wageningen University, 69 p.

Nguyen, H.V., J.L. Nieber, C.J. Ritsema, L.W. Dekker, and T.S. Steenhuis, 1999. *Modeling gravity driven unstable flow in a water repellent soil.* J. Hydrol., 215: 202-214.

Nielsen, D.R., M.Th. van Genuchten and J.W. Biggar, 1986. *Water flow and solute transport in the unsaturated zone.* Water Resour. Res., 22, supplement: 89S-108S.

Nimmo, J.R., J. Rubin and D.P. Hammermeister, 1987. *Unsaturated flow in a centrifugal field: measurement of hydraulic conductivity and testing of Darcy's law.* Water Resour. Res., 32: 124-134.

Norton, J.P., 1986. *An introduction to identification.* Academic Press, San Diego, California, 310 p.

Olsthoorn, T.N., 1998. *Groundwater modelling: calibration and the use of spreadsheets.* PhD-thesis, Delft University, The Netherlands, 114 p.

Ommen, H.C. van, 1985. *Systems approach to an unsaturated-saturated groundwater quality model, including adsorption, decomposition and bypass.* Agric. Water Manage., 10: 193-203.

Ommen, H.C. van, 1988. *Transport from diffuse sources of contamination and its application to a coupled unsaturated-saturated system.* PhD-thesis, Wageningen University, 142 p.

Ommen, H.C. van, R. Dijksma, J.M.H. Hendrickx, L.W Dekker, J. Hulshof and M. van den Heuvel, 1989a. *Experimental and theoretical analysis of solute transport from a diffuse source of pollution.* J. Hydrol., 105: 225-251.

Ommen, H.C. van, M.Th. van Genuchten, W.H. van der Molen, R. Dijksma, and J. Hulshof, 1989b. *Experimental assessment of preferential flow paths in a field soil.* J. Hydrol., 105: 253-262.

Oostindie, K., and J.J.B. Bronswijk, 1992. *FLOCR - a simulation model for the calculation of water balance, cracking and surface subsidence of clay soils.* Report 47, Alterra Green World Research, Wageningen.

Otjens, A.J., M. van Elswijk, and R.M. Lokers, 1999. *Introduction to modeling and programming with Frameworks Integral Watermanagement.* Technical document 59, Alterra Green World Research, Wageningen, 67 p. (in Dutch)

Pan, L., and P.J. Wierenga, 1995. *A transformed head-based approach to solve Richards equation for variably saturated soils.* Water Resour. Res., 31: 925-931.

Pan, L., A.W. Warrick, and P.J. Wierenga, 1996. *Finite elements methods for modelling water flow in variably saturated porous media: Numerical oscillation and mass distributed schemes.* Water Resour. Res., 32: 1883-1889.

Parker, J.C., J.B. Kool, and M.Th. van Genuchten, 1985. *Determining soil hydraulic properties from One-step outflow experiments by parameter estimation: II. Experimental studies.* Soil Sci. Soc. Am. J., 49: 1354-1359.

Parlange, J.-Y., and D.E. Hill, 1976. *Theoretical analysis of wetting front instability in soils.* Soil Sci., 122: 236-239.

Passioura, J.B., 1976. *Determining soil water diffusivities from one-step outflow experiments.* Aust. J. Soil Res., 15: 1-8.

Peerboom, J. 1987. *Adaptions of the model SWATRE in order to simulate the behaviour of swelling and shrinking clay soils.* MSc-thesis, Subdep. Water Resources, Wageningen University, 104 p. (in Dutch)

Philip, J.R., 1975. *Stability analysis of infiltration.* Soil Sci. Soc. Am. Proc., 39: 1042-1049.

Prathapar, S.A., A.S. Quereshi, and S.M.P. Smets, 1997. *Mechanically reclaiming abandoned saline soils: a numerical evaluation.* In 'Drainage for the 21st century', Proc. Int. Drainage Workshop, Nov. 1997, Penang, Malaysia, Vol. 3, 17 p.

Press, W.H., B.P. Flannery, S.A. Teukolsky and W.T. Vetterling, 1989. *Numerical recipes in Fortran, the art of scientific computing.* Cambridge University Press, 759 p.

Qureshi, A.S., and S.A. Hussain, 1996. *Soil water simulations in a lysimeter.* In 'Sustainability of irrigated agriculture: crop-water-environment models', R. Ragab, D.E. El-Quosy, B.J. van den Broek and L.S. Pereira (Eds.), Proc. ICID congress, Sept. 1996, Cairo, Egypt, p. 163-174.

Raats, P.A.C., 1973. *Unstable wetting fronts in uniform and nonuniform soils.* Soil Sci. Soc. Am. J., 37: 681-685.

Rijniersce, K. 1983. *A simulation model for physical ripening in the IJsselmeerpolders.* Report, Rijksdienst voor IJsselmeerpolders, Lelystad, The Netherlands, 216 p.

Rijtema, P.E., P. Groenendijk and J.G. Kroes, 1997. *ANIMO, a dynamic simulation model for transport and transformation of nutrients and organic materials in soils.* Report 30, Alterra Green World Research, Wageningen.

Rijtema, P.E., P. Groenendijk and J.G. Kroes, 1999. *Environmental impact of land use in rural regions: the development, validation, and application of model tools for management and policy analysis.* Vol. 1, Series on environmental science and management, Imperial College Press, London, 321 p.

Ritchie, J.T., 1972. *Model for predicting evaporation from a row crop with incomplete cover.* Water Resour. Res., 8: 1204-1213.

Ritsema, C.J., L.W. Dekker, J.M.H. Hendrickx and W. Hamminga, 1993. *Preferential flow mechanism in a water repellent sandy soil.* Water Resour. Res., 29: 2183-2193.

Ritsema, C.J., and L.W. Dekker, 1994. *How water moves in a water repellent sandy soil. 2. Dynamics of fingered flow.* Water Resour. Res., 30: 2519-2531.

Ritsema, C.J., 1998. *Flow and transport in water repellent sandy soils.* PhD-thesis Wageningen University, 213 p.

Ritsema, C.J., J.L. Nieber, T.S. Steenhuis, L.W. Dekker and J.C. van Dam, 2000. *Principles and modeling approaches of preferential flow in hydrophobic soils.* AGU Spring Meeting, June 2000, abstract and poster.

Ritzema, H.P., 1994. *Subsurface flow to drains.* In 'Drainage principles and applications', H.P. Ritzema (Ed.), ILRI publication 16, 2nd edition, Wageningen, p. 263-304.

Romano, N., B. Brunone, and A. Santini, 1998. *Numerical analysis of one-dimensional unsaturated flow in layered soils.* Adv. Water Resour., 21: 315-324.

Roo, A.P.J. de, C.G. Wesseling, and C.J. Ritsema, 1996. *LISEM, a single event physically based hydrological and soil erosion model for drainage basins. Theory, input and output.* Hydrol. Process., 10: 1107-1117.

Rooij, G.H. de, 1996. *Preferential flow in water-repellent sandy soils. Model development and lysimeter experiments.* PhD-thesis, Wageningen University, 229 p.

Ross, P.J., 1990. *Efficient numerical methods for infiltration using Richards' equation.* Water Resour. Res., 26: 279-290.

Runhaar, J., J.P.M. Witte, and P.H. Verburg, 1997. *Groundwater level, moisture supply, and vegetation in The Netherlands.* Wetlands, 17: 528-538.

Santini, A., N. Romano, G. Ciollaro, and V. Comegna, 1995. *Evaluation of a laboratory inverse method for determining unsaturated hydraulic properties of a soil under different tillage practices.* Soil Sci., 160: 340-351.

Sarwar, A., 2000. *A transient model approach to improve on-farm irrigation and drainage in semi-arid zones.* PhD-thesis, Wageningen University, 143 p.

Saxena, R.K., N.J. Jarvis and L. Bergström, 1994. *Interpreting non-steady state tracer breakthrough experiments in sand and clay soils using a dual-porosity model.* J. Hydrol., 162: 279-298.

Schaaf, S. van der, 1999. *Analysis of the hydrology of raised bogs in the Irish Midlands. A case study of Raheenmore Bog and Clara Bog.* PhD-thesis, Wageningen University, 375 p.

Schaap, M.G., 1996. *The role of soil organic matter in the hydrology of forests on dry sandy soils.* PhD-thesis, University of Amsterdam, 145 p.

Schoen, R., J.P. Gaudet, and T. Bariac, 1999. *Preferential flow and solute transport in a large lysimeter, under controlled boundary conditions.* J. Hydrol., 215: 70-81.

Schultz, E., 1992. *Water management of Dutch polders.* PhD-thesis, Delft University, 507 p. (in Dutch)

Scientific Software Group, 2000. *HydroGeoChem.* Http://www/scisoftware.com.

Scott, P.S., G.J. Farquhar and N. Kouwen, 1983. *Hysteretic effects on net infiltration.* In 'Advances in infiltration', ASAE, St. Joseph, Michigan, p. 163-170.

Selker, J.S., T.S. Steenhuis, and J.-Y. Parlange, 1996. *An engineering approach to fingered vadose pollutant transport.* Geoderma, 70: 197-206.

Shalhevet, J., 1994. *Using water of marginal quality for crop production: major issues.* Agric. Water Manage., 25: 233-269.

Šimunek, J., and M.T. van Genuchten, 1996. *Parameter estimation of soil hydraulic properties from the tension disc infiltrometer experiment by numerical inversion.* Water Resour. Res., 32: 2683-2696.

Šimunek, J., M. Sejna, and M.Th. van Genuchten, 1996. *The HYDRUS-2D software package for simulating water flow and solute transport in two-dimensional variably saturated media.* Version 1.0, Int. Groundwater Model Cent., TPS-53, Colorado School of Mines, Golden, Colorado.

Šimunek, J., and M.T. van Genuchten, 1997. *Estimating unsaturated soil hydraulic properties from multiple tension disc infiltrometer data.* Soil Sci., 162: 383-398.

Šimunek, J., O. Wendroth, and M.T. van Genuchten, 1998a. *A parameter estimation analysis of the evaporation method for determining soil hydraulic properties.* Soil Sci. Soc. Am. J., 62, 894-905.

Šimunek, J., M. Sejna, and M.Th. van Genuchten, 1998b. *The HYDRUS-1D software package for simulating one-dimensional water, heat, and multiple solutes in variably saturated media.* Version 2.0., Report, Oct. 1998, US Salinity Laboratory, Riverside, California, 178 p.

Šimunek, J., R. Kodesova, M.M. Gribb and M.T. van Genuchten, 1999. *Estimating hysteresis in the soil water retention function from cone permeameter experiments.* Water Resour. Res., 35: 1329-1345.

Smedt, F. de, and P.J. Wierenga, 1979. *A generalized solution for solute flow in soils with mobile and immobile water.* Water Resour. Res., 15: 1137-1141.

Smets, S.M.P., M. Kuper, J.C. van Dam, and R.A. Feddes, 1997. *Salinization and crop transpiration of irrigated fields in Pakistan's Punjab.* Agric. Water Manage., 35: 43-60.

Smith, M., 1992. *CROPWAT, a computer program for irrigation planning and management.* Irrigation and Drainage Paper 46, FAO, Rome, Italy.

Soil Survey Staff, 1975. *Soil taxonomy: A basic system of soil classification for making and interpreting soil surveys.* USDA-SCS Agric. Handb. 436, U.S. Gov. Print. Office, Washington DC, Maryland.

Spieksma, J.F.M., J.M. Schouwenaars, and J. Blankenburg, 1996. *Combined modelling of groundwater table and open water level in raised mires.* Nordic Hydrol., 27: 231-246.

Spitters, C.J.T., H. van Keulen and D.W.G. van Kraalingen, 1989. *A simple and universal crop growth simulator: SUCROS87.* In 'Simulation and systems management in crop protection', R. Rabbinge, S.A. Ward and H.H. van Laar (Eds.), Simulation Monographs, Pudoc, Wageningen, p. 147-181.

Starr, J.L., H.C. DeRoo, C.R. Frink, and J.-Y. Parlange, 1978. *Leaching characteristics of a layered field soil.* Soil Sci. Soc. Am. J., 42: 386-391.

Stroosnijder, L. 1975. *Infiltration and redistribution of water in the soil.* PhD-thesis, Wageningen University, 213 p. (in Dutch)

Tedeschi, A., G. Barbieri, and M. Menenti, 1996. *Impact of saline water on soil properties and crop yield: a simulation study.* In 'Sustainability of irrigated agriculture: crop-water-environment models', R. Ragab, D.E. El-Quosy, B.J. van den Broek and L.S. Pereira (Eds.), Proc. ICID congress, Sept. 1996, Cairo, Egypt, p. 126-139.

Ten Berge, H.F.M., 1986. *Heat and water transfer at the bare soil surface: aspects affecting thermal images.* PhD-thesis, Wageningen University, 287 p.

Tiktak, A., 1999. *Modeling non-point source pollutants in soils. Applications to the leaching and accumulation of pesticides and cadmium.* PhD-thesis, University of Amsterdam, 232 p.

Tiktak, A., F. van den Berg, J.J.T.I. Boesten, M. Leistra, A.M.A. van der Linden, and D. van Kraalingen, 2000. *Pesticide Emission at Regional and Local scales: Pearl version 1.1 User Manual.* RIVM report 711401008, report 29, Alterra Green World Research, Wageningen.

Tol, C. van der, 2000. *Soil evaporation and plant transpiration as simulated by the FAO-56 method and the agrohydrological model SWAP.* MSc-thesis, Subdep. Water Resources, Wageningen University.

Toorman, A.F., P.J. Wierenga, and R.G. Hills, 1992. *Parameter estimation of hydraulic properties from One-step outflow data.* Water Resour. Res., 28: 3021-3028.

Topp, G.C., 1969. *Soil water hysteresis measured in a sandy loam and compared with hysteretic domain model.* Soil Sci. Soc. Am. J., 33: 645-651.

Vachaud, G., and J.L. Thony, 1971. *Hysteresis during infiltration and redistribution in a soil column at different initial water contents.* Water Resour. Res., 7: 111-127.

Valiantzas, J.D., D.G. Kerkides, and A. Poulovassilis, 1988. *An improvement to the One-step outflow method for the determination of soil water diffusivities.* Water Resour. Res., 24: 1911-1920.

Vanclooster, M., P. Viaene, J. Diels, and K. Christiaens, 1994. *WAVE, a mathematical model for simulating water and agrochemicals in the soil and vadose environment. Reference and user's manual, release 2.* Inst. for Land and Water Management, Katholieke Univers. Leuven, Belgium, 150 p.

Veen, J.R. van de, F. van den Berg, H.A.J. Pellikaan-van Harten, M. Leistra, and J.J.T.I. Boesten, 1997. *Leaching of pesticides from soils in greenhouses to open water ditches.* Report 481.2, Alterra Green World Research, Wageningen.

Vos, J.A. de, 1997. *Water flow and nutrient transport in a layered silt loam soil.* PhD-thesis, Wageningen University, 284 p.

Vries, D.A. de, 1963. *Thermal properties of soils.* In 'Physics of plant environment', W.R. van Wijk (Ed.), North Holland Publishers, Amsterdam.

Vries, D.A. de, 1975. *Heat transfer in soils.* In 'Heat and mass transfer in the biosphere. I. Transfer processes in plant environment', De Vries, D.A. and N.H. Afgan (Eds.), Scripts Book Company, Washington DC, Maryland, p. 5-28.

Wang, Z., J. Feyen, and C.J. Ritsema, 1998a. *Susceptibility and predictability of conditions for preferential flow.* Water Resour. Res., 34: 2169-2182.

Wang, Z., J. Feyen, and D. Elrick, 1998b. *Prediction of fingering in porous media.* Water resour. Res., 34: 2183-2190.

Warrick, A.W., 1991. *Numerical approximations of Darcian flow through unsaturated soil.* Water Resour. Res., 27: 1215-1222.

Wendroth, O., W. Ehlers, J.W. Hopmans, H. Kage, J. Halbertsma and J.H.M. Wösten, 1993. *Reevaluation of the evaporation method for determining hydraulic functions in unsaturated soils.* Soil Sci. Soc. Am. J., 57: 1436-1443.

Wesseling, J.G., 1985. The effect of soil type and soil water content on soil temperatures. Report 1645, ICW, currently Alterra Green World Research, Wageningen, 27 p. (in Dutch)

Wesseling, J.G., J.G. Kroes, and K. Metselaar, 1998. *Global sensitivity analysis of the Soil-Water-Atmosphere-Plant (SWAP) model.* Report 160, Alterra Green World Research, Wageningen, 67 p.

Wijk, W.R. van, 1966. *Physics of plant environment.* Second edition, North Holland Publ. Comp., Amsterdam, 382 p.

Wit, C.T. de, J. Goudriaan, H.H. van Laar, F.W.T. Penning de Vries, R. Rabbinge, H. van Keulen, L. Sibma, and C. de Jonge, 1978. *Simulation of assimilation, respiration and transpiration of crops.* Simulation Monographs, Pudoc, Wageningen, 141 p.

White, I., P.M. Colombera, and J.R. Philip, 1977. *Experimental studies of wetting front instability induced by gradual change of pressure head gradient and by heterogeneous porous media.* Soil Sci. Soc. Am. J., 41: 483-489.

Wösten, J.H.M., J. Bouma and G.H. Stoffelsen, 1985. *Use of soil survey data for regional soil water simulation models.* Soil Sci. Soc. Am. J., 49: 1238-1244.

Wösten, J.H.M., 1990. *Use of soil survey data to improve simulation of water movement in soils.* PhD-thesis, Wageningen University, 103 p.

Wösten, J.H.M., C.H.J.E. Schuren, J. Bouma and A. Stein, 1990. *Functional sensitivity analysis of four methods to generate soil hydraulic functions.* Soil Sci. Soc. Am. J., 54: 832-836.

Wösten, J.H.M., G.H. Veerman and J. Stolte, 1994. *Water retention and hydraulic conductivity functions of top- and subsoils in The Netherlands: The Staring series.* Technical Document 18, Alterra Green World Research, Wageningen, 66 p. (in Dutch)

Wösten, J.H.M., P.A. Finke, and M.J.W. Jansen, 1995. *Comparison of class and continuous pedotransfer functions to generate soil hydraulic characteristics.* Geoderma, 66: 227-237.

Wösten, J.H.M., A. Lilly, A. Nemes and C. Le Bas, 1998. *Using existing soil data to derive hydraulic parameters for simulation models in environmental studies and in land use planning.* Report 156, Alterra Green World Research, Wageningen, 106 p.

Yassoglou, N., C.S. Kosmas, N. Moustakas, E. Tzianis, and N.G. Danalatos, 1994. *Cracking in recent alluvial soils as related to easily determined soil properties.* Geoderma, 63: 289-298.

Yates, S.R., M.Th. van Genuchten, A.W. Warrick and F.J. Leij, 1992. *Analysis of measured, predicted and estimated hydraulic conductivity using the RETC computer program.* Soil Sci. Soc. Am. J., 56: 347-354.

Yeh, W.W.G., and Y. S. Soon, 1981. *Aquifer parameter identification with optimum dimension in parameterization.* Water Resour. Res., 17: 664-672.

Yeh, W.W.G, 1986. *Review of parameter identification procedures in groundwater hydrology: the inverse problem.* Water Resour. Res., 22: 95-108.

Youngs, E.G, 1958. *Redistribution of moisture in porous materials after infiltration, 1 and 2.* Soil Sci., 86: 117-125, 202-207.

Youngs, E.G., and A. Poulovassilis, 1976. *The different forms of moisture profile development during redistribution of soil water after infiltration.* Water Resour. Res., 12: 1007-1012.

Youngs, E.G., and R.I. Price, 1981. *Scaling of infiltration behaviour in dissimilar porous materials.* Water Resour. Res., 17: 1065-1070.

Yule, D.F., and J.T. Ritchie, 1980a. *Soil shrinkage relationships of Texas Vertisols: I. Small cores.* Soil Sci. Soc. Am. J., 44: 1285-1291.

Yule, D.F., and J.T. Ritchie, 1980b. *Soil shrinkage relationships of Texas Vertisols: II. Large cores.* Soil Sci. Soc. Am. J., 44: 1291-1295.

Zaidel, J., and D. Russo, 1992. *Estimation of finite difference interblock conductivities for simulation of infiltration into initially dry soils.* Water Resour. Res., 28: 2285-2295.

Zee, S.E.A.T.M. van der, 1988. *Transport of reactive contaminants in heterogeneous soil systems.* PhD-thesis, Wageningen University, 283 p.

Zijlstra, J., and J.H. Dane, 1996. *Identification of hydraulic parameters in layered soils based on a quasi-Newton method.* J. Hydrol., 181: 233-250.

Zurmühl, T., and W. Durner, 1996. *Modeling transient water and solute transport in a biporous soil.* Water Resour. Res., 32: 819-829.

Appendix A of Chapter 4.

First order approximation of parameter covariance matrix

Close to the optimal values we assume a linear response of the observations to the parameter values [*Norton*, 1986]:

$$y = J b + e \tag{A1}$$

with e the observation error array. This gives for the objective function Φ:

$$\Phi = e^{\mathrm{T}} Q e = \left(y^{\mathrm{T}} - b^{\mathrm{T}} J^{\mathrm{T}} \right) Q \left(y - b J \right) \tag{A2}$$

The minimum of Φ is found at the parameter set where the gradient of Φ with respect to b is zero:

$$\frac{\partial \Phi}{\partial b} = \left[\frac{\partial \Phi}{\partial b_1} \frac{\partial \Phi}{\partial b_2} \cdots \frac{\partial \Phi}{\partial b_{\mathrm{k}}} \right]^{\mathrm{T}} = 0 \tag{A3}$$

To evaluate the expression $\partial\Phi/\partial b$ we use the following matrix standard operations (*Norton*, 1986):

$$\frac{\partial \left(a^{\mathrm{T}} b \right)}{\partial b} = a \tag{A4}$$

$$\frac{\partial \left(b^{\mathrm{T}} A b \right)}{\partial b} = \left(A + A^{\mathrm{T}} \right) b \tag{A5}$$

We multiply out the expression for Φ in Eq. A1, take the derivative with respect to b, note that $b^{\mathrm{T}} J^{\mathrm{T}} Q y$ is identical to $y^{\mathrm{T}} Q J b$ since both are scalars, put $J^{\mathrm{T}} Q y$ for a and $J^{\mathrm{T}} Q J$ for A in Eqs. A4 and A5, and obtain:

$$\frac{\partial \Phi}{\partial b} = -2 J^{\mathrm{T}} Q y + 2 J^{\mathrm{T}} Q J b \tag{A6}$$

The parameter set b that makes the gradient of Φ zero is therefore:

$$\hat{b} = \left[J^{\mathrm{T}} Q J \right]^{-1} J^{\mathrm{T}} Q \hat{y} \tag{A7}$$

Using Eqs. A1 and A7, the covariance of the parameter estimates can be calculated as:

$$
\begin{aligned}
C\left(\hat{b}\right) &= E\left[\left(\hat{b} - b\right)\left(\hat{b} - b\right)^{\mathrm{T}} \right] \\
&= E\left\{ \left[\left(J^{\mathrm{T}} Q J\right)^{-1} J^{\mathrm{T}} Q y - b \right]\left[\left(J^{\mathrm{T}} Q J\right)^{-1} J^{\mathrm{T}} Q y - b \right]^{\mathrm{T}} \right\} \\
&= E\left\{ \left[\left(J^{\mathrm{T}} Q J\right)^{-1} J^{\mathrm{T}} Q (Jb + e) - b \right]\left[\left(J^{\mathrm{T}} Q J\right)^{-1} J^{\mathrm{T}} Q (Jb + e) - b \right]^{\mathrm{T}} \right\} \\
&= E\left\{ \left[\left(J^{\mathrm{T}} Q J\right)^{-1} J^{\mathrm{T}} Q e \right]\left[\left(J^{\mathrm{T}} Q J\right)^{-1} J^{\mathrm{T}} Q e \right]^{\mathrm{T}} \right\} \\
&= E\left[\left(J^{\mathrm{T}} Q J\right)^{-1} J^{\mathrm{T}} Q e e^{\mathrm{T}} Q^{\mathrm{T}} J \left(J^{\mathrm{T}} Q J\right)^{-1} \right]
\end{aligned}
\tag{A8}
$$

If we assume the residuals to be independent of each other, and define the weighting matrix according to Eq. 4.2, we may write:

$$E\left[\boldsymbol{Q}\boldsymbol{e}\boldsymbol{e}^{\mathrm{T}}\right]=\boldsymbol{s}_{\mathrm{res}}^{2}\boldsymbol{I}=\frac{\Phi(\hat{\boldsymbol{b}})}{n}\boldsymbol{I} \tag{A9}$$

Combination of Eqs. A8 and A9 and multiplication, results in the given expression (Eq. 4.2) of the estimated parameter covariance matrix:

$$C\left(\hat{\boldsymbol{b}}\right)=\frac{\Phi(\hat{\boldsymbol{b}})}{n}\left(\boldsymbol{J}^{\mathrm{T}}\boldsymbol{Q}\boldsymbol{J}\right)^{-1} \tag{A10}$$

Appendix B of Chapter 5.

Equation set to solve Richards' equation, including boundary conditions

The implicit, backward, finite difference solution as discussed in Chapter 5, reads (Eq. 5.4):

$$C_i^{j+1,p-1}\left(h_i^{j+1,p}-h_i^{j+1,p-1}\right)+q_i^{j+1,p-1}-q_i^{j}=$$

$$\frac{\Delta t^{j}}{\Delta z_i}\left[K_{i-\frac{1}{2}}^{j}\left(\frac{h_{i-1}^{j+1,p}-h_i^{j+1,p}}{\Delta z_u}\right)+K_{i-\frac{1}{2}}^{j}-K_{i+\frac{1}{2}}^{j}\left(\frac{h_i^{j+1,p}-h_{i+1}^{j+1,p}}{\Delta z_\ell}\right)-K_{i+\frac{1}{2}}^{j}\right]-\Delta t^{j}S_i^{j} \qquad (B1)$$

Application of Eq. B1 to each node results in a tridiagonal matrix, for which we may define the following coefficients:

$$\begin{bmatrix} b_1 & g_1 & & & & & \\ a_2 & b_2 & g_2 & & & & \\ & a_3 & b_3 & g_3 & & & \\ & & & & & & \\ & & & & & & \\ & & & a_{n-1} & b_{n-1} & g_{n-1} \\ & & & & a_n & b_n \end{bmatrix}\begin{bmatrix} h_1^{j+1,p} \\ h_2^{j+1,p} \\ h_3^{j+1,p} \\ \\ \\ h_{n-1}^{j+1,p} \\ h_n^{j+1,p} \end{bmatrix}=\begin{bmatrix} f_1 \\ f_2 \\ f_3 \\ \\ \\ f_{n-1} \\ f_n \end{bmatrix} \qquad (B2)$$

In this appendix the expressions for the coefficients α_i, β_i, γ_i, and f_i are listed for each node and for both flux and head controlled boundary conditions.

B.1 Intermediate nodes

Rearrangement of Eq. B1 to B2 results in the coefficients:

$$a_i=-\frac{\Delta t^{j}}{\Delta z_i\Delta z_u}K_{i-\frac{1}{2}}^{j} \qquad (B3)$$

$$b_i=C_i^{j+1,p-1}+\frac{\Delta t^{j}}{\Delta z_i\Delta z_u}K_{i-\frac{1}{2}}^{j}+\frac{\Delta t^{j}}{\Delta z_i\Delta z_\ell}K_{i+\frac{1}{2}}^{j} \qquad (B4)$$

$$g_i=-\frac{\Delta t^{j}}{\Delta z_i\Delta z_\ell}K_{i+\frac{1}{2}}^{j} \qquad (B5)$$

$$f_i=C_i^{j+1,p-1}h_i^{j+1,p-1}-q_i^{j+1,p-1}+q_i^{j}+\frac{\Delta t^{j}}{\Delta z_i}\left(K_{i-\frac{1}{2}}^{j}-K_{i+\frac{1}{2}}^{j}\right)-\Delta t^{j}S_i^{j} \qquad (B6)$$

B.2 Top node

B.2.1 Flux boundary condition q_{sur}

The right hand side of Eq. B1 transforms to:

$$\frac{\Delta t^j}{\Delta z_i}\left[-q_{\text{sur}} - K_{1\frac{1}{2}}^j\left(\frac{h_1^{j+1,p} - h_2^{j+1,p}}{\Delta z_\ell}\right) - K_{1\frac{1}{2}}^j\right] - \Delta t^j S_1^j \tag{B7}$$

Rearrangements of Eq. B1 to the first line of Eq. B2 gives the coefficients:

$$\boldsymbol{b}_1 = C_1^{j+1,p-1} + \frac{\Delta t^j}{\Delta z_1 \Delta z_\ell} K_{1\frac{1}{2}}^j \tag{B8}$$

$$\boldsymbol{g}_1 = -\frac{\Delta t^j}{\Delta z_1 \Delta z_\ell} K_{1\frac{1}{2}}^j \tag{B9}$$

$$f_1 = C_1^{j+1,p-1} h_1^{j+1,p-1} - \boldsymbol{q}_1^{j+1,p-1} + \boldsymbol{q}_1^j + \frac{\Delta t^j}{\Delta z_1}\left(-q_{\text{sur}} - K_{1\frac{1}{2}}^j\right) - \Delta t^j S_1^j \tag{B10}$$

B.2.2 Head boundary condition h_{sur}

The right hand side of Eq. B1 transforms to:

$$\frac{\Delta t^j}{\Delta z_1}\left[K_{\frac{1}{2}}^j\left(\frac{h_{\text{sur}} - h_1^{j+1,p}}{\Delta z_u}\right) + K_{\frac{1}{2}}^j - K_{1\frac{1}{2}}^j\left(\frac{h_1^{j+1,p} - h_2^{j+1,p}}{\Delta z_\ell}\right) - K_{1\frac{1}{2}}^j\right] - \Delta t^j S_1^j \tag{B11}$$

Rearrangements of Eq. B1 to the first line of Eq. B2 gives the coefficients:

$$\boldsymbol{b}_1 = C_1^{j+1,p-1} + \frac{\Delta t^j}{\Delta z_1 \Delta z_u} K_{\frac{1}{2}}^j + \frac{\Delta t^j}{\Delta z_1 \Delta z_\ell} K_{1\frac{1}{2}}^j \tag{B12}$$

$$\boldsymbol{g}_1 = -\frac{\Delta t^j}{\Delta z_1 \Delta z_\ell} K_{1\frac{1}{2}}^j \tag{B13}$$

$$f_1 = C_1^{j+1,p-1} h_1^{j+1,p-1} - \boldsymbol{q}_1^{j+1,p-1} + \boldsymbol{q}_1^j + \frac{\Delta t^j}{\Delta z_1}\left(K_{\frac{1}{2}}^j - K_{1\frac{1}{2}}^j\right) + \frac{\Delta t^j}{\Delta z_1 \Delta z_u} K_{\frac{1}{2}}^j h_{\text{sur}} - \Delta t^j S_1^j \tag{B14}$$

B.3   Bottom node

B.3.1   Flux boundary condition q_{bot}

The right hand side of Eq. B1 transforms to:

$$\frac{\Delta t^j}{\Delta z_n}\left[K_{n-\frac{1}{2}}^j \left(\frac{h_{n-1}^{j+1,p}-h_n^{j+1,p}}{\Delta z_u} \right) + K_{n-\frac{1}{2}}^j + q_{bot} \right] - \Delta t^j S_n^j \tag{B15}$$

Rearrangements of Eq. B1 to the last line of Eq. B2 gives the coefficients:

$$\boldsymbol{a}_n = -\frac{\Delta t^j}{\Delta z_n \Delta z_u} K_{n-\frac{1}{2}}^j \tag{B16}$$

$$\boldsymbol{b}_n = C_n^{j+1,p-1} + \frac{\Delta t^j}{\Delta z_n \Delta z_u} K_{n-\frac{1}{2}}^j \tag{B17}$$

$$f_n = C_n^{j+1,p-1}h_n^{j+1,p-1} - \boldsymbol{q}_n^{j+1,p-1} + \boldsymbol{q}_n^j + \frac{\Delta t^j}{\Delta z_n}\left(K_{n-\frac{1}{2}}^j + q_{bot} \right) - \Delta t^j S_n^j \tag{B18}$$

B.3.2   Head boundary condition h_{bot}

The right hand side of Eq. B1 transforms to:

$$\frac{\Delta t^j}{\Delta z_n}\left[K_{n-\frac{1}{2}}^j \left(\frac{h_{n-1}^{j+1,p}-h_n^{j+1,p}}{\Delta z_u} \right) + K_{n-\frac{1}{2}}^j - K_{n+\frac{1}{2}}^j \left(\frac{h_n^{j+1,p}-h_{bot}}{\Delta z_\ell} \right) - K_{n+\frac{1}{2}}^j \right] - \Delta t^j S_n^j \tag{B19}$$

Rearrangements of Eq. B1 to the last line of Eq. B2 gives the coefficients:

$$\boldsymbol{a}_n = -\frac{\Delta t^j}{\Delta z_n \Delta z_u} K_{n-\frac{1}{2}}^j \tag{B20}$$

$$\boldsymbol{b}_n = C_n^{j+1,p-1} + \frac{\Delta t^j}{\Delta z_n \Delta z_u} K_{n-\frac{1}{2}}^j + \frac{\Delta t^j}{\Delta z_n \Delta z_\ell} K_{n+\frac{1}{2}}^j \tag{B21}$$

$$f_n = C_n^{j+1,p-1}h_n^{j+1,p-1} - \boldsymbol{q}_n^{j+1,p-1} + \boldsymbol{q}_n^j + \frac{\Delta t^j}{\Delta z_n}\left(K_{n-\frac{1}{2}}^j - K_{n+\frac{1}{2}}^j \right) + \frac{\Delta t^j}{\Delta z_n \Delta z_\ell} K_{n+\frac{1}{2}}^j h_{bot} - \Delta t^j S_n^j \tag{B22}$$

List of main symbols

Roman alphabet

Symbol	Interpretation	Dimension	Applied unit
A	Parameter correlation matrix	-	-
A	Relative surface	-	-
C	Parameter covariance matrix	variable	variable
C	Differential soil water capacity $(\mathrm{d}\theta/\mathrm{d}h)$	L^{-1}	cm^{-1}
C_{air}	Specific heat capacity of air	$L^2T^{-2}\Theta^{-1}$	$J\ kg^{-1}\ K^{-1}$
C_{heat}	Soil heat capacity	$ML^{-1}T^{-2}\Theta^{-1}$	$J\ cm^{-3}\ K^{-1}$
CV	Coefficient of variation	-	-
D	Total dispersion coefficient	L^2T^{-1}	$cm^2\ d^{-1}$
D_{dif}	Solute diffusion coefficient	L^2T^{-1}	$cm^2\ d^{-1}$
D_{heat}	Soil heat diffusivity	L^2T^{-1}	$cm^2\ d^{-1}$
D_{lat}	Lateral solute transfer coeff. between cracks and matrix	L^{-1}	cm^{-1}
D_{root}	Rooting depth	L	cm
D_s	Crop development stage	-	-
E_{max}	Maximum soil water evaporation flux according to Darcy	LT^{-1}	$cm\ d^{-1}$
E_p	Potential evaporation rate	LT^{-1}	$cm\ d^{-1}$
EC_e	Electrical conductivity of saturated soil sample	$L^{-3}M^{-1}T^3I^2$	$dS\ m^{-1}$
EC_{sw}	Electrical conductivity of soil water at actual θ	$L^{-3}M^{-1}T^3I^2$	$dS\ m^{-1}$
ET_p	Potential evapotranspiration rate	LT^{-1}	$cm\ d^{-1}$
F_{mob}	Mobile fraction of soil volume	-	-
G	Soil heat flux density	MT^{-3}	$J\ m^{-2}\ d^{-1}$
GW_c	Groundwater level in crack	L	cm
G_c	Solute flux density from mobile to immobile region	$ML^{-3}T^{-1}$	$g\ cm^{-3}\ d^{-1}$
G_w	Water flux density from mobile to immobile region	T^{-1}	d^{-1}
H	Soil water hydraulic head	L	cm
I	Irrigation amount	L	cm
I	Soil water infiltration flux at soil surface	LT^{-1}	$cm\ d^{-1}$
I_{max}	Maximum soil water infiltration flux according to Darcy	LT^{-1}	$cm\ d^{-1}$
J	Derivative matrix	variable	variable
J	Solute flux density	$ML^{-2}T^{-1}$	$g\ cm^{-2}\ d^{-1}$
K	Soil hydraulic conductivity	LT^{-1}	$cm\ d^{-1}$
K_f	Freundlich coefficient	$M^{-1}L^3$	$cm^3\ g^{-1}$
K_r	Preference factor for solute uptake by roots	-	-
K_y	Yield response factor	-	-
L_{dis}	Dispersion length	L	cm
LAI	Leaf area index $(m^2\ m^{-2})$	-	-
NAL	New Amsterdam Level	L	m
N_f	Freundlich exponent	-	-
P	Precipitation amount	L	cm
P_i	Interception amount	L	cm
Q	Diagonal weighing matrix	variable	variable
Q	Solute fraction adsorbed to soil particles $(g\ g^{-1}\ soil)$	-	-

Symbol	Interpretation	Dimension	Applied unit
Q	Cumulative outflow from soil sample	L^3	cm^3
R	Water recharge to groundwater	LT^{-1}	$cm\ d^{-1}$
RE	Relative efficiency	-	-
R_n	Net radiation flux density	MT^{-3}	$J\ m^{-2}\ d^{-1}$
S	Root water extraction rate ($cm^3\ cm^{-3}\ d^{-1}$)	T^{-1}	d^{-1}
S_c	Solute storage in cracks	ML^{-2}	$g\ cm^{-2}$
S_p	Salt storage in soil profile	ML^{-2}	$g\ cm^{-2}$
SC	Soil cover fraction ($m^2\ m^{-2}$)	-	-
$\boldsymbol{T}$	Cumulative transpiration	L	cm
T	Transpiration rate	LT^{-1}	$cm\ d^{-1}$
T	Temperature	Θ	$°C$
$T_{c,d}$	Mean residence time of water in crack due to $q_{c,d}$	T	d
V	Volume	L^3	cm^3
W_c	Crack water storage	L	cm
W_{frac}	Fraction of day that crop is wet	-	-
X	Solute concentration (dissolved + adsorbed)	ML^{-3}	$g\ cm^{-3}$
$\boldsymbol{Y}$	Crop yield	ML^{-2}	$kg\ ha^{-1}$
Z_c	Crack depth	L	cm
$\boldsymbol{b}$	Parameter vector	variable	variable
c	Solute concentration of soil water	ML^{-3}	$g\ cm^{-3}$
c_c	Mean solute concentration of crack reservoir	ML^{-3}	$g\ cm^{-3}$
c_{in}	Solute concentration of rain- or irrigation water	ML^{-3}	$g\ cm^{-3}$
d_{aquif}	Thickness of aquifer	L	cm
d_{pol}	Diameter soil polygon	L	cm
d_{temp}	Damping depth in soil of surface temperature wave	L	cm
e	Vapour pressure	$ML^{-1}T^{-2}$	kPa
e	Void ratio ($cm^3\ cm^{-3}$)	-	-
h	Soil water pressure head	L	cm
h_{air}	Air pressure head	L	cm
$h_{c,i}$	Water pressure head in crack at node i	L	cm
k_c	Crop coefficient	-	-
k_{ads}	Linear adsorption coefficient in saturated zone	$M^{-1}L^3$	$cm^3\ g^{-1}$
n	Shape factor Mualem-Van Genuchten functions	-	-
q	Soil water flux density (positive upward)	LT^{-1}	$cm\ d^{-1}$
$q_{c,i}$	Infiltration flux density from crack to soil matrix at node i	LT^{-1}	$cm\ d^{-1}$
$q_{c,d}$	Direct drainage flux density from cracks to drains	LT^{-1}	$cm\ d^{-1}$
$q_{c,m}$	Infiltration flux density from crack to soil matrix	LT^{-1}	$cm\ d^{-1}$
q_{heat}	Soil heat flux density (positive upward)	MT^{-3}	$J\ cm^{-2}\ d^{-1}$
r	Diffusion resistance	$L^{-1}T$	$s\ m^{-1}$
r_s	Geometry factor for shrinkage	-	-
$s_{c,in}$	Solute flux density entering the crack reservoir	$ML^{-2}T^{-1}$	$g\ cm^{-2}\ d^{-1}$
$s_{c,out}$	Solute flux density leaving the crack reservoir	$ML^{-2}T^{-1}$	$g\ cm^{-2}\ d^{-1}$

Symbol	Interpretation	Dimension	Applied unit
$s_{lat,i}$	Lateral solute transfer between crack and soil matrix	$ML^{-2}T^{-1}$	$g\ cm^{-2}\ d^{-1}$
t	Time	T	d
v	Pore water velocity	LT^{-1}	$cm\ d^{-1}$
z	Vertical coordinate, positive upward, zero at soil surface	L	cm

Greek alphabet

Symbol	Interpretation	Dimension	Applied unit
Φ	Objective function	-	-
α	Shape factor Mualem-Van Genuchten functions	L^{-1}	cm^{-1}
α_{rs}	Reduction factor root water uptake due to salinity stress	-	-
α_{rw}	Reduction factor root water uptake due to water stress	-	-
α_{sh}	Shape factor of shrinkage characteristic	-	-
β_{sh}	Shape factor of shrinkage characteristic	-	-
ϕ	Hydraulic head, positive upward, zero at soil surface	L	cm
ϕ_{gwl}	Phreatic level midway between drains or ditches	L	cm
ϕ_{por}	Soil porosity ($cm^3\ cm^{-3}$)	-	-
γ	Drainage or sub-irrigation resistance	T	d
γ	Confidence level	-	-
γ_{air}	Psychrometric constant	$ML^{-1}T^{-2}\Theta^{-1}$	$kPa\ K^{-1}$
γ_{sh}	Shape factor of shrinkage characteristic	-	-
κ	Radiation extinction coefficient	-	-
κ_{dir}	Extinction coefficient for direct radiation	-	-
κ_{df}	Extinction coefficient for diffuse radiation	-	-
κ_{gr}	Extinction coefficient for global radiation	-	-
λ	Shape factor Mualem-Van Genuchten functions	-	-
λ_i	Characteristic length similar media	L	cm
λ_{heat}	Soil thermal conductivity	MLT^{-3}	$J\ cm^{-1}\ d^{-1}\ K^{-1}$
λ_w	Latent heat of vaporization	L^2T^{-2}	$J\ kg^{-1}$
μ	First order rate coefficient of transformation	T^{-1}	d^{-1}
π_{root}	Root length density ($cm\ cm^{-3}$)	L^{-2}	cm^{-2}
ν	Moisture ratio	-	-
ν	Degrees of freedom number	-	-
ω	Angular frequency	T^{-1}	d^{-1}
θ	Volumetric water content ($cm^3\ cm^{-3}$)	-	-
ρ	Density	ML^{-3}	$g\ cm^3$
ρ_b	Dry soil bulk density	ML^{-3}	$g\ cm^3$
ρ_i	Scale factor of similar media method	-	-
σ	Standard deviation	variable	variable
τ	Value of Student's t distribution	-	-
τ	Period of temperature wave	T	d

Subscripts and superscripts

a	actual	lab	laboratory
ads	adsorption	lat	lateral
air	air	m	matrix
atm	atmosfeer	max	maximum
bot	bottom	md	main drying
c	crack	mw	main wetting
cal	calculated	mob	mobile
con	convection	obs	observed
crop	crop	p	potential
dif	diffusion	p	pores
dis	dispersion	prec	precipitation
drain	drain	rad	radial
dry	drying	ref	reference
entr	entry	res	residual
gr	groundwater	resis	resistance
gwl	groundwater level	s	solid
fing	finger	sat	saturated
heat	heat	sca	scaling
hor	horizontal	sim	simulated
i	index	sur	surface
inf	infiltration	top	top
im	immobile	tot	total
imp	impermeable	ver	vertical
iw	irrigation water	w	water
j	index	wet	wetting
l	liquid		

Curriculum vitae

Jos van Dam was born at the 'boezemwater' of polder 'De Schermer' in North Holland, The Netherlands, on June 17th, 1961. After finalizing high school in 1978, he studied the Bachelor of Science program of Civil Engineering at the Hogere Technische School in Alkmaar, which he finished with honor degree in 1982. Next for a period of one year he was involved in daily supervision of small engineering works by contractor W. Woestenburg from De Rijp, North Holland. In the period 1983-1988 he studied a Master of Science program on Land and Water Use at Wageningen University. After graduation he worked for two years on a project by the European Community to improve the description of land surface processes in global climate models. Since 1990 he works as researcher and lecturer in soil physics and agrohydrology at Wageningen University.